DISSERTATION

submitted to the
Combined Faculties for the Natural Sciences and for Mathematics
of the Ruperto-Carola University of Heidelberg, Germany
for the degree of

Doctor of Natural Sciences

presented by

Dipl.-Bioinf. Univ. **Anna Katharina Dieckmann**
Born in: Goch, Germany
Oral-examination: 29 February 2016

Systems Biological Analysis of Signal Transduction in Telomere Length Maintenance

Referees: Prof. Dr. Roland Eils
Dr. Brian Luke

To David and Lea, for their patience and endurance. Their love of life and happiness sweetened the efforts put into this dissertation.

To Lorenz, if I would not have you.

To my parents. Without their faith in me, their endless backing, and my fathers teaching to think, I would not have come so far.

Acknowledgements

My great journey of doctoral research has been an incredible experience and a success thanks to a multitude of supporters. I have learnt so much — thanks a lot.

To begin with, I would like to express my particular gratitude to Prof. Dr. Roland Eils not only for giving me the opportunity to fulfil my dissertation in his research group, but also for his scientific advice and strong support, especially during the last third of my PhD and whenever trouble arose.

Moreover, I thank Prof. Dr. Rainer König who not only offered this interesting research project to me, but who also allowed me to follow unforeseen aspects of this project. The lively discussions with him greatly enriched my work.

I want to acknowledge the generous funding from the German-Israeli Cooperation DKFZ-MOST (project Ca145 "A Systems-level Dissection of Telomere Biology"). I also thank the current (Prof. Dr. Peter Angel and Dr. Hagit Schwimmer) and the former (Prof. Dr. Dr. Wolfgang Semmler, Nurit Topaz, and Dr. Shlomo Sarig) program coordinators for organising the great workshops in Jerusalem and Heidelberg offering a platform for scientific exchange.

Brian, thanks, thanks so much. Undoubtedly, I owe gratitude to you for inviting me to conduct experiments and your guidance therein. I am deeply grateful for your endless patience, commitment, and encouragement whenever necessary. I really enjoyed my time in your lab and I am very sure my doctoral research improved a lot thanks to your support.

I give thanks to Dr. Jörg Hoheisel for enriching my thesis advisory committee and for his valuable ideas and comments on my research.

For serving as examiner in my thesis defense committee, I thank PD Dr. Karsten Rippe.

I am much obliged to Prof. Dr. Martin Kupiec for exchange of data and knowledge and for giving helpful hints. I very much appreciated the interesting insights into Israeli history as well as the guided tours of Jerusalem, Ein Kerem, and their environs.

Many thanks to Prof. Dr. Maria Pia Longhese for conducting the resection kinetics assay in her laboratory.

I thank Dr. Carl Hermann for his precious help and advice as well as for mentoring me during the critical final phase of my PhD. Thanks for your helpful comments on my thesis.

I am strongly indebted to Sarah, Martina, Rebecca, André, Arianna, Heiko, Katharina, Julia, Lisa, Marco, René, Tina, and Vanessa. I deeply appreciated the tremendous help of you all, enabling me to gain a foothold in the wet lab with its accompanying techniques and processes. To all of you my greatest thanks for your support in every sense. Working together with you was a great pleasure, I have learnt a lot from you. Moreover, thanks a lot for your assistance during my pregnancy which forbid me to complete certain aspects of the lab work myself; I am grateful for your standing-in for me when proteins had to be extracted, gels had to be run or zeocin spottings had to be done. Without you, I would not have been able to finish my thesis. A special thank you to Julia and Katharina for answering every no matter how silly questions and your patience. Katharina, you were a great bench partner.

I also thank Dr. Barbara Di Ventura for her imaging support and Dr. Tobias Bauer for sharing his enrichment script with me.

Ashwin and Alexandra, I will not forget the many fruitful discussions with you two, your help and companionship during the last years.

All dear fellow eilslabs members, thanks a lot for the great working environment and atmosphere.

Jan, I am very grateful for your backing and for always having a sympathetic ear.

I say thanks to Corinna and Manuela for their support in all administrative matters and for boosting my morale every now and then.

I would like to acknowledge the support by the Helmholtz International Graduate School for Cancer Research in Heidelberg.

My doctoral research would not have been possible without an excellent education and training preceding it. Thus and hereby, I would like to express my gratitude to Prof. Dr. Hans-Werner Mewes and Prof. Dr. Thomas Rattei who were convinced of my abilities, supported me during my studies and continued to do so during my PhD. Bearing this in mind, moments of self-doubt lost their basis.

In the end, the last four years were only possible because of the wholehearted support by my family and friends. My PhD would not have been possible without their moral support, without Sarah, Maria, especially Lea, or my mum spending weekends with us, looking after David and Lea whenever necessary, or the financial support by Erna. All of you, thanks that you endured me during the last years. Sarah, thanks a lot for being such a good critic of my thesis.

Abstract

Eukaryotic chromosomal ends are formed by special structural and functional units, termed telomeres, protecting them from fusion, degradation, and unwanted DNA damage repair events. In this way, telomeres preserve genome stability and integrity that are vital to every cell and organism, whereas genomic instability is a hallmark of cancer and ageing. Telomere length is maintained mainly by telomerase which is expressed in 85–90 % of human malignancies, although most human cancer types arise from somatic tissue that is telomerase negative. Thus, telomerase can serve as a nearly universal marker for cancer, as well as a drug target against tumour cells. Genome-wide studies in *Saccharomyces cerevisiae* identified approximately 7 % of the genome (roughly 400 genes) to be associated with telomere length maintenance (*TLM* genes).

Based on these studies, a strong enrichment of genes encoding endosomal sorting complex required for transport (ESCRT) factors has been found within the *TLM* genes that led to telomere shortening when deleted. ESCRT factors define a system of five multi-protein complexes which is involved in deforming and scissioning cytosol filled membrane stalks. Although they can be linked to genomic stability and integrity, only little literature exists on the relationship of telomere homoeostasis and the ESCRT machinery. The data presented here shows that the whole ESCRT system is required to safeguard proper telomere length maintenance. More in-depth experimental investigations of the ESCRT-0 factor Vps27 suggested a model of impaired Exo1-mediated resection resulting in too little telomeric overhang such that Cdc13 binding is suppressed, preventing either telomerase recruitment or telomeric overhang protection. A protein-protein-interaction network analysis indicated a potential feedback mechanism to regulate telomere homoeostasis via the ESCRT system.

The results from the present thesis uncovered the ESCRT system, especially Vps27, as promising drug candidate directed against malignant growth of cancer or diseases caused by dysfunctional telomeres.

Zusammenfassung

Die Enden eukaryotischer Chromosomen werden durch spezielle strukturelle und funktionelle Einheiten gebildet, sogenannte Telomere, und damit vor unerwünschten DNA Reparaturmechanismen, Abbau und Chromosomen-Fusionen geschützt. Auf diese Weise tragen Telomere zum Erhalt von Genom-Stabilität und -Integrität bei, welche lebenswichtig für jede Zelle und jeden Organismus sind. Genomische Instabilität ist ein Schlüsselmerkmal von Krebs- und alternden Zellen. Die Telomerlänge wird hauptsächlich durch Telomerase aufrechterhalten, welche in 85–90 % menschlicher Tumoren exprimiert wird, obwohl sich die meisten menschlichen Krebsarten aus somatischem Gewebe entwickeln, das Telomerase-negativ ist. Daher kann Telomerase als nahezu universeller Tumormarker und als medikamentöser Ansatzpunkt gegen Tumorzellen dienen. In *Saccharomyces cerevisiae* wurde für rund 7 % des Genoms (ca. 400 Genen) durch genomweite Studien ein Einfluss auf die Balance der Telomerlänge festgestellt (*Telomere Length Maintenance* oder *TLM* Gene).

Basierend auf diesen Studien wurde innerhalb der *TLM* Gene eine starke Anreicherung von ESCRT (Endosomal Sorting Complex Required for Transport) Faktoren gefunden, deren Deletion zu einer Telomer-Verkürzung geführt haben. ESCRT Faktoren umfassen ein System aus fünf Multiproteinkomplexen, das an der Verformung und Abschnürung Zytosol-gefüllter Membranknospen beteiligt ist. Obwohl sie bereits mit genomischer Stabilität und Integrität in Verbindung gebracht wurden, existiert nur wenig Literatur über ihre Bedeutung für die Telomer-Homöostase. Die hier präsentierten Daten zeigen, dass das gesamte ESCRT System erforderlich ist, um die richtige Telomerlänge zu bewahren. Tiefergehende experimentelle Untersuchungen des ESCRT-0 Faktors Vps27 führten zu einem Modell, in dem eine geschädigte durch Exo1 vermittelte Resektion einen zu kurzen telomerischen DNA-Sequenz-Überhang nach sich zieht, sodass die Cdc13 Bindung unterdrückt wird und entweder die Telomerase-Rekrutierung oder der Schutz des telomerischen Überhangs verhindert wird. Eine Protein-Protein-Interaktions-Netzwerk Analyse legte einen möglichen Rückkopplungsmechanismus nahe, um Telomer-Homöostase über das ESCRT System zu regulieren.

Die Ergebnisse der vorliegenden Dissertation verweisen auf das ESCRT System, insbesondere Vps27, als vielversprechenden Medikamentenkandidaten gegen bösartiges Wachstum von Krebs oder Krankheiten, die durch dysfunktionalen Telomere verursacht werden.

Contents

List of Figures

List of Tables

List of Abbreviations

A	Adenine (nucleotide)
AA	Amino acid
AnAge	Animal Ageing and Longevity Database ([1])
α	Anti
ATP	Adenosine triphosphate
bactExo1	Bacterial Exo1 (derived from *E. coli*)
BP	Biological process (GO domain)
bp	Base pairs
C	Cytosine (nucleotide)
CA	Chronological ageing
CHX	Cycloheximide
cm	Centimetre
CST	Cdc13-Stn1-Ten1 (3' ssDNA telomere capping complex)
ctrl	Control
DAmP	Decreased Abundance by mRNA Perturbation (yeast mutant library of essential genes)
DB	Database
dCTP	Deoxycytidine triphosphate
dd	Double-distilled (water)
DDR	DNA damage response
DIG	Digoxigenin
DMSO	Dimethyl sulfoxide
DNA	Deoxyribonucleic acid
dNTP	Deoxyribonucleotide triphosphate
DSB	DNA double-strand break
dsDNA	Double-stranded DNA
e.g.	*exempli gratia*
ESCRT	Endosomal sorting complex required for transport
$escrt \cap tlm_{short}$	Overlap of ESCRT factor encoding genes and short *tlm* mutants
EST	Ever shorter telomere (telomerase genes)
EUROSCARF	EUROpean *Saccharomyces Cerevisiae* ARchive for Functional Analysis
EV	Empty vector control
FC	Fold-change
f.c.	Final concentration
FDR	False discovery rate
fig.	Figure (plural: figs.)
FunCat	Functional category
FYVE	(Fab1, YOTB/ZK632.12, Vac1, and EEA1) zinc finger domain (protein domain that binds phosphatidylinositol 3-phosphate, [2])
G	Guanine (nucleotide)
g	Gram
G1	Gap 1 (cell cycle phase)
G2	Gap 2 (cell cycle phase)
Gal	Galactose (GAL)
gDNA	Genomic DNA (also referred to as DNA)
GFP	Green fluorescent protein
GIS	Genetic interaction score

GO	Gene Ontology ([3, 4])
GSEA	Gene set enrichment analysis
h	Hour
HAGR	Human Ageing Genomic Resources
HCl	Hydrogen chloride
HF	High fidelity
HIS	Histidine (used as auxotrophic marker)
HIV	Human immunodeficiency virus
HR	Homologous recombination
HYG	Hygromycin (used as antibiotic selection marker)
ID	Identifier
i.e.	*id est*
ILV	Intralumenal vesicle
KAN	Kanamycin (used as antibiotic selection marker)
kbp	Kilo base pairs
KEGG	Kyoto Encyclopedia of Genes and Genomes ([5–7])
KO	Knock-out
Ku	Yku70-Yku80 heterodimer
Leu	Leucine (used as auxotrophic marker)
LiAc	Lithium acetate
M	Molar
MAT	Mating type
Mb	Mega base pairs
MDP	Mean density profile
mg	Milligram
min	Minute
MIPS	Munich Information Centre for Protein Sequences ([8, 9])
ml	Millilitre
MM	Master mix
mM	Millimolar
mq	MilliQ® (water)
mRNA	Messenger RNA
MRX	Mre11-Rad50-Xrs2
MVB	Multivesicular body
NaCl	Sodium chloride
NaOH	Sodium hydroxide
NAT	Nourseothricin (used as antibiotic selection marker)
NES	Normalised enrichment score
ng	Nanogram
NHEJ	Non-homologous end joining
Ni	Biological replicate of index i (also referred to as n_i)
nt	Nucleotides
NW	Network
OD	Optical density
OE	Overexpression plasmid
ON	Overnight
ORF ID	Systematic open reading frame identifier
P	P-value
PCR	Polymerase chain reaction
PD	Population doubling
PI(3)P	Phosphatidylinositol 3-phosphate
PK	Protein kinase
PPI	Protein-protein-interaction
Raf	Raffinose
RNA	Ribonucleic acid
rpm	Rounds per minute
rRNA	Ribosomal RNA
RA	Replicative ageing
RT	Room temperature
s	Seconds
S	Synthesis (cell cycle phase)
SC	Synthetic complete (yeast medium, expendable as dropout medium)
S. cerevisiae	*Saccharomyces cerevisiae* (official ID: SCE; alias: baker's or budding yeast)

SD	Synthetic dextrose (yeast minimal medium)
SGD	*Saccharomyces* Genome Database ([10])
siRNA	Small interfering RNA
ssDNA	Single-stranded DNA
ssRNA	Single-stranded RNA
suppl.	Supplemental
T	Thymine (nucleotide)
TAP	Tandem Affinity Purification (protein tag)
TLM\DAmP	Non-essential *TLM* genes
TLM	Telomere length maintenance
TRP	Telomere related protein
U	Unit
UEV	Ubiquitin E2 variant (ubiquitin binding domain)
µg	Microgram
UIM	Ubiquitin-interacting motif (ubiquitin binding domain)
µl	Microlitre
µm	Micrometre
Ura	Uracil (used as auxotrophic marker; alias: URA)
V	Volt
VPS	Vacuolar protein sorting
WB	Western Blot
w/o	Without
WT	Wild-type
W×L	Width times length
YPD	Yeast extract peptone dextrose (yeast complete medium)
ZMBH	Zentrum für Molekulare Biologie der Universität Heidelberg (life science faculties of the University of Heidelberg)

Approved Gene Symbols

Standard symbols as provided by the *Saccharomyces* Genome Database (SGD) are used in the present dissertation. The descriptions given in the following list of used gene symbols correspond always to the first sentence of the particular gene description taken from the SGD [10].

Comments On Typesetting of Yeast Identifiers The typesetting of the identifiers follows the general yeast nomenclature [11]. Gene names are presented in italic letters. In case of wild-type of chromosomal-dominant alleles, capital letters are used (e.g. *CDC13*) while recessive mutant alleles are put in lower-case letters and are followed by a hyphen and an Arabic number to indicate the specific mutation (e.g. *cdc13-1*). A protein is symbolised with the corresponding gene symbol that is typeset with only the first character in upper case and is not in italics (e.g. Cdc13). Deletion of a particular gene is denoted with the Greek character Δ and gene disruptions with a double colon (*vps27Δ::KAN* indicates deletion of the *VPS27* gene and its replacement by a kanamycin cassette). Abbreviations of gene families are typeset according to these, too.

escrt	Endosomal sorting complex required for transport (mutant notation)
ESCRT	Endosomal sorting complex required for transport (gene notation)
tlm	*TLM* gene deletion (mutant notation)
TLM	Telomere length maintenance (gene notation)
vps	Vacuolar protein sorting (mutant notation)
VPS	Vacuolar protein sorting (gene notation)
yfgΔ	Your favourite gene deletion
yfts	Your favourite temperature-sensitive mutant

List of Used Gene Symbols

Q0060	Endonuclease I-SceIII (mitochondrial gene; *AI3*)
AIM3	Protein that inhibits barbed-end actin filament elongation
ALIX	Programmed cell death 6 interacting protein (mammalian homologue of Bro1, [12])
ARG3	Ornithine carbamoyltransferase (involved in arginine biosynthesis)
ATG5	Conserved protein involved in autophagy and the Cvt pathway
BRO1	Cytoplasmic class E vacuolar protein sorting (VPS) factor
CDC13	Single stranded DNA-binding protein found at TG1-3 telomere G-tails
Cep55	Centrosomal protein 55kDa (mammalian protein, [12])
DID2	Class E protein of the vacuolar protein-sorting (Vps) pathway (ESCRT-III associated)
EST1	TLC1 RNA-associated factor involved in telomere length regulation
EST2	Reverse transcriptase subunit of the telomerase holoenzyme
EST3	Component of the telomerase holoenzyme
Exo1	5'–3' exonuclease and flap-endonuclease
HGS	Hepatocyte growth factor-regulated tyrosine kinase substrate (alias: HRS, mammalian homologue of Vps27, [12])
HO	Homothallic switching endonuclease
HRS	Refer to HGS

HSE1	Subunit of the endosomal Vps27-Hse1 complex (ESCRT-0)
IPK1	Inositol 1,3,4,5,6-pentakisphosphate 2-kinase
IST1	Protein with positive role in the MVB sorting pathway (ESCRT-III associated)
YKU70	Subunit of the telomeric Ku complex (Yku70p-Yku80p)
YKU80	Subunit of the telomeric Ku complex (Yku70p-Yku80p)
LAS17	Actin assembly factor
MEC1	Genome integrity checkpoint protein
MRE11	Nuclease subunit of the MRX complex with Rad50 and Xrs2
MVB12	ESCRT-I subunit required to stabilize ESCRT-I core complex oligomers
PGK1	3-phosphoglycerate kinase
PIF1	DNA helicase, potent G-quadruplex DNA binder/unwinder
RAD50	Subunit of MRX complex with Mre11 and Xrs2
RAD52	Protein that stimulates strand exchange
RAD53	DNA damage response protein kinase
RAD9	DNA damage-dependent checkpoint protein
RAP1	Essential DNA-binding transcription regulator that binds many loci
RIF1	Protein that binds to the Rap1 C-terminus
RIF2	Protein that binds to the Rap1 C-terminus
SAE2	Endonuclease required for telomere elongation
SIR3	Silencing protein
SIR4	SIR protein involved in assembly of silent chromatin domains
SLA1	Cytoskeletal protein binding protein
SNF7	One of four subunits of the ESCRT-III complex
SNF8	Component of the ESCRT-II complex
SRN2	Component of the ESCRT-I complex
STN1	Telomere end-binding and capping protein
STP22	Component of the ESCRT-I complex
TEL1	Protein kinase primarily involved in telomere length regulation
TEN1	Protein that regulates telomeric length
TIF1	Translation initiation factor eIF4A
TLC1	RNA template component of telomerase
TSG101	Tumor susceptibility 101 (mammalian homologue of Stp22, [12])
DID4	Class E Vps protein of the ESCRT-III complex (alias VPS2)
VPS20	Myristoylated subunit of the ESCRT-III complex
VPS24	One of four subunits of the ESCRT-III complex
VPS25	Component of the ESCRT-II complex
VPS27	Endosomal protein that forms a complex with Hse1 (ESCRT-0)
VPS28	Component of the ESCRT-I complex
VPS36	Component of the ESCRT-II complex
VPS4	AAA-ATPase involved in MVB protein sorting (ESCRT-III associated)
VPS60	Protein involved in late endosome to vacuole transport (ESCRT-III associated)
VTA1	Multivesicular body protein (ESCRT-III associated)
XRS2	Protein required for DNA repair (component of MRX complex)
YDR133C	Dubious open reading frame (unlikely to encode a functional protein)

CHMP	Chromatin modifying protein
CPY	Carboxypeptidase Y (a vacuolar protease)
EAP	ELL-associated proteins
ELL	RNA polymerase II elongation factor

List of Publications

Results obtained and described during the present dissertation contributed to the following publications.

Dieckmann, A. ; Babin, V. ; Harari, Y. ; Eils, R. ; König, R. ; Kupiec, M. ; and Luke, B.: *Role of the ESCRT complexes in telomere biology.* – (manuscript in preparation, working title)

Harari, Y. ; Dieckmann, A. ; and Kupiec, M.: *The relationship between telomere length, cellular aging and fitness in Saccharomyces cerevisiae.* – (manuscript in preparation)

Furthermore, independently of the present thesis — in terms of content — I contributed to the following manuscript.

Schellhaas, R. ; Dieckmann, A. ; and Luke, B.: *The regulation of telomere looping.* – (manuscript in preparation, working title)

1 Introduction

Not that long ago, biology was considered by many to be a simple science, a pursuit of expedition, observation and experimentation. [...] *The molecular revolution that dawned with the discovery of the structure of DNA in 1953 changed all that, making biology more quantitative and respectable, and promising to unravel the mysteries behind everything from evolution to disease origins.*

(Erika Check Hayden, [16])

1.1. The Complexity of Life

The basic structural and functional unit of life is the *cell* [17]. However, life's complexity is defined by the interplay of diverse organisational levels from basic cellular building blocks such as proteins up to tissues and organs [18,19]. Understanding the structure and dynamics of their functional interplay is a key challenge for biology in the twenty-first century [20] as it has become increasingly clear that research "limited to individual genes, cells, and chemical reactions" [21] is insufficient to fully disentangle the complexity of life, visualised in fig. 1.1. The elementary molecular building blocks of a cell are organised into small recurrent patterns that form functional modules which in turn assemble into large-scale entities. Systems biology aims at understanding "how complex systems underlie life" [21].

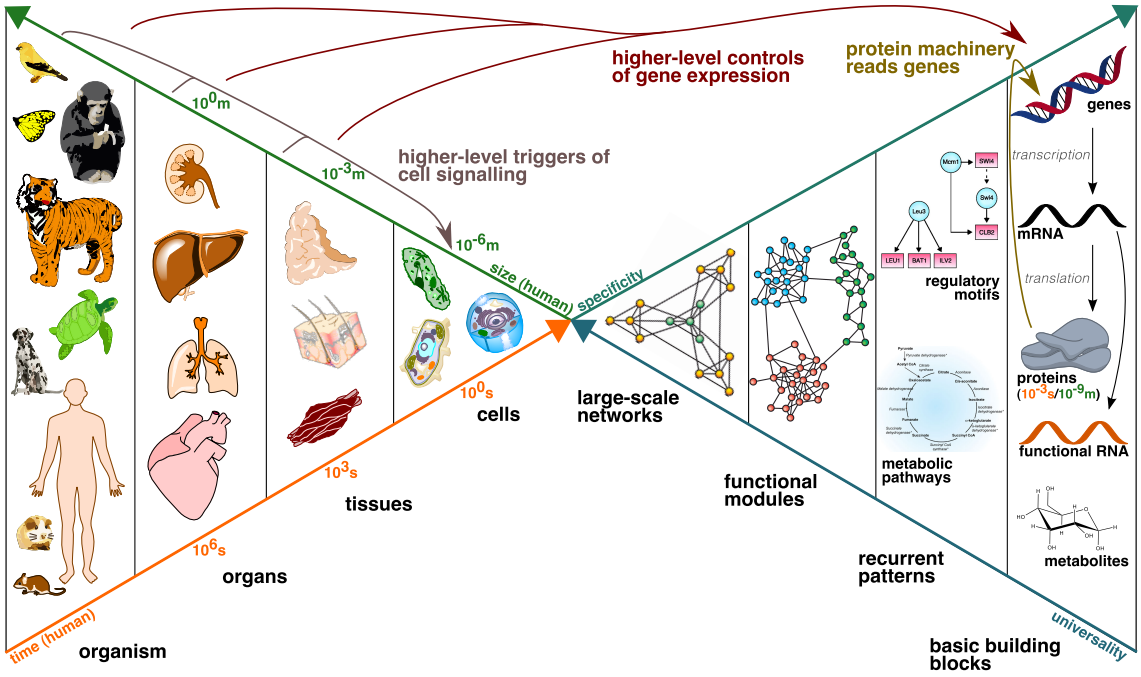

Figure 1.1.: Complexity of life is defined by the interplay of diverse levels. From left to right, we zoom from the organism into its cells that are composed of a hierarchy of different levels. Cellular functions are "distributed among groups of heterogeneous components that all interact within larger networks" [19]. These larger networks consist of functional modules that are formed by either genetic-regulatory motifs or metabolic pathways. The basic building blocks for those components are metabolites or gene products encoded in an organism's genome. "Loops of interacting downward and upward causation can be built between all levels of biological organisation" [18]. This is already apparent on the very lowest level: the protein machinery decodes genes which in turn encode proteins. The time and size scale on the left apply for various levels of the human body. The figure has been devised on the template of the life's complexity pyramid presented by Oltvai and Barabási [19] and extended with ideas of the causal chain of life by Denis Noble [18]. It has been drawn using biological entities from ChemDraw Professional except for the regulatory motifs [22], the TCA cycle [23], and the functional modules as well as the large-scale network [19]. An enlarged version of this figure can be found in the supplement (fig. B.1).

The entire information for building and maintaining an organism is stored in its *genome*. Except for some viruses storing it in a ribonucleic acid (RNA) molecule, the genome is encoded in a double-stranded and helical deoxyribonucleic acid (DNA) molecule. A *gene* is defined as "a union of genomic sequences encoding a coherent set of potentially overlapping functional products" [24] (e.g. a protein). The genome comprises genes and non-coding elements. A process termed *gene expression*, decodes genes into functional products. Initially, the DNA sequence corresponding to a single gene is transcribed into an intermediary RNA sequence (messenger RNA or mRNA). The mRNA is either translated

into a linear amino acid sequence or post-transcriptionally processed into a functional RNA molecule. Finally, the amino acid sequence is folded into a three-dimensional fully functional protein representing a cellular building block or molecular machine. The DNA molecule of each cell is highly condensed into thread-like structures called *chromosomes* (fig. 1.2).

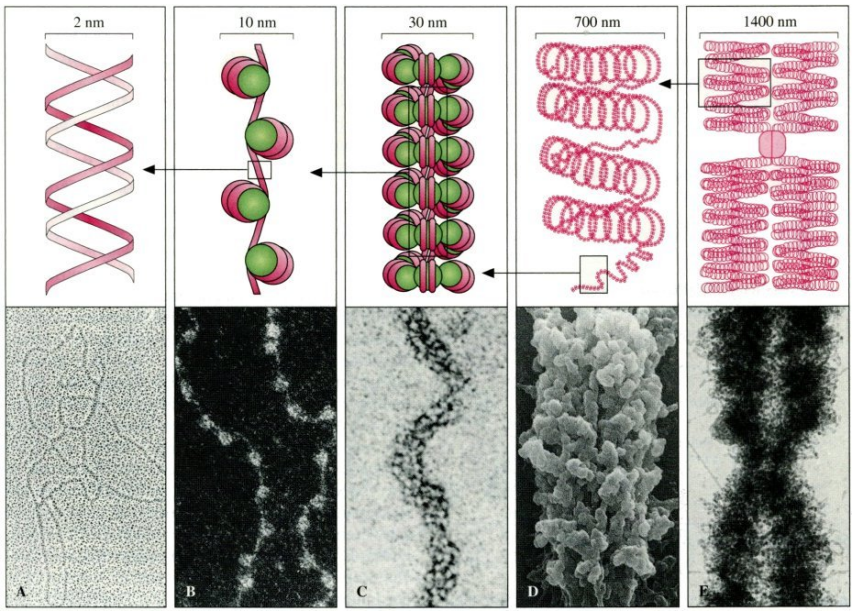

Figure 1.2.: The different states of DNA condensation from a double-stranded helical structure (A) into a thread-like structure called *chromosome* (E). Both schematic and electron microscopic images are depicted. Green balls represent histones that support and strengthen the folding of the DNA molecule. The images have been taken from Hafner and Hoff [25].

Every cell of an organism is challenged by the fundamental and continuous need to maintain genomic stability [26, 27] while being faced with either endogenous sources of DNA damage (e.g. routine errors in DNA replication) or exogenous genotoxic agents (e.g. ultraviolet light or chemical compounds) [27, 28]. As can be seen by the myriad of human syndromes, neurodegenerative diseases, and immunodeficiency, as well as cancer associated with defects in factors sensing and responding to DNA damages [26–30], a proper repair of DNA lesions is rather critical for cells and organisms. Besides being a hallmark of cancer, genomic instability is also a hallmark of ageing, since chromosomal instabilities increase with age [26]. "DNA double-strand breaks (DSBs) are among the most serious and lethal types of DNA damage, as a single DSB is sufficient to kill a cell or to disturb its genomic integrity" [27, 30]. For maintaining genomic integrity, a well orchestrated DNA damage response (DDR) is required [27,31,32], wherein multiple players and processes are employed.

Thus, understanding the mechanisms leading to genomic instability is crucial for improving and developing promising treatments and therapeutic targets, successfully tackling cancer and other health burdens. With its integrative and system-wide view, systems biology is an auspicious approach unravelling the complex intercellular network of genes, proteins, and biochemical reactions underlying diseases [33]. As "a gene can do nothing without [its] interpretation by the system" [18], we have to strive for the comprehension of biological systems in its entirety.

1.2. DNA Maintenance

The following section on DNA Maintenance has been adapted from the book "Molecular Biology of the Cell" by Bruce Alberts [34].

As stated before, the entire information for building and maintaining an organism is stored in its genome. The necessity of duplicating the entire DNA sequence previous to each cell division becomes evident as requirement for growth, development and maintenance of health. "Multicellular organisms like ourselves depend on the remarkably high fidelity with which their DNA sequences are maintained" [34]. DNA maintenance relies strongly on accurate *DNA replication* and transmission to daughter cells as well as on DNA damage repair. These damages might be caused by radiation, chemicals or naturally arising errors during DNA replication and transmission. Although species as a whole can benefit in the long run from occasional genetic changes, each individual relies on genetic stability for its survival. In humans, most body or *somatic* cells regularly undergo cell division. Except for *germ cells* (eggs or sperm), all human cells are somatic. The sequence of events in the life of a cell from its creation until division is called *cell cycle* [35]. Broadly, one cell cycle comprises a phase of growth and activity and a phase of division. The first phase (*interphase*) consists of phases G1 (growth), S (DNA replication or synthesis), and G2 (growth, preparing for division). The actual cell division requires division of the genetic material (*mitosis*) followed by division of the cytoplasm (*cytokinesis*). At the end of the G1 and G2 phase, cell cycle checkpoints ensure that the cell cycle faultlessly continuous. Upon detection of any DNA damage or mistakes occurred during replication, the cell cycle is arrested, allowing the cellular machinery to correct such errors [35,36].

1.2.1. DNA Replication

In order to distribute a full complement of its genome to both of the daughter cells, the mother cell has to faithfully replicate its whole DNA sequence preceding cell division. The process of DNA replication, visualised in fig. 1.3, takes place during S phase and engages various different enzymes that have to properly cooperate. Due to the complementary and double-stranded structure of the DNA, it can serve as template for its own copying. Initially, the double helical DNA structure is unwound by an enzyme called *helicase* opening the DNA helix into a Y-shaped replication fork. Subsequently, the new strands are synthesised while both parental strands serve as corresponding templates. Synthesis is catalysed by a self-correcting DNA polymerase that can act only in 5' to 3' direction. Hence, the *leading* strand can be continuously extended. As the DNA double helix is antiparallel, the opposing *lagging* strand cannot be continuously extended. In fact, it is processed in so called *Okazaki* fragments using small RNA primers as starting points. Those primers are later removed and the resulting gaps are then filled with nucleotides. Once both strands are completely replicated, each of both newly synthesised DNA molecules contains a new and an old strand (*semi-conservative* replication). In this way the whole genome is copied with remarkable fidelity. In addition to the self-correcting abilities of DNA polymerases, further proofreading processes minimise the number of inappropriate nucleotide additions. As soon as replication of the entire genome is achieved and no replication errors are detected that would lead to a cell cycle arrest, cell division further continues [35,36].

Semi-conservative replication of linear DNA ends entails the *end replication problem*. Although it has originally been considered "to be a problem of incomplete lagging strand

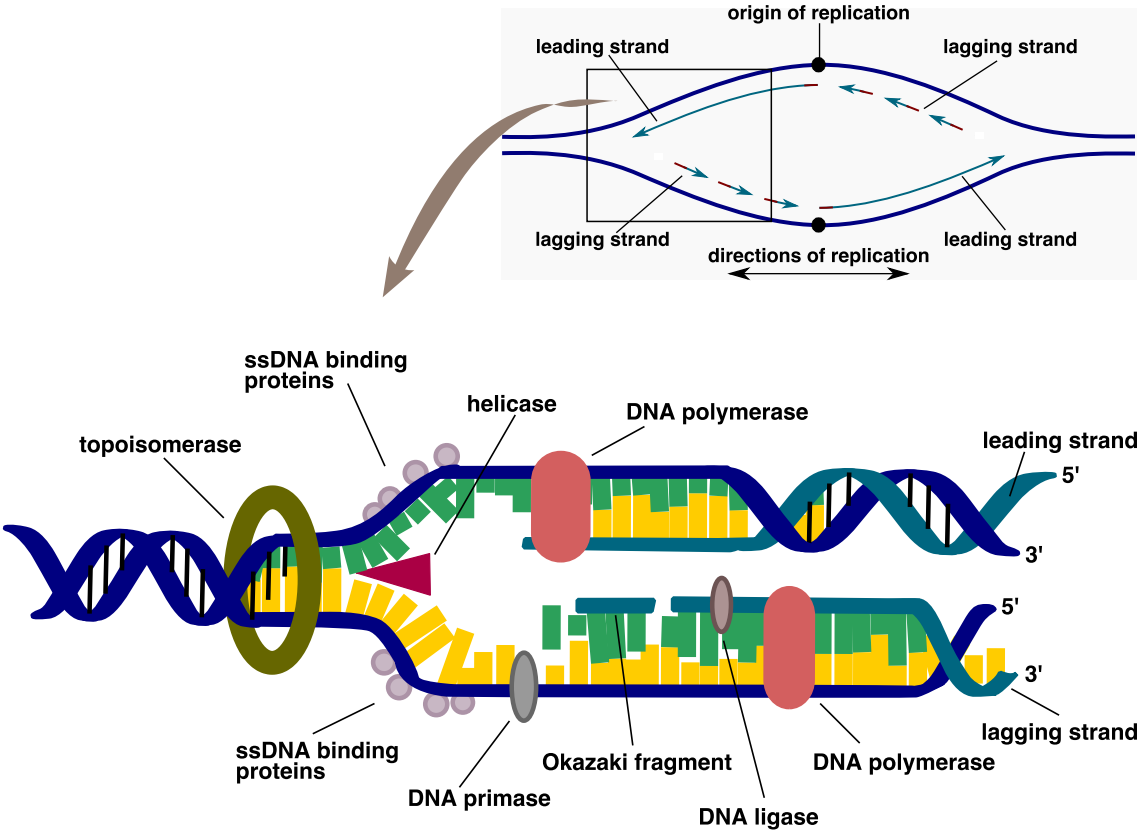

Figure 1.3.: DNA replication describes the process of duplicating the entire genome preceding cell division. Various enzymes are tightly orchestrated to synthesise two new DNA strands in 5'–3' direction. The schematic has been adapted from Campbell et al. [36] using biological entities from ChemDraw Professional.

synthesis" [37], this is only half of the truth. The lagging strand can only discontinuously be synthesised in short Okazaki fragments, each of which requires its own primer. At the very end of a chromosome, the removal of the last primer leaves a gap resulting in a 3' overhang that "cannot be overcome by the replication complex" [38] and results in 5' DNA sequence loss (fig. 1.4a). Without taking care of this lagging strand end problem, the 5' sequence loss will potentiate with cell generations [39–42]. The theory of a lagging strand end problem assumes *blunt*-ended chromosomal termini, i.e. a dsDNA molecule that ends in a common base pair. However, single-stranded overhangs at the 3' chromosomal termini have been found as "a general feature of eukaryotic chromosomes" [37] and thus the replication of DNA termini has to be reconsidered. In the presence of a 3' overhang or *sticky* DNA ends, lagging strand synthesis does not cause problems to the DNA replication machinery as the final RNA primer can be positioned complementary to this 3' overhang. Thus, no 5' sequence loss occurs. In contrast, continuous synthesis of the leading strand results in loss of the 3' overhang causing a lagging strand problem in the next round of DNA replication [37]. Figure 1.4b illustrates the end replication of sticky DNA termini. Hence, depending on the DNA terminus either a leading (sticky ends) or a lagging (blunt ends) strand problem occurs.

1.2.2. DNA Damage Response

The error detection and correction of the DNA replication machinery only rarely fails, producing permanent changes in the DNA (*mutations*). Lesions on one strand or even on both can accidentally occur. If vital positions in the DNA sequence are affected by unintentional

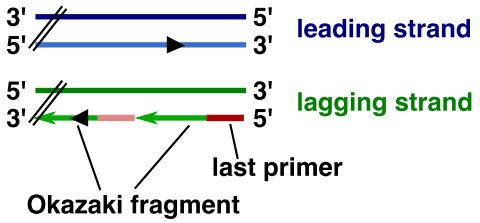

(a) Blunt DNA termini.

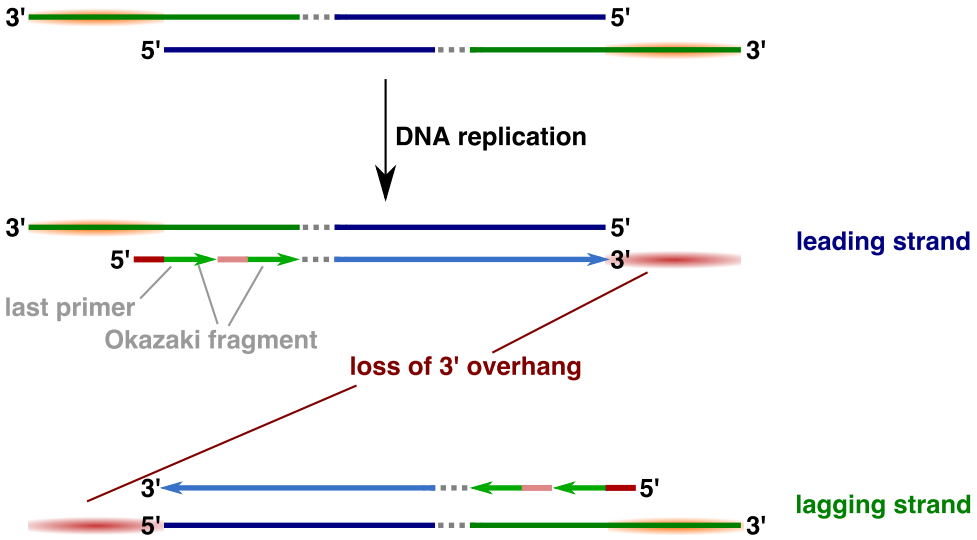

(b) DNA termini with 3' overhangs.

Figure 1.4.: Depending on the DNA terminus either a lagging or a leading strand end replication problem occurs. (a) In the case of blunt ends, the DNA replication machinery is incapable of fully synthesising the lagging strand. Upon removal of the last primer a gap at the newly synthesised DNA strand a 3' overhang arises. This end replication problem results in 5' sequence loss during each cell cycle. (b) In the presence of 3' overhangs, the final Okazaki primer can be positioned complementary to the overhang such that the lagging strand is completely synthesised. However, the continuous replication of the leading strand results in loss of the 3' overhang causing a lagging strand problem in the next round of DNA replication. The figure has been created according to Lingner et al. [37].

changes or lesions, the resulting cellular imbalance can result in detrimental effects on the cellular and organismal level. To circumvent severe defects and genome instability, a multitude of proteins have evolved to tackle those DNA damages. These repair proteins constantly scrutinise the DNA for damage sites. *Base* or *nucleotide excision repair* treat wrongly inserted bases or nucleotides. Whole double-strand lesions (*DNA double-strand breaks* or DSBs) are dealt by either the *non-homologous end joining* (NHEJ) or *homologous recombination* (HR) mechanism. Unlike repair of errors in a single strand, DSB repair cannot fall back to an intact template. For ensuring the transmission of faultless DNA to daughter cells, the cell cycle is delayed until DNA repair is completed, otherwise cells would be prone to apoptosis. In *Saccharomyces cerevisiae*, the incidence of DNA damage can interfere at different stages of the cell cycle: (i) the entry into G1 can be blocked, (ii) DNA replication can be slowed down once begun, and (iii) the transition from S to M phase can be hindered.

Both, cell type and cell cycle stage influence the type of repair event that also depends on the kind of the damaged DNA end. Blunt DNA ends initiate NHEJ whereas single-stranded DNA (ssDNA) stimulates HR [43]. Moreover, NHEJ is active throughout the cell cycle

although preferred during G1, while HR is most active in the S and G2 phase [44, 45]. (Refer to fig. 1.5 for an outline of the NHEJ and the HR repair mechanisms.) Upon detection of a DSB, the yeast Mre11-Rad50-Xrs2 (MRX) complex binds to it and depending on the cell cycle phase either NHEJ (G1) or HR (S or G2) is initiated. In case of NHEJ activation, the Yku70-Yku80 heterodimer (Ku) is recruited to the damage site and prevents nucleolytic attack at the DSB. The two DNA ends are then simply rejoined by DNA ligation without the need for a template, making NHEJ an error-prone process.

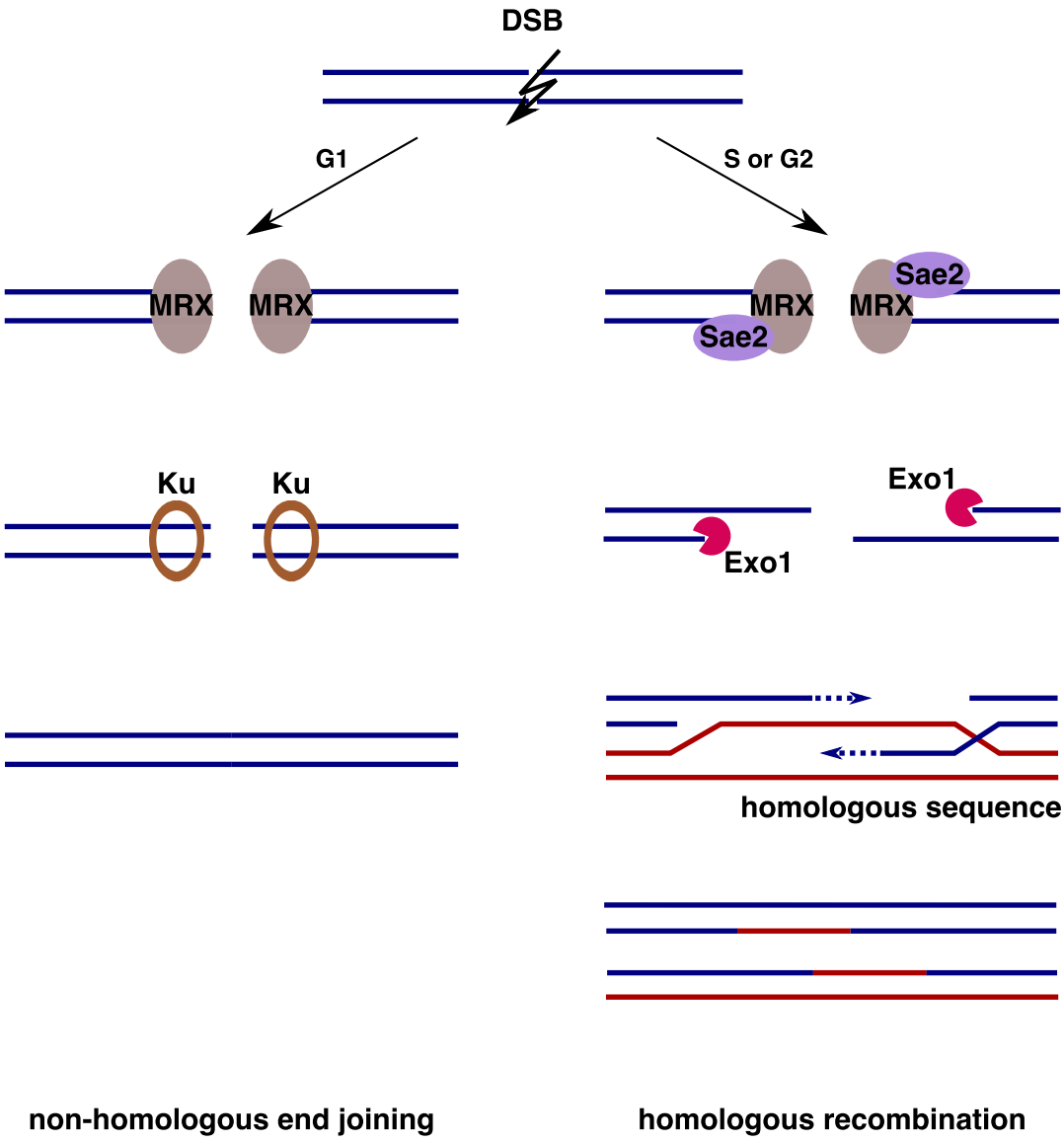

Figure 1.5.: Two major pathways exist in order to repair DNA double-strand breaks (DSBs). Initially, a DSB site is bound in yeast by the Mre11-Rad50-Xrs2 (MRX) complex and depending on the cell cycle stage either non-homologous end joining (NHEJ) or homologous recombination (HR) is initiated. While NHEJ relies on the simple rejoining of the two DNA ends, HR incorporates several steps to repair the lesion. Following extensive 5'–3' resection and homology search, strand invasion, synthesis, and annealing take place.

If HR is stimulated, Sae2 degrades the 5' end into a 3' ssDNA overhang preparing for subsequent extensive Exo1-mediated 5'–3' resection (strand resection). Afterwards, a homologous sequence is searched matching the produced ssDNA sequences, invading the duplex and forming a heteroduplex DNA (strand invasion). Beginning from the 3' ends, new DNA strands are synthesised and the ssDNA tail is annealed to the displaced strand (strand

displacement and annealing). Finally, the heteroduplex is resolved and the ssDNA is fully ligated to the invaded duplex [45,46]. NHEJ is accompanied by loss of nucleotides at the joining site [34]. In contrast to the intrinsic mutagenic nature of NHEJ, HR accurately repairs DSBs as it relies on the usage of an undamaged homologous DNA template and thus fully restores the lost sequence [47].

Depending on the type of damage, either Mec1 (ssDNA) or Tel1 (DSB) activate Rad9, leading to Rad53 phosphorylation and subsequent cell cycle arrest until DNA damage repair is finished [48].

1.3. Telomeres

The natural linear ends of eukaryotic chromosomes — *telomeres* — resemble DNA breaks [49]. However, they neither induce DNA damage repair pathways nor DNA damage checkpoint responses [50]. Telomeres represent essential nucleoprotein caps of the chromosomal ends to preserve genomic integrity and cell viability [49, 51] by prevention of chromosome fusions or degradation and unwanted DSB repair events [51]. Moreover, to maintain genomic stability, it is crucial that telomeres and DSBs do not interconvert [50]. The homoeostasis of telomeres underlies tightly controlled mechanisms. Telomere dysfunction has not only been linked to rare disorders such as Ataxia telangiectasia, Werner Syndrome or dyskeratosis congenita, but also to certain malignancies [49,52].

1.3.1. The Nucleoprotein Structure of Telomeres

Telomeres are nucleoprotein complexes (fig. 1.6) composed of repetitive DNA regions and well-defined coating proteins [51, 53]. The *G strand* directed from 5' to 3' is guanosine-rich

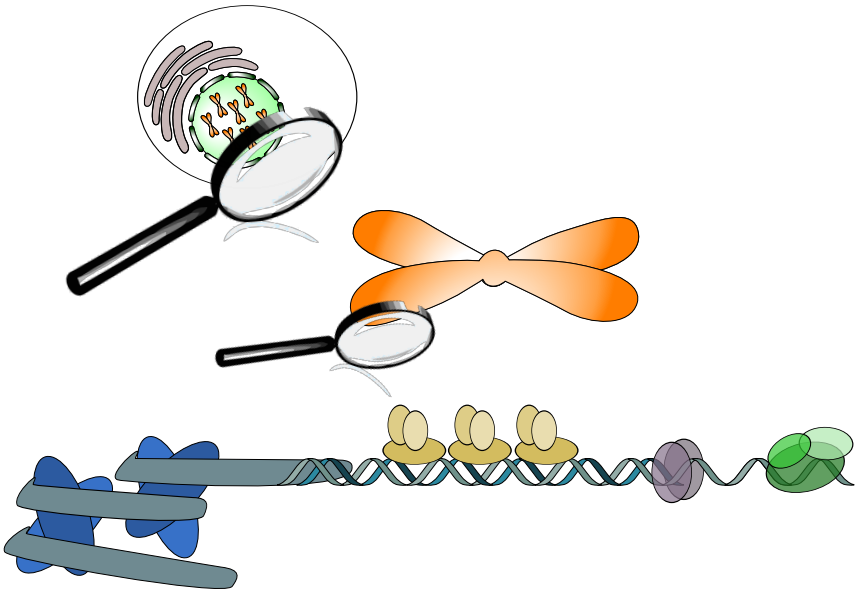

Figure 1.6.: Schematic of the nucleoprotein structure of telomeres. The ends of eukaryotic chromosomes consist of tandem repeats of guanosine-rich sequences and coating proteins. The 5' to 3' strand ends in a 3' ssDNA overhang. The schematic has been drawn using entities from ChemDraw Professional.

and extends into a single-stranded DNA overhang (G-tail) [54]. Tandem array GT-rich repeats are found at every telomere, however their composition and number differ across

species [50]. In contrast to the human 5'-$[T_2AG_3]_n$-3' repeat extending from 2–50 kbp, *Saccharomyces cerevisiae* telomeres bear a more heterogeneous 5'-$[TG_{1\text{-}3}]_n$-3' motif spanning from 250 to 400 bp [53]. The length of G-tails can range from 50–100 nt in yeast up to 50–300 nt in humans [49, 53, 54]. Alternative telomere structures have been observed in *Caenorhabditis elegans* that in addition to 3' G-tails can also form 5' C-tails. The latter have also been detected in mammalian cells while in plants blunt-ended telomeres can be found [55].

In addition, less conserved DNA elements precede telomeric repeats. These subtelomeric regions (fig. 1.7) can be found in most organisms and are at least a few hundred base pairs long. Human individuals as well as yeast strains show high variability in their subtelomeric composition [56]. In yeast, two structural and functional distinct subtelomeric repeats exist, whose distribution separates yeast chromosomes into either the X or the X-Y' class. Y' subtelomeres contain one to four copies of the Y' element. X elements are more diverse, despite that they contain a X-core repeat. While X-subtelomeres lack histones, Y' regions possess high nucleosome density and exhibit transcriptional activity [50,57].

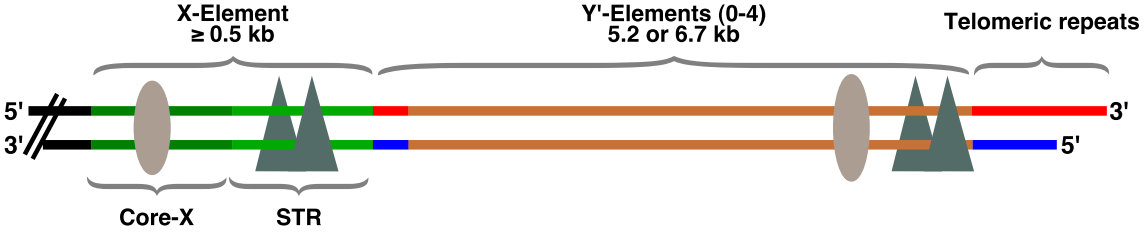

Figure 1.7.: Schematic of the subtelomeric composition of X and Y' elements extending into the terminal repeat sequences. Red indicates G-rich and blue indicates C-rich sequences. The X element can be separated into core and subtelomeric repeated (STR) subregions [58]. The figure has been reproduced according to Wellinger and Zakian [59].

Telomeric DNA can adopt different topological conformations by invasion of the G-tail into upstream dsDNA regions (t-loops, fig. 1.8b) or other structural arrangements such as G-quadruplex structures (fig. 1.8a) [55]. The exact function of t-loops remains to be elucidated.

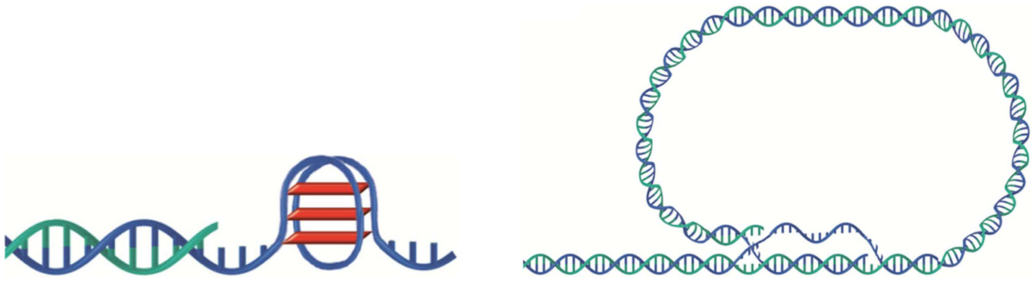

(a) G-Quadruplex. (b) T-Loop.

Figure 1.8.: Telomeric DNA can adopt different topological conformations. (a) Four hydrogen-bonded guanosine bases form a plane or a G-tetrad which are stacked on top of each other to form a G-quadruplex. (b) The 3' telomeric overhang can fold back into a loop and invade into upstream dsDNA regions. The figure has been adapted from Giraud-Panis et al. [55].

Nonetheless, it has been inferred that t-loops contribute to the protection of chromosomal ends from being recognized as DSBs and that they influence the access of telomeric DNA binding proteins to the DNA [55]. Stabilisation of telomeric G-quadruplex structures has been found to support tumour regression in mice [60,61] and interferes with telomeric maintenance mechanisms [55].

"Because of the unusual properties of telomeres, a *bona fide* telomeric protein complex has evolved" [49]. This complex comprises proteins endemic at telomeres or proteins that are also involved in the DNA damage response (DDR) and DSB repair. Telomeric proteins ensure the complex interplay of "telomere length regulation, protection from enzymatic attack [(capping)] and recruitment of required enzymatic activities" [49]. Furthermore, they are involved in the signalling cascades stemming from the telomeres [49]. Although protein capping of telomeres is conserved throughout the eukaryotic lineage, their organisation shows considerable diversity [55]. In baker's yeast, the

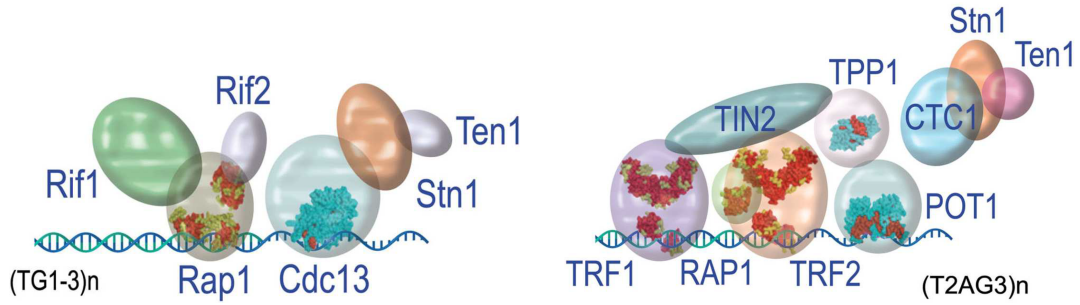

(a) *Saccharomyces cerevisiae*. (b) Mammals.

Figure 1.9.: Telomere capping proteins in (a) baker's yeast and (b) mammals. In yeast the ssDNA overhang and the dsDNA region are bound by two different complexes whereas the Shelterin complex bridges both DNA regions in mammals. The figure has been adapted from Giraud-Panis et al. [55].

ssDNA is capped by the Cdc13-Stn1-Ten1 (CST) complex and the dsDNA is bound by the Rap1-Rif1-Rif2 complexes (fig. 1.9a). The capping complex in mammals (*Shelterin*, fig. 1.9b) comprises six proteins and bridges the single-stranded and double-stranded telomeric DNA [51, 55, 62]. Lack or disruption of those capping protein complexes have been associated with several telomere phenotypes amongst which are improper length control, chromosome fusions, DNA damage checkpoint activation or elevated levels of ssDNA [50].

1.3.2. Telomere Homoeostasis and Maintenance

Linear ends of eukaryotic chromosomes are faced with the leading strand end replication problem as described above (section 1.2.1 and fig. 1.4b) [37,56,63] by which telomeres gradually shorten with each cell division (DNA replication) leading to loss of sequence information. In fungi and flies, telomeres shorten at rather modest rate of approximately 3–5 bp per chromosome end and cell division. The rate of shortening of human and mouse telomeres is much faster, namely 50–100 bp per end and cell division [63]. Upon a critical minimal length defined as the Hayflick limit [64], the progressive shortening leads to replicative senescence (cell ageing) or apoptosis (cell death) [51]. Telomere erosion occurs in most somatic cells while germline and stem cells are equipped with a mechanism to counteract telomere attrition [51,63].

Telomere length homoeostasis is mainly achieved by a two-component ribonucleoprotein enzyme — *telomerase* — consisting of a highly conserved reverse transcriptase and a RNA moiety serving as replication template [51, 63]. Telomerase shares extensive homology with viral reverse transcriptases [56, 63], both being able to re-transcribe a RNA molecule into the corresponding complementary DNA sequence. In humans, telomerase activity is suppressed in soma, whereas it is active in ovaries, testes, and proliferative tissues [63]. This explains the telomere erosion phenotype in somatic cells. Most unicellular organism (e.g.

baker's yeast) express telomerase on housekeeping levels [63]. The constitutive telomerase expression renders *Saccharomyces cerevisiae* an excellent model organism for studying telomere biology. Section 1.5.1 elaborates on the advantages of yeast as a model organism. The following sections will focus on the telomere maintenance by telomerase mainly in yeast.

To maintain telomeres in the absence of telomerase, alternative mechanisms on the basis of homologous recombination exist (reviewed in [65] and [66]).

1.3.2.1. Telomere Replication

In the course of every cell cycle, telomere replication plays an essential part involving multiple steps and components. Failures in the regeneration of the telomeric nucleoprotein architecture lead to DDR and genomic instability [67]. Yeast telomere replication occurs during the late S phase [51] and requires the divestment of the coating proteins to allow the access of telomerase to the telomere. Although the general steps of telomere replication are well conserved, the timing differs amongst various species [67]. Figure 1.10 depicts the integration of telomere extension subsequent to ordinary DNA replication into the baker's yeast cell cycle. Following conventional replication of the telomeric dsDNA region, the chromosomal ends are specifically processed to reconstitute the 3' G-tail.

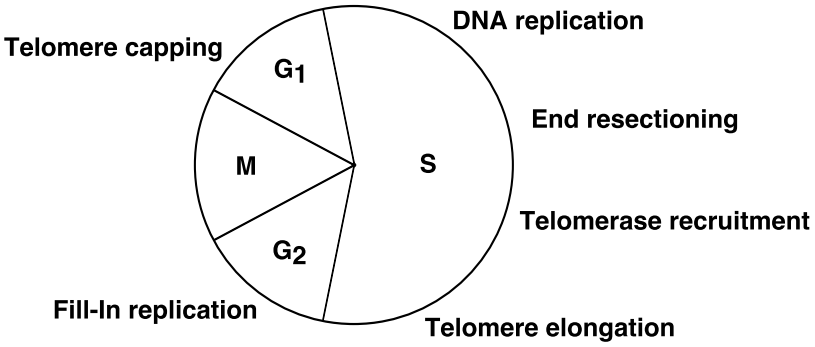

Figure 1.10.: Telomere homoeostasis is well integrated into the cell cycle. In yeast, telomere replication takes place during late S phase.

While the newly synthesised C-strand (lagging strand replication) naturally ends in an overhang after removal of the final Okazaki fragment, the new G-strand is blunt-ended (fig. 1.11). Thus, the formation of an overhang requires 5' to 3' nuclease digestion (*end resection*). Subsequent to end resectioning and in concordance with its reverse transcriptase nature, telomerase extends the 3' ends of the newly replicated G-strands. Afterwards, complementary C-strand fill-in takes place by the DNA polymerase α/primase complex [50, 51, 56, 63, 67]. The 3' overhang serves as primer for telomerase, whose inherent RNA template is positioned such that it is adjacent to the overhang [63]. Telomerase activity comprises multiple iterations of elongation and translocation to the 3' end [56].

1.3.2.2. Recruitment of Telomerase

Telomere elongation correlates with the binding of several proteins assisting in this process [51]. Moreover, telomerase needs to be recruited to the telomeric end and its

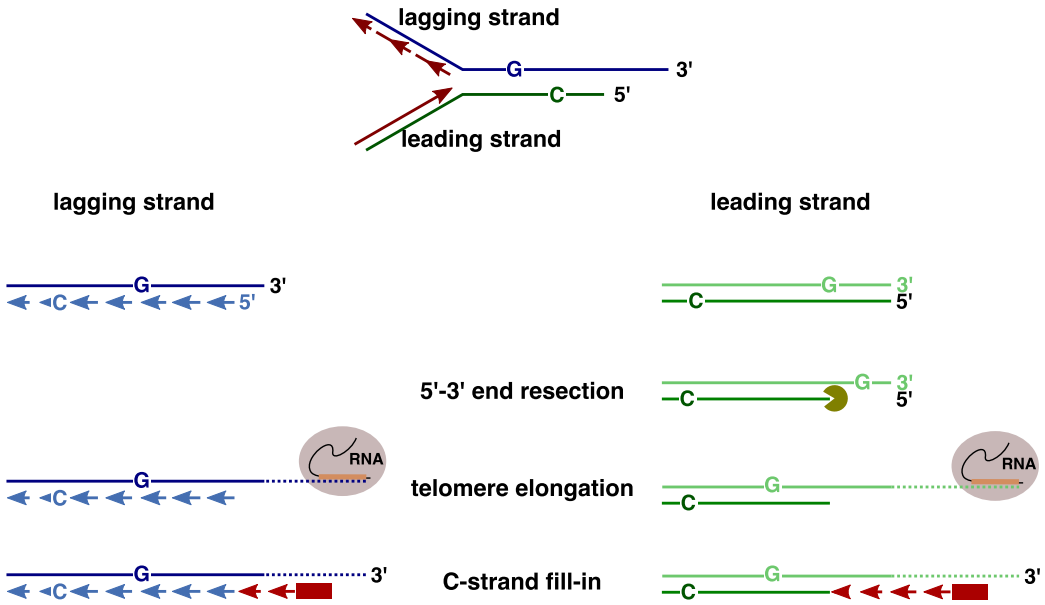

Figure 1.11.: Schematic of telomere replication. While the lagging strand synthesis produces a 3' overhang on its own, leading strand replication results in a blunt-ended DNA duplex. 5'–3' resection reconstitutes the telomeric overhang enabling telomerase attachment. Telomerase action is followed by C-strand fill-in facilitated by the DNA polymerase α/primase complex. The figure has been drawn on the basis of Lydall [50] and Schluth-Bolard et al. [38].

activity has to be tightly regulated to circumvent indefinite elongation. Control of telomerase can be achieved in several ways: (i) at the level of its recruitment, (ii) during the initiation of elongation, or (iii) by the rate and processivity of the elongation cycles [63]. The *S. cerevisiae* telomerase holoenzyme core (reverse transcriptase, Est2 and RNA template, Tlc1) is complemented by two accessory factors (Est1 and Est3) that are not required for *in vitro* telomerase activity. Nevertheless, mutations in any of the *Ever Shorter Telomeres* (*EST*) or the *TLC1* genes lead to progressive telomere shortening [51, 63, 68]. Hence, Est1 and Est3 are necessary for *in vivo* telomerase function [53].

Depending on the cell cycle, two different recruitment pathways exit for telomerase in *S. cerevisiae* [69]. The initial interaction of Est1 with Cdc13 is essential to the recruitment of telomerase during S phase [51, 63, 68]. "Cdc13 is a single-stranded DNA binding protein with a preference for the G-rich strand of yeast telomeric DNA" [63, 70]. It is bound to the telomere all through the cell cycle [53, 69]. Est1 has been reported to promote telomerase activation [68, 71]. Telomerase recruitment (fig. 1.12) continues with an interaction of Est1 and Tlc1 establishing the linkage Est2-Tlc1-Est1-Cdc13-telomeric DNA [68, 72].

Nuclear localisation of telomerase is mediated by the Yku70-Yku80 heterodimer (Ku). Ku binds Tlc1 promoting nuclear import of the telomerase ribonucleoprotein in G1. Thereby, local concentration of telomerase might be increased preparing for and supporting the assembly of Cdc13 and telomerase in S phase [69]. Besides, Ku is involved in the localisation of telomeres at the nuclear envelope [63, 68]. Carl Rabl observed that telomeres localise close to the nuclear envelope on one side of the nucleus opposite of the centromeres [55]. This "Rabl" organisation has been confirmed in various species. Yeast telomeres tether in three to eight foci at the nuclear envelope [55], which is associated with chromatin silencing [55, 73]. The tethering itself is thought to protect against unwanted recombination events [55, 74].

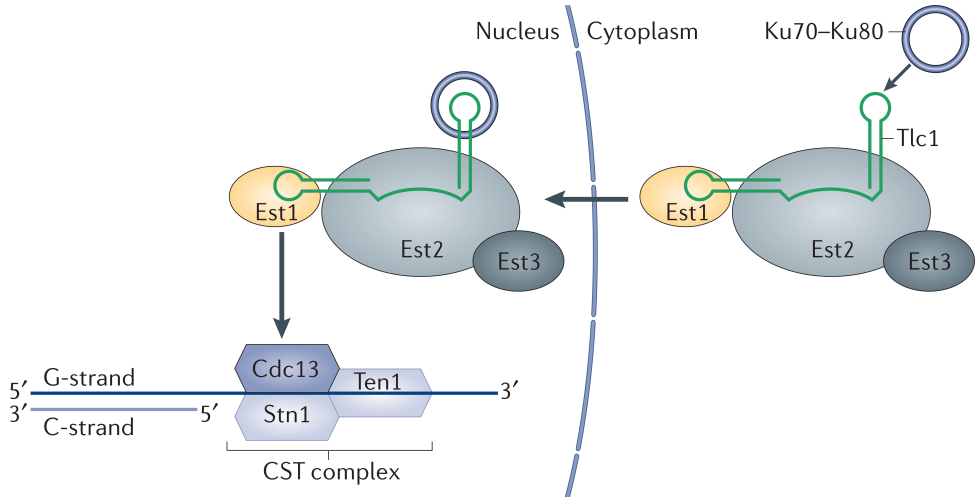

Figure 1.12.: Telomerase localisation into the nucleus is facilitated by the interaction of the Yku70-Yku80 heterodimer (Ku) with Tlc1 (telomerase inherent RNA template). Recruitment to the telomeric end is initiated by the interaction of Cdc13 and Est1 that also binds to Tlc1. The figure has been taken and adapted from Nandakumar and Cech [68].

Accompanying the recruitment of telomerase, the DNA damage checkpoint kinases Tel1 (in G1) and Mec1 (during late S phase) have been found to also associate with the telomere. Furthermore, the Mre11-Rad50-Xrs2 (MRX) complex is required for the efficient progress of Mec1, Cdc13, and Est1 recruitment [69]. According to Bianchi and Shore, Tel1 and Mec1 are necessary for telomerase activation [56].

1.3.2.3. Telomere Binding Proteins

As previously touched on, numerous proteins associate with telomeres throughout the cell cycle. In this way, telomeres become a "unique non-nucleosomal chromatin domain" [53] whose proteins are necessary for the overall telomere structure. Table 1.1 gives an overview of these proteins and their role in yeast telomere homoeostasis.

Table 1.1.: Overview of the diverse telomere binding proteins in yeast and their functions. The table has been taken and adapted from Vega et al. [53].

	Factor	Functions
Telomerase catalytic core	Tlc1 Est2	RNA template reverse transcriptase/catalytic subunit
Telomerase accessory factors	Est1, Est3	Est1 interacts with Cdc13, binds Tlc1
G-tail binding factors	Cdc13	binds ssDNA overhang, interacts with Stn1 & Ten1
dsDNA binding proteins	Rap1	binds dsDNA, telomere length regulator
Telomeric PPIs	Rif1, Rif2 Stn1, Ten1	recruited by Rap1, telomere length regulation recruited by Cdc13, G-tail protection
Others	Yku70-Yku80 Mre11-Rad50-Xrs2 Mec1, Tel1 Pif1	telomere localisation, binds to Tlc1 ATP binding, nuclease activity activation of telomerase 5'–3' helicase activity

G-Tail Protection Cdc13 is the major telomeric ssDNA binding protein. In addition to its function in telomerase recruitment and repression, it is responsible for shading the G-tail from nucleolytic degradation (together with Stn1 and Ten1) [53, 69]. Overhang capping by the Cdc13-Stn1-Ten1 (CST) complex, whose encoding genes are all essential, is critical for cell viability [69]. In the absence of Cdc13, 5'–3' resection degrades the C-strand (fig. 1.13) resulting in increased levels of ssDNA that activate a Rad9-mediated cell cycle arrest [69, 75]. In concordance with its assembly to the extended 3' overhang,

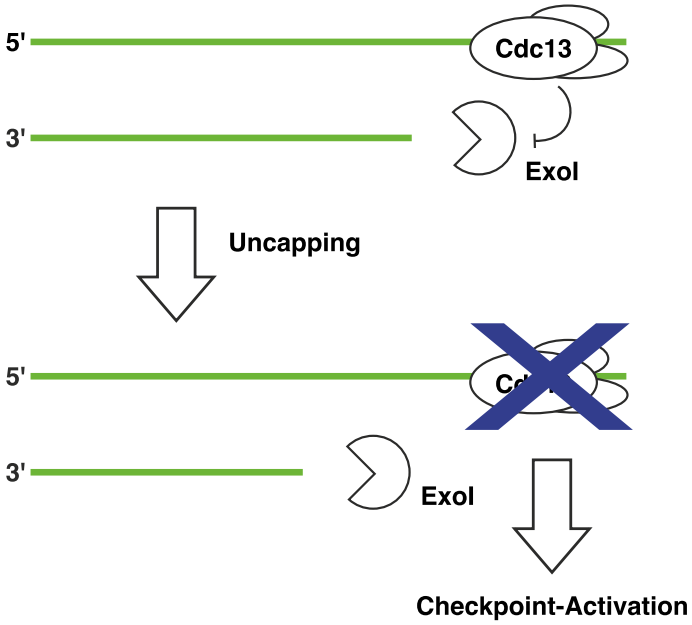

Figure 1.13.: The 3' ssDNA is capped by the Cdc13-Stn1-Ten1 complex of which Cdc13 is the key component. The CST complex prevents Exo1-mediated degradation of the 5' end by 5'–3' resection. Upon telomere uncapping the CST complex is released leading to Exo1 action and robust activation of a cell cycle checkpoint.

its levels peak during late S phase [69]. Telomerase repression limiting the telomerase-dependent telomere elongation is facilitated by Cdc13 in conjunction with its complex partners [63, 69, 76]. There is further evidence that Cdc13 might be also involved in the coordination of G- and C-strand synthesis, probably by assisting in the recruitment of DNA polymerase α [53,69].

Negative Feedback Control Telomere length is kept at a species-specific average value (see section 1.3.1). Several experiments suggest a model of negative feedback control of telomere length by a protein-counting mechanism. This model hypothesises that the number of dsDNA bound proteins correlates with telomere length regulation. In *S. cerevisiae* the main actor of this *cis* inhibition of telomerase is thought to be Rap1 that specifically binds to the telomeric dsDNA repeats [53, 56, 63, 69]. Approximately 10–20 Rap1 molecules bind to each telomere [53]. Via its C-terminus, Rap1 recruits Rif1 and Rif2 which are both contributing to the negative feedback control and whose deletion leads to telomere lengthening. Furthermore, the silencing proteins Sir3 and Sir4 bind to the C-terminus of Rap1, too [63]. A schematic of this Rap1-Rif1-Rif2 counting model is shown in suppl. fig. B.2a. According to the present doctrine, this protein complex remodels telomeric chromatin structure during the cell cycle together with the Sir proteins, thereby restricting the telomerase access to telomeres [53]. Due to suppressed telomerase action, telomeres are exposed to replicative attrition, and shortening of their ends leads to loss of Rap1 binding sites and reactivation of telomerase. Hence, telomeres are kept in a dynamic length equilibrium [56].

One nucleus can bear telomeres having different lengths [63]. However, telomerase is not acting on every telomere in each cell cycle, but it preferentially acts on short telomeres (suppl. fig. B.2b). In contrast to only 6–8 % telomere elongation frequency at wild-type

length, telomeres shortened to 100 nt are elongated with a frequency of 50 %. Moreover, the number of nucleotides added to telomeres does not correlate with telomere length; it rather varies between a few to more than 100 nucleotides. Telomere elongation itself is not regulated in a length-dependent manner [69, 77]. Teixeira et al. have widened the protein counting model by the knowledge how telomerase is actually inhibited. Their data has suggested that telomere length homoeostasis is achieved by controlling a binary switch (fig. 1.14) [78]. The longer a telomere, the more Rap1-Rif1-Rif2 complexes are bound and the telomere

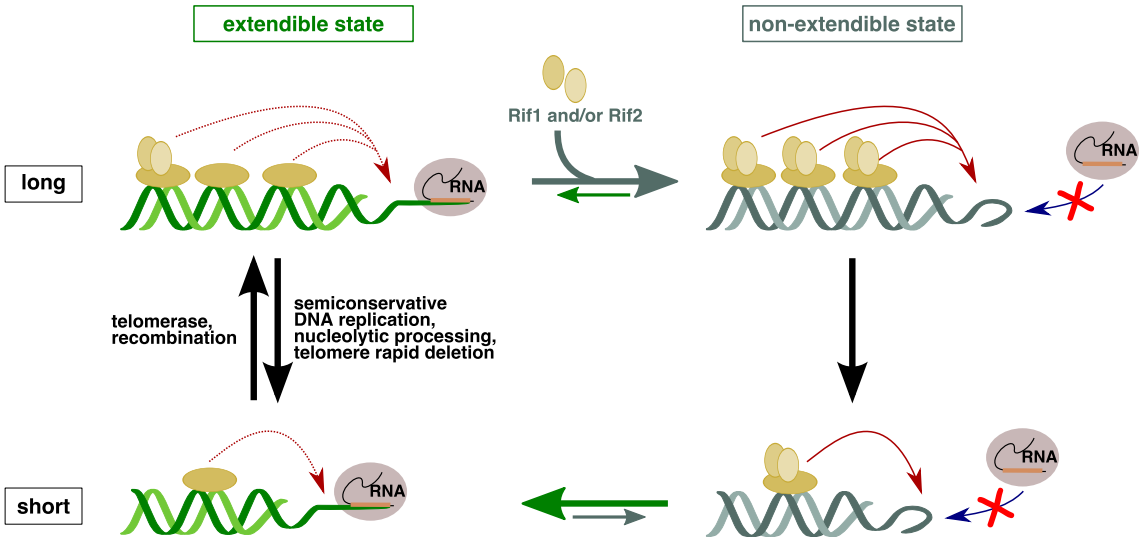

Figure 1.14.: Telomere length homoeostasis is achieved by controlling the binary switch between two states. Depending on their length, telomeres exist either in an extendible (left side) or in a non-extendible state (right side). Rif1 and Rif2 promote the non-extendible state. Hence, the number of Rap1-Rif1-Rif2 complexes determines the state of a telomere. The figure has been reproduced according to Teixeira et al. [77].

switches more likely to a non-extendible state. With decline in length, Rap1 complexes are lost and telomeres adopt an extendible state. According to the model of binary switch control, the protein complex count determines the state of a telomere. Rif1 and Rif2 have been identified as critical mediators of the binary switch as they promote the non-extendible state [69,77,78].

1.3.3. Dysfunctional Telomeres and DNA Damage Response

Genome integrity relies inter alia on cellular distinction between DSBs and telomeres, albeit both of them represent physical ends of chromosomes [53]. In addition to their shielding of chromosomal ends, telomeric binding proteins have been shown to suppress checkpoint and repair responses as well as recombination events [79]. Failure of any of these capping factors stimulates a DNA damage response [43, 79]. Wellinger has called this phenomenon an identity crisis of telomeres [80] whose outcome ranges from chromosome-chromosome fusion events to permanent cell cycle arrest and even apoptosis [43, 79]. Figure 1.15 depicts a schematic of the relationship between telomere “health” and DNA damage associated responses. In yeast already a single DSB is sufficient in causing a robust cell cycle arrest and is subjected to either homologous recombination (HR) or non-homologous end joining (NHEJ) [43]. Thus, it is quite conceivable that even a temporary deprotection of a single telomere could trigger DDR. Repair via NHEJ creates highly unstable dicentric chromosomes by fusion of two telomeres and leads to ongoing genome instability [67, 79, 81]. The incorrect recognition of telomeres as DNA damage

is associated with "a diverse number of pathologies, from cellular ageing and tumourigenesis to the genetic disease *dyskeratosis congenita*, obesity, and diabetes" [43, 82–87].

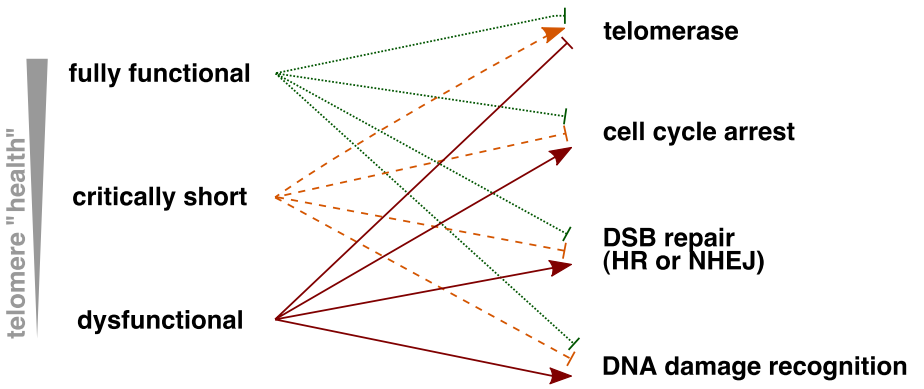

Figure 1.15.: Schematic of the relationship between telomere "health" and DNA damage associated responses. The figure has been created based on Wellinger [80] and Longhese [79].

Generally, two scenarios of telomere deprotection seem to be plausible. The CST complex could eventually become non-functional uncovering the telomeric overhang, or alternatively, the telomeric DNA erodes to such a degree that the CST complex capping function is no longer supported (lack of Cdc13 binding sites) [67, 80]. Both scenarios have been described in human cells [49, 80] and seem to be imaginable in baker's yeast, too. Due to the constitutive expression of telomerase in yeast, the second situation is usually prevented. Nonetheless it is possible to engineer a yeast strain lacking telomerase activity [80, 88, 89]. However, the cellular response to altered telomeric structure (uncapping) is generally different from eroded telomeres due to the lack of telomerase action [77].

Several DNA damage repair proteins have been found at telomeres [53, 63]. Even more, telomere maintenance relies on the presence of Tel1 and Mec1, both being DNA damage response kinases that are influenced by the Rap1 complex [63]. Replication of short telomeres and DSB-repair comprise a number of analogous steps applying the same factors, but it is less well known how these activities are actually driven to telomere elongation and away from DNA repair [80]. Subsequent to inactivation of Cdc13, the C-rich telomeric strand is degraded by 5'–3' resection resulting in drastic elongation of the ssDNA overhang and loss of viability [43, 79]. The accumulation of very long ssDNA is referred to as a hallmark of telomere dysfunction by Longhese et al. [79]. The excessive amounts of ssDNA stimulate a Mec1-dependent checkpoint activation culminating in a robust cell cycle arrest in G2 preventing anaphase entry [43, 75, 79]. Although both uncapped telomeres and DSB repair employ nuclease activities, they are distinct from each other. At DSBs the MRX complex initiates resection together with initial Sae2 nucleolytic activity preparing for extensive exonucleolytic resection by Exo1 [43]. In contrast, the MRX is suppressing resection at uncapped telomeres [43, 90]. Even though Exo1 is not essential for resection at DSBs, it is the major nuclease acting on uncapped telomeres [43, 91]. Moreover, the DNA helicase Pif1 has been shown in having a critical role in the resection of uncapped telomeres while not being involved in DSB repairs [43, 92]. Dewar and Lydall prove that Cdc13 protects telomeres from Pif1- and Exo1-mediated resection [92].

In addition to the CST, the Rap1 complex interferes with telomeric DDR. Its loss results in telomere fusion events by NHEJ [79]. Consistent with the model of telomere length homoeo-

stasis (fig. 1.14), long arrays of Rap1 bound TG tracts prevent exonucleolytic resection and activation of the Mec1-dependent DNA damage checkpoint [79,93].

1.3.4. Telomeres, Ageing and Diseases

Telomeres are essential to preserve genome integrity [52]. The gradual telomere erosion results in loss of telomeric function and triggers cells to enter a non-dividing state (replicative ageing or RA) [51,94]. Telomere-dependent RA is considered as a tumour-suppressive mechanism. In 85 % of human malignancies, telomerase expression can be detected [94,95], although most human cancer types arise from somatic tissue that is telomerase negative. Figure 1.16 outlines the relationship of telomere length and replicative ageing or rather the number of cell divisions. Reactivation and overexpression of telomerase enables tumour cells to gain almost unlimited proliferative capacity [52]. Thus, telomerase can confer cellular immortality, explaining the great medical interest in it [62]. However, telomerase activation *per se* is not sufficient to induce neoplastic transformation [63,94].

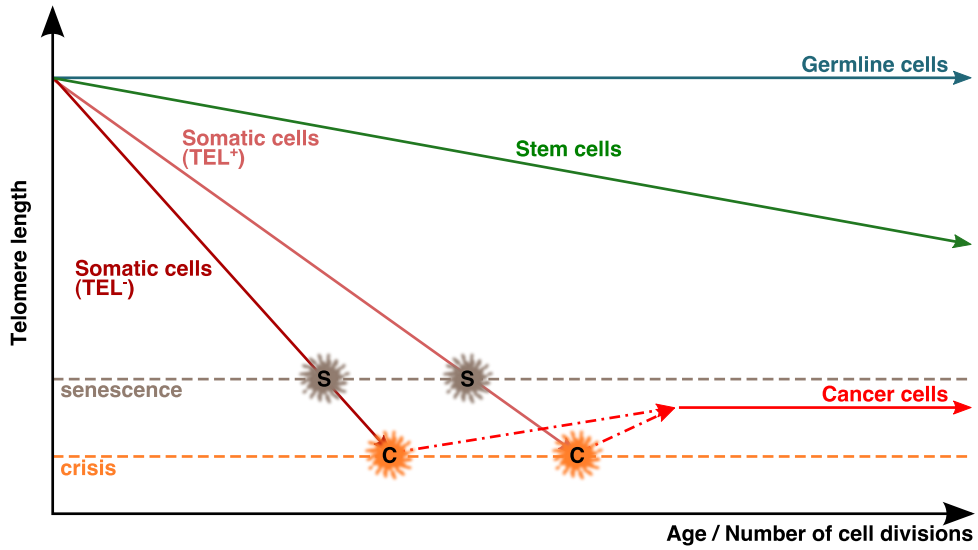

Figure 1.16.: Relationship between telomere length and cell divisions (replicative senescence). Germline immortality is achieved by robust telomerase activity leading to continuous telomere length maintenance while ageing. Somatic stem cells express telomerase, too, however to a smaller extent than germline cells. Thus, with age or increased number of cell divisions, telomeres do shorten in these cells. The majority of somatic cells is telomerase negative (TEL^-) such that telomere erosion occurs with ongoing cell divisions. Upon a critical minimal length, cells enter senescence (S), but can continue to divide if the DNA damage checkpoint is deactivated. In this way, telomere erosion continues eventually leading to crisis which is characterised by extensive genomic instability and even cell death. Cancer cells can escape this stage by either reactivation of telomerase or alternative telomere lengthening based on homologous recombination. Afterwards, telomeres are maintained at greatly reduced lengths, nevertheless enabling limitless proliferation in cancer cells. The figure has been created on the basis of Baird [94], Buseman et al. [95], and Finkel et al. [26].

Telomere loss also represents a function of age in human tissues. The accumulation of senescent cells contributes to age-related tissue deterioration and has the potential to disrupt tissue homoeostasis. The extent of telomere erosion varies greatly between tissues and correlates with the levels of cellular turnover. While it is stable in adulthood, telomere shortening mainly occurs during early and later life. Telomere length is significantly correlated with age-related diseases and life styles, i.e. short telomeres correlate with physiological stress. Upon short telomere detection in blood, mortality of heart

disease and infection is increased by 3.2-fold and 8.5-fold, respectively. The latter findings hold true for individuals with an age above 60, but is no longer significant for an age of 75 and higher. Malfunctioning telomerase is causal of several genetic disorders that are based on mutations affecting telomerase [94]. A 2-fold reduction of telomerase function results in "the failure of proliferating tissue" [62] giving rise to e.g. dyskeratosis congenita. Already a single critical short telomere is sufficient to induce cellular senescence [96].

Furthermore, proteins involved in telomere homoeostasis could have an impact on human health, as they regulate telomerase action and telomere structure. Future research dealing with the impact of defective telomere related proteins has to be undertaken [97].

With respect to the strong impact of telomerase dysfunction for human health, therapeutic approaches targeting telomerase or its regulation would be beneficial. "The ideal cancer treatment would specifically target cancer cells yet have minimal or no adverse effect on normal somatic cells" [95]. Multiple therapeutic strategies utilising telomerase as target have been devised. Telomerase inhibitors represent a potential chemotherapeutic agent against cancer (driving cancer to apoptosis) while medicinal reactivation of telomerase would have to be strictly controlled. The latter could help to cure diseases caused by accelerated telomere erosion (premature ageing syndromes) [94, 97]. Moreover, telomerase-targeted immunotherapies [95, 98, 99] as well as telomerase-driven virotherapies [95, 100, 101] have been hatched. Clinical trials are well underway examining the proposed therapies. Intermediary results emphasise the great potential of telomerase-based treatments to cure or ameliorate cancer and telomerase syndromes [95]. The different therapeutic approaches are well described and summarised by Buseman and Shay [95].

1.4. The Class E Vacuolar Protein Sorting Family

In addition to having chromosomes in a membrane enclosed nucleus, eukaryotic cells are defined by also possessing membrane-bound organelles. The endomembrane system comprises the major subcellular compartments that are dynamically interconnected either by continuous membranes or by vesicles that shuttle back and forth between the individual parts of the cell. Amongst others, the nuclear envelope, the Golgi apparatus, and the lysosome/vacuole belong to this system, which is primarily responsible for the biosynthesis, modification, packaging, and transport of proteins [102, 103]. Furthermore, it is involved in protein degradation, a fundamental mechanism of protein regulation and quality control [104]. In addition to soluble proteins, transmembrane proteins (e.g. cell surface receptors) are also subjected to control and degradation to ensure proper cell signalling and metabolism [103–105]. Proteins slated for degradation are marked by ubiquitylation. They are delivered to lysosomes (mammals) or the vacuole (yeast) [106] by multivesicular bodies (MVBs, also referred to as multivesicular endosomes) [105, 107, 108]. In yeast this process is termed the vacuolar protein sorting (VPS) pathway [108, 109]. Its implication on human health becomes apparent considering the involvement of the MVB (VPS) pathway in cell death [110], budding of retroviruses (e.g. HIV [111]), and tumour suppression [112].

Genetic and genome-wide studies in yeast have identified approximately 150 genes involved in vacuolar protein sorting, with approximately 50 % having a mammalian homologue [113]. Subsets can be distinguished, depending on the transport step at which they are required. All twenty [103] class E *VPS* genes function in MVB biogenesis [114, 115]. Deletion of any of them leads to defects in the formation of MVBs and the accumulation

of "aberrant structures adjacent to the vacuole" [105]. All members of the class E *VPS* family are highly conserved in the eukaryotic lineage as well as is their function in MVB sorting. Mammalian cells express one or more homologues for each of the class E Vps proteins [105].

1.4.1. The Endosomal Sorting Complex Required for Transport System

The class E Vps proteins form five distinct cytoplasmic complexes — the endosomal sorting complex required for transport (ESCRT) complexes 0, I, II, III, III-associated [103,106]. In endosomal sorting, most data suggest a sequential activity of the different sub-complexes to accomplish cargo-protein recognition and sorting as well as MVB formation [107,116–118]. In addition to endosomal sorting, certain ESCRT complexes are also involved in cytokinesis [106,119–121], enveloped viral budding [106,122,123], autophagy [106,124–126], and nuclear envelope reformation [127]. Figure 1.17 shows the different cellular states of ESCRT factor actions.

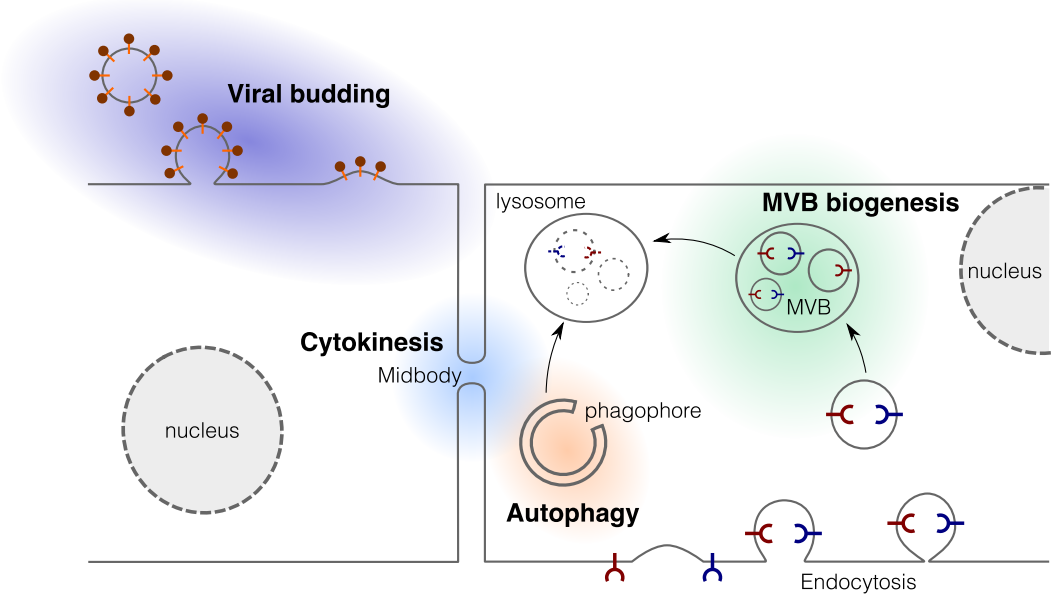

Figure 1.17.: ESCRT factors are involved in several cellular processes that rely on the same topological membrane deformation and abscission. Those processes are multivesicular body (MVB) biogenesis, cytokinesis, viral budding, and autophagy. Nuclear functions of certain ESCRT factors are not indicated. The figure has been created on the basis of Hurley and Hanson [106].

Furthermore, some Vps factors are associated with transcriptional elongation in yeast [128] and chromatin remodelling in humans [129]. Deletions of ESCRT proteins have been shown to cause defects in chromosomal segregation in humans [130] as well as in yeast [131], linking them to genomic stability and integrity.

1.4.1.1. Composition of the ESCRT Machinery

The individual sub-complexes of the ESCRT machinery are recruited one after another by the preceding complex to accomplish endosomal sorting [103]. The structural biology of the ESCRTs has been reviewed in detail by Hurley et al. [104, 132] as well

as by Williams et al. [133]. In the following sections the ESCRT system will be examined on the basis of *S. cerevisiae*. Figure 1.18 depicts the composition and molecular interactions of the ESCRT machinery and table 1.2 lists its individual components.

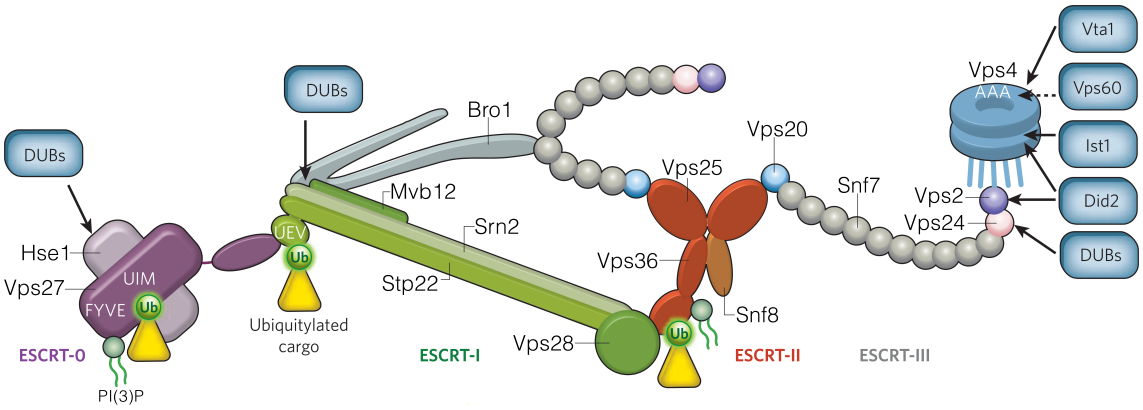

Figure 1.18.: In multivesicular body biogenesis, the individual sub-complexes of the ESCRT machinery are sequentially recruited one after another. Interactions between the individual complexes, ESCRT-III accessory factors, and ubiquitinated cargo or PI(3)P are indicated. The figure has been adapted from Raiborg and Stenmark [107]. DUB, deubiquitylating enzyme; PI(3)P, phosphatidylinositol 3-phosphate; Ub, ubiquitin; UIM, ubiquitin-interacting motif; UEV, ubiquitin E2 variant.

ESCRT-0 Initially, endosomal phosphatidylinositol 3-phosphate (PI(3)P) recruits ESCRT-0 to the endosome via the FYVE zinc-finger domain of Vps27 [134, 135]. Both ESCRT-0 subunits (Vps27 and Hse1) harbour ubiquitin-interacting motifs (UIMs) enabling the binding of ubiquitylated cargo proteins [135, 136]. The C-terminus of Vps27 serves as docking site for the ESCRT-I complex. The "Vps27 protein appears to direct the compartment-specific activation of MVB sorting, and Vps27 function is regulated by specific interactions with both PI(3)P and ubiquitinated cargo at the late endosome" [104].

ESCRT-I ESCRT-I is a heterotetramer comprising Stp22, Vps28, Srn2, and Mvb12 of which Stp22 binds to Vps27 and ubiquitin (cargo-protein). Recruitment of ESCRT-I is suppressed in absence of ESCRT-0. Vps28 interacts with Vps36, a subunit of ESCRT-II [106,107].

ESCRT-II Vps36 can also bind ubiquitinated cargo and is complemented by Snf8 and two molecules of Vps25 to form the ESCRT-II complex [106]. This complex connects the endosomal membrane and ubiquitinated cargo in combination with ESCRT-I and -III complexes [104].

ESCRT-III The ESCRT-III complex is a dynamic polymer of four core proteins (Snf7, Vps20, Did4, and Vps24) and three accessory subunits having a regulatory role. In humans the list of ESCRT-III subunits includes twelve proteins [106]. The core subunits are assembled "in a highly ordered manner" [137]. Attachment to the ESCRT-II complex is achieved by the interaction of Vps25 and Vps20. As ESCRT-II comprises two molecules of Vps25, two filaments of ESCRT-III can be nucleated. Vps20 interacts with Snf7 which assembles into filamentous oligomers capped by a Did4/Vps24 sub-complex [107, 137]. The latter recruits the ATPase Vps4 that can also interact with Snf7 and other ESCRT-III proteins indicating no strict specificity of Vps4 [104, 107].

Further ESCRT-III accessory factors are involved in the regulation of the activity and recruitment of Vps4. Those elements comprise the Ist1–Did2 and the Vta1–Vps60 subcomplexes [107]. The core subunits of ESCRT-III cycle between a "closed monomeric state in the cytosol and an open polymerised state on the endosomal membrane" [106].

Table 1.2.: The individual ESCRT subunits, associated proteins and their biological role. Alternative metazoan names are provided in brackets. The table follows Hurley and Hanson [106] as well as Raiborg and Stenmark [107]. MVB, MVB biogenesis; A, autophagy; V, viral budding; and C, cytokinesis.

Complex	Yeast	Metazoan	Biological Role			
			MVB	A	V	C
ESCRT-0	Vps27	HRS (HGS)	×	×		
	Hse1	STAM1,2	×	×		
ESCRT-I	Stp22	TSG101	×	×	×	×
	Vps28	VPS28	×	×	×	×
	Srn2	VPS37A–D	×	×	×	×
	Mvb12	MVB12A,B	×	×	×	×
ESCRT-II	Snf8	VPS22 (EAP30)	×	×		
	Vps25	VPS25 (EAP20)	×	×		
	Vps36	VPS36 (EAP45)	×	×		
ESCRT-III	Vps20	VPS20 (CHMP6)	×	×		
	Did4	VPS2A,B (CHMP2A,B)	×	×	×	×
	Vps24	VPS24 (CHMP3)	×	×	×	×
	Snf7	SNF7A–C (CHMP4A–C)	×	×	×	×
ESCRT-IIIa	Did2	DID2A,B (CHMP1A,B)	×		×	×
	Vps60	CHMP5	×			×
	Ist1	IST1	×			×
Other	Vps4	VPS4A,B	×	×	×	×
	Vta1	VTA1 (LIP5)	×	×	×	×
	Bro1	ALIX (AIP1)	×	×	×	×

1.4.1.2. Sequential Activity in MVB Biogenesis

According to the present opinion, different ESCRT complexes act sequentially in the VPS pathway and the complexes 0 to II "might function as a supercomplex" [107,118]. Raiborg and Stenmark suggest a reception of cargo proteins by ESCRT-0 that senses ubiquitin-bound cargo proteins which are then sequentially passed on to other ESCRT complexes in the numerical order (fig. 1.19a) [107]. ESCRT-I and -II induce membrane invagination and stabilise the resulting membrane bud (figs. 1.19a and 1.19b) [106,138]. Subsequently, ESCRT-III catalyses scission of the membrane neck (fig. 1.19c) [106,139]. With progressive membrane budding, the contained cargo proteins are enclosed and their ubiquitin-mark is dissolved by deubiquitylating enzymes (fig. 1.19b). Finally, Vps4 causes the disassembly of the ESCRT-III complex [103,140,141].

1.4.2. ESCRTs Beyond Multivesicular Body Formation

Certain ESCRT factors are also found at other sites of membrane deformation (fig. 1.17). Biogenesis of MVBs requires the "severing [of] thin stalks of membrane filled with cytosol" [107]. This type of membrane deformation and scission event is equivalently necessary at the midbody during cytokinesis and for budding of enveloped viruses. Such membrane fission events

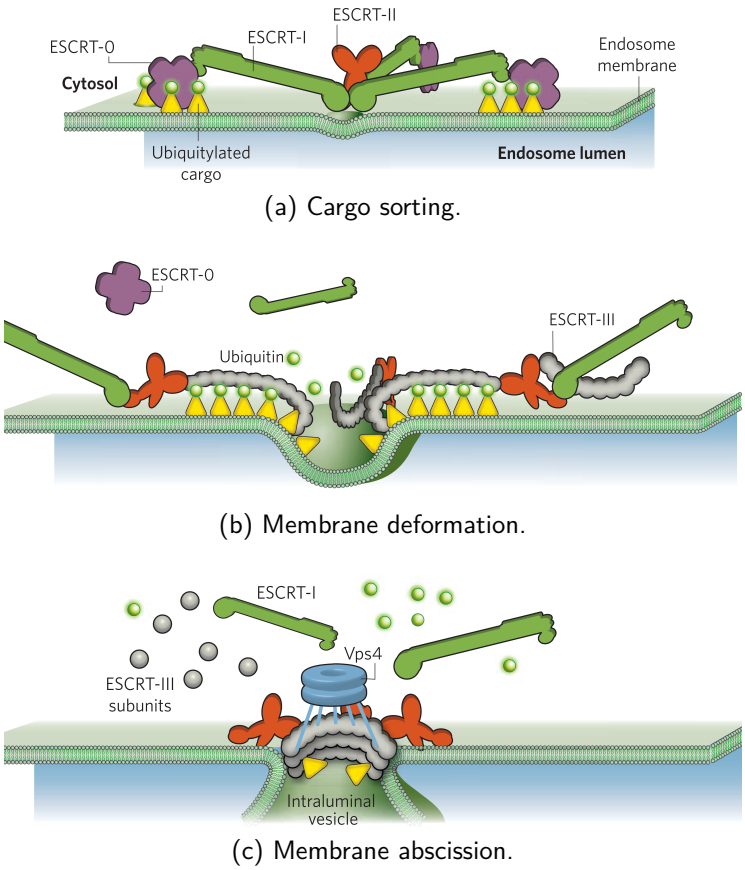

Figure 1.19.: In the MVB pathway, the ESCRT system is responsible for three major steps to fulfil endosomal sorting. (a) Recognition and sorting of ubiquitinated cargo by ESCRT-0. (b) ESCRT-I and ESCRT-II induce membrane invagination and stabilise the resulting membrane bud. (c) ESCRT-III facilitates the membrane abscission continuously assembling into circular arrays. Vps4 causes the disassembly of ESCRT-III. The figure has been adapted from Raiborg and Stenmark [107].

are catalysed by ESCRT-III and Vps4 [106,107]. Further, the ESCRT machinery is involved in autophagy [106,124–126] and several nuclear functions [127].

1.4.2.1. Cytokinesis and Viral Budding

Both mammalian cytokinesis and most enveloped viruses (e.g. HIV) utilise the ESCRT complexes I and III, as well as Vps4 and Alix (mammalian homologue of Bro1) for the final abscission event. While ESCRT-0 recruits those factors in intralumenal vesicle (ILV) budding, the centrosome/midbody protein Cep55 recruits the ESCRT core machinery to the midbody during cytokinesis, and viral structural proteins take care of this recruitment in virus budding. The actual pinch-off is mediated by ESCRT-III, whereas the exact mechanism is still unknown. The ability of Vps4 to hydrolyse ATP represents the sole energy source for this process. The assembly of ESCRT-III subunits into circular arrays is essential for membrane fission [106, 107]. Figure 1.20 outlines the just described involvement of ESCRT complexes.

1.4.2.2. Autophagy

In autophagy, cells extract building blocks from superfluous or defective cellular components such as damaged organelles, aggregated proteins, or even invading microorganisms [107]. Initially, this “rubbish” is enclosed together with cytosol in a double-membrane phagophore that matures into an autophagosome which finally fuses with a lysosome (autolysosomes) for degradation of its content [106, 107]. Autophagosomes and the phagophore closure are topologically equivalent to MVBs and the abscission of ILVs into them [106]. Multiple

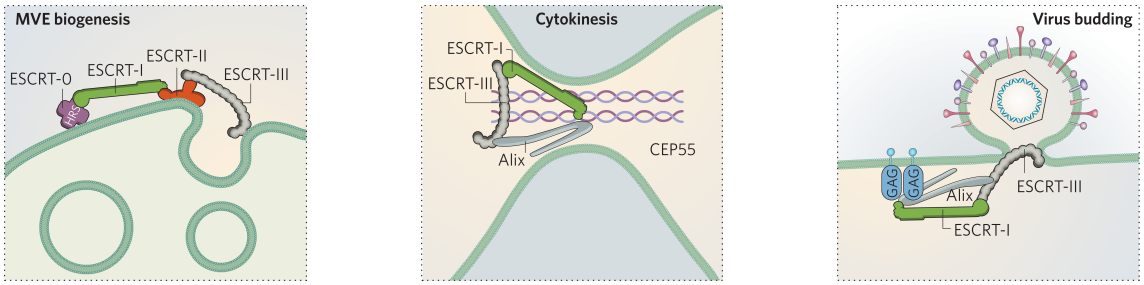

Figure 1.20.: The ESCRT machinery is involved at three topologically similar sites of membrane abscission. The actual abscission of cytosol filled membrane stalks is catalysed by ESCRT-III which is recruited differently depending on the context. In MVB biogenesis (left) recruitment is achieved by ESCRT-0–II, in cytokinesis (middle) this is done by the centrosome/midbody protein Cep55, and in virus budding (right) viral structural proteins take care of ESCRT-III recruitment. The figure has been adapted from Raiborg and Stenmark [107].

evidence show that the entire ESCRT machinery is necessary for autophagy [142], suggesting a "deeper relationship between the two pathways" [106]. On one hand, the number of autophagosomes increases in the absence of a functional ESCRT system [124, 143, 144] and autolysosomes are rare [107], and on the other hand phagophore closure is topologically equivalent to ILV scission. Raiborg and Stenmark assume that the fusion between an autophagosome and a lysosome is probably inhibited when the ESCRT machinery is inactive [107].

1.4.2.3. Nuclear Functions of Mammalian ESCRT Factors

In addition to the aforementioned roles, some ESCRT factors have acquired nuclear functions. Quite recently, Vietri and colleagues have reported the recruitment of human ESCRT-III and Vps4 to the reassembling nuclear envelope at the end of mitosis [127]. The exact mode of action remains unknown, but it seems that ESCRT-III is recruited to the intersection of the reassembly site and microtubules. Subsequent to the severing of the microtubules by spastin, ESCRT-III and VPS4 mediate "constriction and sealing of the holes in the nuclear envelope" [127]. The authors emphasise the protection of the genome through mitotic exit by ESCRT-III [127].

Most of human ESCRT-II and -III factors have been originally identified as nuclear proteins, as indicated by their naming: EAP for ELL-associated proteins (ELL is a RNA polymerase II elongation factor) and CHMP for chromatin modifying protein [145, 146]. Thus, both EAPs and CHMPs control transcription on different levels: CHMPs by modifying chromatin for gene silencing [147] and EAPs by regulating RNA polymerase activity [129]. TSG101 (ESCRT-I, mammalian homologue of Stp22) is implicated in several nuclear functions, too. Depending on the cell-cycle phase, it is translocated to the nucleus (G1 and S phase) while its expression levels are unchanged [148]. During mitosis, TSG101 colocalises with the mitotic apparatus [149] and in *Drosophila melanogaster* its inactivation leads to loss of cell polarity. TSG101 even seems to function as a transcriptional regulator of nuclear receptors that are important transcriptional regulators [150]. For all ESCRT factor mediated regulatory influences on transcription the exact mechanisms are still unknown [145,146].

1.4.3. From Cell Division to Garbage Collection

The ESCRT system is well conserved throughout all major eukaryotic taxa [133], although the different complexes have not evolved simultaneously (fig. 1.21). ESCRT-III is the most

ancient and conserved complex [107,109], whereas ESCRT-0 has been added just recently and is unique to the group of opisthokonta (animals and fungi) [109,133]. Furthermore, viability in baker's yeast does not depend on the presence of any of the ESCRT factors, however some of them are essential in mammals pointing to "potential evolutionary differences between yeast and metazoa" [109, 151, 152]. In order to achieve minimal ESCRT function, especially membrane deformation and biogenesis of intralumenal vesicles, presence of complexes III and III-a is sufficient [103, 133]. Albeit in Archaea no endocytosis system exists, Did4-like and Vps4-like family homologues have been found and were suggested to be involved in cytokinesis in Archaea, too [103,153].

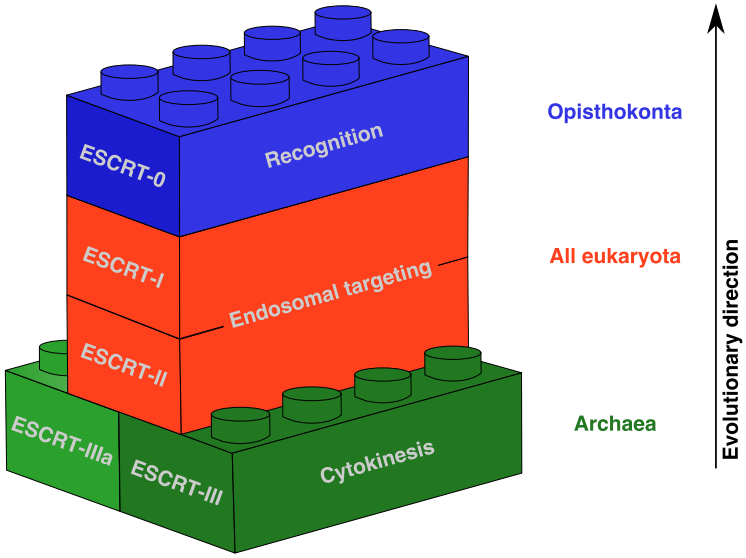

Figure 1.21.: The ESCRT system has gradually evolved, beginning at the most ancient ESCRT-III/-III-a complexes, ranging to the latest ESCRT-0 complex. Initially, the core III complexes have been only involved in cytokinesis which is also apparent from the fact that those two are sufficient for minimal ESCRT function in mammals. With ongoing evolution and development of endocytosis and MVB biogenesis, the ESCRT system has expanded and specialised. The figure has been created based on Field and Dacks [103] using building blocks from Openclipart as base [154].

The current data strongly supports ESCRT-III/-III-a as the most ancient complex originally involved in cytokinesis. As the endocytotic system evolved, ESCRT-I and -II developed and the earlier ESCRT-III system has been co-opted [103, 109]. The final addition of ESCRT-0 "may be important for increased levels of cargo selection and recognition" [103].

1.4.4. Implications of ESCRT Factors in Human Diseases

The ESCRT machinery is involved in multiple fundamental biological processes by varying degree: (i) MVB biogenesis being a part of endocytosis, (ii) final abscission at the midbody during cytokinesis, (iii) autophagy, and (iv) nuclear functions such as transcription elongation and chromatin remodelling. Furthermore, certain ESCRT factors are hijacked by some enveloped viruses to mediate their budding from host cells. Not surprisingly, disturbances of the ESCRT system is associated with several human disorders including cancer, neurodegeneration, and bacterial infections [107].

While some viruses take advantage of the ESCRT system for their spread, the ESCRT machinery "is crucial for lysosomal killing of certain intercellular bacteria and parasites" [155]. The innate immune system utilises the endocytotic and autophagic pathways to engulf and destroy invading microorganisms [107, 155]. A screen in *Drosophila melanogaster* has identified several ESCRT factors as host factors restricting mycobacterial replication. This implication has been verified in mammalian cells [156], although the exact mechanism of the ESCRT involvement is still unknown [107,155].

According to Nixon and Cataldo, protection against neurodegenerative diseases (e.g. Alzheimer's, Huntington's, or Parkinson's disease) requires accurate lysosomal functions [157].

Both, endocytosis/MVB pathway and autophagy, lead to the lysosome and are responsible for garbage collection in order to maintain cellular health. “Individuals with missense mutations in the ESCRT-III subunit VPS2B develop [...] amyotrophic lateral sclerosis and frontotemporal dementia” [107], both being characterised by the accumulation of ubiquitin-positive protein agglomerates [107, 155] as a result from impaired autophagy [124]. Recently, a mouse study has associated ESCRT proteins with an improved therapeutic potential of the immunotherapy of Parkinson’s disease and dementia [158].

Finally, ESCRT factors are implicated in cancer both with positive and negative regulatory roles [159]. On one hand, “incomplete cytokinesis can result in aneuploid cells” [155], and on the other hand defective endocytosis results in sustained receptor signalling [107]. The relevance of ESCRT factors for tumourigenesis is further underlined by their association to nuclear envelope reformation [127] and chromatin remodelling [129]. As chromosomal segregation [130] is disturbed upon deletion of ESCRT proteins, they are even more linked to genomic stability and integrity whose disruption is a hallmark of cancer.

Stuffers and Stenmark have summarised the effects of individual ESCRT factor dysfunction in cancer and other diseases [155]. Due to their role in a variety of human diseases and fundamental cellular processes, ESCRT factors represent interesting targets for diagnostic and therapeutic developments [155,159].

1.5. Systems Biology

The tremendous diversity of biological systems (fig. 1.1) and their complex, but well-defined orchestra of processes maintaining homeostasis, motivate *systems biology*, a branch of life sciences aiming at understanding “how complex systems underlie life” [21]. Doubting the hypothesis of a common origin of life is comprehensible regarding how different e.g. humans and water fleas are. However, both organisms share the same set of amino acids, nucleotides, and phospholipids. Beyond the unity in biochemistry, also the organisation on the cellular level is substantially similar between organisms [160]. Obviously, the reductionist approach to understand life’s complexity is not sufficient. Studying entire pathways or organismal processes instead of individual genes or proteins represents a paradigm shift in modern biological research [161]. Nonetheless, “before systems biology could develop fully, molecular biology had first to come to maturity on its own right” [21]. Without the knowledge how to investigate genes or exogenously express proteins, it would be impossible to characterise “gene–gene, gene–protein, or protein–protein based systems” [21]. Systems biology employs and integrates methodologies from various fields such as molecular and computational biology, mathematics, physics, and engineering [19]. Data from the multitude of genome-wide *omics* technologies are combined in an iterative procedure of model construction, testing, and refinement. The iterative interplay between hypotheses and observation is visualised in fig. 1.22. Based on experimental data or prior knowledge, either a hypothesis is derived or an existing one is refined (*induction* or top-down approach). Conversely, in a bottom-up approach (*deduction*) e.g. individual well-defined pathway models are integrated into a model for the entire system [163, 164]. While the former approach, in general, targets at the identification of new molecular mechanisms (e.g. regulatory models), the latter aims at “mechanism-based descriptions of subsystems of organisms” [164].

In the early and mid-1990s, the first pioneering large-scale studies have been carried out [161]. Due to the ease of culturing, manipulation and the profound knowledge about its genetics,

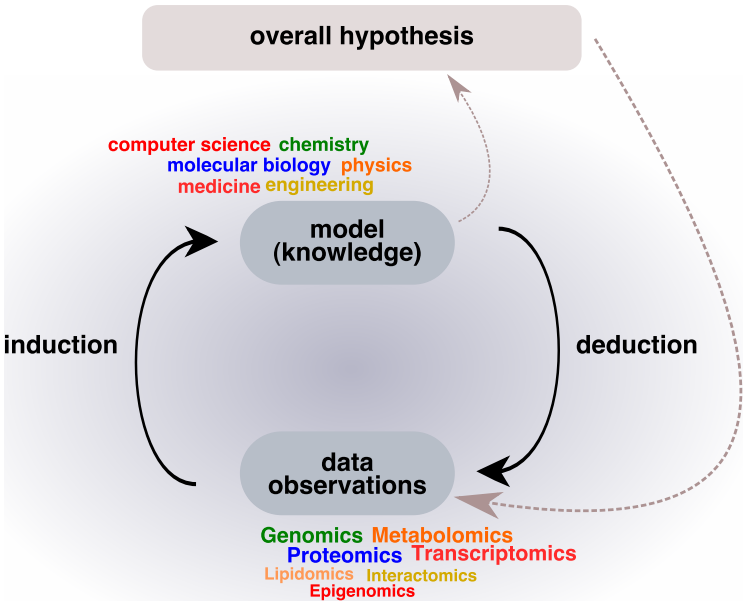

Figure 1.22.: Systems biological analyses employ an iterative procedure of elaborating hypothesis, testing and refining them. By deduction biological systems are perturbed in a specific and well-defined manner to monitor the response(s) and refine the hypothesis. The inductive approach derives a hypothesis based on prior knowledge and subsequently validates it. The outline of the schematic has been adapted from Westerhoff and Kell [162].

most of these studies have been conducted in the baker's yeast [161, 165]. According to Botstein and Fink, yeast has become the pioneer organism "that facilitated the establishment of [...] systems biology" [166].

1.5.1. Baker's Yeast as a Systems Biological Tool

Saccharomyces cerevisiae (*S. cerevisiae*) (colloquially referred to as yeast) might be the oldest domesticated organism. In addition to its usage for wine production, already Sumerian and Babylonian have used *S. cerevisiae* for beer brewing, and in old Egypt it has been used for dough leaving. That is why *S. cerevisiae* often is referred to as baker's or brewer's yeast [167]. In the mid-1930s, H. Roman has introduced it as an experimental organism [167, 168]. Although being an unicellular organism, baker's yeast bears all major characteristics of an eukaryote, e.g.: it comprises membrane-bound organelles (e.g. nucleus, mitochondria) [169]. However, as it grows on defined media, it allows complete control over environmental parameters [167]. Yeast unites a number of advantages: (i) it is remarkably inexpensive, (ii) it is readily available, (iii) it grows rapidly, (iv) it is easy to culture and store, (v) its entire genome is known, and (vi) its genome can be quite simply manipulated. Under optimal growth conditions, yeast cells divide every 90 min by budding off smaller daughter cells. *S. cerevisiae* can exist either in a stable diplophase or in a stable haplophase, wherein it can alternate between both phases (fig. 1.23). Haploid cells of the two different mating types (MATa or MATα) can mate with each other forming a/α diploids. Upon starvation, a diploid cell undergoes meiosis and sporulates resulting in so called *tetrads* — four haploid spores surrounded by the wall of the mother cell (ascus) [167, 169]. Thus, yeast cells allow studying both types of cell division: mitosis and meiosis. Yeast stocks can be stored in glycerol at $-80\,^{\circ}\mathrm{C}$ [169].

In April 1996, the genome sequencing of *S. cerevisiae* has been completed [166] by which it has become the first fully sequenced eukaryote [169]. A haploid yeast cell harbours roughly 6000 genes on a 12 Mb genomic DNA which is wrapped into 16 chromosomes that also contain centromeres and telomeres. Additionally, yeast cells have a mitochondrial genome and one plasmid [167, 169]. For about 85 % of the protein-coding genes a basic knowledge of their biological role is known [166] and approximately 17 % of them belong

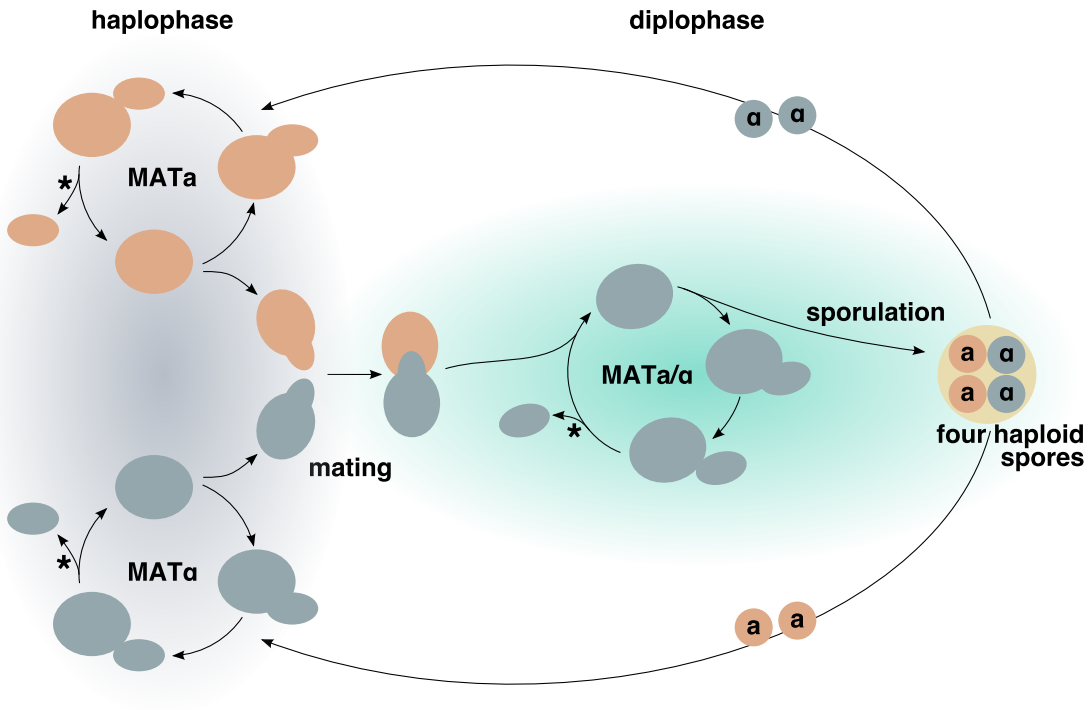

Figure 1.23.: Budding yeast's life cycle comprises haplo- and diplophases. Two haploid cells of differing mating types can mate resulting in a diploid cell. Under nitrogen-poor conditions, diploids undergo meiosis and sporulate forming four haploid spores. Those spores germinate and join the haplophase of the corresponding mating type. Both, haploid and diploid cells can proliferate through mitosis increasing the pool of the respective genotype (marked with an asterisk). MAT, mating type. The figure has been drawn on the basis of Duina et al. [169] and Masur [170].

to orthologous gene families associated with human diseases [166, 171]. The basic cellular mechanisms such as replication, recombination, cell division, and the metabolism are well conserved between yeast and mammals. The yeast genome can be easily manipulated, i.e. genes can be introduced by plasmids (*transformation*), deleted, or otherwise mutated [167].

"As *S. cerevisiae* has the most advanced selection of genetic tools available for any eukaryotic organism, perhaps even any model organism, it has served as the launch pad for landmark discoveries in gene regulation mechanisms and other cellular processes over the past several decades" [169]. Various generally available resources have been established to be exploited in small- and large-scale studies [166]. Amongst those are comprehensive mutant collections [172–176], libraries of fusions to GFP [177] or TAP [178] tags, and the *Saccharomyces* Genome Database (SGD) [10] which combines all the available data on yeast (genes) into one resource [165, 166, 169]. Only recently, the Holstege lab released a collection of genetic perturbation profiles measuring gene expression for a subset of the mutant collection under standard growth conditions [179]. A selection of the available tools is collected in table 1.3.

Such libraries allow systematic screening of all conceivable yeast mutants in order to search for mutants defective in a certain assay or under a particular condition. Heretofore, myriads of genome-wide screens searching for all kinds of phenotypes have been conducted. To name only a few, Yoshikawa and colleagues have utilised the deletion collection to find genes that affect growth under ethanol stress [180]. On a genome-scale, the Boone lab has explored the genetic interaction of yeast by examining 5.4 million gene–gene pairs for their synthetic genetic interactions [181, 182]. A consortium of Israeli researchers has explored the mutant libraries to find genes whose deletions affect telomere

length maintenance [183–185]. The screens in the mutant libraries are complemented by e.g. comprehensive analyses of protein-protein interactions in baker's yeast [186–188].

Table 1.3.: Selection of yeast genetics and bioinformatics resources has been adapted from Duina et al. [169].

Name	Access/Reference
Saccharomyces Genome Database	http://www.yeastgenome.org/ [10]
Yeast deletion project	http://www-sequence.stanford.edu/group/yeast_deletion_project/deletions3.html [172–174]
Yeast deletion collection	GE Healthcare Dharmacon Inc. [189, 190]
Yeast DAmP Collection	GE Healthcare Dharmacon Inc. [175, 191]
Yeast temperature-sensitive collection	Boone Lab [176]
Yeast GFP-tagged ORF IDs	Life Technologies GmbH [177]
Yeast TAP-tagged ORF IDs	Open Biosystems [178]
Yeast GFP Fusion Localisation DB	http://yeastgfp.yeastgenome.org/ [177, 178]
Yeast Deletome	http://deleteome.holstegelab.nl/ [179]
Yeast Search & Mining Tool	http://yeastmine.yeastgenome.org/ [192]
Yeast Genetic Interactions	http://drygin.ccbr.utoronto.ca/ [181, 182, 193]

However, *Saccharomyces cerevisiae* lacks some critical regulatory levels of higher eukaryotes, like hormone signalling and the associated receptors (e.g. nuclear receptors and their co-regulators), and due to its unicellular nature, yeast cells cannot be used for inferring data on the multicellular level. Hence, its suitability for the verification of a particular question or hypothesis has to undergo thorough consideration [194].

1.5.2. Systems Biology of Telomeres

As mentioned previously, telomeres represent vital structures to maintain genome integrity and cell viability. Imbalance in telomere homoeostasis or dysfunction of any involved protein can impinge severely on human health. Hence, there is a great interest in understanding telomere homoeostasis. *S. cerevisiae* is an excellent model organism to study telomere biology. In addition to its advantages as model organism (section 1.5.1), yeast presents all basic characteristics of mammal telomeres (section 1.3). A fine-tuned equilibrium of positive and negative regulation keeps telomeres at a steady length. The complex interplay of the two opposed mechanisms (elongation by telomerase, degradation by nucleases) and the multitude of involved factors reach out for a system-wide approach to unravel the principles underlying telomere homoeostasis.

Over the last few years, in particular a consortium of Israeli researchers have carried out multiple genome-wide screens to widen the knowledge about telomere length maintenance in baker's yeast. Initially, mutant collections have been systematically screened to identify roughly 400 mutants that affect telomere length (either shorter or longer than the wild-type length) [183–185] representing approximately 7 % of the yeast genome [165, 183]. The corresponding genes are termed *telomere length maintenance* or *TLM* genes. Protein-protein-interaction (PPI) networks have been investigated [195, 196] to find "pathways connecting *TLM* gene functions to telomere length maintenance" [165]. A third network-based approach has uncovered that the observed phenotype of a gene deletion is not necessarily caused due to the consequence of the deletion itself, but rather by the effect the deletion has on a neighbouring locus [197]. Considering those PPI analyses and correcting for the neighbouring gene effect, the overall *TLM* list has been expanded to a near-complete list of almost 500 *TLM* genes comprising almost all functions in the cell (e.g. DNA and

chromatin maintenance, RNA and protein synthesis, metabolic pathways, and mitochondrial functions) [165]. Based on this list, various studies have broaden the knowledge about those genes. Rog and colleagues have analysed the role of vacuolar protein sorting (VPS) proteins in telomere length maintenance and have revealed that their influence on telomere length depends on telomerase and the Ku complex while being independent of Tel1 and Rap1 [165,198]. The influence of environmental stimuli on telomere homoeostasis has been tested by Romano et al. They have systematically exposed *tlm* mutants to ethanol and caffeine and have observed that telomere length is either increased (ethanol) or reduced (caffeine) [165,199].

Apart from that, many other telomere related studies have been conducted. The Lydall lab has contributed immense information about the telomere capping protein Cdc13 by crossing a temperature-sensitive allele (*cdc13-1*) to the whole non-essential deletion library. A genetic interaction score has been derived describing whether the second mutant enhances or suppresses the telomere capping defect of *cdc13-1* mutants exposed to high temperature [200]. This analysis has been extended with the cross of *yku70* to the whole deletion library [201]. Visualisation of the three-dimensional conformation of yeast telomeres cannot be done as in mammals [165]. Nevertheless, the Luke laboratory has devised a genome-wide screening for finding mutants affecting the fold-back structure of yeast telomeres [202]. Finally, a genome-wide study aiming for the identification of pathways affecting telomere-initiated senescence in yeast has been performed by Chang and co-workers [203]. These briefly introduced studies represent only a small selection of the huge number of telomere related screens.

The huge efforts in the field of yeast telomere research have led to many valuable and crucial insights into telomere structure and homoeostasis. Even though many aspects of the telomere system and also the DNA damage response are highly conserved throughout the eukaryotic lineage, "some critical aspects of both [...] have changed over the course of evolution" [63]. Hence, all regulatory pathways have to be confirmed for every species separately [63]. Findings from one species can only serve as starting points in another species. This is apparent from the differences of yeast as a model organism and humans, too. Furthermore, the data from Ben-Shitrit et al. emphasises the importance of validating the identified (key) players from large-scale experiments [165,197].

1.6. Scope of this Thesis

Genomic instability is a hallmark of cancer and ageing [26]. A myriad of human syndromes, neurodegenerative diseases, immunodeficiency, and cancer are associated with defects in factors sensing and responding to DNA lesions [26–30]. Eukaryotic chromosomal ends are formed by special structural and functional units termed telomeres. Although they resemble DNA breaks [49], telomeres neither induce DNA damage repair pathways nor DNA damage checkpoint responses [50]. The proper maintenance of their homoeostasis and the distinction between DSBs and telomeres is crucial to preserve genome stability and integrity that are vital to every cell and organism.

Saccharomyces cerevisiae represents an excellent model organism to study telomere biology. In baker's yeast, telomere homoeostasis employs several endemic proteins, but also a multitude of factors involved in DNA damage response pathways to keep telomeres at a steady length. The constitutive telomerase expression in yeast resembles the telomerase activity in human proliferative tissue, germ cells [63], and tumour cells. Most of the latter reactivate telomerase to gain almost unlimited proliferative capacity [52].

Approximately 7 % of the *Saccharomyces cerevisiae* genome (roughly 400 genes) has previously been associated with telomere length maintenance. Genes whose respective deletions have been found to affect telomere length (increased shortening or lengthening) are termed telomere length maintenance (*TLM*) genes [183–185, 195, 197]. Based on these *TLM* genes, the present thesis aims at understanding the genetic regulation that affects telomere length maintenance and at suggesting novel drug targets to tackle human syndromes, diseases, and malignancies. The number of *TLM* genes and the complexity of telomere homoeostasis reach out for a system-wide exploration of those signals.

An initial analysis of the *TLM* gene list for over-represented KEGG pathways [5–7] or functional categories (MIPS FunCat; [8, 9]) has revealed a strong enrichment of genes encoding endosomal sorting complex required for transport (ESCRT) factors within the short *tlm* mutants. ESCRT factors define a system of five multi-protein complexes which are involved in deforming and scissioning cytosol filled membrane stalks. Deletion of certain ESCRT factors causes defects in chromosomal segregation in yeast [131] and in humans [130], linking them to genomic stability and integrity. As only little literature exists on the relationship of telomere homoeostasis and vacuolar sorting, a process that the ESCRT machinery is involved in, a more in-depth experimental analysis of this association has been performed. The experimental investigations of *VPS27*, which has been chosen as representative of the enriched genes, have showed that upon its deletion telomerase-dependent telomere elongation is disturbed and that it hampers Exo1-mediated resection, leading to a rescue of *cdc13-1* capping-defective telomeres. In addition to proper elongation of telomeres, their homoeostasis relies on a functional capping system, especially of the 3' ssDNA overhang. The Cdc13-Stn1-Ten1 complex shelters this overhang from Exo1-mediated resection as part of a DNA damage response that is not desirable at telomeres. Besides being the key player of this capping complex, Cdc13 is also involved in the recruitment of telomerase during telomere replication. The experimental data from the present thesis suggest that the whole ESCRT system is required for proper telomere length maintenance. Furthermore, a protein-protein-interaction network analysis has found that several protein kinases interlink Cdc13 and Vps27, possibly constituting a feedback loop to regulate telomere homoeostasis via the ESCRT system. Overall, my observations have led to a model which states that impaired Exo1-mediated resection results in too little 3' telomeric overhangs such that Cdc13 binding is suppressed, preventing either telomerase recruitment or telomeric overhang protection. Moreover, *escrt* mutants have exhibited an increased sensitivity to DSBs, indicating that defects in Exo1-mediated resection can cause improper DNA damage repair in these mutants, too.

Although ESCRT factors are essential to mammals, they could still serve as new targets to tackle telomerase reactivation and up-regulation in tumour cells. Knock-down of one or multiple ESCRT factor(s) could hyper-sensitise cancer cells to DNA damage, which would allow lowering the dosage and side effects of radio- or chemotherapy. Vps27 represents a potentially promising drug target belonging to a sub-complex of the ESCRT system whose absence seems to have less severe consequences for human cells. Neothyonidioside could be a good starting point for these investigations, as it is a compound reported to mimic the morphological defects of *VPS27* deletion [204] on Cdc13 defective cells. Nevertheless, observations made in *S. cerevisiae* generally have to be thoroughly verified when translated to humans or mammals.

2 Materials and Methods

Blues is to jazz what yeast is to bread — without it, it's flat.
(Carmen McRae, [205])

2.1. *in silico* Analyses

All *in silico* analyses were based on a list of genes that were previously associated with telomere length maintenance (*TLM* genes) [183–185, 195, 197] and performed using the R environment [206]. A *TLM* gene is defined as a gene whose corresponding yeast deletion strain has an altered telomere length — either shorter or longer than the wild-type length of 350 bp [183]. The *TLM* list contained non-essential genes from screening a haploid, homozygous yeast deletion strain collection [183, 184] and essential genes from testing the DAmP (Decreased Abundance by mRNA Pertubation) collection [185]. Telomere length was measured by analysing gDNA from different mutant strains compared to the wild-type on Southern Blots (separation of DNA fragments by electrophoresis). Figure 2.1a shows an exemplary Southern Blot for gene deletions leading to telomere shortening (short *tlm* mutants) and fig. 2.1b depicts a typical Southern Blot for long *tlm* mutants.

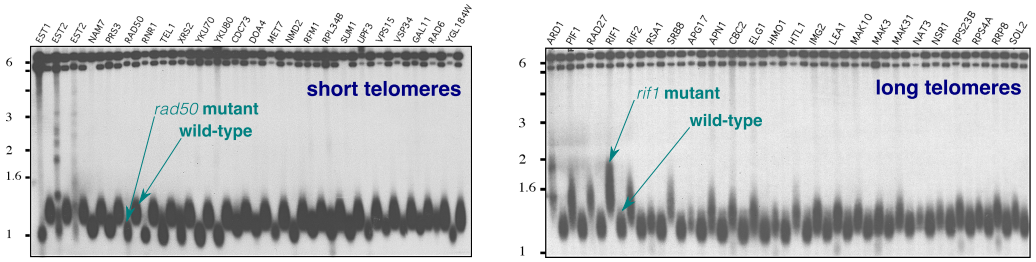

(a) Short *tlm* mutants. (b) Long *tlm* mutants.

Figure 2.1.: Exemplary Southern Blots of *tlm* mutants as used in the telomere length maintenance (TLM) screens [183–185, 195, 197]. The longer a DNA fragment, the slower it migrates through the agarose gel. Numbers on the left indicate fragment size in kbp. The blots shown here have been adapted from Gatbonton et al. [184].

The *TLM* gene list was compiled, cleaned from duplicates and identifier (ID) problems using R [206]. If required, ID mappings were done with the Bioconductor [207] package for yeast annotations (*org.Sc.sgd.db* [208]). The original categorisation of the telomere length phenotype into six classes (suppl. table C.3) was summarised into either *short* or *long*. Of the final 482 *TLM* genes, 286 referred to short *tlm* mutants and 182 to long *tlm* mutants. Thirteen *TLM* genes were not annotated with any telomere phenotype upon deletion and one genes was annotated with both phenotypes. Table 2.1 gives an overview of the composition of the *TLM* gene list.

Table 2.1.: Overview of the composition of the *TLM* gene list.

***tlm* Phenotype**	**Non-Essential**	**DAmP**
short	234	52
long	139	43
no info	13	0
short/long	1	0

As the overall list of screened genes was not tracked, I derived this list from the mutant collections themselves. To this end, I downloaded the following data: the data sheet for (i) the yeast haploid MATa knock-out strain collection (YSC1053) [189], (ii) the yeast haploid MATα knock-out strain collection (YSC1054) [190], and (iii) the yeast DAmP haploid strain collection (YSC5090) [175, 191] from Open Biosystems. Based on the union of these tables and the *TLM* list, I compiled a list of unique gene IDs representing the list of genes that were tested in the original *TLM* screens [183–185, 195, 197].

This list will be later referred to as the *TLM* universe (containing 5882 genes). Unfortunately there was no list of genes providing information whether a mutant strain showed wild-type telomere length or whether the measurement failed for it during the original screens.

As the strains from the DAmP collection behave very heterogeneously in the sense that results obtained with these strains are not always biologically reproducible, I decided to use only the non-essential *TLM* sublist. Thus, the *TLM* universe comprised the Mata and Matα collection (4990 genes). The *TLM*\DAmP universe contained only 189 short and 126 long *tlm* mutants.

2.1.1. Enrichment Analyses

In case of simple contingency table tests, the default two-side Fisher's Exact test functionality from R [206] was employed. For testing the functional association of two gene sets, I used an R [206] script written by Dr. Tobias Bauer. This script calculates the Fisher Exact test based on the default R [206] functionality for two user-defined gene sets. Multiple testing correction was done applying the false discovery rate (FDR) correction provided by R [206]. Either the KEGG pathway [5–7] annotation (*KEGG.db* package [209]) or the assignment of functional categories (FunCat v2.1) from the Munich Information Centre for Protein Sequences (MIPS) [8,9] as well as the aforementioned *TLM*\DAmP universe were used for calculating the enrichments. The MIPS FunCat data was downloaded from the MIPS website [210].

2.1.2. Protein-Protein-Interaction Network

A manually curated *Saccharomyces cerevisiae* interaction network (NW) was provided by Christine Brun. The network was compiled analogously to the human protein interaction network prepared by Chapple and colleagues [211]. The interaction network consisted exclusively of experimentally verified binary PPIs making it a highly reliable interaction source. The network contained 5592 vertices connected by 28581 edges. Christine Brun sent the network as Cytoscape session file from which I exported it as edge table to import it into the *igraph* [212] library within R [206]. All network examinations were done using the *igraph* library while network visualisation was done in Cytoscape [213].

2.1.3. Knock-Out Gene Expression Data

In April 2014, the Holstege laboratory released a genome-wide mRNA expression dataset which was measured in the corresponding haploid deletion strains of one quarter of the yeast genes (1484 deletion mutants) [179]. They selected genes having "a (putative) role in regulating gene expression" and "also included characteristics such as nuclear location or the capacity to modify other proteins" [179]. Deletions strains were classified as responsive (different from the wild-type) if "at least four transcripts showed robust changes" (fold-change or FC > 1.7 and p-value or P < 0.05) [179]. The data table for all responsive mutants was downloaded from the supplementary information (http://deleteome.holstegelab.nl/) and contained all relevant key quantities for expression data (M ratio and p-values). The M ratio (FC) was calculated for the comparison of a particular mutant versus the wild-type while the p-value described the significance of this FC. The downloaded data

table contained expression data for 700 responsive deletion strains (columns, also referred to as samples) and a total of 6112 target genes (rows). Duplicated target gene rows (11 altogether) were united by calculating the mean value per sample and target gene.

This data set was used to perform a gene set enrichment analysis (GSEA) of differentially expressed genes and to assess whether there is a change in the expression levels of telomere related protein encoding genes upon deletion of any *ESCRT* gene. Twelve of the nineteen ESCRT factor encoding genes were contained within the samples of this data (fig. 3.24). Data pre-processing and visualisation was done using R [206].

The gene set enrichment analysis for KEGG pathways [5–7] against a pre-ranked list of genes was carried out using the GSEA software (default settings) offered by the Broad Institute of MIT and Harvard [214, 215]. Initially, I ranked the target genes in descending order by the t statistic from a Student's t-Test for all *escrt* samples versus the remaining samples. In addition, I extracted the pathway annotations from the *KEGG.db* R package [206, 209] to create a gene set database. Figure 2.2 outlines the idea of this analysis.

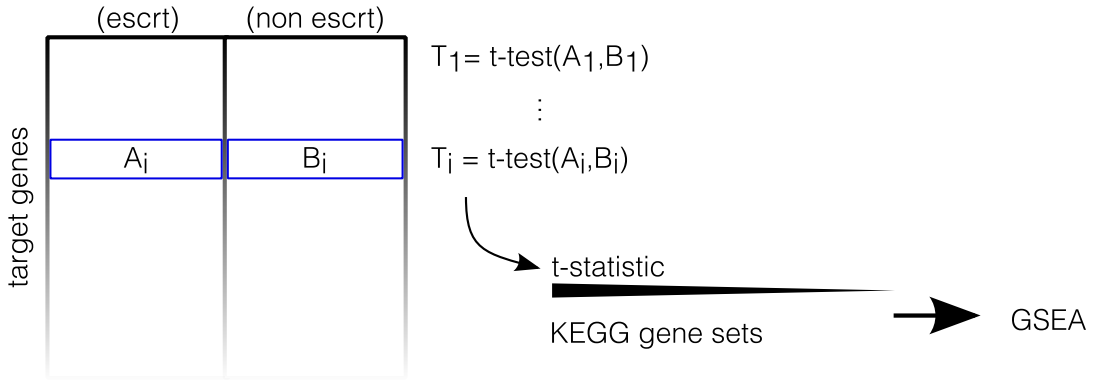

Figure 2.2.: Scheme of the GSEA run against a pre-ranked gene list to find significantly changed KEGG pathways. Student's t-Test was calculated for all *escrt* samples versus the remaining samples. Subsequently, the target genes were ranked in descending order by the t statistic.

To assess the change in expression levels of TRP encoding genes upon deletion of any *ESCRT* gene, I extracted a sub-matrix of the M values composed of *escrt* only columns and *TRP* rows. For ease of visualisation, I plotted this matrix using the *corrplot* package for R [206,216].

2.2. Experimental Analyses

All experimental analyses were performed by myself in the former laboratory of Dr. Brian Luke at the Zentrum für Molekulare Biologie (ZMBH) of the Heidelberg University.

2.2.1. Materials

Standard chemicals for usual media and solutions were ordered from AppliChem GmbH or Sigma-Aldrich Co. LLC. Source of supply of any further material is indicated in the following sections.

2.2.1.1. Yeast Strains

Most of the yeast strains used in this study were derivatives from the BY4741 background (*his3Δ1*, *leu2Δ0*, *ura3Δ0*, *met15Δ0*). Haploid strains were derived from the listed diploids. Experiment identifiers correspond to the mapping listed in suppl. table C.1.

Code	Genotype	Experiment ID
yAM223	MATa *vps27Δ::KAN*	B, O
yAM224	MATα *vps27Δ::KAN*	D
yAM225	MATa/MATα *EST2/est2Δ::HIS VPS27/vps27Δ::KAN*	H, I, K
yAM229	MATa *CDC13::cdc13-1 HIS vps27Δ::KAN*	T
yAM234	MATα *CDC13::cdc13-1 HIS vps27Δ::KAN*	E, L, M, O, P
yAM235	MATa EXO1-TAP (HIS) *vps27Δ::KAN*	X
yAM269	MATa/MATα *HSC82/hsc82Δ::KAN CDC13/CDC13::cdc13-1 HIS*	T
yAM270	MATa/MATα CDC13-TAP (HIS) *VPS27/vps27Δ::KAN*	T, U
yAM274	MATa *stp22Δ::KAN*	B
yAM275	MATa *vps28Δ::KAN*	B
yAM278	MATa *snf8Δ::KAN*	B
yAM282	MATa *snf7Δ::KAN*	B
yAM285	MATa *did2Δ::KAN*	B
yAM290	MATa *bro1Δ::KAN*	B
yAM297	MATα vps27Δ::NAT	X
yAM325	MATa/MATα SAE2-TAP (HIS) *VPS27/vps27Δ::KAN*	X
yAM326	MATa/MATα *RAD52/rad52Δ::KAN VPS27/vps27::HIS*	C
yAM329	MATa/MATα *ATG5/atg5Δ::NAT CDC13/CDC13::cdc13-1 HIS VPS27/vps27Δ::KAN*	K
yAM342	MATa *CDC13::cdc13-1 HIS exo1Δ::ura vps27Δ::KAN*	M
yAM346	MATa *exo1Δ::ura CDC13::cdc13-1 HIS*	M
yAM382	MATα EXO1-GFP (HIS)	G
yAM386	MATa/MATα *CDC13/CDC13::cdc13-1 KAN VPS27/vps27Δ::NAT* EXO1-TAP (HIS)	W
yAM387	MATa *CDC13::cdc13-1 KAN vps27Δ::NAT* EXO1-TAP (HIS)	V
yAM392	MATa *CDC13::cdc13-1 KAN vps27Δ::NAT* EXO1-GFP (HIS)	G
yAM394	MATa *CDC13::cdc13-1 KAN* EXO1-GFP (HIS)	G
yAM396	MATa *vps27Δ::NAT* EXO1-GFP (HIS)	G
yAM441	MATa/MATα *STN1/STN1::stn1-13 KAN VPS27/vps27Δ::NAT*	R
yAM443	MATa/MATα *CDC13/CDC13::cdc13-1 HIS HSE1/hse1Δ::KAN*	L
yAM444	MATa/MATα *CDC13/CDC13::cdc13-1 HIS STP22/stp22Δ::KAN*	L
yAM445	MATa/MATα *CDC13/CDC13::cdc13-1 HIS VPS28/vps28Δ::KAN*	L
yAM446	MATa/MATα *CDC13/CDC13::cdc13-1 HIS SRN2/srn2Δ::KAN*	L
yAM447	MATa/MATα *CDC13/CDC13::cdc13-1 HIS VPS4/vps4Δ::KAN*	L
yAM448	MATa/MATα *CDC13/CDC13::cdc13-1 HIS VTA1/vta1Δ::KAN*	L
yAM449	MATa/MATα *CDC13/CDC13::cdc13-1 HIS MVB12/mvb12Δ::KAN*	L
yAM450	MATa/MATα *CDC13/CDC13::cdc13-1 HIS SNF8/snf8Δ::KAN*	L
yAM451	MATa/MATα *CDC13/CDC13::cdc13-1 HIS VPS25/vps25Δ::KAN*	L

Continued on next page.

Continued from previous page.

Code	Genotype	Experiment
yAM452	MATa/MATα *CDC13/CDC13::cdc13-1 HIS VPS36/vps36Δ::KAN*	L
yAM453	MATa/MATα *CDC13/CDC13::cdc13-1 HIS VPS20/vps20Δ::KAN*	L
yAM454	MATa/MATα *CDC13/CDC13::cdc13-1 HIS SNF7/snf7Δ::KAN*	L
yAM455	MATa/MATα *CDC13/CDC13::cdc13-1 HIS VPS24/vps24Δ::KAN*	L
yAM456	MATa/MATα *CDC13/CDC13::cdc13-1 HIS VPS2/vps2Δ::KAN*	L
yAM457	MATa/MATα *CDC13/CDC13::cdc13-1 HIS DID2/did2Δ::KAN*	L
yAM458	MATa/MATα *CDC13/CDC13::cdc13-1 HIS VPS60/vps60Δ::KAN*	L
yAM459	MATa/MATα *CDC13/CDC13::cdc13-1 HIS IST1/ist1Δ::KAN*	L
yAM460	MATa/MATα *CDC13/CDC13::cdc13-1 HIS BRO1/bro1Δ::KAN*	L
yAM461	MATa/MATα *SAE2/sae2::HIS STN1/STN1::stn1-13 KAN VPS27/vps27Δ::NAT*	Q
yAM544	MATa/MATα *CDC13/CDC13::cdc13-1 HIS RAD53/RAD53::rad53-11 URA VPS27/vps27Δ::KAN*	N
yAM552	MATa/MATα *ARC15/ARC15::arc15-0 KAN VPS27/vps27Δ::NAT*	S
yAM556	MATa/MATα *ARP7/ARP7::arp7-E411K KAN VPS27/vps27Δ::NAT*	S
yAM559	MATa/MATα *GFA1/GFA1::gfa1-97 KAN VPS27/vps27Δ::NAT*	S
yBL7	MATa	B, M, O, Y
yBL679	MATα	D, P
yJK162	MATa EXO1-TAP (HIS)	X
yJK199	MATα *CDC13::cdc13-1 HIS*	E, M, O, P
yJK244	MATa *CDC13::cdc13-1 KAN* EXO1-TAP (HIS)	V
ySLG60	MATα *rad9Δ::KAN*	T
ySLG70	MATα *CDC13::cdc13-1 KAN rad9Δ::KAN*	T

Yeast strains used for the DSB-repair experiments (ID A and F, suppl. table C.1) were derivatives from either JKM139 (MATa) or YKM179 (MATα) having the following background *hmlΔ::ADE1 hmrΔ::ADE1 ade1-100 leu2-3,112 lys5 trp1::hisG ade3::GAL-HO* [217].

Code	Genotype	Experiment ID
yAM433	MATa vps27::KAN	F
yAM436	MATa vps27::KAN	F
yAM437	MATa vps27::KAN	F
yBL317	MATα MATinc-URA3 ura3-52	A
yBL319	MATα ura3-52	A
yBL320	MATα	A

2.2.1.2. Plasmids

Code	Name	Genotype	Source
pBL211	empty vector	pRS425 GAL, LEU2	Matthias Peter
pSLG44	Exo1-OE	pBL211-EXO1, LEU2	Bradley Johnson

2.2.1.3. Oligonucleotides

Code	Name	Sequence	Experiment
oBL29	KAN/NAT reverse	CTGCAGCGAGGAGCCGTAAT	A, F
oBL207	telomeric repeat	CACCACACCCACACACCACACCCACA	E
oBL358	1L forward	GCGGTACCAGGGTTAGATTAGGGCTG	H, J
oBL359	oligo dG	$CGGGATCCG_{18}$	H, J, Y
oBL361	6Y' forward	TTAGGGCTATGTAGAAGTGCTG	H, J, Y
oJK73	*VPS27* forward	AGTTAGCACGCGCATATCCA	A, F
oJK74	*VPS27* reverse	AGAACAAGAGCTGGACGGTG	A, F
oJK75	*VPS27* forward	CCTGTGGTATGTTTTGAAGGGC	A, F

2.2.1.4. Yeast Media and Plates

plates (1 l)	**YPD**	**+KAN**	**+NAT**	**+HYG**
YPD Agar	65 g	65 g	65 g	65 g
dd H_2O	1 l	1 l	1 l	1 l
Autoclave: 20 min, 121 °C				
KAN (G418, 50 mg/ml; f.c. 250 µg/ml)	—	5 ml	—	—
NAT (100 mg/ml; f.c. 100 µg/ml)	—	—	1 ml	—
HYG (100 mg/ml; f.c. 300 µg/ml)	—	—	—	3 ml

liquid or plates (1 l)	**YPGal/Raf**
Bacto Pepton	20 g
Yeast extract	10 g
Raffinose x 5 H_2O (f.c. 1 %)	11.8 g
dd H_2O	900 ml
for solid medium + Agar	20 g
Autoclave: 20 min, 121 °C	
20 % Galactose (f.c. 2 %)	100 ml

plates (60 ml)	**YPD+zeocin** (f.c. 5 µg/ml)	**YPD+zeocin** (f.c. 10 µg/ml)	**YPD+zeocin** (f.c. 15 µg/ml)
YPD Agar	3.9 g	3.9 g	3.9 g
dd H_2O	60 ml	60 ml	60 ml
Autoclave: 20 min, 121 °C			
Zeocin (100 mg/ml)	3 µl	6 µl	9 µl

liquid or plates (1 l)	**SC**	**+KAN**
Yeast Synthetic Dropout Medium Supplement w/o AAs	1.92 g	1.92 g
Yeast Nitrogen Base w/o AAs	6.7 g	6.7 g
for solid medium + Agar	24 g	24 g
100x AAs	10 ml	10 ml
dd H_2O	950 ml	950 ml
Autoclave: 20 min, 121 °C		
50 % Glucose (f.c. 2 %)	40 ml	40 ml
KAN (G418) 50 mg/ml (f.c. 250 µg/ml)	—	5 ml

liquid or plates (1 l)	**SC−AA**	**+KAN**
Yeast Synthetic Dropout Medium Supplement w/o AAs	1.92 g	1.92 g
Yeast Nitrogen Base w/o AAs	6.7 g	1.7 g
Monosodium Glutamate	—	1.0 g
for solid medium + Agar	24 g	20 g
dd H_2O	960 ml	960 ml
Autoclave: 20 min, 121 °C		
50 % Glucose (f.c. 2 %)	40 ml	40 ml
KAN (G418) 50 mg/ml (f.c. 250 µg/ml)	—	5 ml

liquid or plates (1 l)	**SC−2 AA**
Yeast Synthetic Dropout Medium Supplement w/o AAs	1.92 g
Yeast Nitrogen Base w/o AAs	6.7 g
for solid medium + Agar	24 g
100x/50x first AAs	10 ml/20 ml
100x second AAs	10 ml
dd H_2O	940 ml/930 ml
Autoclave: 20 min, 121 °C	
50 % Glucose (f.c. 2 %)	40 ml

liquid or plates (1 l)	**SD**
Yeast Nitrogen Base w/o AAs	6.7 g
for solid medium + Agar	24 g
dd H_2O	960 ml
Autoclave: 20 min, 121 °C	
50 % Glucose (f.c. 2 %)	40 ml

liquid or plates (1 l)	**SGal/Raf complete**	**SGal/Raf−AA**
Yeast Synthetic Dropout Medium Supplement w/o AAs	1.92 g	1.92 g
Yeast Nitrogen Base w/o AAs	6.7 g	6.7 g
Raffinose x 5 H_2O (f.c. 1 %)	11.8 g	11.8 g
for solid medium + Agar	20 g	20 g
100x AAs	10 ml	—
dd H_2O	890 ml	900 ml
Autoclave: 20 min, 121 °C		
20 % Galactose (f.c. 2 %)	100 ml	100 ml

plates (1 l)	**Pre-Sporulation**
Standard nutrient broth	30 g
Yeast extract	10 g
Agar	20 g
dd H_2O	900 ml
Autoclave: 20 min, 121 °C	
50 % Glucose	100 ml

liquid medium (100 ml)	**Sporulation Medium**
Potassium acetate	1 g
Zinc acetate 5 mg/ml	1 ml
dd H_2O	100 ml
Autoclave: 20 min, 121 °C	

plates (5 l)	**LB ampicillin**
LB Agar	200 g
dd H_2O	5 l
Autoclave: 20 min, 121 °C	
Ampicillin	100 µg/ml

liquid medium (500 ml)	**2x YT + carb Medium**
2x YT medium	500 ml
Carbenicillin disodium salt (100 mg/ml)	500 µl

2.2.1.5. Stock Solutions and Buffers

10x TBE (1 l)	
Tris base	108 g
Boric Acid	55 g
EDTA (0.5 M, set to pH 8.0 with NaOH)	20 ml
dd H_2O	1 l
Autoclave: 20 min, 121 °C	

10x PBS (1 l)	
NaCl	80 g
KCl	2 g
Na_2HPO_4 – 7x H_2O	26.8 g
KH_2PO_4	2.4 g
Adjust to pH 7.4 with HCl	
dd H_2O	1 l
Autoclave: 20 min, 121 °C	

1x PBS + 0.1 % Tween 20 (1 l)	
10x PBS	100 ml
dd H_2O	900 ml
Tween 20	1 ml

SDS (200 ml)	**10 % SDS**	**20 % SDS**
SDS	20 g	40 g
dd H_2O (sterile)	200 ml	200 ml
Sterilise: millipore filter 0.22 µm		

Solution 1 (20 ml)	
10 M NaOH (f.c. 1.85 M)	3.7 ml
14.34 M β-mercaptoethanol (f.c. 1.09 M)	1.52 ml
dd H_2O	14.78 ml

Solution 2 (20 ml)	
100 % TCA (f.c. 50 %)	10 ml
dd H_2O	10 ml

Solution 3 (20 ml)	
100 % Acetone	20 ml

10x Running buffer (1 l)	
Tris base	30 g
Glycin	144 g
SDS	10 g
dd H_2O	1 l

1x Running buffer (1 l)	
10x running buffer	100 ml
dd H_2O	900 ml

Urea loading buffer (10 ml)	
1 M Tris-HCl (pH 6.8; f.c. 120 mM)	1.2 ml
70 % Glycerol (f.c. 5 %)	714 µl
Urea (f.c. 8 M)	4.8 g
14.3 M β-mercaptoethanol (f.c. 143 mM)	100 µl
20 % SDS (8 %)	4 ml
dd H_2O	4 ml
Add bromophenol blue to color the buffer	

0.2 M NaOH (5 ml)	
2 M NaOH	0.5 ml
dd H_2O	4.5 ml

20x SSC (1 l)	
NaCl	175.3 g
Sodium citrate	88.2 g
Adjust to pH 7.0 with HCl	
dd H_2O	1 l
Autoclave: 20 min, 110 °C	

SSC (1 l)		+ **0.1 % SDS**		
	2x	**2x**	**0.5x**	**0.2x**
20x SDS	100 ml	100 ml	25 ml	10 ml
10 % SDS	—	10 ml	10 ml	10 ml
dd H_2O	900 ml	890 ml	965 ml	980 ml

PIPES 1 M pH 6.4 (100 ml)	
PIPES (f.c. 1 M)	30.2 g
dd H_2O	100 ml
Adjust to pH 6.4 with NaOH	
Autoclave: 20 min, 121 °C	

Hybridisation solution (100 ml)	
Formamide	50 ml
20x SSC	25 ml
50x Denhardt's solution	10 ml
0.5 M EDTA	1 ml
PIPES (1 M pH 6.4)	1 ml
Yeast RNA *(heat to 65°C, filter sterilise)*	40 mg in 3 ml H_2O
10 % SDS	10 ml
Sterilise: heat to 65°C, use millipore filter 0.22 µm	

TMAC buffer (1 l)	
TMAC (f.c. 3 M)	328.8 g
1 M Tris-HCl (pH 8.0; f.c. 50 mM)	50 ml
0.5 M EDTA (pH 8.0; f.c. 0.1 mM)	200 µl
dd H_2O	950 ml

Maleic acid buffer (1 l)	
Maleic acid (f.c. 0.1 M)	11.67 g
Adjust to pH 7.5 with NaOH	
NaCl (f.c. 0.15 M)	8.76 g
dd H_2O	1 l
Autoclave: 20 min, 121°C	

10x Blocking solution (100 ml)	
Blocking solution powder	10 g
Maleic acid buffer	100 ml
Heat on thermoblock while mixing; aliquot & store at −20°C	

1x Blocking solution (40 ml)	
10x Blocking solution	4 ml
Maleic acid buffer	36 ml

5x DIG wash buffer (1 l)	
Maleic acid (f.c. 0.5 M)	58 g
Adjust to pH 7.5 with NaOH	
NaCl (f.c. 0.75 M)	43.8 g
Tween 20 (f.c. 1.5 %)	15 ml
dd H_2O	1 l
Autoclave: 20 min, 121°C	

1x DIG wash buffer (1 l)	
5x DIG wash buffer	200 ml
dd H_2O	800 ml

DIG detection buffer (1 l)	
Tris base (f.c. 0.1 M)	12.1 g
NaCl (f.c. 0.1 M)	5.8 g
dd H_2O	1 l
Adjust to pH 9.5 with HCl	
Autoclave: 20 min, 121 °C	

10x TE (4 l)	
TRIS (1 M, set to pH 7.5 with HCl; f.c. 0.1 M)	400 ml
EDTA (0.5 M, set to pH 8.0 with NaOH, autoclaved; f.c. 10 mM)	80 ml
dd H_2O	4 l
Autoclave: 20 min, 121 °C	

LiAc Mix (100 ml)	
1 M LiAc (sterile; f.c. 0.1 M)	10 ml
10x TE (sterile; f.c. 1x)	10 ml
dd H_2O (sterile)	80 ml

PEG Mix (100 ml)	
Polyethylene glycol 4000	40 g
LiAx mix (sterile)	100 ml
Autoclave: 20 min, 121 °C	

10x Telomere PCR Buffer (10 ml)	
Tris base (f.c. 670 mM)	810 mg
$(NH_4)_2SO_4$ (f.c. 160 mM)	211 mg
70 % Glycerol (f.c. 50 %)	7.1 ml
Tween-20 (f.c. 0.1 %)	10 µl
mq H_2O	2.9 ml
Adjust to pH 8.8 with 37 % HCl	*approx. 125 µl*
Store 1 ml aliquots at −20 °C	

Zeocin stock solution (100 mg/ml)
Aliquot and store at −20 °C in the dark

2.2.1.6. Other Materials

Enzyme	**Source**	**Item No.**
Exonuclease (*E. coli*)	New England Biolabs GmbH	M0293L
Phusion® HF 2x Master Mix	New England Biolabs GmbH	M0536S
Phusion® Hot Start Flex DNA Polymerase	New England Biolabs GmbH	M0535L
Proteinase K	QIAGEN GmbH	19131
Q5® HF DNA Polymerase	New England Biolabs GmbH	M0491S
Taq 2x Master Mix	New England Biolabs GmbH	M0270L
Terminal transferase	New England Biolabs GmbH	M0315L
Lyticase (zymolyase yeast lytic enzyme)	Sigma-Aldrich Co. LLC	L4025

Kit	Source
DIG Oligonucleotide 3' End Labeling Kit, 2nd generation	Roche Diagnostics GmbH
Gentra Puregene Yeast/Bact. Kit (200 ml)	QIAGEN GmbH
QIAprep® Spin Miniprep Kit	QIAGEN GmbH
QIAquick® PCR Purification Kit (250)	QIAGEN GmbH

Ladder	Source	Item No.
Broad range protein ladder	New England Biolabs GmbH	P7708L
100 bp DNA ladder	New England Biolabs GmbH	N3231L
1 kbp DNA ladder	New England Biolabs GmbH	N3232L

Primary Antibody	Source	Item No.	Host	Dilution
α-Actin	Merck Millipore, Merck KGaA	MAB1501	Mouse	1:1000
α-PAP	Sigma-Aldrich Co. LLC	P1291	Rabbit	1:3000
α-PAP	Sigma-Aldrich Co. LLC	P1291	Rabbit	1:6000
α-Pgk1	Life Technologies GmbH	22C5D8	Mouse	1:20000
α-Pgk1	Gift from Michael Knop	—	Mouse	1:25000
AP-coupled α-DIG Fab	Roche Diagnostics GmbH	11093274910	Sheep	1:5000

Secondary Antibody	Source	Item No.	with 1st	Dilution
α-mouse-HRP	Bio-Rad Laboratories GmbH	1705047	Actin	1:3000
α-mouse-HRP	Bio-Rad Laboratories GmbH	1705047	Pgk1	1:15000
α-mouse IRDye® 680RD	LI-COR Biosciences GmbH	926-68070	Pgk1 (Knop)	1:10000
α-rabbit IRDye® 800CW	LI-COR Biosciences GmbH	926-32211	PAP	1:10000

Additional Material	Source
β-mercaptoethanol	Fluka
4–15 % Mini/Midi-PROTEAN® TGX™ Precast Protein Gels	Bio-Rad Laboratories GmbH
50x Denhardt's solution	AppliChem GmbH
6x LB buffer	New England Biolabs GmbH
Agarose	AppliChem GmbH
Amersham Hybond-N+ (Dot Blot membrane)	GE Healthcare Europe GmbH
Blocking solution powder	Roche Diagnostics GmbH
Bromophenol blue indicator	Sigma-Aldrich Co. LLC
Cycloheximide (CHX)	Sigma-Aldrich Co. LLC
CPD-Star	Roche Diagnostics GmbH
Dimethyl sulfoxide (DMSO)	Sigma-Aldrich Co. LLC
dNTPs	New England Biolabs GmbH
Ethanol	Sigma-Aldrich Co. LLC
Exonuclease I Reaction Buffer	New England Biolabs GmbH
G418 (kanamycin)	AppliChem GmbH
Glycin	Sigma-Aldrich Co. LLC
NAT (nourseothricin)	WERNER BioAgents GmbH
NEBuffer 4	New England Biolabs GmbH
Ponceau S solution	Sigma-Aldrich Co. LLC
RedSafe Nucleic Staining Acid Solution	iNtRO Biotechnology
SDS	Fluka
SuperSignal™ West Pico Chemiluminescent Substrate	Thermo Firsher Scientific Inc.
TCA	Sigma-Aldrich Co. LLC
Trans-Blot® Turbo™ Mini/Midi Nitrocellulose Transfer Packs	Bio-Rad Laboratories GmbH
Tween 20	Sigma-Aldrich Co. LLC
Yeastmaker™ Carrier DNA	Clontech Laboratories Inc.
Zeocin (phleomycin D1)	Invitrogen™ Life Technologies

2.2.1.7. Electronic Devices and Software

Electronic device	Source
Astacus LifeScience (dd H_2O machine)	MembraPure GmbH
Bio-Dot Microfiltration Apparatus (dot blot)	Bio-Rad Laboratories GmbH
C1000 Touch™ Thermal Cycler	Bio-Rad Laboratories GmbH
Centrifuge 5430R	Eppendorf AG
Centrifuge 5417R	Eppendorf AG
Centrifuge Heraeus Pico 17	Thermo Fisher Scientific Inc.
Centrifuge MCF-2360	neoLab Migge Laborbedarf-Vertriebs GmbH
Dissection Microscope MSM manual	Singer Instruments
DNA Gel chambers	Feinmechanische Werkstatt, ZMBH, Heidelberg University
Hybridisation oven MS incubator	UniEquip Laborgerätebau- und Vertriebs GmbH
LAS-4000	Fujifilm Life Science
Mini-PROTEAN® Tetra Cell	Bio-Rad Laboratories GmbH
MIR-154 cooled incubator	SANYO E&E Europe BV
Multishaker (e.g.WB-wash)	neoLab Migge Laborbedarf-Vertriebs GmbH
Multitron Standard incubation shakers	Infors AG
NanoDrop 2000c	Thermo Fisher Scientific Inc.
Odyssey® Infrared Imaging System	LI-COR Biosciences GmbH
PowerPac™ Basic Power Supply	Bio-Rad Laboratories GmbH
PowerPac™ HC High-Current Power Supply	Bio-Rad Laboratories GmbH
Rotator MBT-TTR79 ("wheel")	neoLab Migge Laborbedarf-Vertriebs GmbH
Spectrophotometer Ultrospec 2100 pro	GE Healthcare Europe GmbH
Stratalinker® UV Crosslinker 2400	Stragagene
Superflake ice machine MF41	Scotsman Ice Systems
Thermoblock (item No. 2-2504)	neoLab Migge Laborbedarf-Vertriebs GmbH
Thermomixer F1.5	Eppendorf AG
Trans-Blot® Turbo™	Bio-Rad Laboratories GmbH
Vortex Mixer (7-2020)	neoLab Migge Laborbedarf-Vertriebs GmbH
Zeiss Axio Observer.Z1 microscope	Carl Zeiss AG

Software	Source
ChemDraw Professional 15 Suite (free trial)	PerkinElmer Informatics
Cytoscape (v3.2.1)	cytoscape.org [213]
DotBlotAnalyzer	image.bio.methods.free.fr/dotblot.html
Excel 2010	Microsoft Corporation
Fiji Is Just ImageJ (v1.49g)	fiji.sc
FileMaker Pro 10	FileMaker Inc.
GSEA software (v2.2.1.0)	Broad Institute of MIT & Harvard [214, 215]
GIMP (v2.8.10)	gimp.org
ImageStudio™ (v4.0)	LI-COR Biosciences GmbH
Inkscape (v0.48)	inkscape.org
JabRef (v2.10b2)	jabref.sourceforge.net
Kile (v2.1.3)	kile.sourceforge.net
LaTeX (TeXLive 2013)	tug.org/texlive
Multi Gauge (v3.2)	Fujifilm Life Science
R (v3.2.1)	r-project.org [206]
Word 2010	Microsoft

All schematic drawings and figure annotations were prepared using Inkscape.

2.2.2. Methods

The following sections give detailed information about the experimental procedures I applied in the present thesis. All procedures comply to the protocols used in the laboratory of Dr. Brian Luke and as described before [218–221]. Section 2.1 provides the details about the *in silico* analyses I performed.

2.2.2.1. Yeast Preparatory Workflow

Preceding any experiment described below, the required yeast strains had to be prepared. If a particular strain did not already exist in the laboratory-own yeast stock, it either had to be obtained from mutant collections (single mutants) or had to be established by crossing suitable haploid strains carrying the desired mutations. In case of single (non-essential) gene deletions (e.g. any *ESCRT* deletion), haploid strains can be received from e.g. the EUROSCARF BY4741 deletion strain collection [174]. Essential genes (e.g. *CDC13*) can be investigated by utilising temperature-sensitive alleles [176]. If available, required mutants were thawed in a single-colony streak-out from the corresponding −80 °C stock and incubated at appropriate temperature. The permissive temperature of temperature-sensitive strains used in this study was 23–25 °C which was used for routine incubations whereas all other strains were standard incubated at 30 °C. Unless specified otherwise, strains were grown on or in standard yeast extract peptone dextrose (YPD) complete medium.

Figure 2.3 depicts a schematic overview of the general workflow for creating a yeast mutant strain from crossing two haploid strains harbouring mutations that should be combined into one strain. This workflow will be exemplified for crossing two haploid single mutants leading to one double mutant strain. However, it is basically possible to generate mutants of any number of mutations depending on the underlying haploid strains.

Initially, two different haploid strains with distinct mating types and markers (e.g. KAN or NAT) are crossed by mixing corresponding single colonies on YPD plates. Assume the mutant $yfg\Delta^{A}::KAN$ (yfg, your favourite gene) carries the deletion of gene A and has mating type MATa while $yfg\Delta^{B}::NAT$ has mating type MATα and gene B is deleted. Crossing both strains would result in a $yfg\Delta^{A}::KAN$ $yfg\Delta^{B}::NAT$ double mutant. After incubation for at least four hours or overnight, the colony is partly streaked out for single colonies on double-selective (KAN and NAT) media to select for diploid (MATa/MATα) cells. Typically, single colonies require 2-3 days to grow to sufficient size to proceed with sporulation. Single colonies are patched on pre-sporulation medium plates overnight and the patches are partly dissolved in sporulation medium (2 ml) the next day. The cultures sporulate at 23 °C for 3–5 d. Upon sporulation yeast cells enter sexual reproduction, undergo meiosis, and form asci containing haploid ascospores (fig. 1.23). Sporulated cultures contain asci with differing numbers of spores as well as unsporulated vegetative cells [194]. To derive the desired mutant, tetrads (asci with four spores) have to be identified and each ascospore has to be relocated to a separate position on a YPD plate to allow forming isolated spore colonies. 10 µl of sporulation culture is mixed with 10 µl of Zymolyase and incubated for 10–15 min to digest the ascus wall. Subsequently, 10–15 µl of this culture is applied in one straight line to a YPD plate. Tetrads are divided by micromanipulation and dissection as described by Fred Sherman [222]. Dissection will result in a matrix of single spore colonies, in which each column contains the four ascospores of an individual ascus. Once the spore colonies have grown to sufficient size (after approximately 2 d), the dissection plate is replica plated onto different plates carrying the markers matching the used haploids. From the evaluation of

these plates (after 2–3 d of growth), the genotypes of the individual spore colonies are derived.

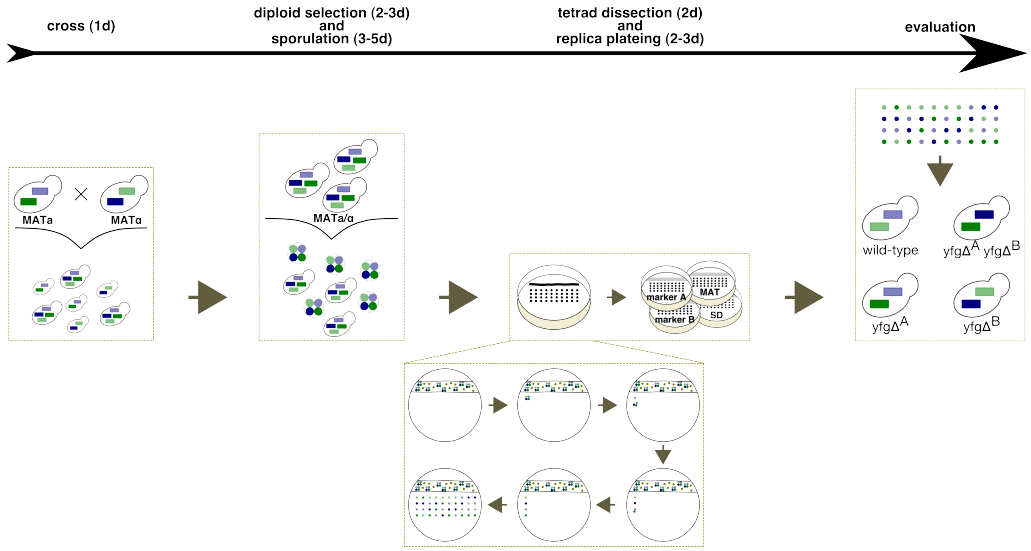

Figure 2.3.: General preparatory workflow to derive mutants from crossing haploid strains. Depicted are the four basic building blocks for deriving a new mutant. Numbers in parentheses represent the amount of incubation days required for a particular step. Initially, two haploid strains of different mating types and carrying the desired genotypes or tags that shall be combined are crossed. Diploid selection on double selective plates allows growth only for diploids which are induced to sporulate and thus undergo meiosis. The four haploid ascospores of one ascus or tetrads are divided by micromanipulation and dissection. As soon as the dissected ascospore colonies have grown to sufficient size, they are replica plated on the corresponding selective plates whose evaluation allows the genotype assignment to the individual spore colonies. The visualisation for tetrad dissection has been adapted from Sherman [194]. An enlarged version of the figure can be found in the supplement (fig. B.3).

Finally, experiments can be initiated from single colonies, spore colonies from dissection plates, or patches of those.

2.2.2.2. Transformation of Yeast

Competent Cells overnight (ON) cultures were diluted in 25 ml of appropriate medium to a final concentration (f.c.) of OD_{600} 0.15 and incubated at appropriate temperature until exponential growth phase was reached (OD_{600}=0.4 – 0.8). Cultures were pelleted at 3000 rpm for 5 min at RT, the supernatant was thrown and cells were resuspended in 5 ml of LiAc mix. Subsequent to repeated centrifugation, cultures were resuspended in 250 µl of LiAc mix (100 µl of LiAc mix per 10 ml culture) again. For the storage of competent yeast cells, aliquots of 93 µl of cell suspension and 7 µl of DMSO were frozen at −80 °C.

Transformation 100 µl of competent cell suspension (one aliquot) was used for transformation with 150 ng of plasmid or 1–2 µg of DNA or PCR product for integration. Following the addition of 10 µl of yeastmaker carrier DNA, 700 µl of PEG mix was added and cells were incubated for 30 min at RT cycling on a rotator. Cells were heat-shocked at 42 °C for 15 min and pelleted at 3000 rpm for 5 min at RT. After resuspension in 300 µl of YPD medium, cells were incubated at appropriate temperature for 30 min in case of plasmid uptake or for 3–4 h for DNA/PCR product integration. Finally, cells were spread on appropriate selective media plates using sterile glass beads and incubation was continued.

2.2.2.3. Genomic DNA Extraction

Genomic DNA was purified on ice from 2 ml of an ON culture using the Gentra Puregene Yeast/Bact. Kit from QIAGEN. All centrifugation steps were performed at 13 000 rpm and thermoblocks were used for incubation at 37 °C and 65 °C. After the addition of Lytic Enzyme Solution (step 6 of the corresponding protocol from QIAGEN), samples were incubated for 45 min instead of 30 min at 37 °C to improve cell lysis. Purified DNA samples were stored at 4 °C for few days or at −20 °C for prolonged storage.

2.2.2.4. Amplification of *vps27*::KAN Cassette

The *vps27*::KAN cassette was amplified by PCR (1.5 µl of 100 ng/µl of DNA from yAM223 and 48.5 µl of PCR master mix) while the master mix (8 reactions) contained 148 µl of mq H_2O, 200 µl of Phusion HF 2x MM, 20 µl of forward primer (oJK73), and 20 µl of reverse primer (oJK74). The PCR program was as follows: 98 °C for 30 s (initial temperature), 34 cycles of 98 °C for 10 s, 64 °C for 30 s, 72 °C for 60 s, followed by final extension at 72 °C for 10 min and holding at 12 °C. PCR product correctness was confirmed on a 1.2 % agarose gel (0.005 % Red Safe, 100 V for 35 min). The PCR product was purified using the QIAquick PCR Purification Kit from QIAGEN and stored at −20 °C.

2.2.2.5. Telomere Length Measurement – Telomere PCR

All reactions were performed using a Bio-Rad thermal cycler. 150 ng DNA in 10 µl of 1x NEBuffer (1.5 µl of 100 ng/µl DNA, 0.9 µl of NEBuffer 4, and 6.6 µl of mq H_2O) was denatured at 96 °C for 10 min and cooled down to 4 °C. For the C-tailing reaction, 1 µl of tailing mix was added and samples were incubated at 37 °C for 30 min, at 65 °C for 10 min, and at 96 °C for 5 min. Per 10 µl reaction, the tailing mix contained 0.2 µl of terminal transferase at 20 U/µl, 0.1 µl of 10x NEBuffer 4, 0.1 µl of 10 mM dCTPs, and 0.6 µl of mq H_2O. After cool-down to 65 °C, PCR-cycling was initiated by the addition of 30 µl (3x the reaction volume) of pre-heated PCR-mix. Per reaction, the PCR-mix contained 0.5 µl of Q5 HF or Phusion Hot Start DNA polymerase, 0.3 µl of oligo-dG reverse primer (oBL359), 0.3 µl of telomere-specific forward primer (6Y', oBL361 or 1L, oBL358), 4 µl of 2 mM dNTPs, 4 µl of 10x PCR buffer, 21 µl of mq H_2O. PCR-cycling: 3 min at 95 °C followed by 45 cycles of 95 °C for 30 s, 63 °C for 15 s, 68 °C for 20 s. Following additional 5 min at 68 °C, cool-down to 4 °C for holding. Samples were separated using an 1.8 % agarose gel (0.005 % Red Safe) at 100 V. Depending on the gel size, it was run for 30 min (50 ml; 6 cm × 9 cm, W×L) or for 2.5 h (150 ml; 12 cm × 14 cm, W×L). After signal detection (LAS-4000), telomere length was quantified using Multi Gauge. Fragment separation on a larger gel allowed more precise band quantification. The telomere PCR product was stored at 4 °C (short-term storage) or −20 °C (long-term storage).

2.2.2.6. Senescence Curve

Spore colonies derived from diploid dissection were dissolved in 500 µl of dd H_2O. Cultures were diluted in 5 ml of YPD medium to a f.c. of OD_{600} 0.01 and incubated at 30 °C for 24 h. Using a spectrophotometer, cell density was measured and cells were re-diluted in 5 ml of YPD medium to a f.c. of OD_{600} 0.01. Cultures were re-diluted and incubated in this way for

eight days. Every 24 h cell samples were taken, pelleted and stored at −20 °C. Population doublings (PDs) were calculated as $\log_2(OD_{600}^{24\,h}/0.01)$. All PD values base on PDs after the spore colony had grown to saturation on the dissection plate and had been diluted in water (about 25 generations).

Rate of Telomere Shortening Genomic DNA was prepared from cell pellets of the indicated days (section 2.2.2.3) and used to run telomere PCR (section 2.2.2.5) to infer the rate of telomere shortening during senescence.

2.2.2.7. Viability Spotting

Unless specified otherwise, cells were spotted onto standard YPD plates, 1:10 serially diluted in dd H_2O, and incubated at 30 °C. Initial cell concentration was OD_{600} 0.5. Images were taken after 2–3 d of growth. For testing the sensitivity to DNA damage, YPD plates containing zeocin (phleomycin D1) with f.c. of 5 µg/ml, 10 µg/ml, or 15 µg/ml were used.

UP-DOWN Assay The UP-DOWN protocol was adapted from Addinall et al. [200]. Temperature oscillation was performed in a pre-heated (23 °C) programmable Sanyo incubator. Controls were incubated at 23 °C.

2.2.2.8. Measurement of Telomeric ssDNA – Dot Blot Assay

ON cultures were diluted in 40 ml of YPD medium to a f.c. of OD_{600} 0.2 and incubated at 23 °C until exponential growth phase was reached. Culture volumes corresponding to 10 OD_{600} units were spun-down by centrifugation at 3000 rpm for 4 min (control samples). Remaining cultures were heat-shocked at 30 °C by addition of pre-warmed (44 °C) YPD medium and incubation for one hour at 30 °C. Again, culture volumes corresponding to 10 OD_{600} units were pelleted (telomere capping-defective samples). DNA was purified for all samples as described in section 2.2.2.3.

All steps involving incubation at 47.5 °C were performed in a pre-heated hybridisation oven. DNA samples were kept on ice in all steps. Per sample, 8 µg of DNA was digested by *E. coli* Exonuclease 1 (2 µl of Exo1, 5 µl of Exo1 buffer, and mq H_2O to 50 µl total volume) for 2 h at 37 °C (digested samples). Further, 1 µg of DNA was diluted in 100 µl of 0.2 M NaOH and denatured for 15 min at 65 °C (denatured samples). For native samples, 8 µg of DNA was diluted in 400 µl of 2x SSC which was also added to digested and denatured samples to a final volume of 400 µl. All samples were spotted in duplicates (190 µl each) onto a positively charged nylon membrane (GE Healthcare Amersham Hybond-N+, rinsed in 2x SSC) using a Bio-Dot Microfiltration Apparatus. The membrane was washed thrice in TMAC and once in 2x SSC (1 min per wash). Subsequent to crosslinking (Stratalinker UV Crosslinker 2400 with auto setting), the membrane was rinsed in 2x SSC and incubated in 10 ml of pre-warmed hybridisation solution for 30–60 min at 47.5 °C. Afterwards, the hybridisation solution was replaced by a DIG-labelled telomeric CA probe (oBL207, denatured for 5 min at 95 °C) diluted in 1–2 ml pre-warmed hybridisation solution. The membrane was incubated overnight rotating at 47.5 °C.

Washing solutions were pre-heated at 47.5 °C. The membrane was washed twice for 5 min in 25 ml of 2x SSC + 0.1 % SDS and twice for 20 min in 25 ml of 0.5x SSC + 0.1 %

SSC at 47.5 °C. All following steps were performed at RT. Subsequent to rinsing in 1x DIG wash buffer, the membrane was blocked for 30 min with 1x blocking solution shaking at 100 rpm and incubated afterwards with an AP-coupled α-DIG Fab antibody (1:5000 diluted in 1x blocking solution) for 30 min. The antibody was spun-down for 5 min at 3000 rpm. The subsequent membrane washing steps were: four times 1x DIG wash buffer and once DIG detection buffer for 15 min each. Finally, the membrane was put into a transparent film, CDP-star solution was pipetted directly onto the membrane and spread by letting the transparent film slide onto the membrane. The membrane was incubated in the dark for 5 min, drained (removal of CDP-star solution), and put into a new transparent film. Subsequent to further incubation in the dark for 5–10 min, the membrane was exposed to chemiluminescent light for signal detection on a LAS-4000. Signal quantification was done using the Dot Blot Analyzer tool. The amount of telomeric overhang was calculated as [(native DNA − Exo1 digested DNA)/denatured DNA].

2.2.2.9. Protein Level Measurement – Western Blot

Control and telomere capping-defective samples were prepared analogously as described in section 2.2.2.8.

Protein Extraction Culture volumes corresponding to 2.0 OD_{600} units were collected by centrifugation at 13 000 rpm for 2 min at RT. Cell pellets were resuspended in 150 µl of solution 1 and incubated on ice for 10 min. Following the addition of 150 µl of solution 2, samples were incubated on ice for 10 min. Samples were centrifuged at 13 000 rpm for 2 min at 4 °C, the cell pellets were resuspended in 1 ml of acetone and centrifuged at 13 000 rpm for 2 min at 4 °C again. Finally, the cell pellets were resuspended in 100 µl of urea buffer.

Western Blot Subsequent to incubation at 75 °C for 5 min and spin-down at 13 000 rpm, protein samples were loaded onto either a mini or a midi PROTEAN TGX TM Precast protein gel (4–15 %). The gel was run at 100 V for roughly 1.5 h and blotted onto a nitrocellulose membrane with a Trans-Blot Turbo machine (high-molecular weight program). Initially, the membrane was rinsed in Ponceau for unspecific staining, washed with dd H_2O and imaged on a LAS-4000. Then, it was blocked in blocking solution (1x PBS + 0.1 % Tween 20 containing 5 % skim milk powder) for one hour at RT shaking on a multishaker. Incubation with primary antibody diluted in blocking solution was performed at 4 °C overnight. Preceding incubation for one hour at RT with the secondary antibody (diluted in blocking solution), the membrane was washed. Washing differed depending on the type of signal detection.

Chemiluminescent-Based WB First washing steps were four times for 15 min in 1x PBS + 0.1 % Tween 20. After the secondary antibody incubation, the membrane was washed thrice for 15 min in 1x PBS + 0.1 % Tween 20 and once for 15 min in 1x PBS. Protein signals were detected using SuperSignal West Pico Chemiluminescent Substrate (mixed 1:1, membrane was kept dark) on a LAS-4000 and quantified in Fiji.

Fluorescence-Based WB Following incubation with primary or secondary antibodies, the membrane was washed four times for 15 min in 1x PBS. The membrane was always kept dark during antibody incubation or washing. Image acquisition was done on an Odyssey Infrared Imaging System (LI-COR). Bands were quantified using Image Studio.

Protein Degradation Kinetics Assay For measuring the kinetics of protein degradation, different samples of the same cultures were taken at different time points and evaluated for their content of the protein in question. ON cultures were diluted in 25 ml of YPD medium to OD_{600} 0.2, grown to OD_{600} 0.5 – 0.6 at 23 °C and control samples (denoted as "bs") were taken. Afterwards, cultures were heat-shocked by addition of pre-warmed (44 °C) YPD medium and incubation at 30 °C. One hour later, samples used as heat-shocked controls (denoted as time point zero) were taken and cycloheximide (CHX, Sigma Aldrich) was added to the cultures to a f.c. of 200 µg/ml. Incubation at 30 °C was continued. After 30, 45, 60, and 75 min of CHX-addition, further samples were taken. All samples correspond to 2.0 OD_{600} units, cells were spun-down at 3000 rpm for 5 min and cell pellets were stored at −20 °C. Protein samples were prepared and analysed with a fluorescence-based WB as described above.

2.2.2.10. Resection Kinetics Assay

DSB end resection was analysed in the laboratory of Prof. Maria Pia Longhese as described by Trovesi et al. [223]. As preparatory steps for this assay, *VPS27* was replaced in the underlying HO-cut strain by a kanamycin cassette amplified from yAM223. All incubation steps were performed at 30 °C. The HO-cut was induced by growth in or on galactose-containing medium. YPD medium or plates were autoclaved when already containing glucose which might convert partly to galactose due to the heat from the autoclave. Thus, SD-complete medium was used in all preparatory steps to avoid unintentional HO-cuts as glucose was added to it after autoclaving the medium itself. Subsequent to receipt of the basal strain from the Longhese lab, it was frozen and stored at −80 °C as yBL1018 and yBL1019, respectively.

As it was impossible to thaw these strains from −80 °C on SD-complete plates, they were thawed on YPD plates and single colonies from streak-outs on SD-complete plates were used for further processing. Competent cells were prepared from ON cultures in SD-complete medium as described in section 2.2.2.2, transformed with a *vps27*::KAN cassette amplified from yAM223 (sections 2.2.2.2 and 2.2.2.4), and spread on SD-complete + KAN plates. The integration of the *vps27*::KAN cassette was confirmed by ordinary PCR reaction using a forward primer (yJK75) upstream of *VPS27* and a reverse primer (yBL29) inside of the kanamycin cassette. DNA was extracted as usual (section 2.2.2.3). The PCR master mix (8 reactions) contained 8 µl of forward primer (oJK75), 8 µl of reverse primer (oBL29), 200 µl of Taq 2x MM, and 168 µl of mq H_2O. PCR was run with 2 µl of 100 ng/µl DNA and 48 µl of PCR master mix. The PCR program comprised 95 °C for 30 s (initial temperature), 30 cycles of 95 °C for 20 s, 52 °C for 30 s, 68 °C for 60 s, followed by final extension at 68 °C for 5 min and holding at 12 °C. PCR products were analysed on a 1.2 % agarose gel (0.005 % Red Safe, 100 V, and 35 min). Colonies with confirmed integrations were streaked out for single colonies on SD-complete and SGal/Raf-complete plates. Strains with confirmed integration and no growth on SGal/Raf-complete plates were frozen at −80 °C (yAM402, yAM403, and yAM433) and sent to the Longhese laboratory for running the desired assay.

3 Results and Discussion

Nature is inherently messy.
(Denis Noble, [18])

Approximately 7 % of the *Saccharomyces cerevisiae* genome (roughly 400 genes) have previously been associated with telomere length maintenance. Genes whose respective deletions were found to affect telomere length (increased shortening or lengthening) are termed telomere length maintenance (*TLM*) genes [183–185,195,197]. The number of *TLM* genes and the complexity of telomere homoeostasis reach out for a system-wide exploration of the signals regulating telomere length maintenance.

3.1. Functional Association of *TLM* Genes and ESCRT Factors

Initially, I tested the *TLM* gene list for enrichment of specific KEGG pathways [5–7] or functional categories (MIPS FunCat; [8,9]) to get a first impression of the contained genes and their biological functions. Due to the unreliability of the DAmP collection (section 2.1.1), only the non-essential *TLM* genes were included into these calculations (denoted as *TLM*\DAmP). Surprisingly, the top-ranking KEGG pathway for short *tlm* mutants was endocytosis with a corrected p-value of 2.612e−5 (two-sided Fisher's Exact test, table 3.1). The remaining pathways (table 3.1) represented biological functions like different DNA repair mechanisms or nucleotide biosynthesis. Those pathways were to be expected in the context of telomere maintenance.

Table 3.1.: KEGG pathways [5–7] enriched with *tlm* mutants corresponding to non-essential genes. The enrichment was calculated based on the default two-sided Fisher's Exact test within R [206]. Multiple testing correction was done with the FDR correction method.

tlm Phenotype	KEGG Pathway	P-Value	Corrected P-Value
short	Endocytosis	1.306e−5	2.612e−5
	Non-homologous end-joining	0.000 13	0.000 27
	Homologous recombination	0.001 27	0.002 53
	Purine metabolism	0.003 15	0.006 29
	Biosynthesis of secondary metabolites	0.003 59	0.007 18
	Metabolic pathways	0.007 23	0.007 23
	DNA replication	0.003 64	0.007 28
	Pyrimidine metabolism	0.022 49	0.044 98
long	Ribosome	7.123e−8	1.425e−7
	RNA transport	0.000 31	0.000 63
	Metabolic pathways	0.000 48	0.000 95
	Base excision repair	0.000 54	0.001 08
	Spliceosome	0.005 03	0.010 06
	DNA replication	0.020 06	0.020 06

Similarly, I conducted an enrichment test with the functional categories as defined by MIPS [8,9]. Among the top-ranking FunCats (suppl. table C.2), categories were found which mirror the biological functions of the top-ranking KEGG pathways (table 3.1) such as FunCats corresponding to vesicular transport. Hence, both analyses delivered coherent results.

Having found the striking and unexpected association of short *tlm* mutants and endocytosis, I took a closer look at the KEGG map for endocytosis (ID sce04144). The KEGG Mapper – Search&Color Pathway tool [224] was used to highlight the enriched *TLM* genes in the particular map (fig. 3.1). Conspicuously, the gene products of the affected genes clustered around the late endosome and almost all of them represented endosomal sorting complex required for transport (ESCRT) factors.

Nine out of nineteen ESCRT factor encoding genes were *TLM* genes. A Fisher's Exact test of this overlap revealed a p-value of 8.84e−9 (*TLM*\DAmP data). The respective contingency table is given in table 3.2. Table 3.3 lists those ESCRT factors that were contained in this overlap. Eight of them were found by the KEGG Mapper tool and were highlighted in red in fig. 3.1. *BRO1* denoted with its mammalian symbol (ALIX) was marked manually, as it was not found by this tool due to naming differences.

As described in section 1.4, ESCRT factor encoding genes belong to the larger vacuolar protein sorting (*VPS*) gene family [104]. Some of the *VPS* genes were described to be involved in

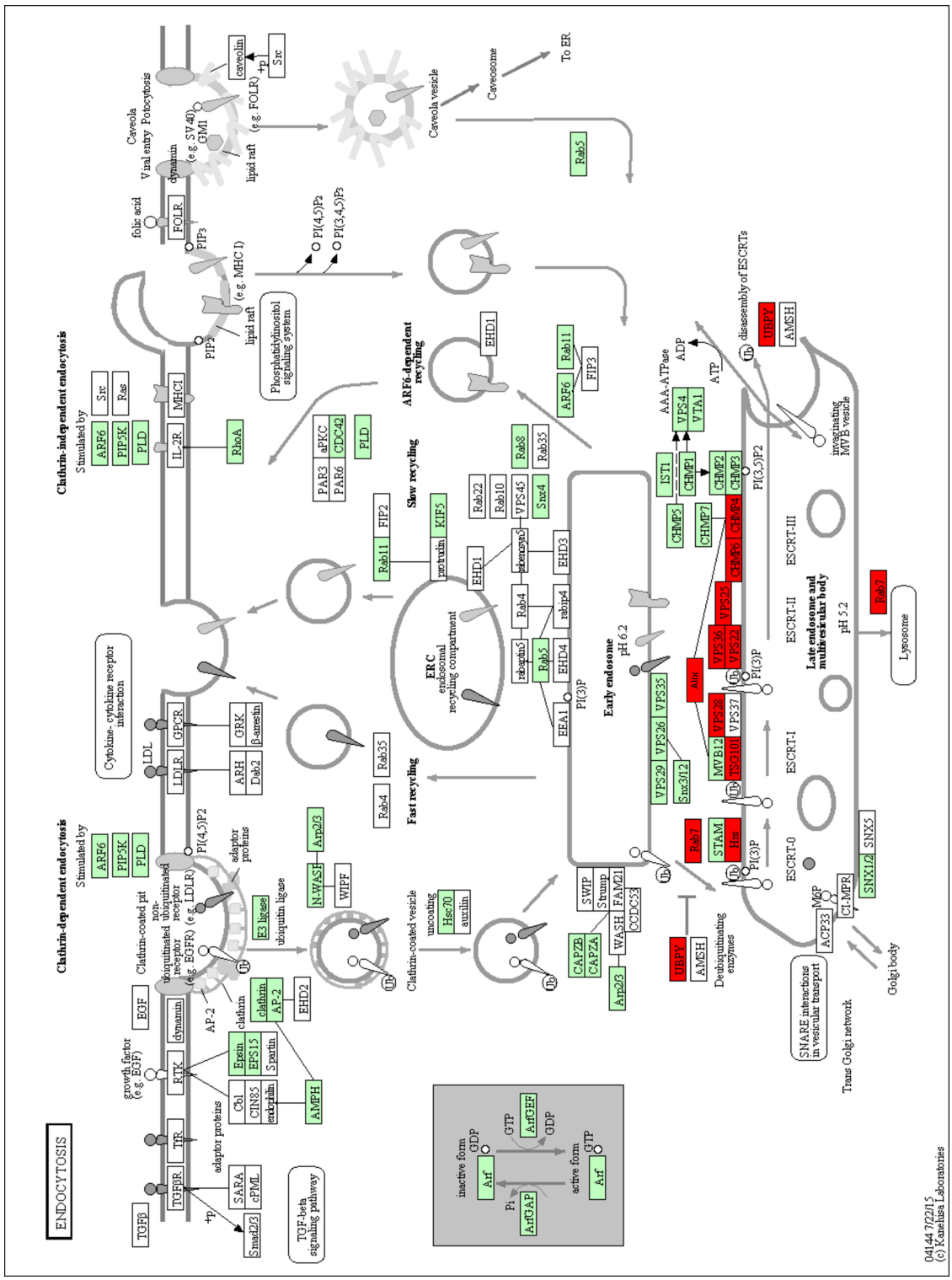

Figure 3.1.: KEGG pathway map for endocytosis (ID sce04144). Proteins were coloured using the KEGG Mapper – Search&Color Pathway tool [224]. *BRO1* (ALIX) was marked manually. Map was downloaded from the KEGG website [5–7]. Green coloured boxes represent pathway elements existing in *Saccharomyces cerevisiae* and red coloured boxed highlight short *tlm* mutants.

Table 3.2.: Contingency table of the overlap of short *tlm* mutants and *ESCRT* genes. The p-value of this overlap was 8.84e−9 (*TLM*\DAmP data).

	ESCRT	$\overline{\textbf{ESCRT}}$	
short	9	180	189
$\overline{\textbf{short}}$	10	4791	4801
	19	4971	$\sum$ 4990

Table 3.3.: List of ESCRT factors that were enriched in the *TLM*\DAmP gene set.

Yeast	**ESCRT Complex**	**Metazoan**
VPS27	0	HRS
STP22	I	TSG101
VPS28	I	VPS28
SNF8	II	EAP30
VPS25	II	EAP20
VPS36	II	EAP45
VPS20	III	CHMP6
SNF7	III	CHMP4A-C
BRO1	other	ALIX

telomere length maintenance before [198]. Amongst other genes involved in vesicular traffic, *vps* mutants exhibit shorter telomeres. Rog et al. tested a subset of these *vps* mutants to gain insights into the functional relationship between telomere homoeostasis and vacuolar sorting mechanisms. Although they found indications that the tested *VPS* genes influence telomere length regulation in a telomerase-dependent pathway, Rog and colleagues could only hypothesise about the causal link between telomere homoeostasis and vacuolar sorting mechanisms [198].

3.2. Experimental Investigations

With respect to the significant enrichment of ESCRT factors within the short *tlm* mutants and the little knowledge about the relationship of telomere homoeostasis and vacuolar sorting, I chose to perform a more in-depth experimental analysis of this association. For this, I decided for *VPS27* as representative of the enriched genes for the experimental investigations reported on in the following sections. Unless specified otherwise, I conducted all experiments myself, in the former laboratory of Dr. Brian Luke at the ZMBH of the Heidelberg University, and under his supervision.

3.2.1. Telomerase-Dependent Telomere Elongation is Disturbed in *vps27* Mutants

Initially, I tested the telomere shortening of *vps27* mutants. Telomere length was measured by telomere PCR for different telomeres (six different Y' telomeres and the 1L telomere) and for both wild-type and *vps27* cells, respectively. To ensure telomere shortening, the respective yeast strains were grown for at least 150 generations by serial restreaks on standard yeast extract peptone dextrose (YPD) medium plates and incubation at 30 °C.

A shortening effect in *vps27* cells could be reproduced for the Y'-element containing telomeres (6 Y', fig. 3.2a) as was previously shown by Shachar et al. [195]. For the X-only telomere (1L) the shortening effect was not as pronounced as for the Y' telomeres, but nonetheless still present (fig. 3.2b). Thus, observable from this test, the deletion of *VPS27* did not affect all telomeres equally. As telomere length is mainly maintained by telomerase, I explored whether telomerase is disturbed in a *VPS27* deleted background. Telomerase is a holoenzyme whose catalytic subunit is encoded by the *EST2* gene. Cells missing this gene senescence faster after a certain number of passages because the

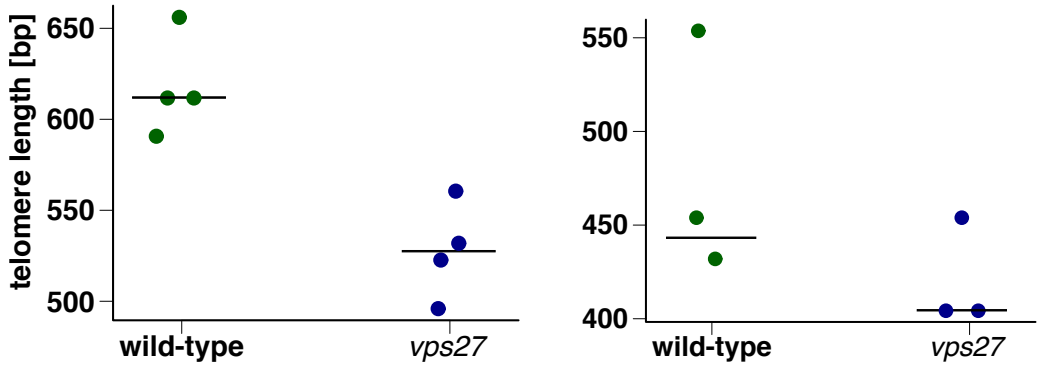

(a) 6 Y' telomeres. (b) X-only telomere.

Figure 3.2.: Telomere length was measured by telomere PCR for wild-type and *vps27* cells after growth to at least 150 generations. Length was examined for (a) six Y' telomeres and (b) the 1L telomere. Bars represent the median of the respective data points. Each data point refers to one individual telomere length measurement. Figure B.4 depicts the images of the underlying agarose gels that were quantified. As the fourth lane for the *vps27* mutant and 1L telomere showed no clear band, this lane was not quantified.

telomerase-dependent telomere elongation is malfunctioning in those cells [88]. Senescence (fig. 3.3a) and the corresponding rate of telomere shortening (fig. 3.3c) was recorded for the double mutant *est2 vps27* and compared to *est2* single mutants. The *est2 vps27* double mutants senesced equally fast as compared to the *est2* single mutants, and telomeres did shorten in both mutants with a roughly similar rate. This result is supported by data from Chang et al. who combined the deletion of *EST1*, another telomerase subunit encoding gene, with the systematic yeast deletion collection and measured senescence for the resulting *est1 yfgΔ* double mutants [203]. Deletion of *EST1* leads to the disruption of telomerase and accelerated senescence. Ten mutant strains corresponding to ESCRT factor encoding genes were included in this data. Chang et al. defined three different senescence archetypes: (i) accelerated entry into senescence (*est1 rad52* archetype), (ii) accelerated entry into and recovery from senescence (*est1 rif1* archetype), and (iii) normal senescence [203]. From the provided supplemental material, the different archetypes were extracted and compared to the average of the mean density profiles (MDPs) for the contained ESCRT factors (fig. 3.3b, dark red line). The profile of the *escrt est1* double mutants was more similar to the average of the double mutants comprising the class of accelerated senescence (fig. 3.3b, light blue line) than to those showing normal senescence (fig. 3.3b, light grey line). Hence, telomerase-dependent telomere elongation seemed corrupted in *VPS27* deleted cells and most likely this holds true for the whole ESCRT family.

3.2.2. *VPS27* Deletion Rescues *cdc13-1* Capping-Defective Telomeres

The effect of deleting *VPS27* on telomere length was mild, which is why also other possible relationships between ESCRT factors and telomere maintenance were considered. In addition to proper telomere elongation, telomere homoeostasis also relies on a functional capping system. The 3' ssDNA overhang of telomeres is protected by the Cdc13-Stn1-Ten1 (CST) capping complex from Exo1-mediated resection as part of a DNA damage response (DDR). Refer to section 1.3.2.3 and fig. 1.13 for a more detailed description. Cdc13 is the key player in this capping complex and thus the question arose whether deletion of *VPS27* affects telomere capping. *CDC13* null-mutants are not viable, but telomere uncapping can be induced with a temperature-sensitive allele of *CDC13* (*cdc13-1*) [43]. Incubation of *cdc13-1* mutants at non-permissive temperatures ($> 27\,^{\circ}\mathrm{C}$) or shifting them to these

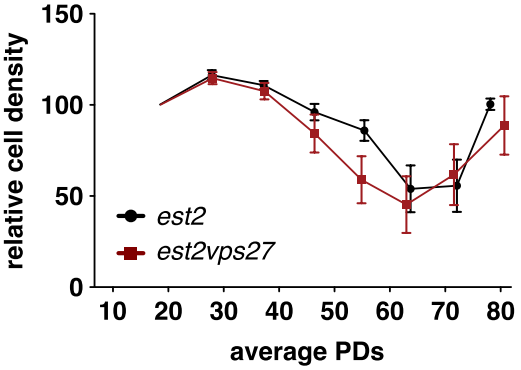

(a) Senescence curve.

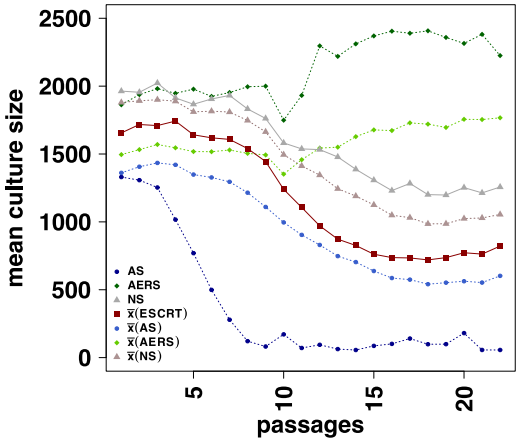

(b) Senescence archetypes.

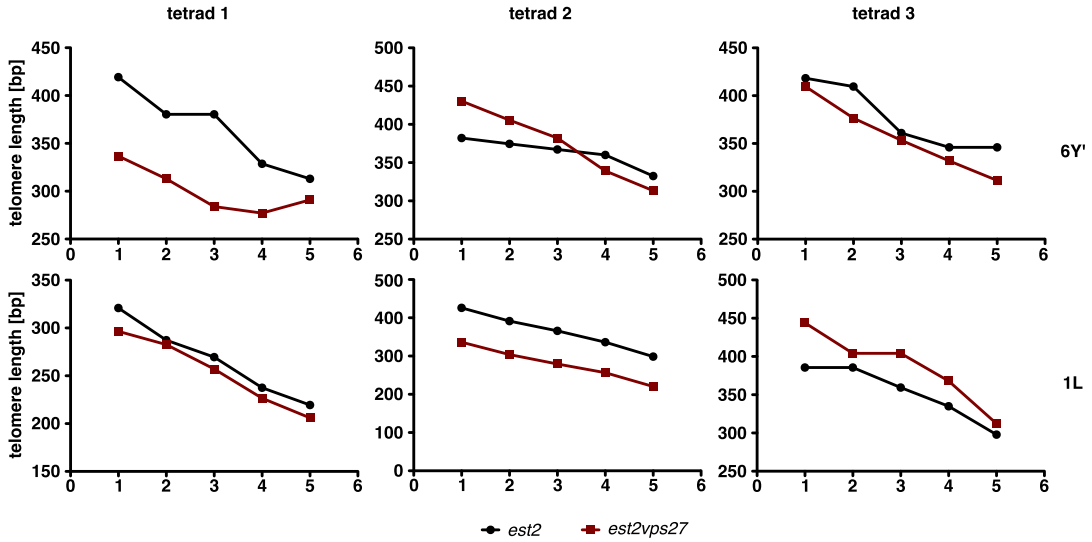

(c) Rate of telomere shortening.

Figure 3.3.: (a) Senescence curve of *est2* single and *est2 vps27* double mutants. Error bars represent the standard error of mean. At each time point six individual samples were measured per mutant type. (b) Senescence archetypes as defined by Chang et al. and reproduced from their supplemental data [203]. Represented are the different mean density profiles (MDPs) of the double mutants that define a certain archetype, as well as the average of those MDPs that belong to one archetype. The class of accelerated senescence (AS) is defined by the *est1 rad52* double mutant (depicted in dark blue), the *est1 rif1* double mutant defines the accelerated entry into and recovery from senescence (AERS, depicted in dark green) and normal senescence (NS) is depicted in dark grey. $\bar{x}$ denotes average of MDPs. (c) Telomere length was measured for samples 1–5 d of the senescence curve in (a) to derive the rate of telomere shortening. Samples referred to three individual initial spore colonies. The underlying agarose gels are represented in suppl. fig. B.5.

temperatures (heat shock) induces telomere uncapping. Subsequently, Exo1-mediated resection takes place activating a cell-cycle arrest as schematically depicted in fig. 3.4.

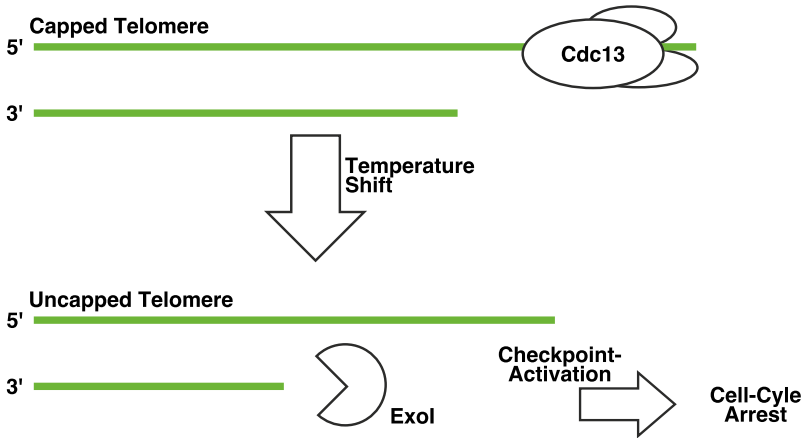

Figure 3.4.: Model of telomere uncapping upon temperature shift and subsequent Exo1-mediated resection leading to a robust cell-cycle arrest.

For investigating whether CST-mediated telomere capping is defective in *vps27* mutants, a *VPS27* deletion strain and a *cdc13-1* strain were crossed. The resulting double mutant was examined for its viability at permissive (23 °C and 25 °C) and non-permissive temperatures (27 °C and 28 °C) and compared to the wild-type as well as both single mutants (*vps27* and *cdc13-1*). As apparent from fig. 3.5, the wild-type and the *vps27* cells grew well at

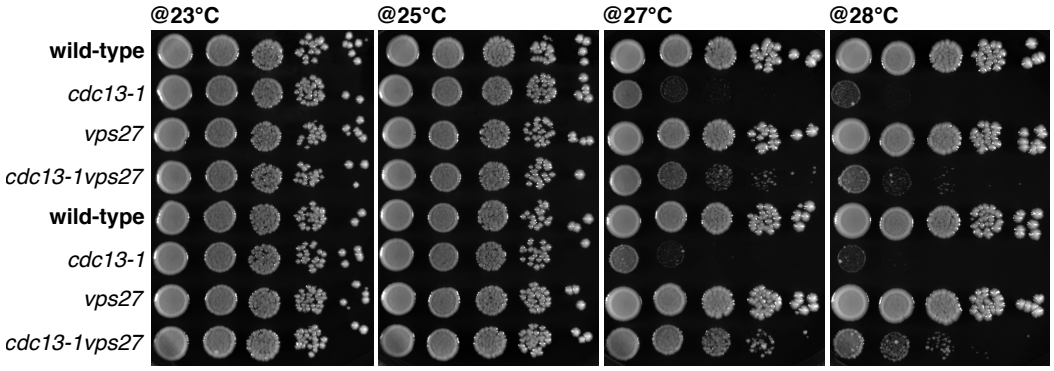

Figure 3.5.: Viability spotting assay of *cdc13-1 vps27* double mutants at permissive (23 °C and 25 °C) and non-permissive temperatures (27 °C and 28 °C). The assay was performed on normal YPD plates and cells were 10-fold serially diluted. Cells were incubated for three days. Two biological replicates were spotted.

all temperatures, while the *cdc13-1* cells grew well at 23 °C and 25 °C only, but not at higher temperatures. However, the double mutants grew at 28 °C. Hence deletion of *VPS27* increased the viability of *cdc13-1* mutants at non-permissive temperatures (rescue of temperature sensitivity). Addinall et al. found a similar suppression of temperature sensitivity of *cdc13-1* mutants by deletion of *HSE1* [200]. This finding is in concordance with the rescue result presented herein as *HSE1* encodes the ESCRT-0 complex partner of *VPS27*. These observations suggested that deletion of the ESCRT-0 complex protects cells from uncapped telomeres.

3.2.3. Exo1-Mediated Resection of Uncapped Telomeres

Uncapped telomeres are recognized as DNA double-strand breaks (DSBs), inducing 5'–3' Exo1-mediated resection and a subsequent robust cell cycle arrest [43] (fig. 3.4). Therefore, both reduced Exo1-mediated resection and defective cell cycle checkpoint activation would explain rescue of a *cdc13-1* capping-defective telomere [200].

3.2.3.1. Slightly Decreased Amounts of 3' Telomeric Overhang in *cdc13-1 vps27* Mutants

First, I explored whether deletion of *VPS27* influences Exo1-mediated resection of uncapped telomeres. Degradation of the 5' end of uncapped telomeres leads to increased amounts of telomeric single-stranded overhang (fig. 3.4). The amount of telomeric single-stranded DNA was measured by a Dot Blot assay in *cdc13-1* single and in *cdc13-1 vps27* double mutants. Genomic DNA (gDNA) samples were taken from cultures of both mutant types in exponential growth phase at 23 °C and after one hour heat shock at 30 °C (induction of telomere uncapping). Figure 3.6 describes the basic principles of this assay. Parts of the DNA samples were treated with a bacterial Exo1 (bactExo1), which is degrading 3' ssDNA. Untreated (native) and the bactExo1 digested DNA samples were spotted together with denatured DNA samples (background) onto a positively charged nylon membrane. The samples were incubated with a digoxigenin (DIG)-labelled probe that specifically binds to the telomeric repeats. The amount of telomeric overhang was than quantified with eq. (3.1) from the individual DIG signals.

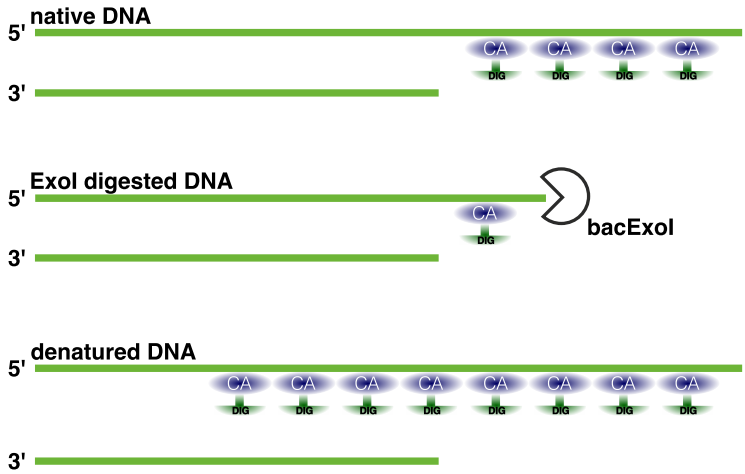

Figure 3.6.: Principles of the Dot Blot assay for measuring the amount of telomeric overhang. Parts of native, denatured and bactExo1 treated DNA samples were spotted onto a positively charged nylon membrane and incubated with a DIG-labelled probe that is specific to the telomeric repeats. The amount of telomeric overhang was quantified using eq. (3.1) from the individual DIG signals.

$$\text{telomeric overhang} = \frac{\text{native DNA} - \text{bactExoI digested DNA}}{\text{denatured DNA}} \tag{3.1}$$

An extrapolated model of the detected spot intensities is represented in fig. 3.7a and an image of the underlying membrane can be found in suppl. fig. B.6. As expected elevated levels of 3' single-stranded DNA in *cdc13-1* cells were present after heat shock treatment (fig. 3.7). Strikingly, the amount of 3' telomeric overhang was slightly decreased in the double mutants (fig. 3.7c). This finding strongly suggested that Exo1-mediated resection is not working properly in *cdc13-1 vps27* mutants.

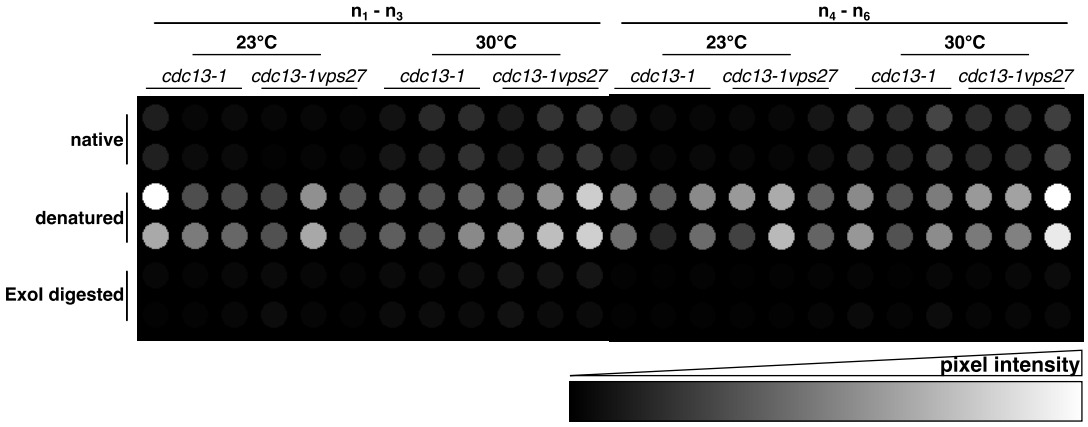

(a) Extrapolated model of spot intensities.

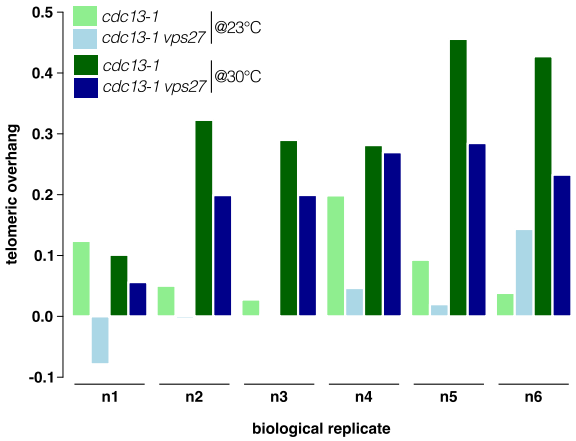

(b) Telomeric overhang per biological replicate.

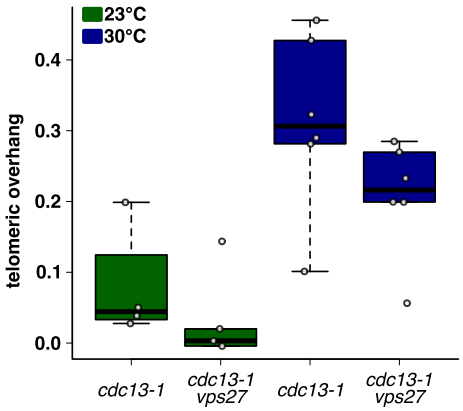

(c) Telomeric overhang per mutant and temperature.

Figure 3.7.: Dot Blot assay for quantifying the amount of 3' ssDNA at telomere ends in *cdc13-1* single and *cdc13-1 vps27* double mutants at permissive temperature and after heat shock at 30 °C. (a) Model of the Dot Blot outcome as extrapolated pixel intensities. Two technical (rows) and six biological (columns) replicates were spotted altogether. An image of the underlying membrane can be found in suppl. fig. B.6. (b) Amount of telomeric overhang plotted as barplot individually for each biological replicate. (c) Boxplot indicating the amount of telomeric ssDNA for the individual mutants before and after heat shock treatment.

3.2.3.2. Overexpression of *EXO1* Abolishes Rescue of *cdc13-1* by Deletion of *VPS27*

Having found that Exo1 is affected in *VPS27* deleted cells, I explored the consequences of Exo1 perturbation for *cdc13-1 vps27* mutants. If a corrupted Exo1 function rescues telomere uncapping, then overexpressing *EXO1* in *cdc13-1 vps27* cells should abolish the temperature rescue seen beforehand. Therefore, wild-type, *cdc13-1*, *vps27*, and *cdc13-1 vps27* cells carrying either an *EXO1* OE or the corresponding empty vector control (EV) were monitored for their viability at different temperatures.

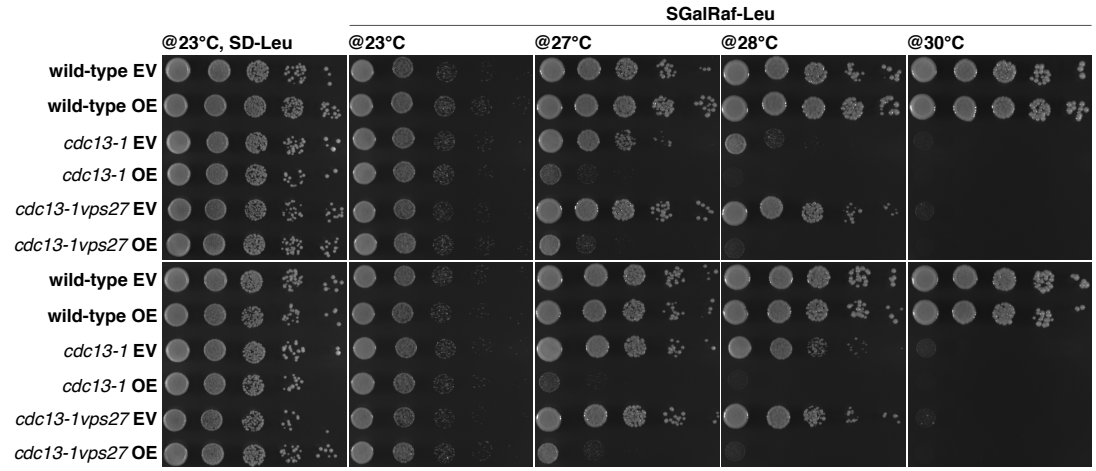

Figure 3.8.: Viability spotting assays at the indicated temperatures. Cells of the indicated genotypes were spotted 10-fold serially diluted onto SGalRaf-Leu plates (overexpression is induced by growth on galactose) and incubated for three days. Controls were grown on SD-Leu plates. The cells carried either an Exo1 overexpression plasmid (OE) or the corresponding empty vector control (EV).

Overexpression of *EXO1* in *cdc13-1 vps27* cells (but not the empty vector) abolished the aforementioned rescue effect (fig. 3.8), supporting the idea of a defective Exo1-mediated resection upon *VPS27* deletion.

3.2.3.3. Protein Levels of Exo1 are Not Affected

So far, all findings strongly suggested a malfunction of Exo1 that can be caused either by decreased protein levels or improper localisation. Thus, the protein levels of Exo1 were assessed in *vps27* single mutants as well as in *cdc13-1 vps27* double mutants after induction of telomere uncapping by heat shock (one hour at 30 °C) using a TAP-tagged Exo1 strain. As Sae2 is also involved in the resection at uncapped telomeres — although to a lower extent than Exo1 — protein levels of this second nuclease were examined, too.
Figure 3.9 depicts the respective Western Blots and their quantifications. Clearly, nuclease levels were not affected in *VPS27* deleted cells (fig. 3.9b). Although the quantification suggested a slightly decreased amount of Exo1 in the double mutant, this was not clearly apparent from the corresponding band intensities. Moreover, the two biological replicates were quite heterogeneous, which is why the indicated difference is probably not dependable.

Moreover, measuring the kinetics of Exo1 protein degradation revealed no difference between *cdc13-1* single and *cdc13-1 vps27* double mutants (fig. 3.10). For this, cultures were incubated at permissive temperature (23 °C) and heat shocked for one hour at 30 °C to induce telomere uncapping. Subsequently, cycloheximide (CHX) was added to the cultures and samples were taken at 30/45/60/75 min following the addition of

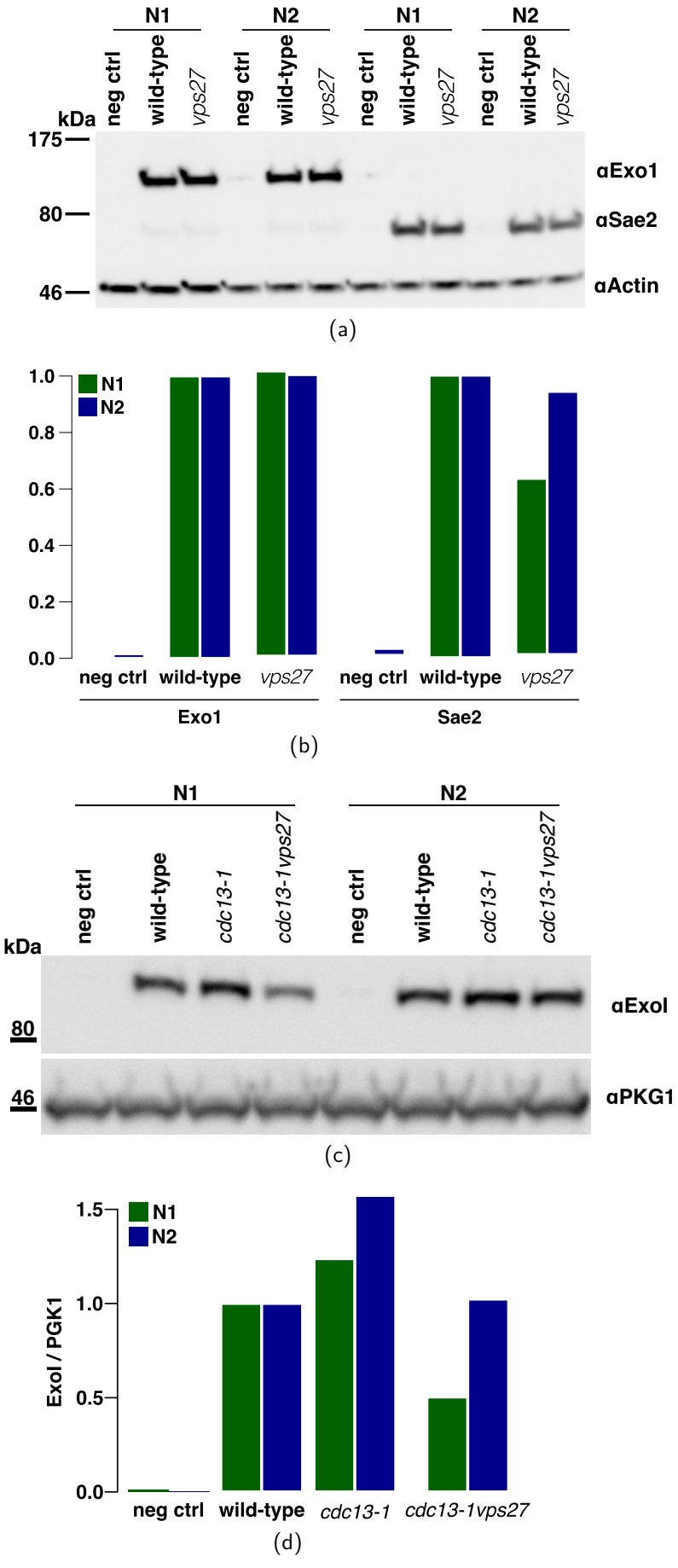

Figure 3.9.: Western Blot for measuring the protein levels of nucleases involved in the resection of uncapped telomeres. Protein samples of the indicated mutants were collected after heat shock treatment for one hour at 30 °C to induce telomere uncapping. Protein levels were measured for two biological replicates. (a) and (c) represent images of the underlying membranes, and (b) and (d) contain the accompanying quantifications. The upper lanes of the membranes represent the Exo1 or Sae2 signal and the lower lanes correspond to either actin or Pgk1 as loading controls. The quantification indicates the relative amount of Exo1 or Sae2 over loading control, respectively. Images with the corresponding Ponceau stained membranes are depicted in suppl. figs. B.10a and B.10b.

CHX which blocks the translational elongation and by this inhibits protein synthesis.

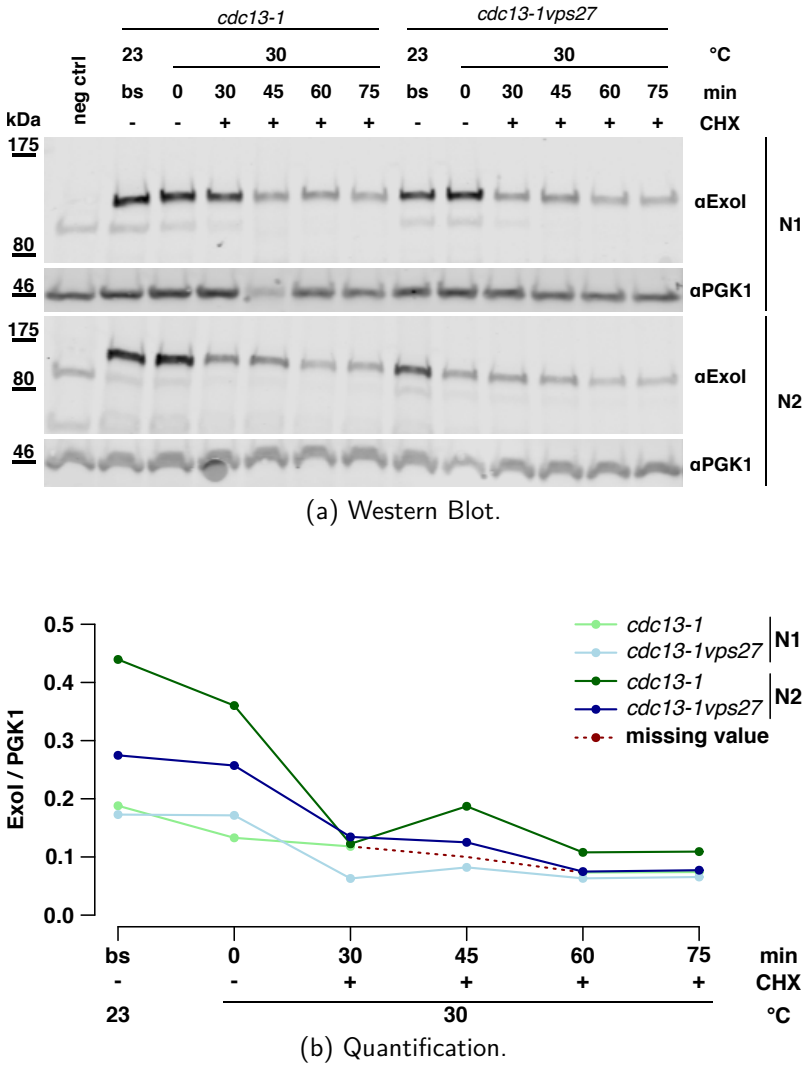

(a) Western Blot.

(b) Quantification.

Figure 3.10.: Western Blot for measuring Exo1 degradation kinetics. Cultures were incubated at permissive temperature (23 °C) and heat shocked for one hour at 30 °C to induce telomere uncapping. Afterwards, cycloheximide (CHX) was added to the cultures and samples were taken at 30/45/60/75 min following the addition of CHX. (a) depicts the underlying membranes whose upper lanes (row 1 and 3) refer to the Exo1 signal and the lower lanes (row 2 and 4) represent the loading control (Pgk1). Its quantification is given in (b). The experiment was conducted for two biological replicates. "bs" denotes samples at 23 °C and time point zero reflects samples at 30 °C before addition of CHX. Figure B.10c depicts an image of the corresponding Ponceau staining.

Hence, as there were no detectable changes in the protein levels of Exo1, I attempted to image GFP-labelled Exo1 to test for localisation defects. Therefore, an Exo1-GFP labelled strain was crossed to the *cdc13-1 vps27* double mutant. Afterwards, the derived wild-type, *cdc13-1*, *vps27*, and *cdc13-1vps27* mutants were examined. As previously done, samples were taken at 23 °C and subsequent to heat shock treatment (one hour at 30 °C). Imaging was performed in the laboratory of Dr. Barbara Di Ventura and with her support using a Zeiss Axio Observer.Z1 microscope, equipped with: objective, Zeiss Plan Apochromat 63x/1.4NA; light source, HXP-120 (Vistron Systems GmbH); camera, Zeiss AxioCam MRm; and filter set, 38 HE (GFP). Unfortunately, a very weak GFP-signal prevented the observation of any difference between the wild-type and any mutant, regardless of the different temperature treatment. Due to the weak GFP-signal, I decided not to further pursue the investigation of possible localisa-

tion problems and therefore the possibility of Exo1-localisation problems cannot be excluded.

3.2.3.4. *vps27* Mutants are Sensitive to DNA Double-Strand Breaks

In addition to acting on uncapped telomeres, 5'–3' Exo1-mediated resection is also important for the homologous recombination (HR) in the DSB repair pathway (section 1.2.2). Upon detection of DNA double-strand breaks, 5'–3' resection by Exo1 is initiated for preparing for the subsequent strand displacement and annealing process [225]. Figure 3.11 briefly describes the involvement of Exo1 in this respect.

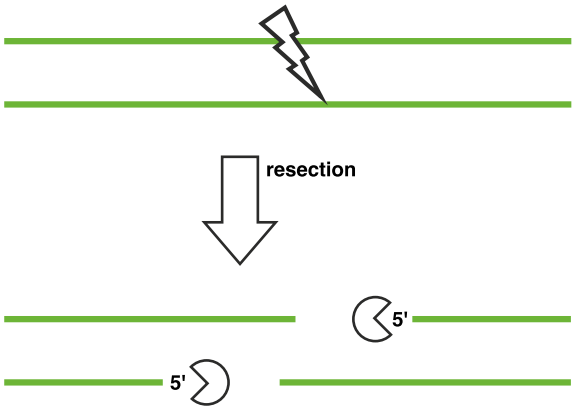

Figure 3.11.: Schematic of Exo1 involvement in homologous recombination during DSB repair. Subsequent to the detection of a DNA double-strand break, 5'–3' resection by Exo1 is initiated. Subsequently, the break is repaired by strand displacement and annealing [225].

This is why sensitivity of *vps27* mutants to DNA damage was tested. Hereto, growth ability of these mutants was verified when incubated on normal yeast complete medium plates (YPD) containing varying concentrations of zeocin (5 µg/ml, 10 µg/ml, and 15 µg/ml; fig. 3.12). Zeocin (phleomycin D1) induces DNA double-strand breaks (DSBs) as described by Chankova and colleagues [226]. Growth was compared to the wild-type. As clearly indicated in fig. 3.12, *vps27* mutants were sensitive to higher levels of zeocin indicating that these mutants are defective for DNA damage repair. For this experiment, YPD plates containing increasing amounts of zeocin were prepared by Martina Dees who also spotted the cultures onto those plates.

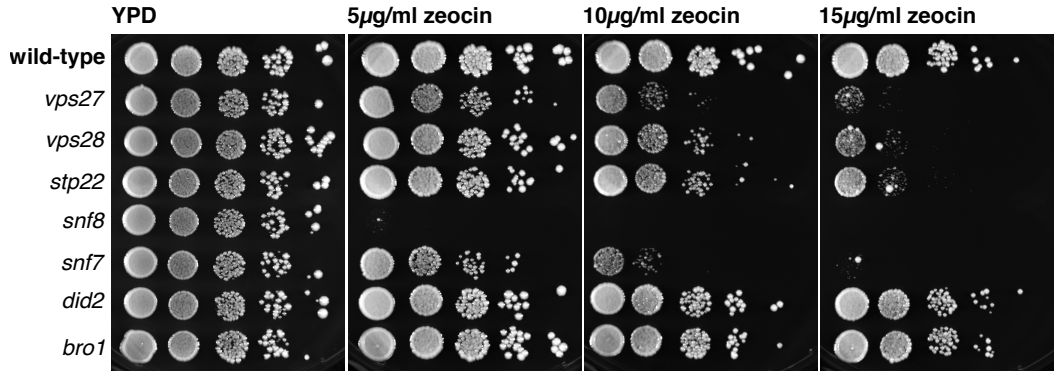

Figure 3.12.: Spotting growth assay for DNA damage sensitivity. Wild-type, *vps27*, and other *escrt* mutants were spotted in 10-fold serial dilutions onto yeast complete medium plates containing increasing concentrations of zeocin. Plates were incubated for three days at 30 °C. Two biological replicates were spotted. Plates were prepared by Martina Dees who also spotted the cultures onto those plates.

For the proper progress of HR, initiation of DNA strand annealing by Rad52 is essential [227,228], which is why the genetic interaction of *VPS27* and *RAD52* was tested. After construction of the double mutant *rad52 vps27*, it was subjected to an analogous DNA damage spotting as the *vps27* single mutant before. Both genes were found to show an additive effect (fig. 3.13).

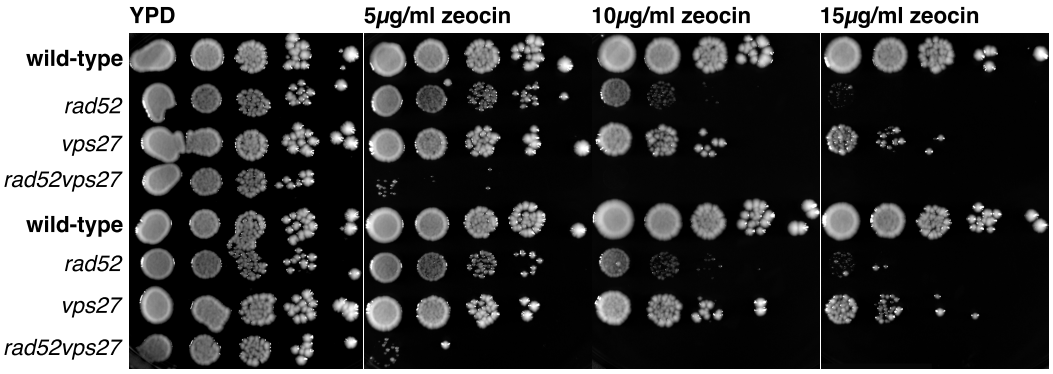

Figure 3.13.: Spotting growth assay for testing the sensitivity of *rad52 vps27* double mutants to DSBs caused by zeocin. The indicated mutants and the wild-type were spotted in 10-fold serial dilutions onto YPD plates containing increasing amounts of zeocin. Plates were incubated for three days at 30 °C. Two biological replicates were spotted.

Having found indications that DSB repair by HR is impaired upon deletion of *VPS27*, I examined an HR proficient strain in the presence of *VPS27* deletion ($vps27_{\mathrm{HR}}$) for its viability. Comparing the wild-type HR-proficient strain ($\mathrm{WT_{HR}}$) with the *VPS27* deleted one, a slight decrease in the growth capabilities was discovered. There were smaller and less dense colonies in the $vps27_{\mathrm{HR}}$ mutant than in the $\mathrm{WT_{HR}}$ (fig. 3.14). This effect was pronounced by the circumstance that in the corresponding control strain colonies were thicker and more dense.

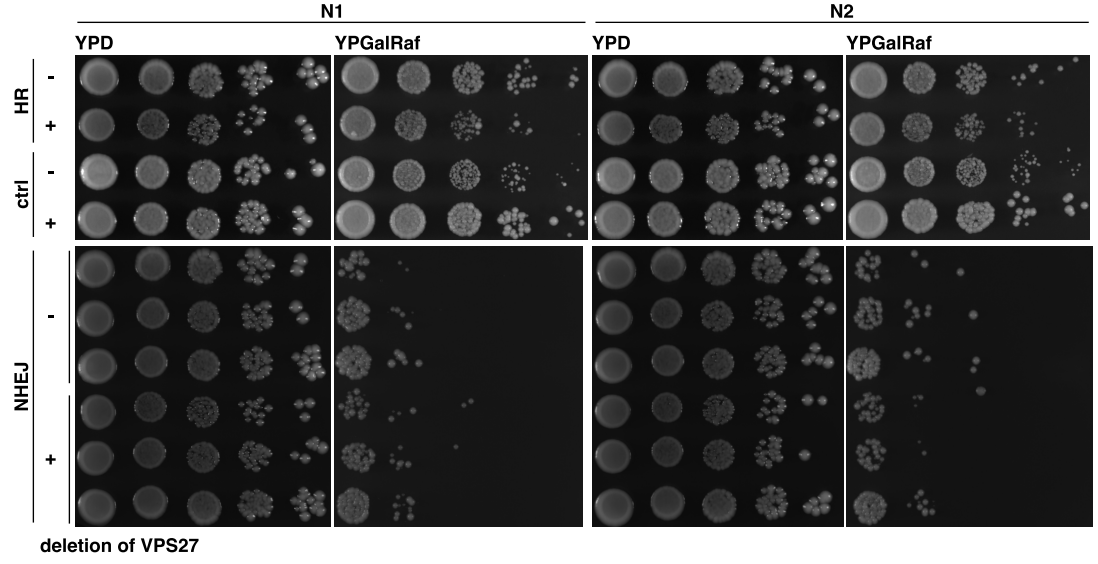

Figure 3.14.: Viability spotting for DNA damage repair proficient cells in the presence of *VPS27* deletion. Cells were spotted in 10-fold serial dilutions onto standard YPD or YPGalRaf plates. Incubation lasted for three days at 30 °C. Two biological replicates were spotted.

In concordance with the previous results, this assay suggested an impaired HR pathway in *vps27* mutants. In order to obtain a complete picture of DNA damage repair pathways,

a NHEJ-proficient strain was included in this experiment. However, no effects were observed for NHEJ in the absence of *VPS27*.

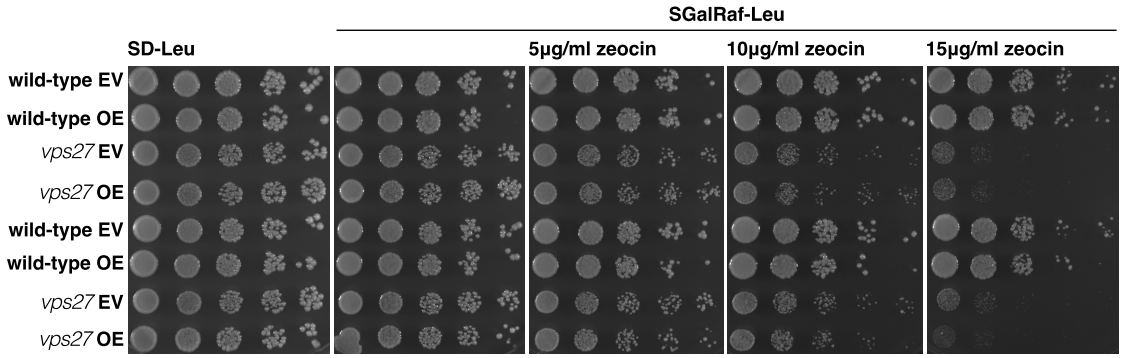

Figure 3.15.: DNA damage spotting of *vps27* single mutants in the presence of *EXO1* overexpression. Wild-type or *vps27* cells carrying either an *EXO1* overexpression plasmid or the corresponding empty vector control were spotted in 10-fold serial dilutions onto SGalRaf-Leu plates (*EXO1* OE is galactose induced) containing increasing concentrations of zeocin. Controls were spotted onto SD-Leu plates or SGalRaf plates without zeocin. Two biological replicates were tested. Incubation lasted for three days at 30 °C.

With respect to the data indicating a corrupted Exo1 function, it was tested whether overexpression of *EXO1* in *vps27* mutants diminishes the sensitivity of those mutants to DSBs induced by zeocin. Similar to the initial DNA damage spotting (fig. 3.12), wild-type and *vps27* cells carrying either an *EXO1* overexpression plasmid or the corresponding empty vector control were spotted onto media plates harbouring different concentrations of zeocin (fig. 3.15). Overexpression of *EXO1* did not have any effect on the sensitivity to zeocin for *VPS27* deleted cells.

3.2.3.5. Examination of the Resection Efficiency in *vps27* Mutants

Finally, the efficiency of 5'–3' Exo1-mediated resection was verified. The laboratory of Prof. Maria Pia Longhese developed an assay that allows to follow the 5'–3' resection after induction of a DSB at the mating type (MAT) locus [223, 229]. The DSB is induced by the homothallic switching endonuclease (HO) that naturally occurs in certain fungi enabling them to switch between their mating types (homothallic switch) [230, 231]. By taking advantage of this assay, it can be examined whether resection in a certain mutant is progressing as fast as in the wild-type. Figure 3.16a gives a schematic of the "system used to detect DSB resection" [229]. Genomic DNA is separated on alkaline agarose gels subsequent to digestion with a SspI restriction endonuclease. The gel is then hybridised with a ssRNA probe that specifically binds to the unresected strand of the MAT locus. The probe indicates HO-cut and uncut fragments at 0.9 kbp and 1.1 kbp, respectively. With progress of 5'–3' resection, SspI sites are gradually removed "producing larger SspI fragments" that are detected by the probe [223, 229].

As described in section 2.2.2.10, the *VPS27* deletion was introduced into the underlying HO-cut strain while the actual resection assay was performed in the laboratory of Prof. Longhese. No difference in the efficiency of 5'–3' resection was obtained between the wild-type and the *vps27* mutants (fig. 3.16c vs. fig. 3.16d). Although this assay indicated correct functioning resection in *vps27* mutants, its outcome was not interpretable as the induction of a DSB site by the HO-cut mechanism did not work properly. Neither Prof. Longhese nor our lab was able to explain this cut deficiency that made it impossible to infer conclusions about the efficiency of Exo1-mediated resection in *vps27* mutants from

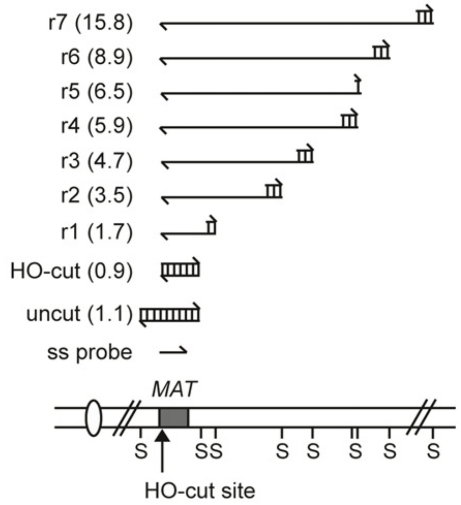

(a) Schematic of the detection of resection at a DSB [229].

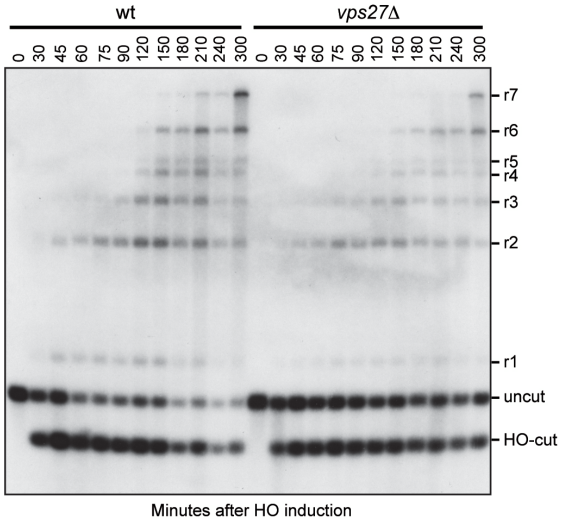

(b) Alkaline agarose Gel.

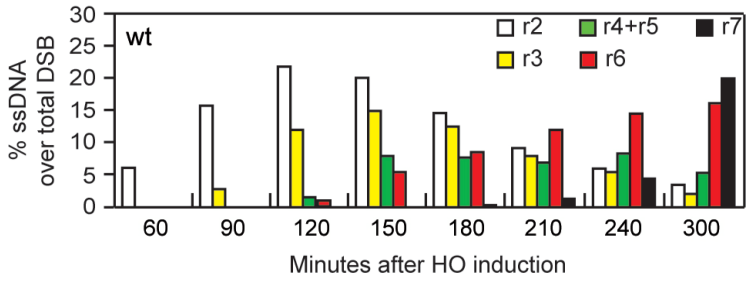

(c) Quantification of for the wild-type.

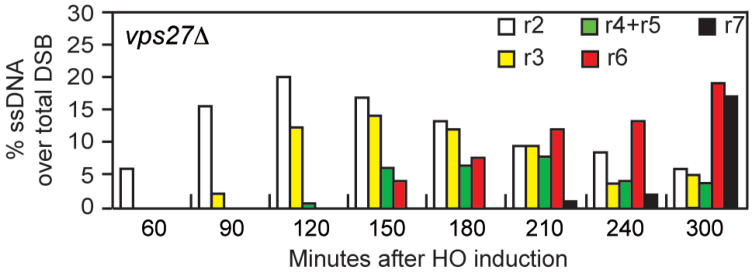

(d) Quantification of for the *vps27* mutant.

Figure 3.16.: (a) 5'–3' resection is examined after a HO-induced DSB. DNA fragments are separated on alkaline agarose gels subsequent to digestion with SspI. Gels are hybridised with a ssRNA probe that binds to the unresected strand of the MAT locus. As resection progresses, SspI sites (S) are gradually eliminated leading to larger SspI fragments (r1–r7) detected by the probe. SspI sites are located 1.7/3.5/4.7/5.9/6.5/8.9/15.8 kbp centromere-distal from the HO-cut site. The sub-figure and its description were taken from [229]. (b) Alkaline agarose gel for the wild-type and *vps27* mutants. The experiment itself was run in the laboratory of Prof. Longhese after the VPS27 deletion was introduced into the underlying HO-cut strain. (c) Quantification of the wild-type lanes in (b) and (d) quantification of the *vps27* lanes. (b) – (d) were provided by the Longhese lab.

the previously described resection assay which is accepted as the gold standard for this issue.

3.2.3.6. Improved Viability of *cdc13-1 exo1 vps27* Mutants

Moreover, the genetic interaction of *CDC13*, *EXO1*, and *VPS27* was tested by generating a triple mutant (*cdc13-1 exo1 vps27*) and examining it in another temperature rescue spotting assay (fig. 3.17). Due to less resection of uncapped telomeres by deleting *EXO1*, *cdc13-1 exo1* mutants are more viable at non-permissive temperatures [200].

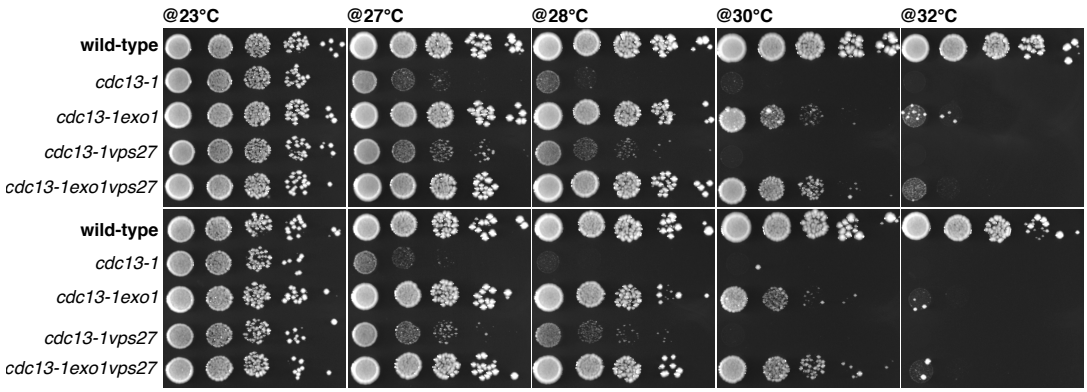

Figure 3.17.: Viability spotting assay at the indicated temperatures. Mutants of the indicated genotypes were spotted in 10-fold serial dilutions. Cells were spotted in duplicates onto standard YPD plates and incubated for three days.

The growth ability of *cdc13-1 exo1 vps27* cells surpassed the *cdc13-1 exo1* and *cdc13-1 vps27* mutants suggesting that Exo1 and Vps27 function independently in the context of dysfunctional telomere capping. This observation was contradictory to the ideas of a defective Exo1-mediated resection due to deletion of *vps27*.

3.2.4. DNA Damage Checkpoint Upon Telomere Uncapping

Other than a defective Exo1-mediated resection, improper DNA damage checkpoint activation could explain the rescue of *cdc13-1* capping-defective telomeres (fig. 3.4). An UP-DOWN assay was developed by the Lydall laboratory in which cells are subjected to cycles of high and low temperature [200]. As the temperature sensitivity of *cdc13-1* mutants is reversible, the cells can maintain viability on short exposures to the non-permissive temperature ($> 27\,^{\circ}\mathrm{C}$) when returned to permissive temperature afterwards. Mutants defective for the DNA damage checkpoint activation fail to arrest in response to DNA damage and recovery is not possible [200]. Under these conditions, mutations in *EXO1* suppress *cdc13-1* defects, whereas a deletion of the *RAD9* checkpoint gene is unable to do so [200]. Figure 3.18 indicates that, contrary to *cdc13-1 rad9* mutants, *cdc13-1 vps27* mutants were viable in this assay, indicating that checkpoint is normal in these cells.

However, the UP-DOWN assay is merely an indicator of checkpoint defects because in *RAD9* deleted cells *MEC1*-mediated auto-phosphorylation of Rad53 could still activate the cell cycle checkpoint in response to DNA damage as outlined in fig. 3.19 [232, 233]. Hence, the viability of *cdc13-1 vps27* mutants was examined in the absence of proper Rad53 function (*rad53-11* mutants [234,235]).

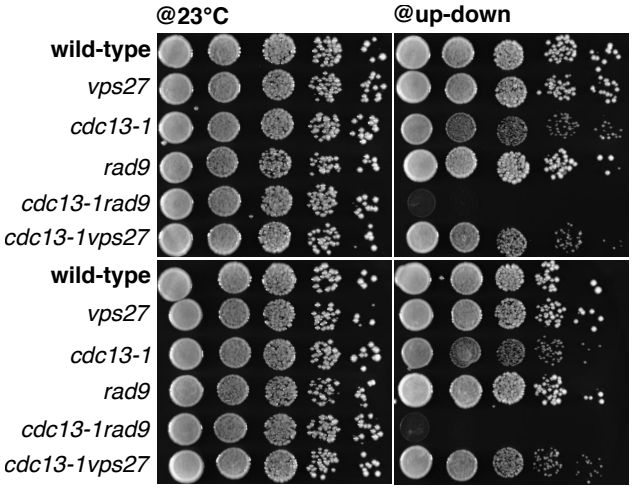

Figure 3.18.: UP-DOWN assay [200] for testing proper cell-cycle checkpoint function in *cdc13-1 vps27* mutants. Cells were spotted in 10-fold serial dilutions onto standard YPD plates that were incubated at oscillating temperatures for three days. Two biological replicates were spotted.

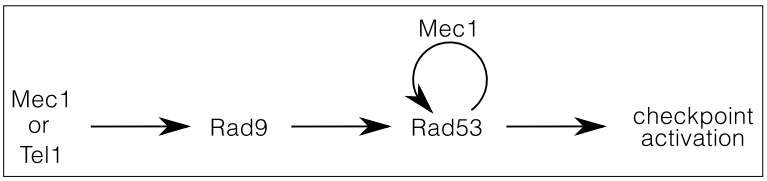

Figure 3.19.: Schematic of checkpoint activation by Rad53 in response to DNA damage. Either Mec1-dependent auto-phosphorylation or Rad9 activate Rad53.

As carried out for the *cdc13-1 vps27* double mutants before, a triple mutant was constructed, spotted onto standard YPD plates and incubated at permissive (23 °C and 25 °C) and non-permissive (27 °C and 28 °C) temperatures. This spotting suggested that *VPS27* and *RAD53* function independently of each other and supported the indication of a proper checkpoint in *vps27* mutants.

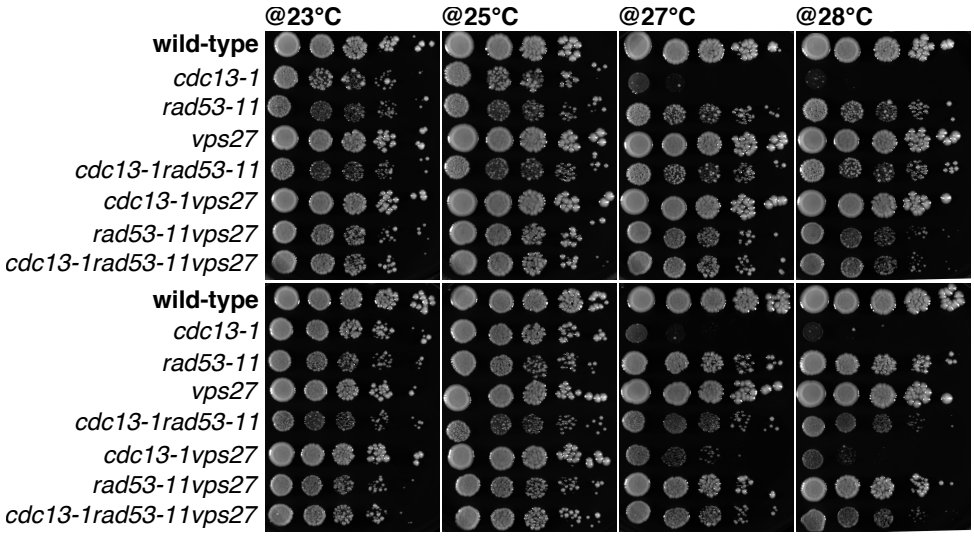

Figure 3.20.: Viability spotting of the indicated strains in duplicate at permissive (23 °C and 25 °C) and non-permissive (27 °C and 28 °C) temperatures. Cells were spotted in 10-fold serial dilutions onto standard YPD plates. Incubation lasted for three days. Two biological replicates were spotted.

3.2.5. All Escrt Factors Show the Same Effects as *VPS27* Deletion

Regarding the fact that only nine out of nineteen ESCRT factor encoding genes were enriched in the *TLM* gene list, the question arose what distinguishes those nine and the remaining ten ESCRT factors. Table 3.4 lists all ESCRT factors and whether an interaction with CDC13 is known.

Table 3.4.: List of all nineteen ESCRT factor encoding genes from baker's yeast. ESCRT complex membership and knowledge about *CDC13* interactions are provided as well as the assignment of the different rescue categories to the *escrt* mutants. A) clear viability at 28 °C, B) clear viability at 27 °C and slight viability at 28 °C, C) viable at 27 °C and D) no enhanced viability. EXP, experimentally derived; DB, database knowledge; ¬, no defect in experimental examination; ↯, contradiction.

	Complex	*cdc13-1* Rescue Effect	Sensitivity to Zeocin	Interaction with CDC13 (SGD)
VPS27	0	A	✓(EXP, DB)	
HSE1	0	C		synthetic rescue
STP22	1	B	✓(EXP, DB)	
VPS28	1	B	✓(EXP, DB)	
SRN2	1	B		synthetic rescue
MVB12	1	C		
SNF8	2	B	✓(EXP, DB)	
VPS25	2	B		
VPS36	2	B	✓(DB)	
VPS20	3	D	✓(DB)	
SNF7	3	B	✓(EXP)	
VPS24	3	B	✓(DB)	positive genetic
VPS2	3	B		
DID2	3-a	B	↯ (DB, ¬EXP)	synthetic rescue
VPS60	3-a	D		synthetic rescue
IST1	3-a	C		
VPS4	a	D		synthetic growth defect
VTA1	a	D		
BRO1	a	A	↯ (¬EXP)	

With respect to the heterogeneous distribution of the *tlm* phenotype and the annotation of known interactions with Cdc13 over the ESCRT family, I examined all *cdc13-1 escrt* double mutants in a temperature rescue spotting, in the same way as *vps27*. Strikingly, almost all *ESCRT* deletions rescued the temperature sensitivity of *cdc13-1* mutants to a varying degree (suppl. fig. B.7). For assessing the overlap of those *escrt* mutants that showed telomere shortening ($escrt \cap tlm_{short}$) with those that rescued the temperature sensitivity of *cdc13-1* cells, the viability of all *cdc13-1 escrt* mutants was categorised as: A) clear viability at 28 °C, B) clear viability at 27 °C and slight viability at 28 °C, C) viable at 27 °C, and D) no enhanced viability (table 3.4). Afterwards, the overlap of $escrt \cap tlm_{short}$ mutants with a corresponding *cdc13-1 escrt* double mutant categorised as either A or B was evaluated. Eight of the nine $escrt \cap tlm_{short}$ mutants showed a *cdc13-1* rescue of type A or B. A Fisher's Exact test revealed a p-value of 0.0399 for this overlap.

Moreover, the DNA damage sensitivity of six additional *escrt* mutants was tested, too. Four of these six mutants showed a clear sensitivity to zeocin (fig. 3.12 and table 3.4) as seen before for *vps27* mutants. To further support this result, I explored the phenotype information

provided by the SGD [10] for known sensitivities of all ESCRT factors against DNA damaging agents. For ease of access, a bipartite drug-sensitivity network was derived from this phenotype information as represented in suppl. fig. B.8. From the sub-network for zeocin resistance (fig. 3.21) it became apparent that some ESCRT factors were already annotated with a decreased resistance to zeocin (marked with "DB" in table 3.4). For four of those factors the decreased resistance to zeocin was confirmed (fig. 3.12 and marked with "EXP" in table 3.4). In addition, information about the decreased resistance to zeocin for three further ESCRT factors was gained. Although the *did2* mutant was described in the SGD [10] to show decreased resistance to zeocin, too, a clear sensitivity could not be obtained (fig. 3.12).

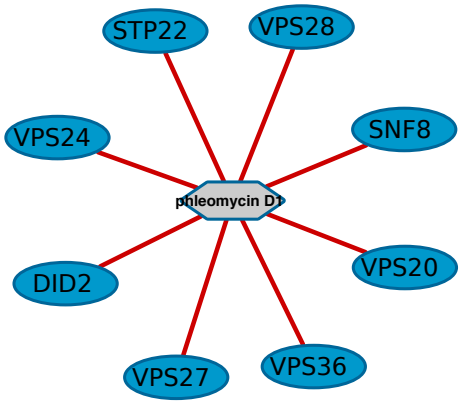

Figure 3.21.: Sub-network for the resistance to zeocin (phleomycin D1). The global bipartite drug-sensitivity network as derived for all ESCRT factors from the phenotype information provided by the SGD [10] is depicted in suppl. fig. B.8. Drugs are denoted with grey and ESCRT factors with blue nodes. Red edges encode a decreased resistance to zeocin of a certain *escrt* mutant. Network manipulation and visualisation was done with Cytoscape [213].

In summary, the data indicated that the whole ESCRT family is rescuing a *cdc13-1* defective telomere-cap and that *escrt* mutants are sensitive to DNA damage.

3.3. *TLM* Genes and the ESCRT System: An *in silico* Examination

Despite all the presented experiments, no clear functional causality could be derived so far. Therefore, I conducted further *in silico* analyses in order to get more insights into the functional relationship of telomere length maintenance and the ESCRT system.

3.3.1. PPI Network of ESCRT Factors and Telomere Related Proteins

Initially, I investigated a manually curated *Saccharomyces cerevisiae* interaction network (provided by Christine Brun) to explore the connections of telomere related proteins and the ESCRT family. As this network consisted exclusively of experimentally verified binary PPIs, it represented a highly reliable interaction source. Shortest path analyses between the set of telomere related proteins (TRPs) and the ESCRT factors revealed that they were mostly connected by more than one traverse step (fig. 3.22). The rationale behind this analysis was that the shortest path between two vertices has the smallest number of edges and thus the least nodes to traverse, enabling the discovery of novel functional relationships.

Finding pathways with only one traverse protein within a global PPI-network, could yield regulatory or functional information about the connected proteins. “Proteins connecting pairs of other proteins with well-defined biological functions [...] have a higher probability to share that function, as compared to those selected at random” [236,237]. The set of TRPs comprised all subunits of the CST (Cdc13, Stn1, and Ten1) capping complex, the Ku complex (Yku70, Yku80), the MRX complex (Mre11, Rad50, and Xrs2), and the proteins Rif1, Rif2, Rap1, Exo1, Est1, Est2, Tel1, and Mec1. Nonetheless, the shortest paths between three ESCRT factors (Vps27, Hse1, and Stp22) and Cdc13 had a distance of only two or one traverse protein, each. Remarkably, those ESCRT factors were also two steps away from Rad53.

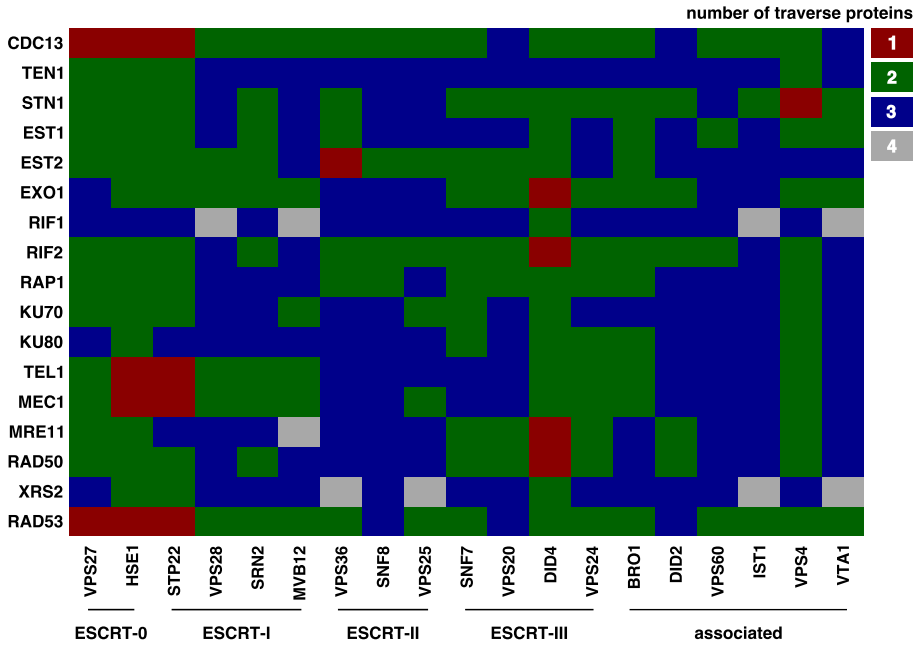

Figure 3.22.: Matrix of shortest path distances between members of the ESCRT family and telomere related proteins. Shortest path investigation was done using the *igraph* library of R [206, 212].

Figure 3.23 represents the induced sub-network for all those PPIs having a distance of two. In there, Cdc13, Rad53 and the ESCRT-0 complex, especially Vps27, form a dense sub-network. In detail, Vps27 (ESCRT-0) is linked with Cdc13 by seven protein kinases (PKs) in parallel (suppl. table C.4). The PPI-NW contains 29 interaction partners for Cdc13 of which 16 are related to protein phosphorylation (P = 2.10e−12, YeastMine GO-BP enrichment [192]). As all nodes interlinking Vps27 and Cdc13 are PKs and as such associated with protein phosphorylation (P = 4.8e−7, YeastMine GO-BP enrichment [192]), I tested whether this enrichment for PK edges was significant. Hence, I derived the representative contingency table (table 3.5) and a two-sided Fisher’s Exact test was calculated, resulting in a p-value of 8.4e−3. This p-value indicated that the amount of PK edges was not to be expected by chance.

Table 3.5.: Contingency table for the PK edges connecting Cdc13 and Vps27. The p-value of this overlap was 8.4e−3.

	protein phosphorylation	**$\overline{\text{protein phosphorylation}}$**	
Cdc13 neighbour is Vps27	7	0	7
$\overline{\text{Cdc13 neighbour is Vps27}}$	9	13	22
	16	13	$\sum$ 29

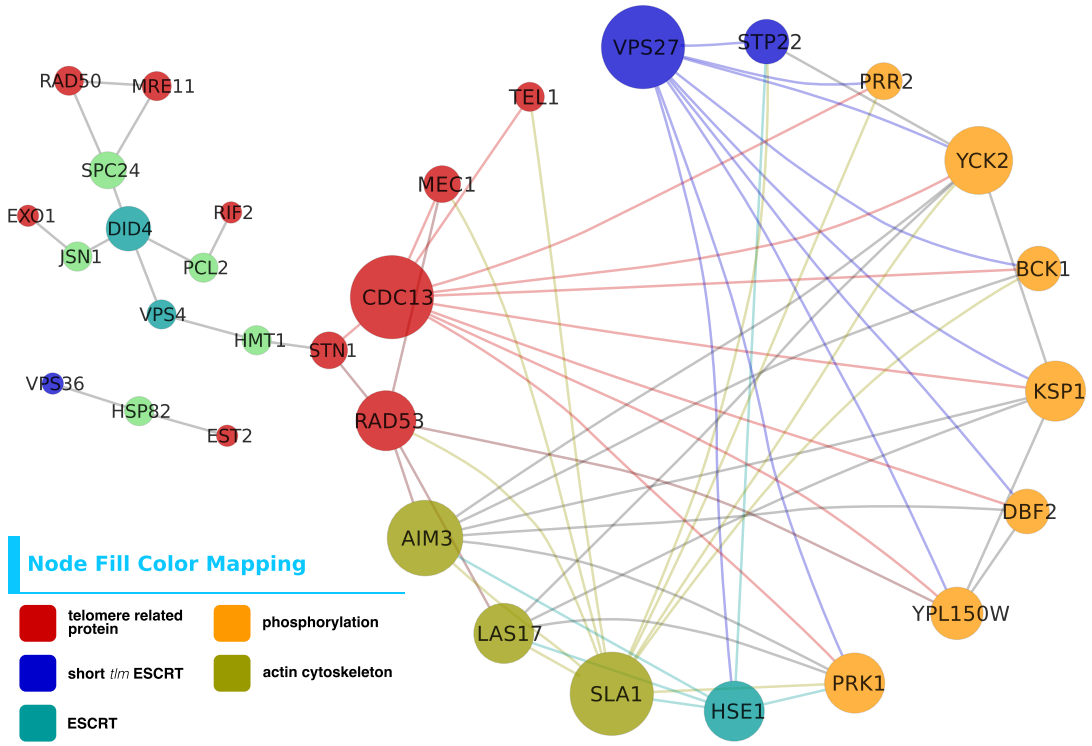

Figure 3.23.: Induced sub-network for all vertices between TRPs and ESCRT factors having a shortest path distance of two. The underlying binary PPI-network was provided by Christine Brun. Overall the network contains 31 vertices and 64 edges. The used symbols correspond to the encoding genes.

Moreover, a cytoskeletal protein binding protein (Sla1) is connecting Tel1 and Mec1 to Hse1 (ESCRT-0) and Stp22 (ESCRT-I). Mec1 and Tel1 are both DNA damage checkpoint kinases that are known to be required for telomerase activation [69]. In the presence of DNA damage, they activate Rad9 leading to Rad53 phosphorylation and subsequent cell cycle arrest (section 1.2.2 and fig. 3.19). Hse1 is linked to Rad53 by Sla1 and two further proteins associated with the actin cytoskeleton (Aim3 and Las17, suppl. table C.4).

Altogether the PPI-NW analysis suggested a strong connection of ESCRT-0 to the telomeric system via Cdc13.

3.3.2. Expression Changes Upon ESCRT Gene Deletions

Furthermore, I analysed gene expression data obtained genome-wide for deletion strains corresponding to one-quarter of the baker's yeast genes [179]. These expression profiles were measured for strains kept under standard growth conditions allowing the study of a particular gene perturbation without side effects caused by special environmental conditions. Twelve deletion strains corresponding to ESCRT factor encoding genes were contained within the samples of this data (fig. 3.24). Most of them were annotated with a clear *cdc13-1* rescue effect (table 3.4). Seven of the nine $escrt \cap tlm_{short}$ mutants were among those twelve deletion strains. Thus, the included *escrt* mutants reflected those that showed the strongest phenotypical association to telomere maintenance.

As described in section 2.1.3, I extracted a matrix of expression values for telomere related protein (TRP) encoding genes (targets, rows) and *escrt* mutants (samples, columns). Figure 3.25 shows this matrix. Only significant changes in expression were plotted ($\log_2(FC)$

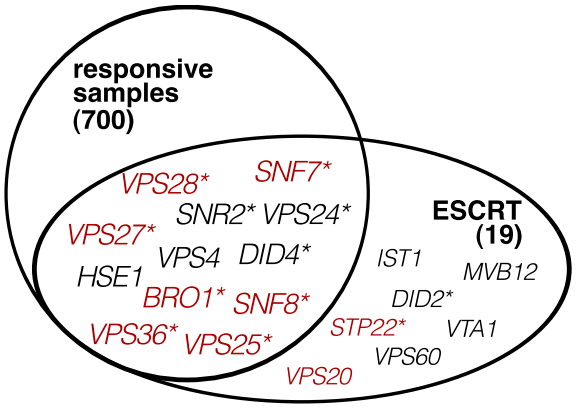

Figure 3.24.: Venn diagram representing the *ESCRT* genes contained within as responsive classified samples in the expression data of Kemmeren et al. [179]. Deletion strains of the genes highlighted in red exhibited shorter telomeres (*tlm* mutants) and those marked with an asterisks showed a clear rescue of the temperature sensitivity of *cdc13-1* (table 3.4).

with P $\leq$ 0.05). In general, deletion of *ESCRT* genes affected the expression of *TRP* genes only occasionally. However, the scale of the fold-changes (FCs) ranged from -0.35 – 0.31, so that these FCs could not be considered as being reliable and the matrix in fig. 3.25 was to be interpreted that the deletion of any *ESCRT* gene does not influence the expression of TRP encoding genes. This interpretation was supported by the circumstance that the scale of the FCs ranged from -3.4 – 3.4 for all target genes. In all contained *escrt* mutants, another *ESCRT* gene was the most up-regulated gene, and one of the following three genes was most down-regulated: *ARG3* (involved in arginine biosynthesis), *Q0060* (a mitochondrial gene), or YDR133C (dubious systematic open reading frame identifier that is unlikely to encode a functional protein).

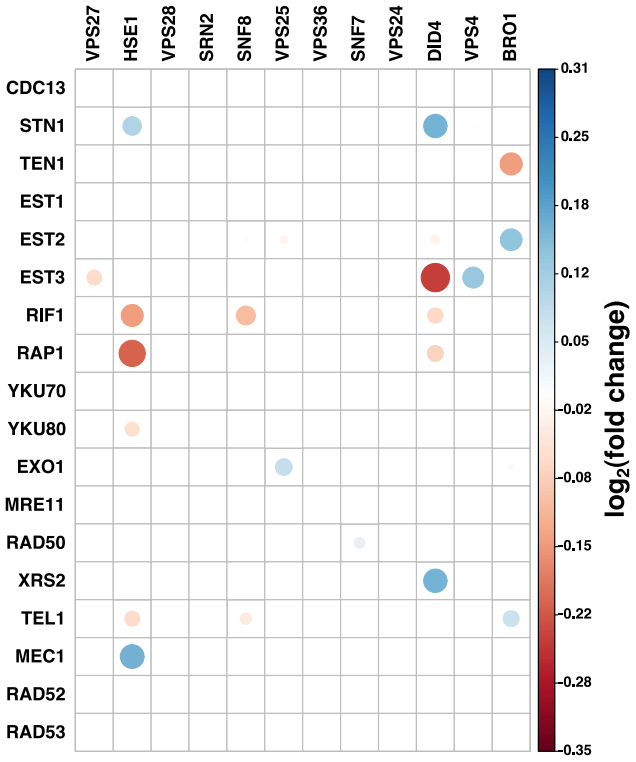

Figure 3.25.: Matrix of gene expression values. Columns refer to *ESCRT* gene deletion strains (samples) and rows contain TRP encoding (target) genes. Only significant changes in expression were plotted. The colour and size of the circles encode the $\log_2(FC)$ with a p-value $\leq$ 0.05. The gene expression data was taken from Kemmeren and colleagues [179].

Nevertheless, having found experimental evidence that the whole ESCRT family rescues *cdc13-1* capping-defective telomeres, I attempted to find up- or down-regulated KEGG pathways [5–7] upon disruption of the ESCRT machinery. To this end, a gene set enrichment analysis (GSEA) against a pre-ranked list of genes was performed. In a preparatory step, the target genes were ranked in descending order by the t-statistic from a Student's

t-Test for all *escrt* samples versus the remaining samples. Figure 3.26 summarises the results.

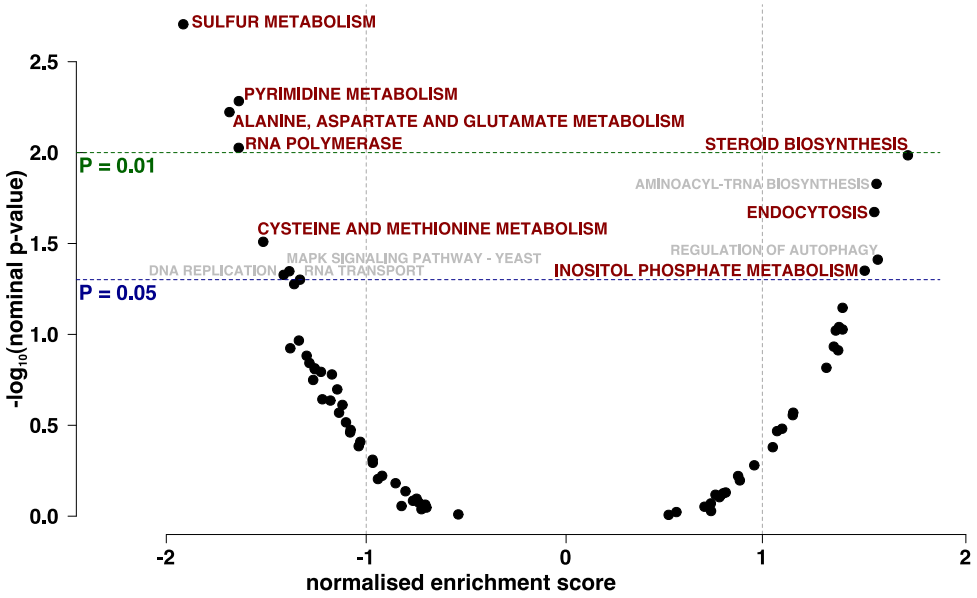

Figure 3.26.: Volcano plot of up- or down-regulated pathways upon disruption of the ESCRT machinery. A GSEA for KEGG pathways [5–7] against a pre-ranked list of genes was carried out using the GSEA software offered by the Broad Institute of MIT and Harvard [214, 215]. The gene expression data was taken from Kemmeren and colleagues [179]. Pathways highlighted in red reached a FDR $\leq 25\,\%$ and those in grey did not. A NES > 0 indicates pathways up-regulated in the *escrt* strains and a NES < 0 reflects down-regulated pathways. NES, normalised enrichment score.

The GSEA highlighted pathways that are known to be up- or down-regulated in response to environmental stress and revealed no peculiarities about the relationship of TLM and the ESCRT family. Keeping the manifold cellular sites in mind that the ESCRT system is acting on, it is plausible that already its disruption puts cells under stress. In the environmental stress response, e.g. growth-related processes and nucleotide biosynthesis are repressed, while pathways required for survival are induced (e.g. autophagy, intracellular signal, and vacuolar functions) [238].

3.3.3. Genetic Interaction Score Exploration for ESCRT Factors

The Lydall laboratory derived a genetic interaction score (GIS) from a "Quantitative Fitness Analysis on thousands of yeast strains containing mutations affecting telomere-capping proteins (Cdc13 or Yku70) in combination with a library of systematic gene deletion mutations" [201]. Hereby, they were able to systematically identify suppressors or enhancers of the capping defects caused by either disrupting CST- or Ku-complex telomere capping. In order to find more information that can be used to understand the functional association of telomere length maintenance and the ESCRT system, I briefly plotted the GISs for *yku70 yfgΔ* mutants against the GISs of *cdc13-1 yfgΔ* mutants and marked short *tlm* and *escrt* mutants (fig. 3.27). Overall, the data set contained merely six *ESCRT* genes of which *VPS27* was the only *TLM* gene. As can be seen in fig. 3.27, all *escrt* mutants received a positive GIS with *cdc13-1*, thus suppressing its defect and supporting the experimental results (suppl. fig. B.7 and table 3.4). The *escrt* mutants were spread all over the positive *cdc13-1* GIS range. They did not form clusters that could have been used to infer additional knowledge about the causality of the defect suppression. Interestingly, the *escrt* mutants yielded only negative GISs in combination with *YKU70* deletion. In

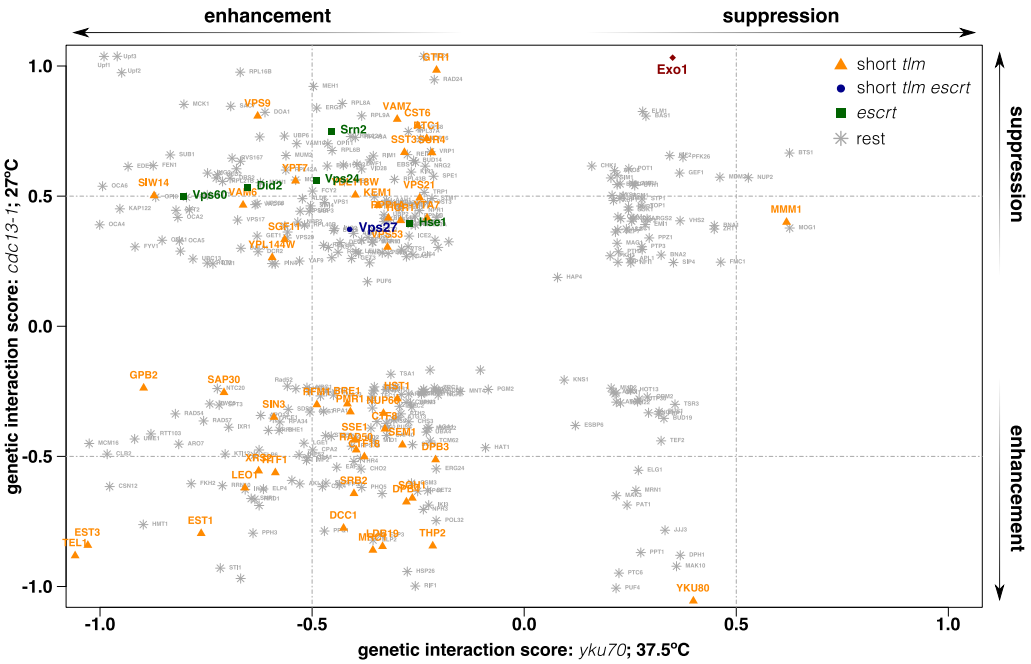

Figure 3.27.: Plot of the GIS for *yku70 yfgΔ* mutants against the GIS of *cdc13-1 yfgΔ* mutants. Short *tlm* and *escrt* mutants were highlighted as follows: Yellow, short *tlm* mutants; blue, *escrt* mutants that showed telomere shortening; green, remaining *escrt* mutants; grey, all other data points. Data was extracted from Addinall et al. [201].

contrast to the *cdc13-1* double mutants, *escrt* mutants enhanced the *yku70* defect. However, as the Ku complex is involved in NHEJ, too, it is difficult to interpret observations gathered by Ku perturbations and assign them to either NHEJ or telomere homoeostasis. I did not evaluate the influences of this complex on telomeres in the background of *ESCRT* deletions.

4 Conclusion

When the absence or aberrance of one component is shown to stop a system working, we have to be careful how we interpret this.
(Denis Noble, [18])

The present dissertation aimed at a systems biological analysis of the genetic regulation effecting telomere homoeostasis. Telomeres represent special structural and functional units forming the ends of eukaryotic chromosomes. Dysfunctional telomeres can give rise to severe imbalance of the genomic stability and reduced integrity that are vital to every cell and organism. A myriad of human syndromes, neurodegenerative diseases, immunodeficiency as well as cancer are associated with defects in factors sensing and responding to DNA damages [26–30] and thus, to telomeres, too. Although profound knowledge has already been gained about telomere biology in general and its homoeostasis, we are far from understanding it in all its details and complexity — especially if it comes to mammalian telomeres (section 1.3). As described in section 1.5.2, *Saccharomyces cerevisiae* serves as an excellent model organism to study telomere biology and to transfer the gained knowledge to humans.

4.1. The ESCRT System is Linked to Telomere Length Maintenance

The system-wide exploration of the signals regulating telomere length maintenance was based on a list of genes — telomere length maintenance (*TLM*) genes — from *Saccharomyces cerevisiae* whose respective deletions were found to affect telomere length (increased shortening or lengthening) [183–185,195,197].

At first, I performed a comprehensive and unbiased analysis to get an overview of the genes within the *TLM* list by testing it for enrichment of specific KEGG pathways [5–7] or functional categories (MIPS FunCat; [8,9]). Surprisingly, the top-ranking KEGG pathway for short *tlm* mutants was endocytosis with a corrected p-value of 2.6e−5 (two-sided Fisher's Exact test, table 3.1), while the remaining pathways were to be expected in the context of (dysfunctional) telomere maintenance (e.g. nucleotide metabolism or DNA damage repair). The enrichment for endocytosis was basically due to an accumulation of nine out of nineteen endosomal sorting complex required for transport (ESCRT) factors within the set of short *tlm* mutants (P = 8.8e−9, two-sided Fisher's Exact test, tables 3.2 and 3.3).

ESCRT factors define a system of five multi-protein complexes which is involved in deforming and scissioning cytosol filled membrane stalks (e.g. MVB formation [107,116–118], cytokinesis [106,119–121], and enveloped viral budding [106,122,123]; section 1.4.1). However, they are linked to genomic stability and integrity, too, as deletion of certain ESCRT proteins were found to cause defects in chromosomal segregation in humans [130] and in yeast [131]. In humans, ESCRT proteins are also associated with chromatin remodelling [129]. Nonetheless, except for Rog et al. [198], there is no literature describing any link or mechanistic insights into the association of telomere length maintenance and vesicular traffic or endosomal sorting. Rog and colleagues have analysed how telomere maintenance is influenced by a subset of proteins belonging to the family of vacuolar protein sorting (VPS) [198] of which ESCRT factors represent the class E VPS subfamily [103–105]. Although they have revealed that the exertion of influence on telomere length by the tested *VPS* genes depends on telomerase and the Ku complex while being independent of Tel1 and Rap1, Rog and colleagues could only hypothesise about the causal link between telomere homoeostasis and vacuolar sorting mechanisms [165,198].

4.1.1. Deletion of *VPS27* Rescues Dysfunctional Telomeres by Impairing Exo1-Mediated Resection

With respect to the significant enrichment of ESCRT factors within the short *tlm* mutants and the little knowledge about the relationship of telomere homoeostasis and vacuolar sorting, I chose to perform a more in-depth experimental analysis of this association. For this, I decided for *VPS27* as a representative of the enriched genes for the experimental investigations. Vps27 and Hse1 form the heterodimeric ESCRT-0 complex. Both proteins are conserved throughout the group of opisthokonts (animals and fungi) [103]. According to Prag et al., ESCRT-0 is a multifunctional complex that (i) is required for recognising and sorting ubiquitinated cargo molecules into multi-vesicle bodies, and (ii) ensures efficient recycling of late Golgi proteins like the carboxypeptidase Y (CPY, a vacuolar protease) sorting receptor [239]. In the absence of the Hse1 core domain, Vps27 can form a stable monomer, whereas Hse1 aggregates and is degraded if expressed in isolation of Vps27 [239].

Shachar et al. have shown that in *VPS27* deleted cells, telomeres are shorter than the wild-type length of 350 bp [195]. I was able to validate this shortening effect in *vps27* mutants, but only for Y'-element containing (fig. 3.2a telomeres, in agreement with Shachar et al.) and not for a X-only (fig. 3.2b, no pronounced shortening) telomere. Thus, the deletion of *VPS27* did not affect all telomeres equally. For testing whether telomerase function is disturbed in a *VPS27* deleted background, senescence and the rate of telomere shortening was recorded and compared to *est2* mutants in which telomerase-dependent telomere elongation is not working properly and therefore these mutants senesce faster [88]. The rate of senescence (fig. 3.3a) as well as telomere shortening (fig. 3.3c) was similar in *est2 vps27* double mutants compared to *est2* single mutants suggesting that telomerase-dependent telomere elongation is corrupted in *VPS27* deleted cells. Data from Chang and colleagues supports the finding of accelerated senescence for *est2 vps27* mutants as the average profile of *est1 escrt* double mutants (fig. 3.3b, dark red line) was more similar to the archetype for accelerated entry to senescence (fig. 3.3b, light blue line) than to normal senescence (fig. 3.3b, light grey line) [203] indicating that most likely a deletion of any ESCRT factor results in accelerated entry to senescence. The indications that the telomerase-dependent telomere elongation is corrupted in *VPS27* deleted cells is further underlined by data from the Kupiec laboratory showing that telomere elongation was drastically decreased in *vps27* mutants in response to ethanol [13, 240], although previous work has discovered that exposure to ethanol stress generally leads to increased telomere elongation by taking advantage of the same mechanisms as under normal conditions [199].

In addition to proper telomere elongation, telomere homoeostasis relies on a functional capping system, especially of the 3' ssDNA overhang. The Cdc13-Stn1-Ten1 (CST) complex shelters this overhang from Exo1-mediated resection as part of a DNA damage response (DDR) that is not desirable at telomeres (section 1.3.2.3 and fig. 1.13). Besides being the key player of this capping complex, Cdc13 is involved in the recruitment of telomerase during telomere replication (section 1.3.2.2 and fig. 1.12). Thus, the question arose whether and how the deletion of *VPS27* affects *cdc13-1* (capping-) defective telomeres. As *CDC13* is an essential gene, only a temperature-sensitive allele (*cdc13-1*) can be used to study *CDC13* impairment [43]. Examining the viability of the corresponding temperature-sensitive strain in combination with the deletion of *VPS27* revealed an increased viability of *cdc13-1* cells at non-permissive temperatures by this deletion (fig. 3.5). This finding is in concordance with an already reported synthetic rescue of *cdc13-1* mutants by the deletion of *HSE1* [200]. Hence, ESCRT-0 seems to protect cells from uncapped telomeres. As the 5' end of uncapped telomeres is degraded by the exonuclease Exo1 leading to a robust cell-cycle arrest (section 1.3.2.3 and fig. 3.4), a dysfunctional Exo1 would explain the rescue effect of *VPS27* deletion on *cdc13-1* defective telomeres. Degrading the 5' end of telomeres leads to an increased amount of telomeric single-stranded overhangs. Indeed, the telomeric overhang was decreased in *cdc13-1 vps27* double mutants subsequent to the induction of telomere uncapping by heat shock (fig. 3.7). Furthermore, overexpression of Exo1 in *cdc13-1 vps27* cells (but not an empty vector) abolished the aforementioned rescue effect (fig. 3.8), supporting the idea of a defective Exo1-mediated resection upon *VPS27* deletion. A malfunction of Exo1 can be caused either by decreased protein levels or improper localisation. At first, no reliable changes in the protein levels of Exo1 were neither detected in *vps27* single (figs. 3.9a and 3.9b) nor in *cdc13-1 vps27* double mutants (figs. 3.9c and 3.9d). Additionally, normal degradation of Exo1 was observed in double mutants (fig. 3.10). Due to a weak GFP-signal, imaging of GFP-labelled Exo1 in the mutants in question failed and therefore the possibility of Exo1-localisation problems as reason for the seen phenotypes cannot be excluded.

The 5'–3' resection mechanism of Exo1 is also important for the HR DSB repair pathway (section 1.2.2 and figs. 1.5 and 3.11). Hence, *vps27* cells were examined in the light of HR. On one hand, *VPS27* deleted cells were sensitive to zeocin induced DSBs (fig. 3.12) and on the other hand the growth capabilities of a HR proficient strain were slightly decreased in the presence of *VPS27* deletion (fig. 3.14). Those results point to an impaired homologous recombination upon deletion of *VPS27*. Consistent with the idea of impaired Exo1-mediated resection at uncapped telomeres, dysfunctional Exo1 action could also explain these observations. However, overexpression of Exo1 did not have any effect on the sensitivity of *vps27* mutants to zeocin (fig. 3.15).

As all results strongly suggested that Exo1-mediated resection is prevented in *VPS27* deleted cells, Prof. Longhese was asked to test the resection efficiency in those mutants. They have developed an assay to follow the 5'–3' resection activity of Exo1 after the induction of a DSB at the mating type locus [223, 229]. No difference in the resection kinetics between the wild-type and *vps27* mutants (fig. 3.16) were observed. But as the induction of the DSB was less efficient in the mutant than in the wild-type, the absence of a difference in the resection efficiency is unreliable and a resection defect is still possible. Furthermore, several experiments were conducted to verify the hypothesis of an impaired resection in *vps27* mutants. First, the deletion of *VPS27* did not rescue every temperature-sensitive yeast strain (suppl. fig. A.3). Second, the rescue of *cdc13-1* defective telomeres was not due to a checkpoint defect (figs. 3.18 and 3.20), and third, autophagy was not involved in that rescue (appendix A).

Altogether, the experimental data supports a model (fig. 4.1) in which deletion of *VPS27* diminishes Exo1-mediated 5'–3'resection of ssDNA overhangs. Although this is beneficial for dysfunctional telomeres, it impairs telomere replication and HR to repair DSBs elsewhere in the genome. In homologous recombination, Exo1-mediated resection is vital to prepare the DNA lesion for subsequent homology search and strand invasion (fig. 1.5). Improper resection renders the foundation of HR impossible, so that the main DNA damage repair pathway of S or G2 phase is suppressed, stalling the cell cycle. The hypothesis of a hampered HR mechanism is supported by the data indicating that *vps27* mutants are sensitive to DSBs induced by zeocin (fig. 3.12) and that HR proficient cells exhibited decreased viability in the presence of *VPS27* deletion (fig. 3.14). In case of 3' capping defective telomeres, the ssDNA is mistakenly recognised as DNA damage, stimulating the cell's DNA damage repair mechanisms and resulting in a robust cell cycle arrest. Dampened Exo1-mediated resection is helpful in this scenario as the amount of arising telomeric overhang by 5'–3' resection is decreased. Several findings support this model: (i) deletion of *VPS27* rescued the temperature sensitivity of *cdc13-1* mutants (fig. 3.5), (ii) *cdc13-1 vps27* double mutants had less telomeric overhangs than *cdc13-1* single mutants after induction of telomere uncapping by heat shock (fig. 3.7), and (iii) overexpression of Exo1 abolished the rescue effect. However, Exo1-mediated resection is also required during the regular replication of eroded telomeres as it reconstitutes the G-tail following DNA replication (section 1.3.2.1 and fig. 1.11). The overhang itself serves as target site for Cdc13 binding. Depending on cell cycle regulated post-translational modifications, Cdc13 forms either a complex with Est1 to recruit telomerase or with Stn1 and Ten1 to protect the telomeric overhang [241]. Hence, according to the cell cycle phase, faulty resection hinders telomere elongation (S phase) or telomeric overhang capping. Nonetheless, the proposed model is not only able to explain the observations gained in the context of a defective Cdc13 (*cdc13-1 vps27* mutants), but also explains the data pointing to an improper telomerase-dependent telomere elongation in *vps27* mutants (figs. 3.2 and 3.3). Only the improved viability of *cdc13-1 exo1 vps27* mutants (fig. 3.17) indicating independence of Exo1 and Vps27 argues against the described model.

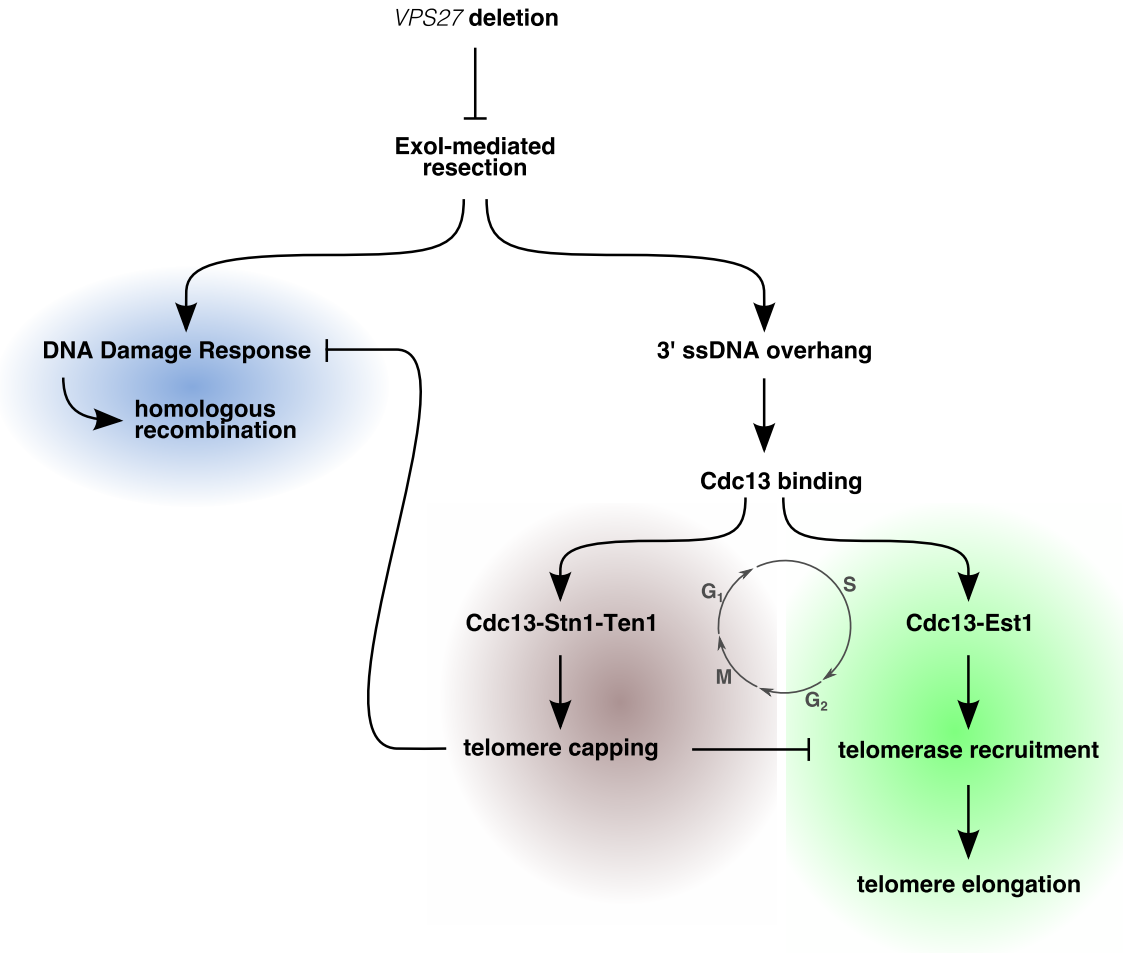

Figure 4.1.: Model of impaired Exo1-mediated 5'–3' resection by the deletion of *VPS27* which is beneficial for dysfunctional telomeres, but impairs telomere replication and homologous recombination to repair DSBs elsewhere in the genome. Proper Exo1-mediated resection at DSB sites is required to prepare the lesion for subsequent homology search and strand invasion. Otherwise homologous recombination is not possible. Uncapped telomeres are recognised as DNA damage, initiating DNA damage response (DDR). 5'–3' resection is fundamental to regular telomere replication. Following DNA replication, it reconstitutes the telomeric overhang that serves as binding site for Cdc13. Depending on the cell cycle stage, Cdc13 is either bound in a complex with Est1 to recruit telomerase or it forms the Cdc13-Stn1-Ten1 (CST) capping complex to shelter the G-tail from unfavourable DDR mechanisms. Grouping is indicated by coloured backgrounds.

4.1.2. Rather the Whole ESCRT System Than Only *VPS27*?

Based on the fact that only nine out of nineteen ESCRT factor encoding genes were enriched in the *TLM* gene list I decided to test whether all or only some ESCRT factor deletions lead to a rescue of *cdc13-1*'s temperature sensitivity and show a decreased resistance to DSBs. Experimental data from the present thesis and existing data from the *Saccharomyces* Genome Database database suggest that the whole ESCRT family is rescuing a *cdc13-1* defective telomere-cap (suppl. fig. B.7) and that any ESCRT factor deletion results in increased sensitivity to DNA double-strand breaks (figs. 3.12 and 3.21). The assumption that the whole ESCRT system is necessary for proper maintenance of telomere length is strongly supported by data from Vera Babin: In her work it was observed that all *escrt* mutants exposed to ethanol stress show a weaker response to ethanol than the wild-type, whereas *vps27* and *snf8* exhibited the strongest effects [13, 240]. Moreover, the telomere elongation kinetics of six *escrt* mutants (*vps27*, *snf8*, *vps20*, *snf7*, *did4*, *doa4*) in the presence of a Cdc13-Est1 fusion protein were evaluated. This fusion protein enforces telomerase to be tethered to

the telomeric overhang that results in vigorous telomere elongation in wild-type cells [242]. Usage of this fusion protein allows distinguishing between defective telomerase recruitment and malfunctioning telomerase activation. Tethering telomerase to the telomere would bypass a defective recruitment mechanism and lead to wild-type levels of telomere elongation. However, if activation of telomerase is affected by the deletion of a particular *ESCRT* gene, telomere elongation would be still reduced in the presence of this Cdc13-Est1 fusion protein. In comparison to wild-type levels, telomere elongation was still reduced in all tested *escrt* mutants, even with the fusion protein. The same held true under ethanol stress in the presence of the Cdc13-Est1 fusion protein in *vps27* and *snf7* mutants [13,240]. According to the rationale of the fusion protein assay, those observations would assume that ESCRT factors are required for the activation of telomerase. Nevertheless, a defective Exo1-mediated resection could lead to an insufficient single-stranded overhang, which is a prerequisite for telomeric Cdc13 binding and subsequent telomere elongation. Therefore, the model proposed in fig. 4.1 explains the decreased telomere elongation response upon deletion of any ESCRT factor, especially *VPS27*, as well as the results from the Cdc13-Est1 fusion protein assay.

For the purpose of gaining more insights into the functional relationship of telomere length maintenance and the ESCRT system, several *in silico* analyses were performed. First, an investigation of the protein-protein-interactions (PPIs) between the ESCRT system and telomere related proteins (TRPs) revealed that only the ESCRT-0 complex and Stp22 (ESCRT-I) are densely connected to the set of TRPs (fig. 3.23). Putting it more precisely, Vps27 is linked by seven protein kinases (PKs) in parallel to Cdc13. This enrichment for PKs yielded a p-value of 8.4e−3. Second, deletion of any *ESCRT* gene did not influence the expression of TRP encoding genes (fig. 3.25). A GSEA highlighted pathways that are known to be up- or down-regulated in response to stress (fig. 3.26), but gave no new insights into the relationship of TLM and the ESCRT family. Keeping the manifold cellular sites in mind that the ESCRT system is acting on, it is plausible that its disruption leads to a stress response. Finally, a dataset of genetic interaction scores for *cdc13-1 yfgΔ* [201] was checked for genes whose deletion have similar effects on *cdc13-1* mutants like the *ESCRT* deletions. As the ESCRT factors are spread all over the range of *cdc13-1* defect suppression levels (fig. 3.27) and do not cluster with particular genes, I decided not to look further into the neighbouring genes.

In conclusion, the present dissertation enriches the current knowledge and understanding of telomere length maintenance with a model of hampered Exo1-mediated resection by the deletion of *VPS27* (fig. 4.1) and the plausible hypothesis that the whole ESCRT system is required for proper telomere length maintenance. The model integrates the *cdc13-1* rescue with the observed telomerase defect. Impaired Exo1-mediated resection results in too little 3' overhang such that Cdc13 binding is suppressed, preventing either telomerase recruitment or telomeric overhang capping (according to cell cycle phase). Furthermore, a PPI network analysis revealed that Cdc13 and Vps27 are tightly interlinked by several PKs in parallel, leaving room to speculate that they serve in a feedback loop to regulate telomere homoeostasis via the ESCRT machinery, whereat Vps27 represents the entry point to it. Indeed, Morvan and co-workers showed that recruitment of the ESCRT machinery depends on the phosphorylation of Vps27 [243].

4.2. Future Perspectives

As pointed out in section 1.5.1, *Saccharomyces cerevisiae* serves as an excellent model organism to study telomere biology. Both, telomere length maintenance and the ESCRT

system share many structural and functional characteristics between yeast and mammals. A major difference is that the ESCRT factors are essential to mammals [155], which is not the case for yeast cells. This fact has to be kept in mind when transferring knowledge about the ESCRT family from baker's yeast to mammals. It is quite likely that "most dominant ESCRT mutations [...] cause prenatal death" [155] and that under stress-free conditions one intact allele of an ESCRT factor encoding gene is sufficient to maintain viability. Moreover, disruption of ESCRT factors bears potential oncogenicity [155]. However, data from various model organisms and tumour samples have as yet failed to find "a unifying concept of how the ESCRT machinery or loss thereof would contribute to cancer" [244]. In general, the role of ESCRT factors in tumourigenesis can be accounted for by either deregulated mitogenic signalling (sustained receptor signalling due to lack of endocytosis) [107, 244] or cytokinetic defects resulting in aneuploidy [155,244].

Having found evidence that the ESCRT machinery is involved in telomere length homoeostasis, ESCRT factors could represent new targets to tackle telomerase reactivation and up-regulation in tumour cells which is a well-known hallmark of human cancer [95], after all 85–90 % of them show telomerase up-regulation. Additionally, the inhibition of one or multiple ESCRT factor(s) could be used to hyper-sensitise cells to DNA damage. This in turn could be combined with radio- or chemotherapy inflicting damage to kill cancer cells. Hyper-sensitising cells to DNA damage might allow lower dosage of chemotherapeutics or x-rays. As most of the ESCRT factors are associated with human diseases to a varying degree (section 1.4.4 and Stuffers et al. [155]), and as the ESCRT system is involved in various critical cellular processes (section 1.4.1), targeting the whole ESCRT system is not advisable. Especially, artificial disruption of ESCRT-III and associated proteins would be difficult to control in mammals due to their involvement in crucial nuclear functions (chromatin remodelling [129], chromosomal segregation [130], and nuclear envelope reformation [127]) and cytokinesis [106, 119–121]. In addition, ESCRT-III is the most ancient and conserved ESCRT complex [107, 109], and sufficient to achieve minimal ESCRT function [103, 133], which is emphasising its requirement. Compared with that, ESCRT-0 is well-suited for additional examinations to test its suitability as drug target. First, it has evolved rather recently [109,133] and might therefore be substitutable more easily and cells may cope better with its loss. Second, up to now ESCRT-0 is not associated with any of the aforementioned nuclear functions or ESCRT functions beyond MVB, that is its dysfunction might not cause side effects as severe as in other ESCRT disruptions. The suitability of ESCRT-0 as an anti-cancer drug target is further strengthened by data from Toyoshima and colleagues showing that Hgs (mammalian homologue of Vps27) is up-regulated in several tumour entities (e.g. melanoma, cervix, and liver) and that its down-regulation by siRNA "reduced the tumourigenic potential" [244,245]. Nevertheless, observations made in the present thesis in *S. cerevisiae* have to be thoroughly verified when translated to humans or mammals in general.

Nonetheless, additional experimental investigations of the association between telomere length maintenance and the ESCRT system in yeast would be advisable to strengthen and to expand the current findings. Exploring the effect of an ESCRT inhibitor on *cdc13-1* cells in yeast would be interesting as this would mimic the deletion of an ESCRT factor and could limit them to the most promising drug targets. Yibmantasiri et al. reported a compound — neothyonidioside — that causes the same morphological defects as the deletion of *VPS27* or *VPS17* [204]. To the best of my knowledge, this is the only compound specifically targeting a member of the ESCRT family in baker's yeast. All other available drugs inhibit the whole endocytosis pathway which is not appropriate.

I chose *VPS27* for an in-depth experimental analysis leading to the model just discussed (fig. 4.1). *VPS27* was also amongst the ESCRT factors with the strongest phenotypes in terms of non-responsiveness to ethanol stress or in the presence of a Cdc13-Est1 fusion protein [13, 240]. Although the presented data strongly supports this model, it would be beneficial to further verify it. The lack or decrease of resection in *vps27* mutants has to be established and potential localisation problems of Exo1 should be examined with an approach allowing better resolution and accuracy. Establishing the localisation route of Exo1 from the cytosol (site of translation) into the nucleus would be beneficial, too, as this could provide new indications if and at which point ESCRT factors or only Vps27 might interfere. Another follow-up strategy could be visualisation of Vps27 and tracking it in *cdc13-1* cells before and after induction of telomere uncapping. In any case it will be important to continue to compare *vps27* mutants with *cdc13-1 vps27* and *cdc13-1* mutants (dysfunctional telomeres) as well as with the wild-type (as control). Of course, all proposed follow-ups could be performed with other *escrt* mutants, too, albeit *VPS27* is the most promising target due to the current findings and its role within the ESCRT machinery.

A Supplemental Experiments

Additional Experiments to Explore the Association of TLM and the ESCRT System

In the context of this work and in addition to the experiments presented in chapter 3, several further experiments were conducted to investigate assumptions raised by previous experiments, but not following the main research scope of the present thesis.

Exo1 Overexpression Does Not Rescue Y'-Telomere Length in *vps27* Mutants

Shachar et al. reported a telomere shortening effect upon *VPS27* deletion for Y'-element containing telomeres [195] that was also visible in the telomere length measurements presented in fig. 3.2. Having received multiple hints that Exo1 might be malfunctioning in *VPS27* deleted cells, I examined whether overexpressing *EXO1* in *vps27* mutants rescues the telomere shortening. Therefore, the same galactose-inducible *EXO1* overexpression plasmid or the respective empty vector control as used in section 3.2.3.2 was introduced into the wild-type and *vps27* mutants. Afterwards, the resulting strains were grown for at least 150 generations by serial restreaks on SGalRaf-Leu plates. The DNA from all strains was extracted and subjected to telomere PCR to measure the length of six Y'-telomeres. Figure A.1 represents the quantification of the underlying agarose gel (fig. B.9).

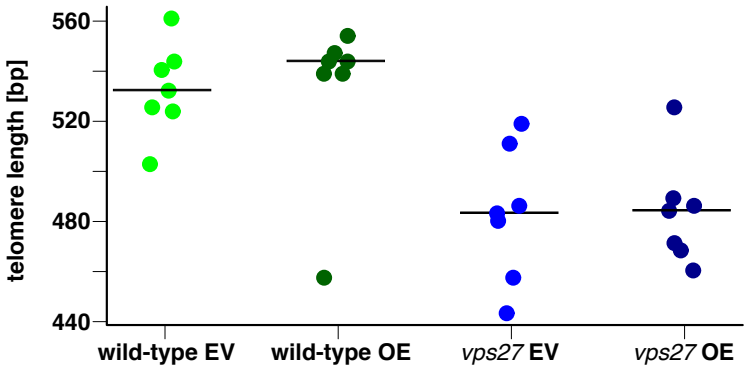

Figure A.1.: Quantification of the telomere PCR (fig. B.9) for wild-type and *vps27* cells containing either an *EXO1* overexpression plasmid (OE) or the corresponding empty vector control (EV) measuring the length of six Y' telomeres. The bars represent the median of the respective data points.

According to the quantification in fig. A.1, the telomere length was not affected by overexpressing *EXO1*. This experiment was only conducted for Y'-element containing telomeres, as the X-only telomere length difference (fig. 3.2b) was not as pronounced as for the Y'-telomeres (fig. 3.2a).

Slight Rescue of *STN1* Defect by Deletion of *VPS27*

As Cdc13 is part of the Cdc13-Stn1-Ten1 (CST) complex capping the telomeric overhang, the question arose whether deletion of *VPS27* does only rescue a *cdc13-1* capping-defective telomere or if the remaining CST subunits exhibit the same effect. Therefore, a temperature-sensitive allele of *STN1* (*stn1-13*) was utilised, because all three genes encoding the different CST subunits are essential. Equivalently to the viability spotting assay for the *cdc13-1 vps27* mutant, a *stn1-13 vps27* mutant was constructed and examined for its viability at non-permissive temperatures ($> 30\,°C$).

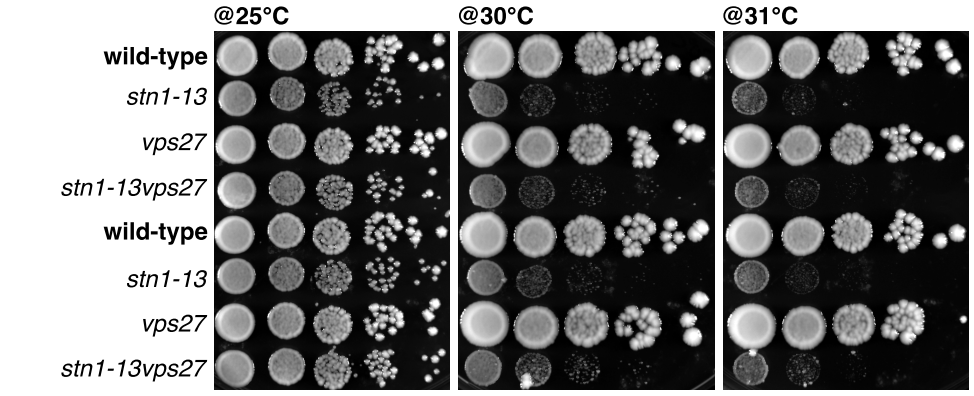

(a)

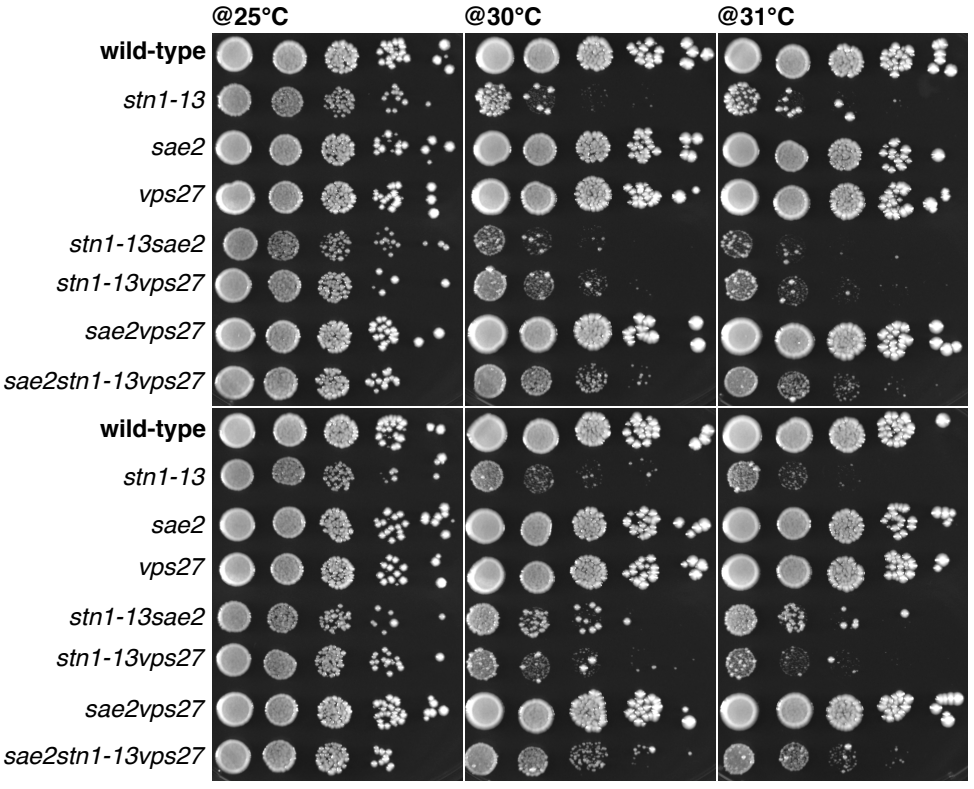

(b)

Figure A.2.: Temperature rescue spotting at the indicated temperatures. Wild-type cells and cells of the indicated mutants were spotted in duplicates in 10-fold serial dilutions onto standard YPD plates and incubated for (a) three or (b) four days.

However, this double mutant did not show any clear increase in viability and the viability of the *stn1-13* single mutant was quite weak at non-permissive temperatures (fig. A.2a). Cells harbouring the *stn1-13* allele are generally less viable than *cdc13-1* mutants as the defect of the *stn1-13* allele is more severe. Although CDC13 is essential, too, the point mutation in *stn1-13* mutants causes a stronger deactivation of the respective protein, resulting in stronger phenotypes than in *cdc13-1* mutants. Introducing a deletion of *SAE2* slightly improves the viability of *stn1-13* mutants because this diminishes nuclease activity at uncapped telomeres. As described in section 1.3.3, Sae2 is another nuclease acting at sites of ssDNA ends, such as uncapped telomeres. I performed a viability spotting assay of all derivatives from crossing a *stn1-13 vps27* double mutant to a *sae2* mutant. The triple mutant exhibited increased viability at higher temperatures compared to the single mutant *stn1-13* (fig. A.2b), pointing to a rescue effect of *VPS27* deletion on any CST telomere capping defects.

Rescue by The Deletion of *VPS27* is Specific to The CST Complex

In order to ensure that the deletion of *VPS27* is not rescuing every temperature-sensitive mutant, I randomly chose three strains from the temperature-sensitive collection and the *vps27 yfts* double mutant was constructed with each of them. All genotypes derived from the individual crossings were examined in a viability spotting assay at different temperatures.

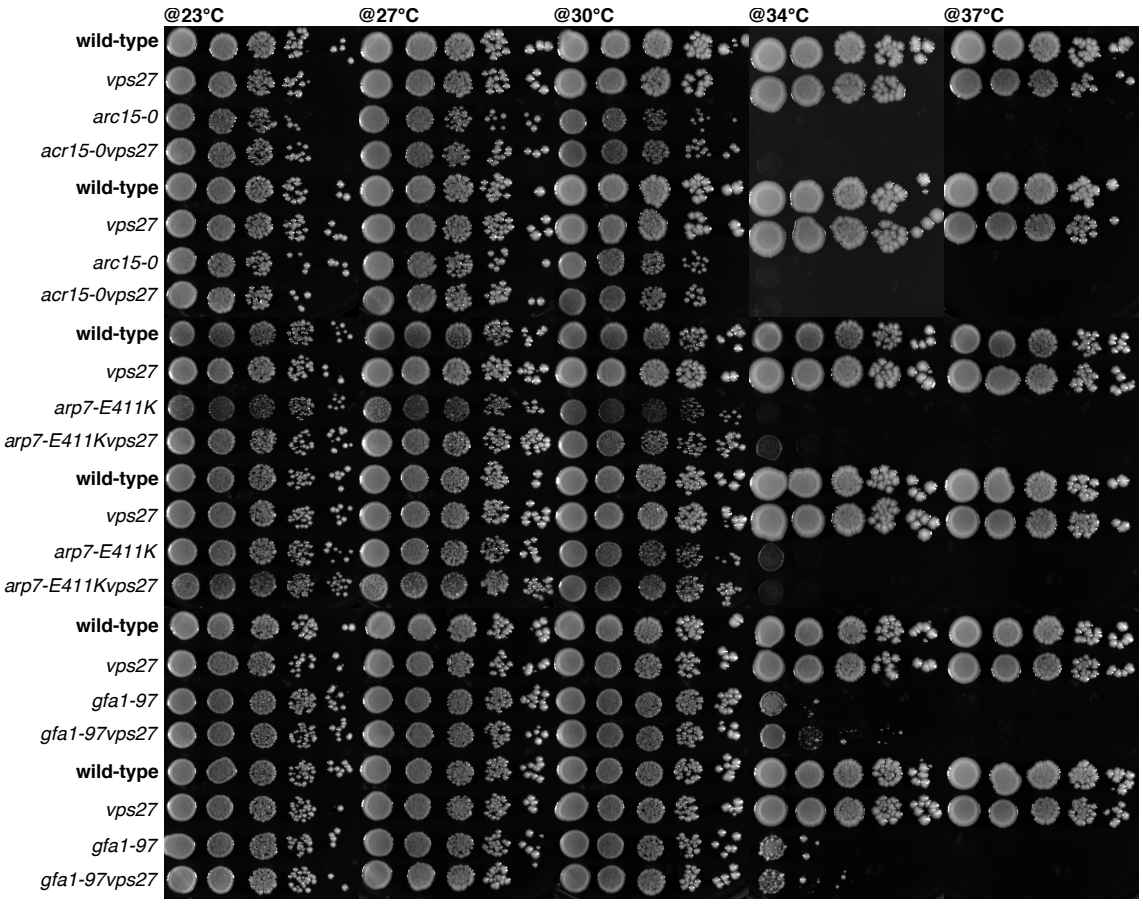

Figure A.3.: Spotting assay for testing the viability of randomly chosen temperature-sensitive mutants at higher temperatures in the presence of *VPS27* deletion. Cells of the indicated genotypes were spotted in duplicates 10-fold serially diluted onto standard YPD plates and incubated for three days.

From comparing the growth spots of the individual temperature-sensitive single mutants and the corresponding double mutants in fig. A.3, it became apparent that the deletion of *VPS27* is not enhancing the viability of every temperature-sensitive mutant. Hence, the rescue effect for *cdc13-1* mutants reported herein was not just arbitrary.

Cdc13 Protein Levels in *VPS27* Deleted Cells

The protein levels of Cdc13 in *vps27* mutants were measured after growth to exponential phase under standard conditions (YPD medium, 30 °C). This Western Blot strongly suggests decreased levels of Cdc13 upon deletion of *VPS27*.

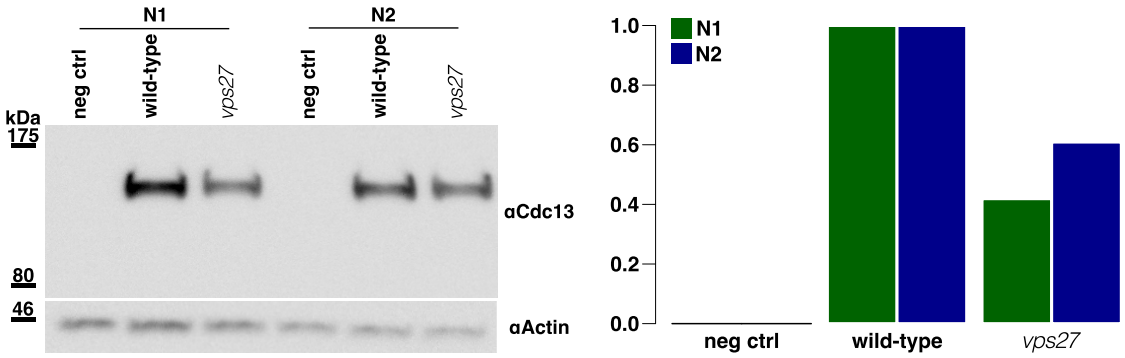

(a) Western Blot. (b) Quantification.

Figure A.4.: Western Blot for measuring Cdc13 protein levels in *vps27* mutants. Protein samples were collected after growth to exponential phase at 30 °C. Protein levels were measured for two biological replicates. (a) shows the underlying membrane quantified in (b). The upper lane of the membranes represent the Cdc13 signal and the lower lanes correspond to actin as loading control. The quantification indicates the relative amount of Cdc13 over actin. Figure B.10d depicts the corresponding Ponceau staining.

Autophagy Does Not Link ESCRT Factors And Telomere Homoeostasis

One possible explanation for the association of ESCRT factors and telomere maintenance was autophagy. "Studies of nematodes, flies and mammals have revealed that the ESCRT machinery has a role in autophagy [142]" (see also section 1.4.2.2). It has been shown that the disruption of the ESCRT machinery leads to autophagosome accumulation and neurodegenerative diseases [124, 143, 144]. Furthermore, Djeddi et al. have found evidence that in *escrt* mutants autophagy is induced as adaptive response for cell survival to counteract the formation of enlarged endosomes [126]. Moreover, Robert and colleagues have reported that Exo1 and Sae2 are degraded via the autophagy pathway [246, 247], indirectly linking telomere homoeostasis to autophagy. Figure A.5a summarises the aforementioned associations.

In order to explore whether autophagy is linking the ESCRT system to telomere maintenance, an *ATG5* deletion strain and the *cdc13-1 vps27* double mutant were crossed. Deletion of *ATG5* has previously been described to effectively block autophagy in yeast and mammalian cells [248–250]. The constructed triple mutant *atg5 cdc13-1 vps27* and the corresponding single and double mutants were examined together with the wild-type in a temperature rescue spotting. In fig. A.5b the triple mutant slightly surpassed the *cdc13-1 vps27* double mutant in its growth abilities, suggesting that autophagy is not involved in the functional association of *VPS27* deletion and its rescue of *cdc13-1* capping-defective telomeres.

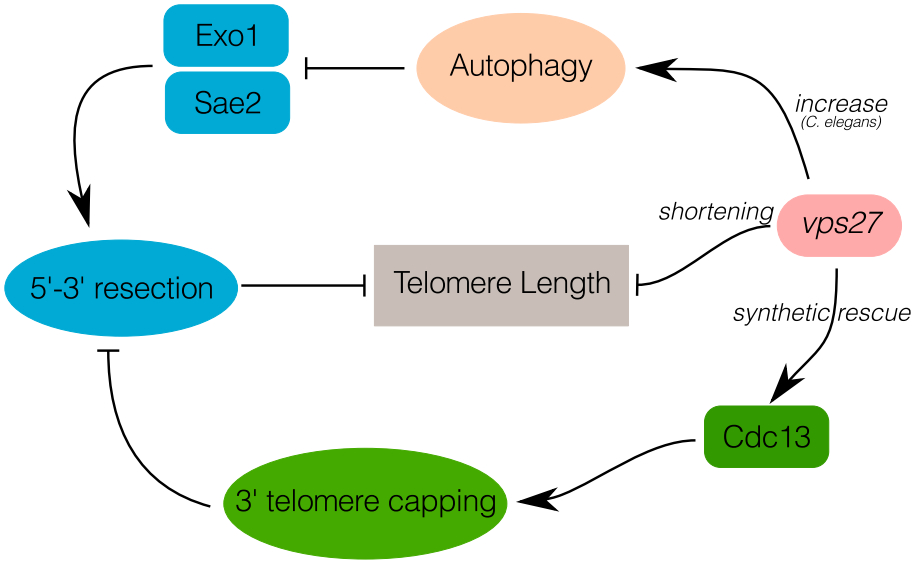

(a) Autophagy and its links to TLM and the ESCRT system.

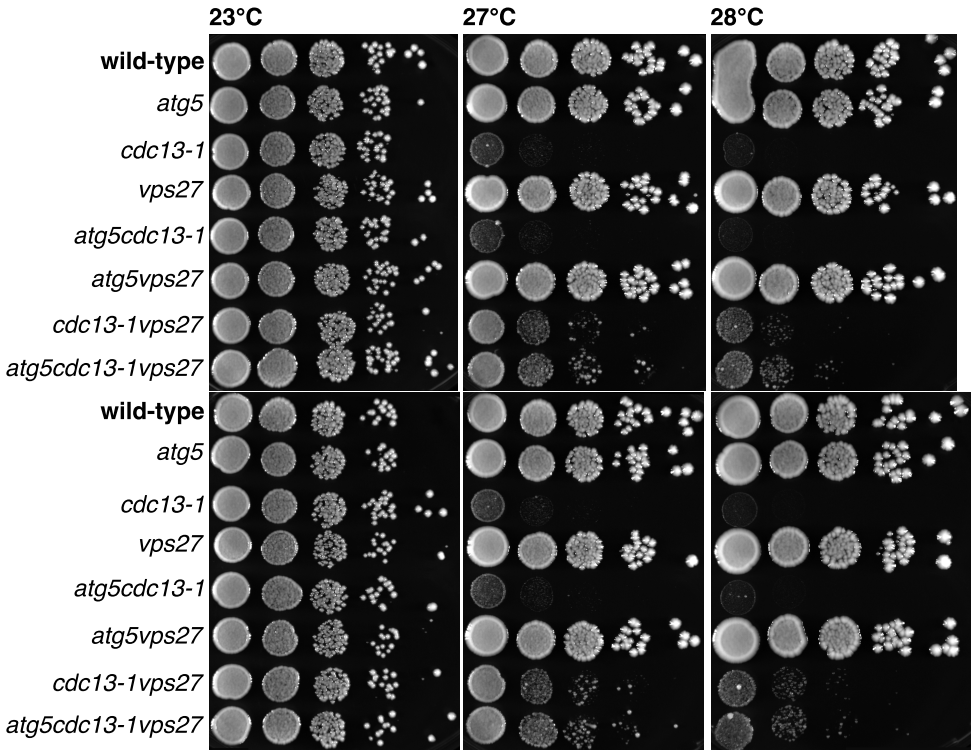

(b) Temperature rescue spotting.

Figure A.5.: (a) Schematic summary of the associations of autophagy to the ESCRT system and telomere homoeostasis. Deletion of any ESCRT factor leads to autophagosome accumulation [124, 126, 143, 144] and induces autophagy [126]. Besides, Exo1 and Sae2 are degraded via autophagy [246, 247]. (b) Viability spotting at different temperatures of the indicated mutants and the wild-type. Cells were spotted in duplicates 10-fold serially diluted onto standard YPD plates that were incubated for three days.

in silico Analysis of The Relation between *TLM* And Ageing in *Saccharomyces cerevisiae*

Data from the following section contributed to the manuscript "The relationship between telomere length, cellular aging and fitness in *Saccharomyces cerevisiae*" by Harari et al. that is currently in preparation [14].

As discussed in section 1.3.4, telomere erosion plays a critical role in ageing. I briefly explored the relation of *TLM* genes and the genes related to life span in baker's yeast. Since more than fifty years budding yeast serves as model organism to study cellular and organismal ageing while harbouring two different types of ageing [251–253]. The number of daughter cells stemming from one mother cell prior to senescence is defined as replicative ageing (RA) or ageing (proliferative capacity) [251, 254, 255]. Chronological ageing (CA) describes "the length of time that a non-dividing yeast cell survives" [255]. Hence, yeast allows studying both mitotic (e.g. epithelial or stem cells) and post-mitotic cells (e.g. muscles and brain) individually and in parallel within a simple unicellular organism [251, 254, 255].

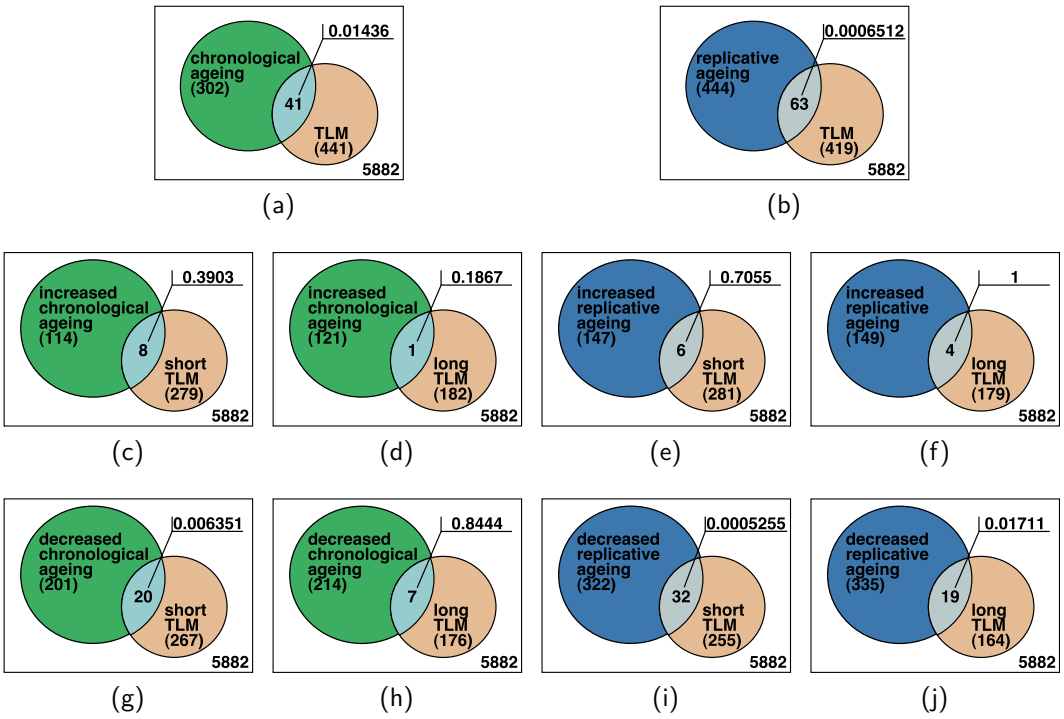

Figure A.6.: Overlap of *TLM* and ageing related genes. Venn diagrams showing the overlap of genes associated with telomere length maintenance and (a) chronological ageing or (b) replicative ageing. The p-values were calculated with a Fisher's Exact test. Please note that the complete set of *TLM* genes in panel (a) and (b) contains additional *TLM* genes for which no telomere phenotype was annotated.

The Animal Ageing and Longevity Database (AnAge) [1] combines curated data on ageing and life span in animals, inter alia data about the RA and CA of *S. cerevisiae*. Thus, I used this database for evaluating the overlap of *TLM* genes with genes affecting life span in yeast. Forty-one *TLM* genes have been annotated to affect chronological life span ($P = 0.014$, fig. A.6a), whereas 63 *TLM* genes have been associated with replicative ageing ($P = 0.001$, fig. A.6b). As expected, genes whose deletion led to telomere shortening were clearly enriched for decreased RA ($P = 0.001$, fig. A.6i), as well as for decreased CA ($P = 0.006$, fig. A.6g). There was no significant enrichment of short *tlm* mutants, increased CA ($P = 0.390$, fig. A.6c), or RA ($P = 0.706$, fig. A.6e). In addition, long *tlm* mutants were

not significantly associated with increased RA (P = 1, fig. A.6f) or CA (P = 0.187, fig. A.6d). Interestingly, nineteen gene deletions have been annotated with decreased RA and their deletion led to telomere lengthening (P = 0.017, fig. A.6j). In contrast to this observation, there was no significant relation between long *tlm* mutants and decreased CA (P = 0.844, fig. A.6h).

Table A.1.: Genes associated with telomere length maintenance and ageing. Genes occurring multiple times are marked as follows (ageing phenotype – *tlm* phenotype): il, increased-long, ds, decreased-short, dl, decreased-long. Gene symbols used in this table do not occur in the list of approved gene symbols.

	TLM Phenotype	**Gene Symbols**
chronological ageing		
increased	short	*ADE12*, *CSR2*, *PDX3*, *PRS3*, *RNH201*, *TLC1*, *VPS75*, *YTA7*
	long	*CYR1*^{il}
decreased	short	*APE3*, *ARF1*, *HDA2*, *MEC1*, *MRE11*, *MRPL38*^{ds}, *MRT4*, *NMD2*, *PHO85*^{ds}, *RAD50*, *RPL13B*, *SAP30*, *SGF73*, *SIF2*, *SIR3*, *UPF3*, *VPS41*^{ds}, *YEL033W*, *YKU70*^{ds}, *YKU80*
	long	*ARD1*, *MAK10*^{dl}, *RAD27*, *SSN3*^{dl}, *TIF1*, *TIF2*, *YBR284W*
replicative ageing		
increased	short	*IPK1*, *PMR1*, *RPL12B*, *RPL1B*, *RPL34B*, *URE2*
	long	*CYR1*^{il}, *IPK1*, *RPS18A*, *TIF1*
decreased	short	*ARG2*, *CTK1*, *DOA4*, *DUN1*, *GTR1*, *HST1*, *LDB19*, *LST7*, *MRPL38*^{ds}, *PCL6*, *PCP1*, *PHO85*^{ds}, *RPN4*, *RPP1A*, *SMI1*, *SWD1*, *SWD3*, *TFP1*, *TLC1*, *UBP8*, *VAM7*, *VPS20*, *VPS21*, *VPS25*, *VPS27*, *VPS34*, *VPS41*^{ds}, *WHI2*, *YFH1*, *YIL077C*, *YKU70*^{ds}, *YPT7*
	long	*ATG17*, *CDC13*, *CDH1*, *FMP26*, *HSP104*, *MAK10*^{dl}, *MAK3*, *MED1*, *NSR1*, *PUB1*, *RIF1*, *RPS17A*, *RPS27B*, *RPS4A*, *RPS4B*, *SOL2*, *SSN3*^{dl}, *VRP1*, *YPL105C*

Table A.1 lists all genes found within the phenotype specific overlaps. Most of these genes occurred only in one overlap. However, ten genes were members of two different intersections. Of those ten, three indicated heterogeneous knock-out effects. *TLC1* deletion showed telomere shortening and increased CA, but also decreased RA. Deletion of *TIF1* led to telomere lengthening and decreased CA, but also increased RA. *IPK1* deletion has been associated with an increase in RA and has been annotated with both, a long and a short *tlm* phenotype (within the original *TLM* gene list).

The laboratory of our Israeli cooperation partner Prof. Martin Kupiec has investigated the relationship of TLM and life span experimentally. Their data revealed mainly that chronological ageing is not affected by telomere length, although my enrichment analyses found telomere shortening to be associated with decreased chronological ageing (fig. A.6g). In general, most of the overlaps between ageing related and *TLM* genes were not significant and those that were significant comprised more or less expected intersections. Knowing that upon a critical shortening of telomeres cells enter senescence (fig. 1.16), the intersection of decreased RA and short *tlm* mutants was not surprising (fig. A.6i). Only the association of decreased RA and long *tlm* mutants was counter intuitive (fig. A.6j). An enrichment test with the nineteen genes corresponding to the latter overlap

for pathways or GO terms using the YeastMine functionality [192] revealed no significant results.

Materials and Methods Data processing and analyses were performed using R [206]. The complete ageing data table for yeast (HAGR-ID 04235) was downloaded from the AnAge database, build 17 [1]. This data set consisted of 825 genes of which 362 were related to chronological ageing and 551 to replicative ageing. Some genes (88) were annotated to affect both ageing types. Genes with contradictory life span annotations were excluded from the analysis.

For overlap examinations, the systematic open reading frame identifiers (ORF IDs) were used. If required, identifier mappings were applied using the Bioconductor [207] package for yeast annotations (*org.Sc.sgd.db* [208]). After partitioning into replicative and chronological ageing subsets, enrichment of *TLM* genes was calculated individually in both. Statistical significance of the intersections was calculated with the default two-sided Fisher's Exact test of R [206]. Venn diagrams were created using Inkscape (v0.48, inkscape.org).

B

Supplemental Figures

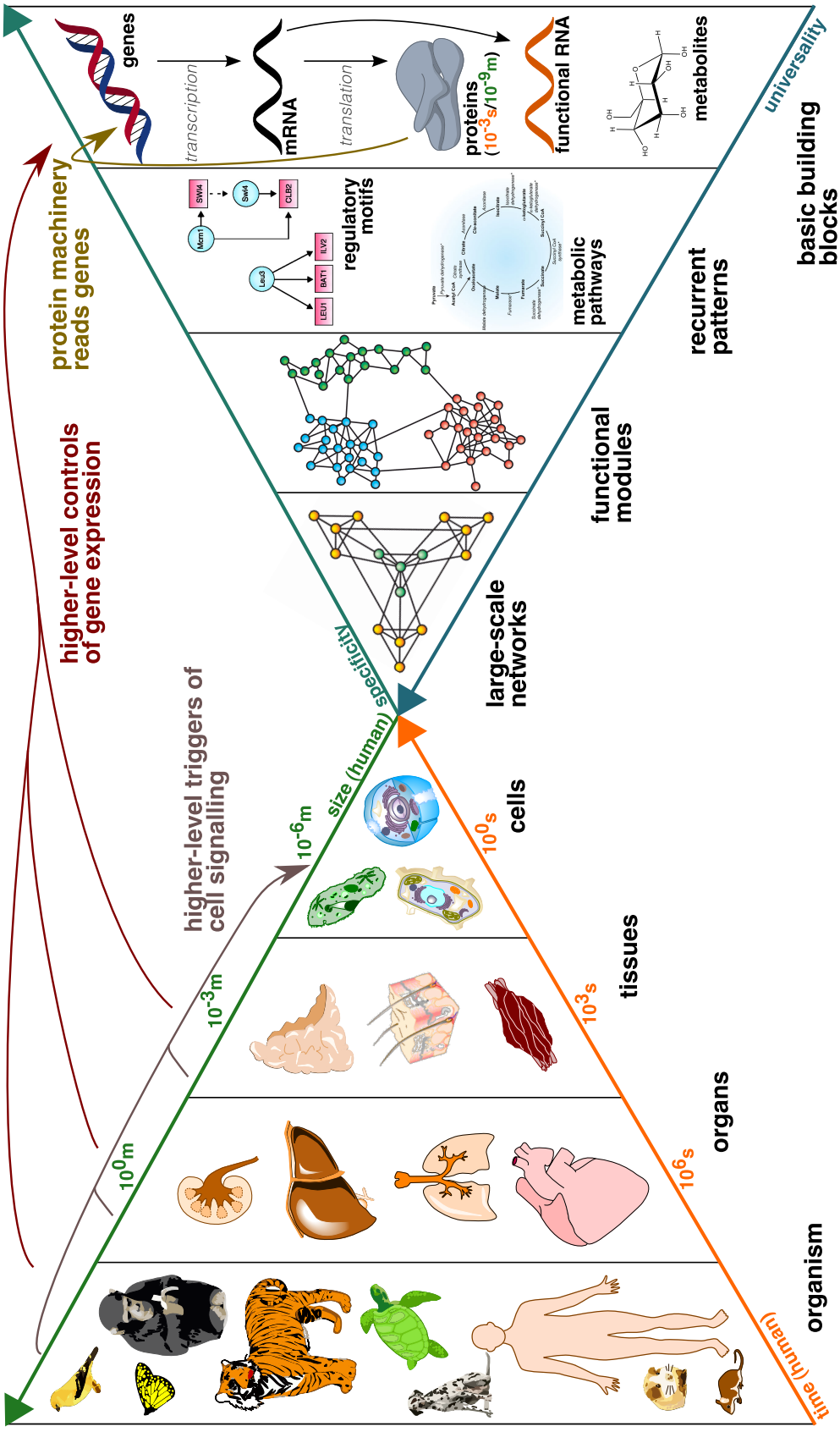

Figure B.1.: Complexity of life is defined by the interplay of diverse levels. (Enlarged version of fig. 1.1.) See next page for the detailed caption.

Figure B.1 (continued from previous page): From left to right, we zoom from the organism into its cells that are composed of a hierarchy of different levels. Cellular functions are "distributed among groups of heterogeneous components that all interact within larger networks" [19]. These larger networks consist of functional modules that are formed by either genetic-regulatory motifs or metabolic pathways. The basic building blocks for those components are metabolites or gene products encoded in an organism's genome. "Loops of interacting downward and upward causation can be built between all levels of biological organisation" [18]. This is already apparent on the very lowest level: the protein machinery decodes genes which in turn encode proteins. The time and size scale on the left apply for various levels of the human body. The figure has been devised on the template of the life's complexity pyramid presented by Oltvai and Barabási [19] and extended with ideas of the causal chain of life by Denis Noble [18]. It has been drawn using biological entities from ChemDraw Professional except for the regulatory motifs [22], the TCA cycle [23], and the functional modules as well as the large-scale network [19].

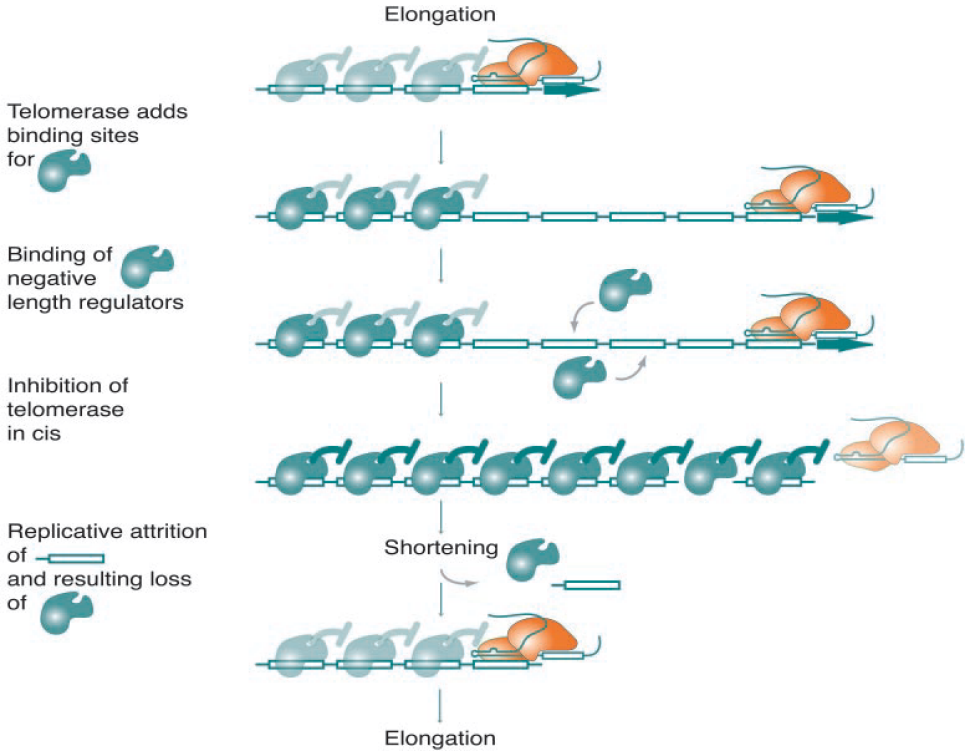

(a) *cis* regulation of telomere length.

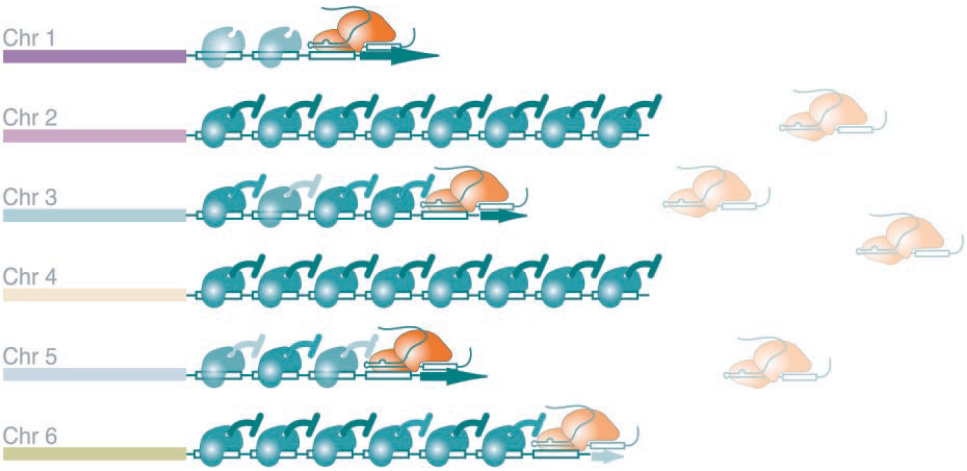

(b) Different telomere length states within one nucleus.

Figure B.2.: Telomere length homoeostasis is achieved by a negative feedback loop involving Rap1, Rif1, and Rif2. (a) Principles of the *cis*-acting telomere length regulation. Telomerase action increases the number of bindings sites for Rap1 that is recruiting Rif1 and Rif2. The more Rap1-Rif1-Rif2 complexes are bound to the telomere, the stronger telomerase is inhibited. Due to suppressed telomerase, telomeres shorten leading to the loss of Rap1 binding sites and reactivation of telomerase. In this manner, telomeres are kept in a dynamic length equilibrium. (b) Within one nucleus, telomeres of different lengths exist and not all telomeres are replicated in the course of one cell cycle. Only short telomeres are elongated, as for them the suppressive capacity of the Rap1-Rif1-Rif2 complexes has diminished. This model has been widened by Teixeira et al. by the knowledge how telomerase is inhibited (fig. 1.14). The figure has been taken from Smogorzewska and de Lange [63].

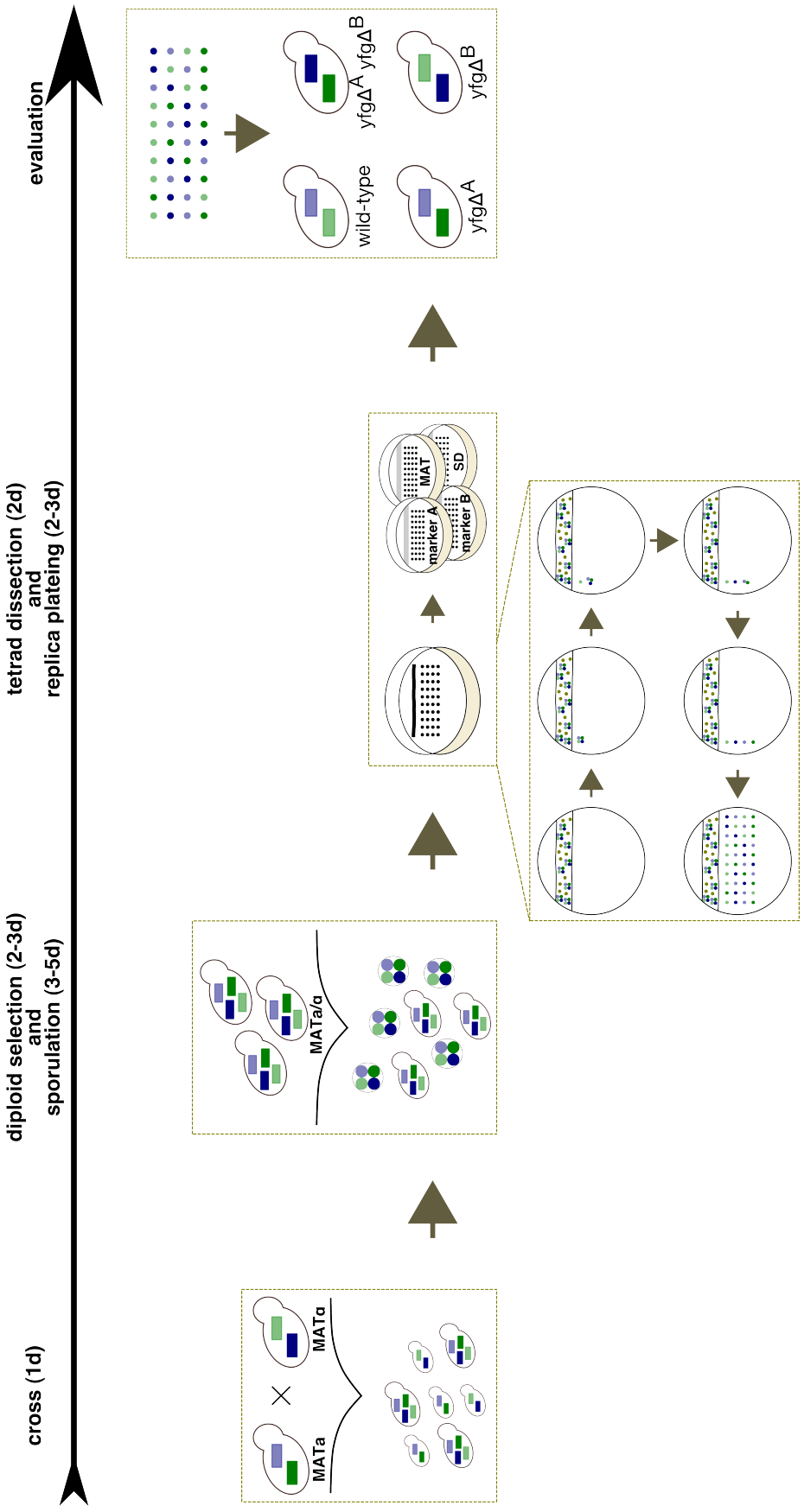

Figure B.3.: General preparatory workflow to derive mutants from crossing haploid strains. (Enlarged version of fig. 2.3.) See next page for the detailed caption.

Figure B.3 (continued from previous page): Depicted are the four basic building blocks for deriving a new mutant. Numbers in parentheses represent the amount of incubation days required for a particular step. Initially, two haploid strains of different mating types and carrying the desired genotypes or tags that shall be combined are crossed. Diploid selection on double selective plates allows growth only for diploids which are induced to sporulate and thus undergo meiosis. The four haploid ascospores of one ascus or tetrads are divided by micromanipulation and dissection. As soon as the dissected ascospore colonies have grown to sufficient size, they are replica plated on the corresponding selective plates whose evaluation allows the genotype assignment to the individual spore colonies. The visualisation for tetrad dissection has been adapted from Sherman [194].

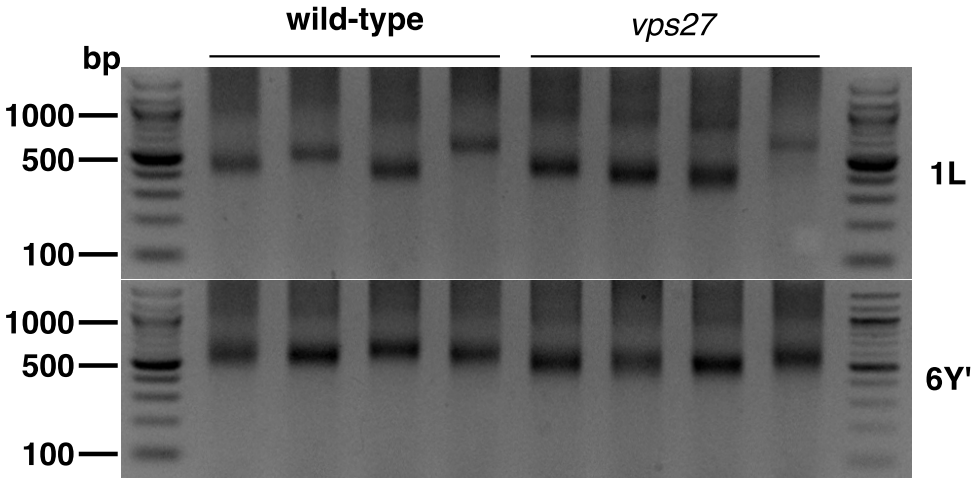

Figure B.4.: Image of the agarose gel quantified in fig. 3.2 for measuring telomere length for wild-type and *vps27* cells of six Y' telomeres as well as of the 1L telomere. The gel was run for 30 min at 100 V. As the fourth lane for the *vps27* mutant and 1L telomere gave no clear band, it was not quantified.

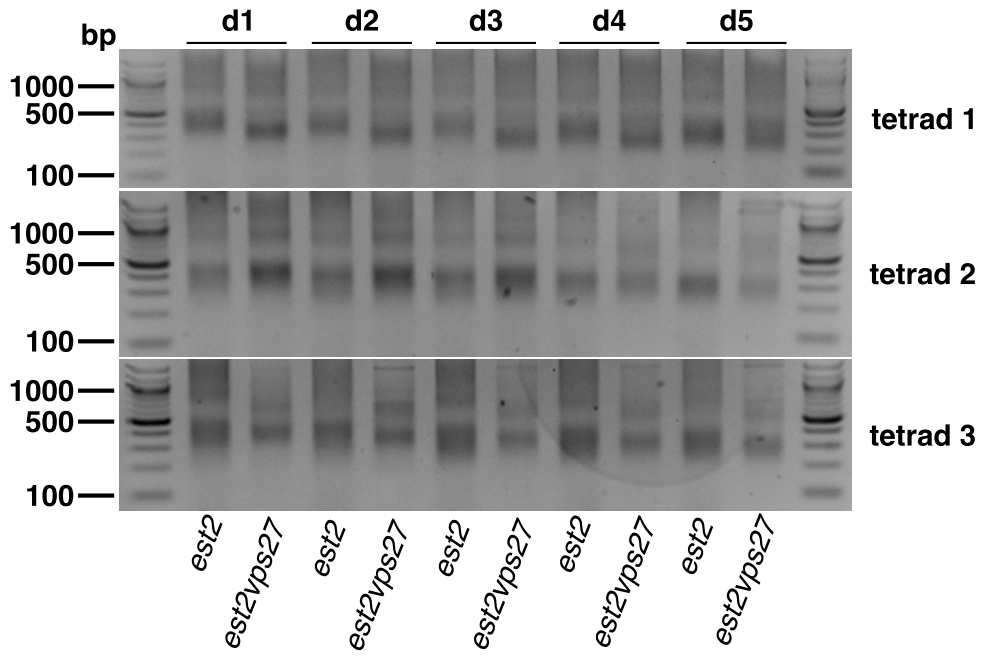

(a) 6 Y' telomeres.

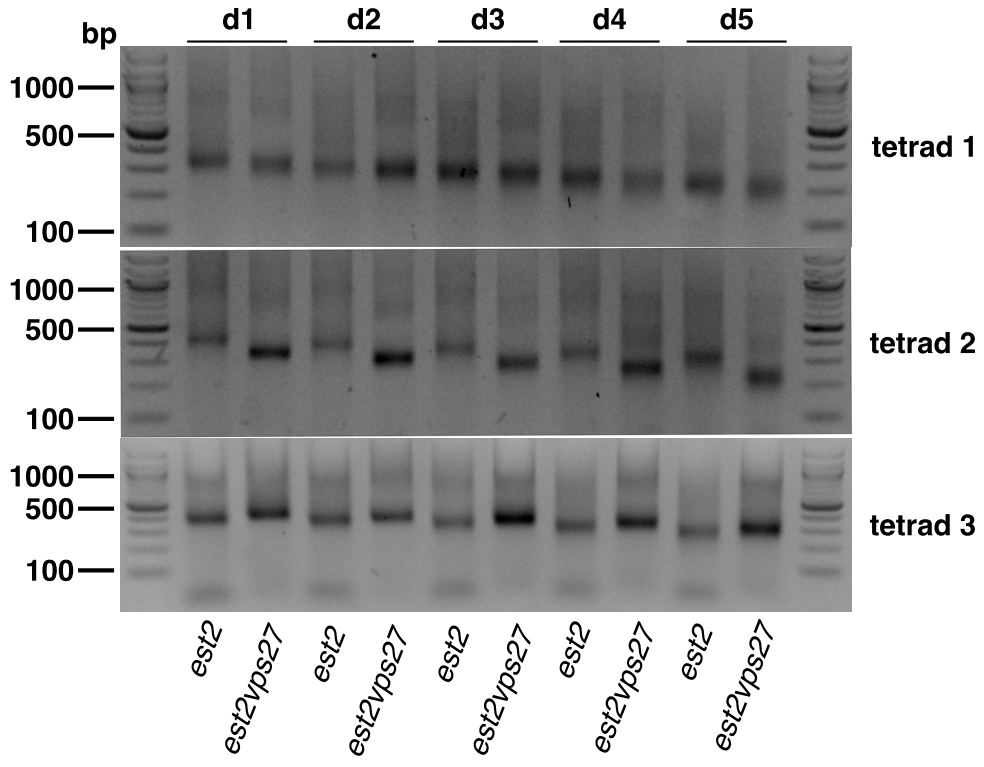

(b) 1L telomere.

Figure B.5.: Image of the agarose gel quantified in fig. 3.3c for measuring the rate of telomere shortening during senescence of *est2* single and *est2 vps27* double mutants. Telomere length was measured for samples 1–5 d of the senescence curve in fig. 3.3a. The gels were run for 30 min at 100 V.

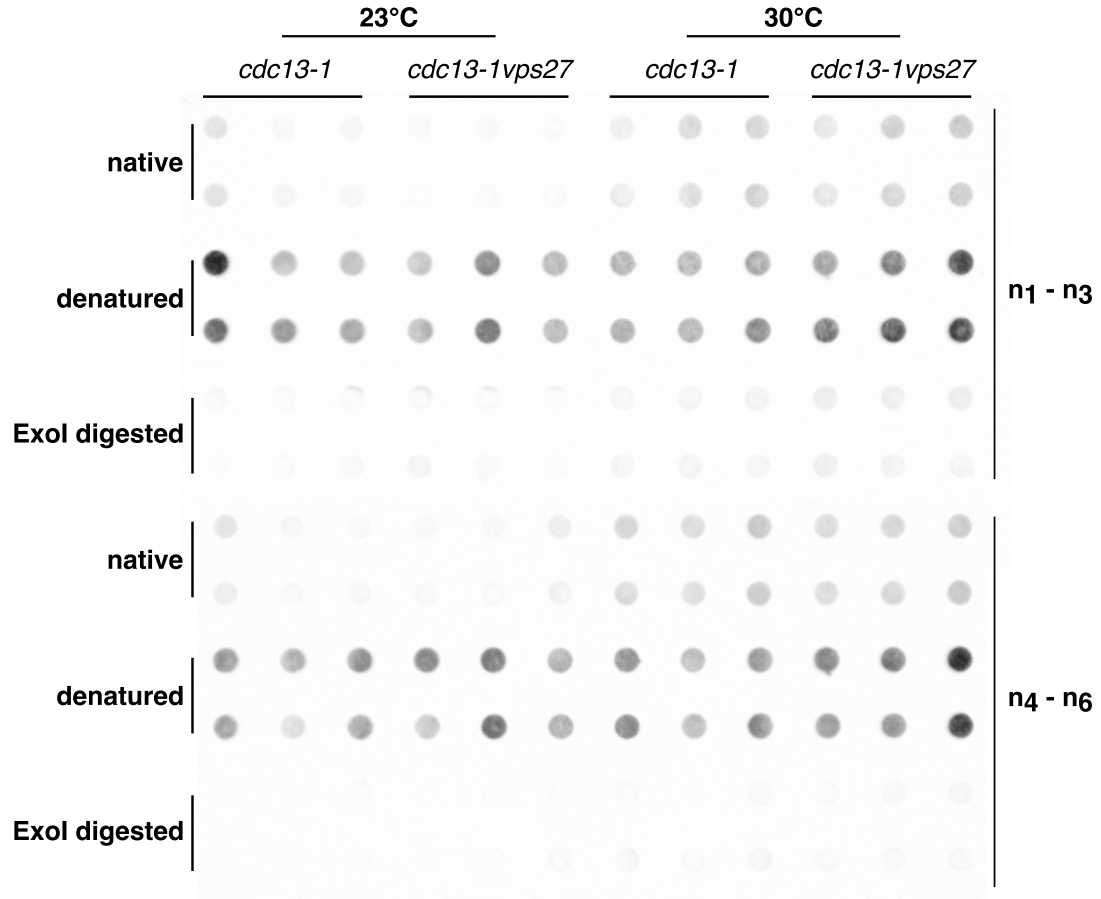

Figure B.6.: Image of the membrane quantified in fig. 3.7 for quantifying the amount of 3' ssDNA at the telomeric ends in *cdc13-1* single and *cdc13-1 vps27* double mutants at permissive temperature and after heat shock at 30 °C.

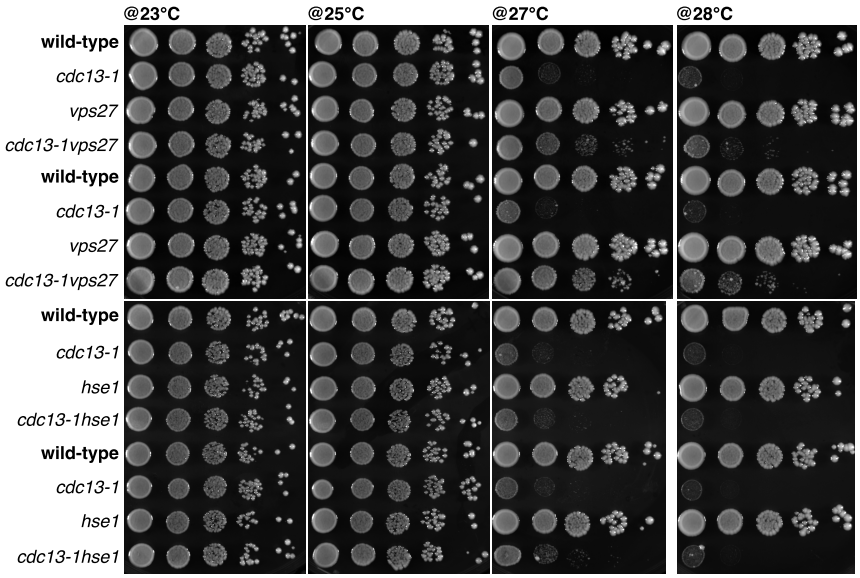

(a) ESCRT complex 0.

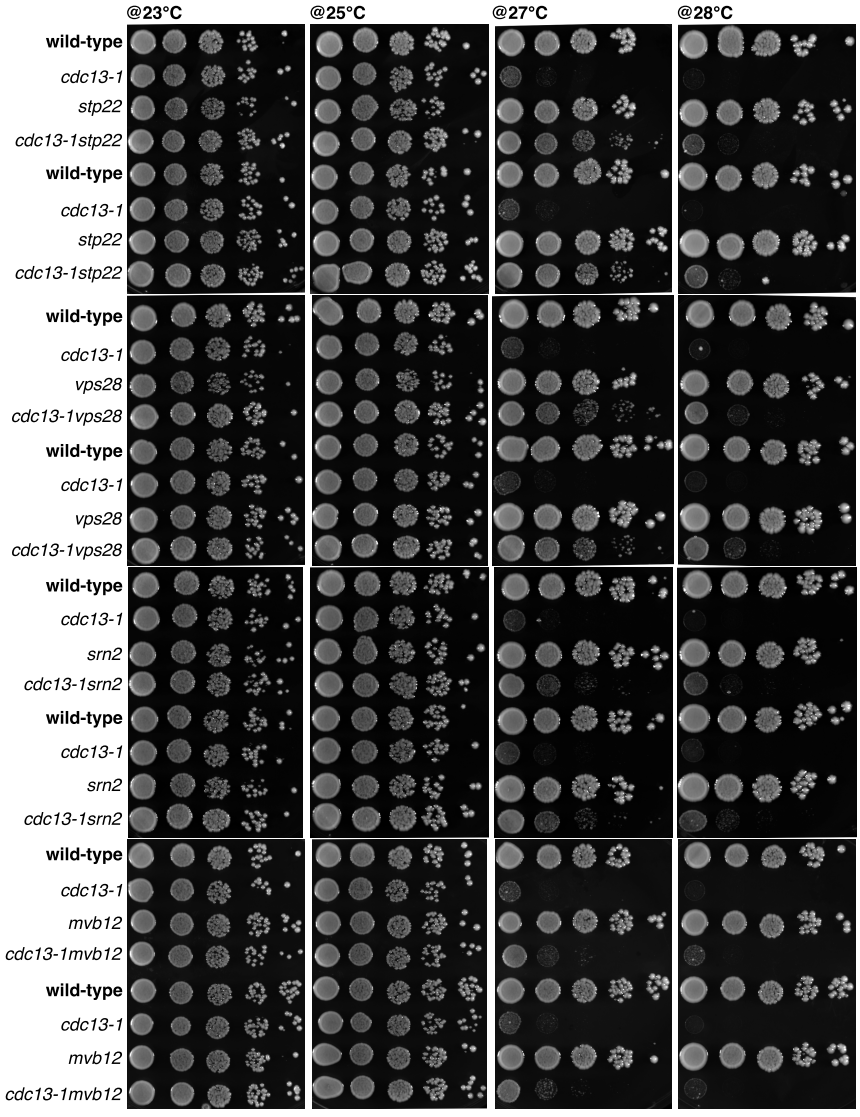

(b) ESCRT complex I.

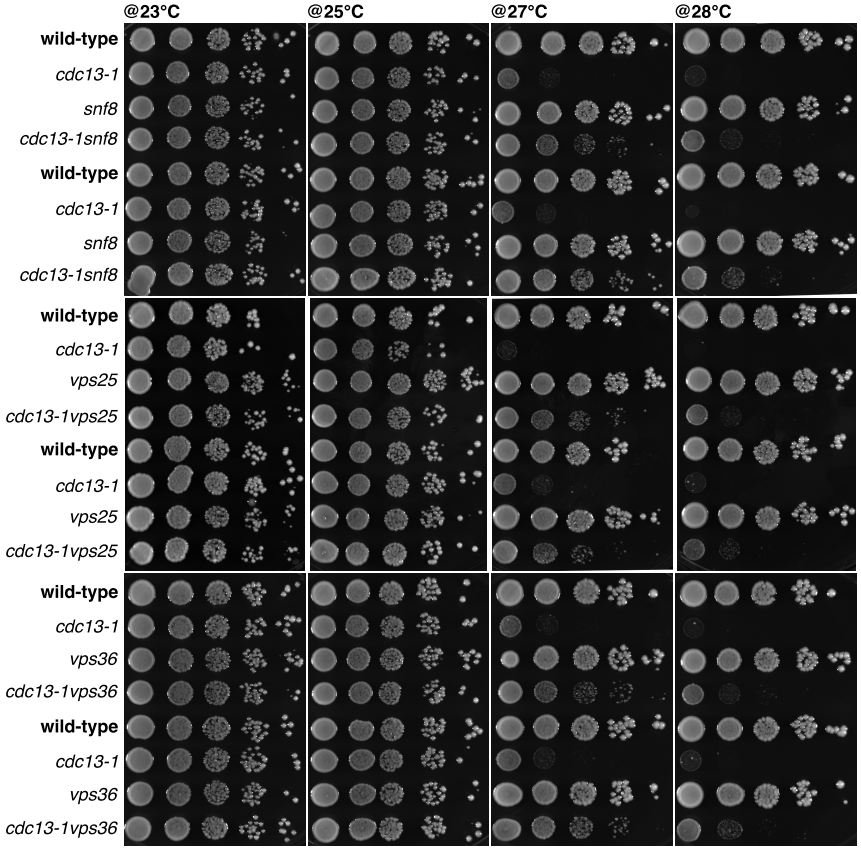

(c) ESCRT complex II.

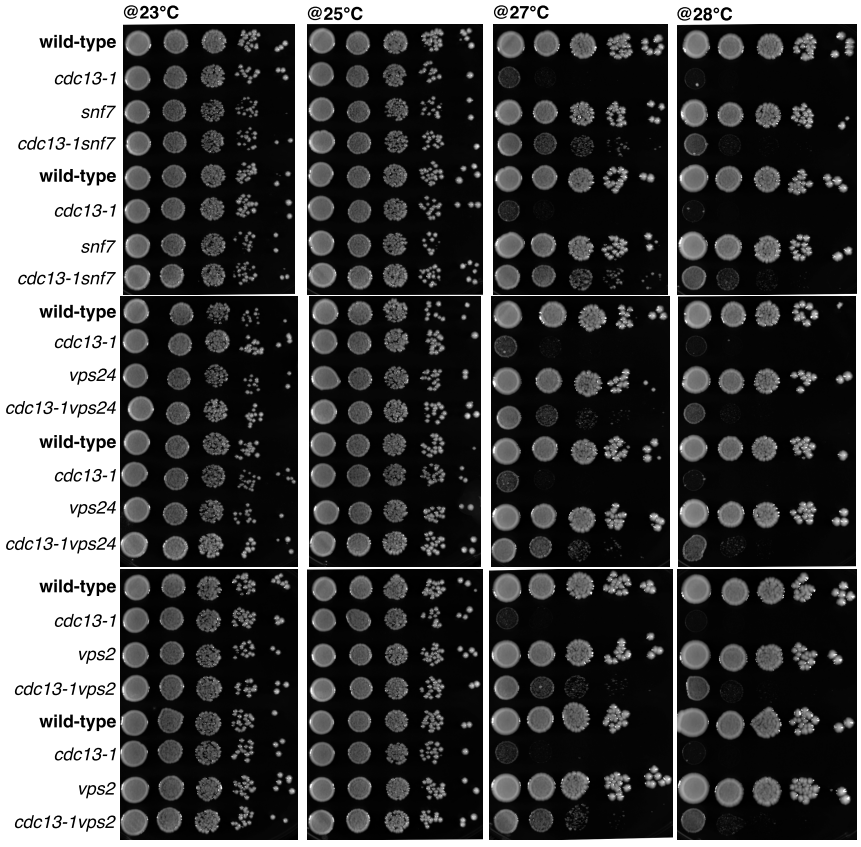

(d) ESCRT complex III.

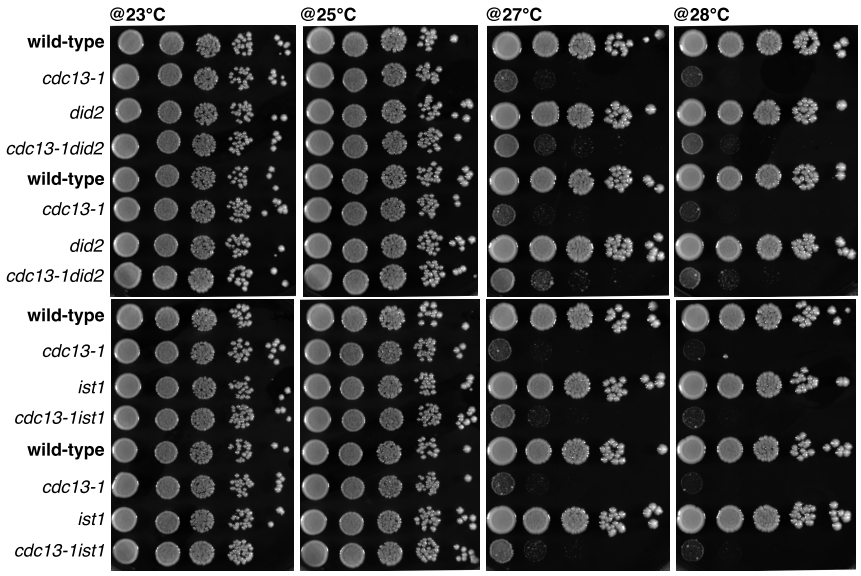

(c) ESCRT complex III associated.

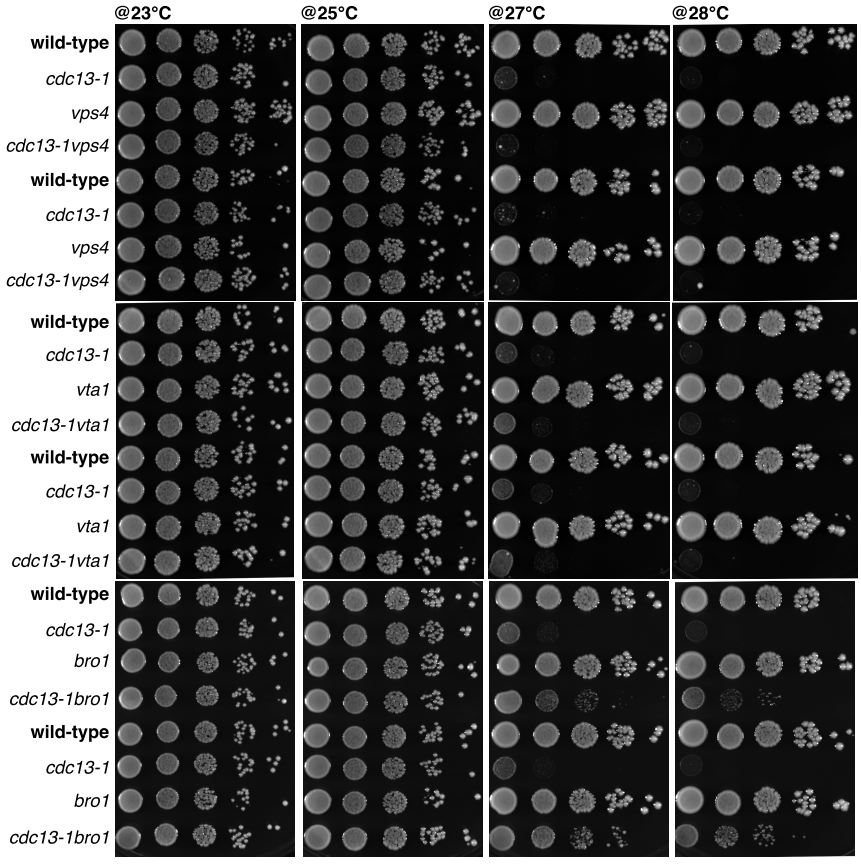

(d) ESCRT system associated.

Figure B.7.: Temperature rescue spotting for all *cdc13-1 escrt* mutants. The indicated strains were spotted 10-fold serially diluted onto standard YPD plates and incubated at permissive (23 °C and 25 °C) as well as non-permissive (27 °C and 28 °C) temperatures for three days. Each *cdc13-1 escrt* mutant and its respective single mutants were spotted in biological duplicates.

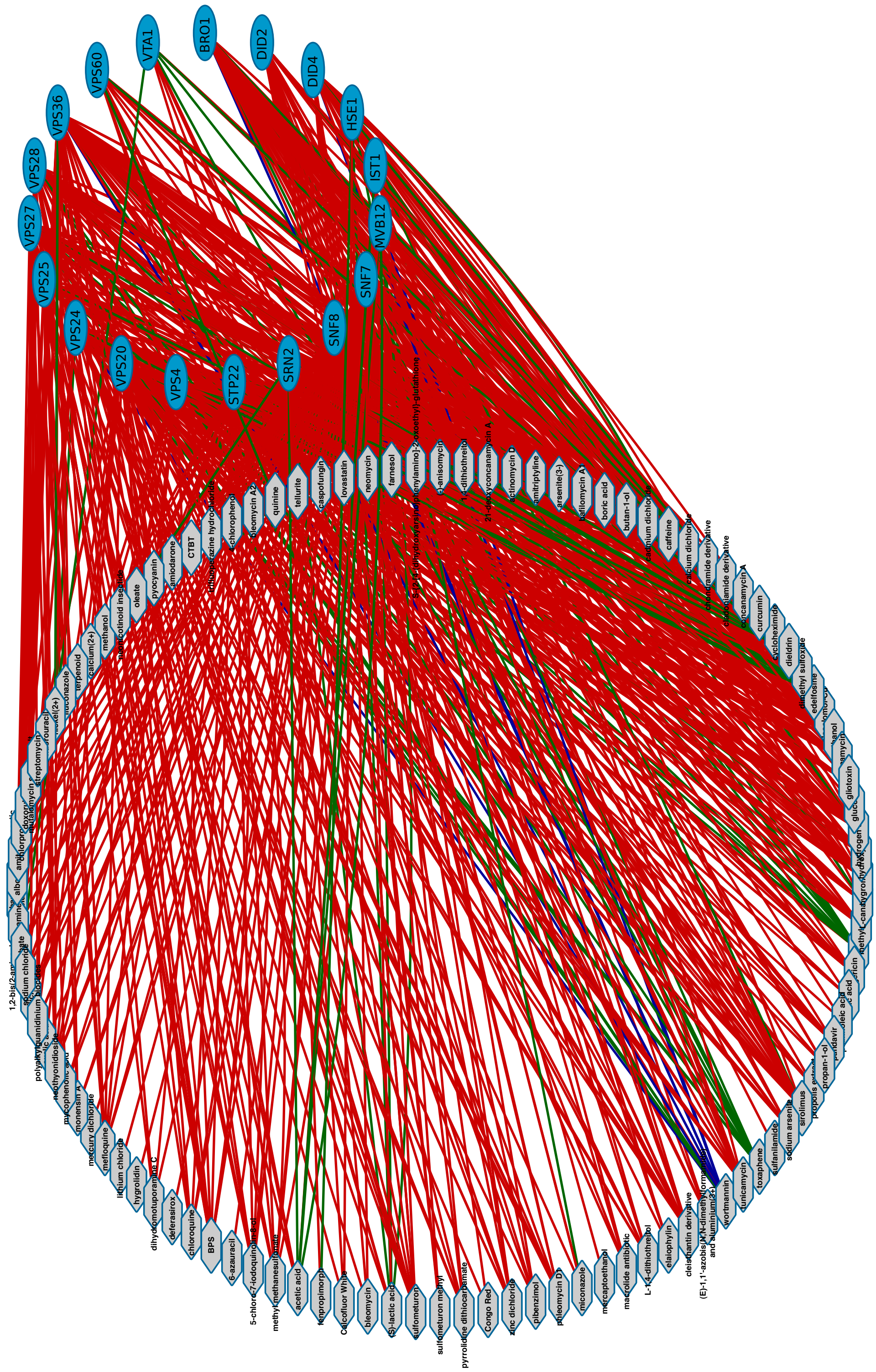

Figure B.8.: Bipartite drug-sensitivity network as derived for all ESCRT factors from the phenotype information provided by the SGD [10]. Drugs are denoted with grey and ESCRT factors with blue nodes. The effect of a certain *escrt* mutant on the resistance to a particular drug is encoded in the edge colour: Red, decreased resistance; green, increased resistance; blue, no change in resistance. Network manipulation and visualisation was done with Cytoscape [213].

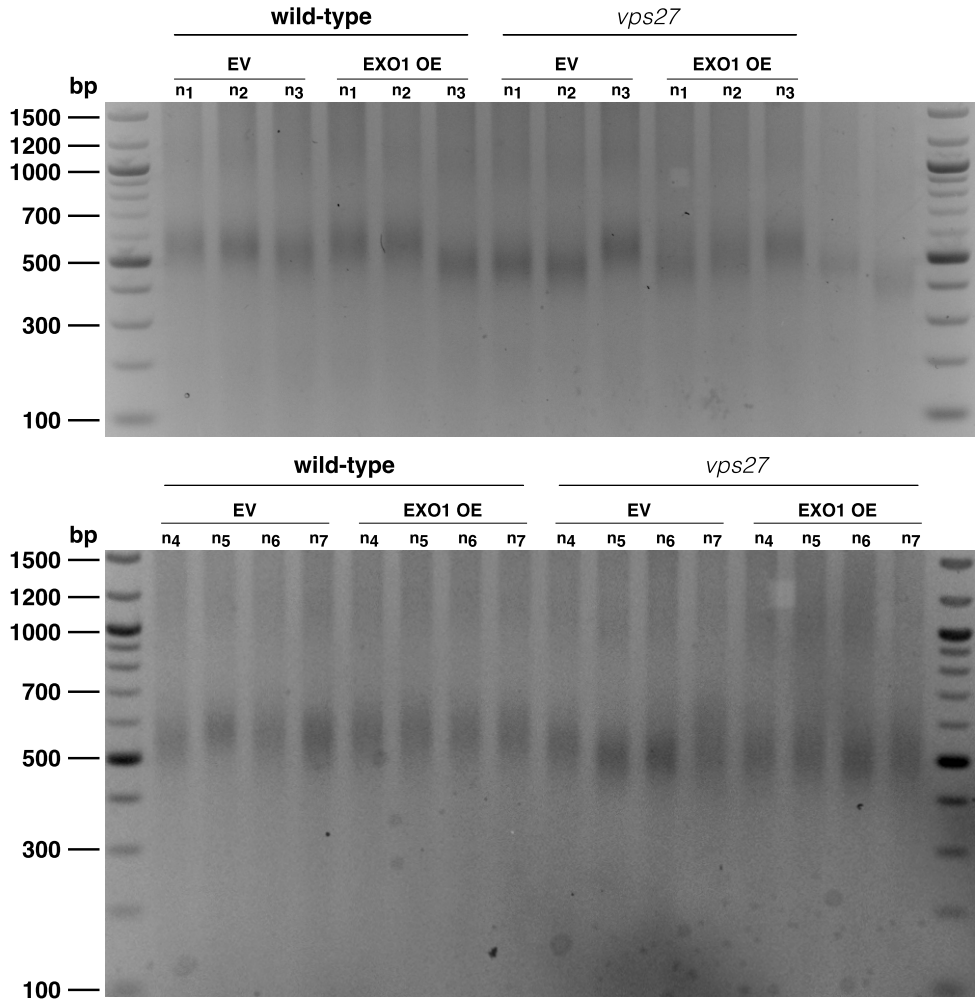

Figure B.9.: Image of the agarose gel quantified in fig. A.1 for measuring the length of six Y' telomeres for wild-type and *vps27* cells containing either an *EXO1* overexpression plasmid (OE) or the corresponding empty vector control (EV). The gels were run for 2.5 h at 100 V.

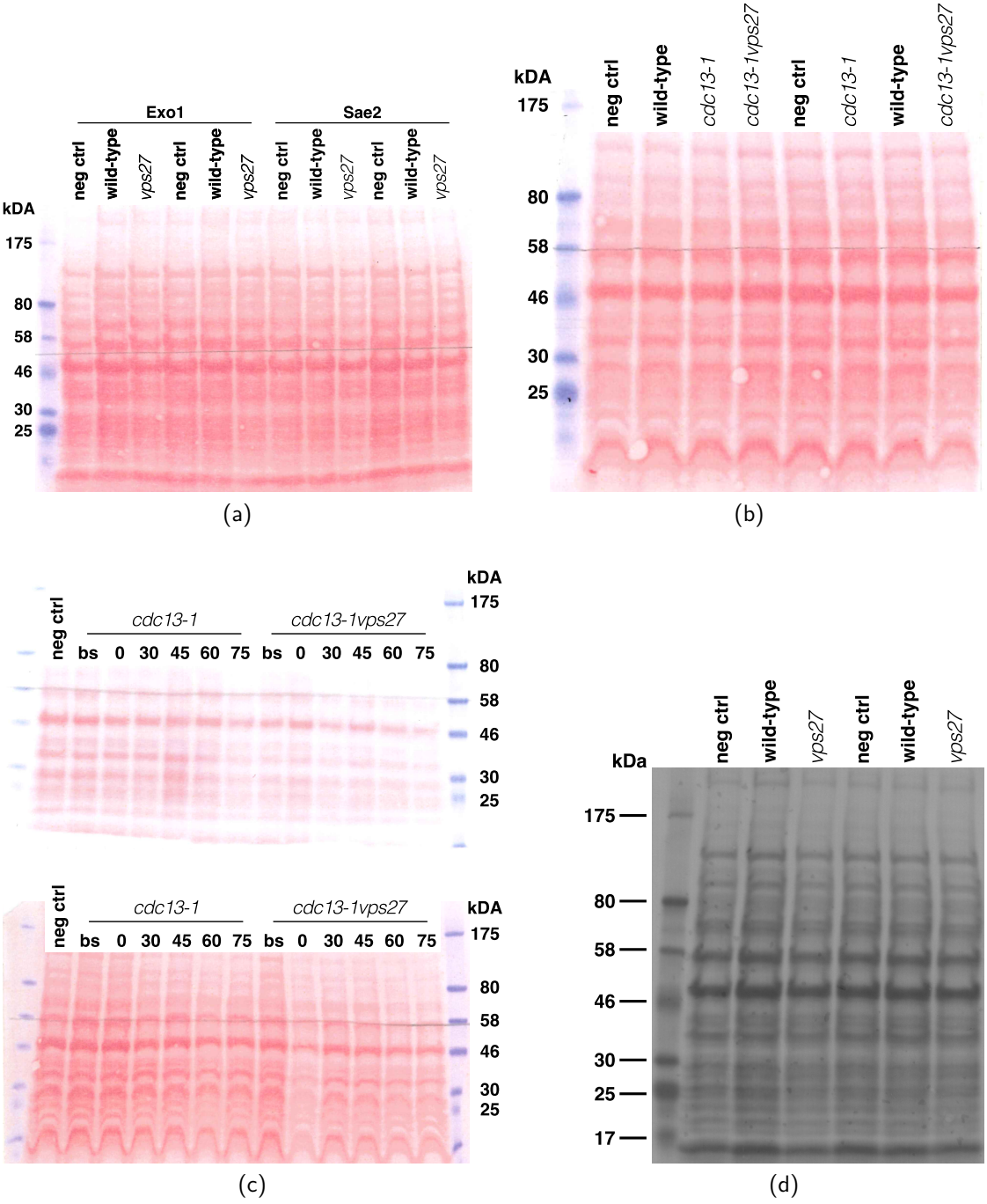

Figure B.10.: Ponceau stainings corresponding to the Western Blots in this work. (a), figs. 3.9a and 3.9b; (b), figs. 3.9c and 3.9d; (c), figs. 3.10a and 3.10b; (d), figs. A.4a and A.4b. Please see the particular captions for details on the individual experiments.

C

Supplemental Tables

Table C.1.: List of experiments conducted in the context of the present thesis.

Experiment	ID	Figure
DDR check spotting *vps27* (HR/NHEJ proficient strains)	A	fig. 3.14
DNA damage spotting *escrt*s	B	fig. 3.12
DNA damage spotting *rad52 vps27*	C	fig. 3.13
DNA damage spotting *vps27* with Exo1 OE	D	fig. 3.15
Dot blot (telomeric overhang)	E	figs. 3.7 and B.6
Exo1 resection assay (Longhese lab)	F	fig. 3.16
Imaging Exo1-GFP	G	
Rate of telomere shortening	H	figs. 3.3c and B.5
Senesencecurve	I	fig. 3.3a
Telomere length in *vps27*	J	figs. 3.2 and B.4
Temperature rescue spotting *atg5 cdc13-1 vps27*	K	fig. A.5b
Temperature rescue spotting *cdc13-1 escrt*s	L	fig. B.7
Temperature rescue spotting *cdc13-1 exo1 vps27*	M	fig. 3.17
Temperature rescue spotting *cdc13-1 rad53-11 vps27*	N	fig. 3.20
Temperature rescue spotting *cdc13-1 vps27*	O	fig. 3.5
Temperature rescue spotting *cdc13-1 vps27* Exo1 OE	P	fig. 3.8
Temperature rescue spotting *sae2 stn1-13 vps27*	Q	fig. A.2b
Temperature rescue spotting *stn1-13 vps27*	R	fig. A.2a
Temperature rescue spotting *vps27 addTS*s	S	fig. A.3
UP-DOWN assay	T	fig. 3.18
Western blot Cdc13 levels in *vps27*	U	figs. A.4 and B.10d
Western blot Exo1 degradation in *cdc13-1 vps27*	V	figs. 3.10 and B.10c
Western blot Exo1 levels in *cdc13-1 vps27*	W	figs. 3.9c and B.10b
Western blot Exo1/Sae2 levels in *vps27*	X	figs. 3.9a and B.10a
Y' telomere length with Exo1 OE in *vps27*	Y	figs. A.1 and B.9

Table C.2.: Functional categories from MIPS [8, 9] enriched with *tlm* mutants corresponding to non-essential genes. Enrichment was calculated based on the default two-sided Fisher's Exact test within R [206]. Multiple testing correction was done with the FDR correction method.

tlm Phenotype	Functional Category	P-Value	Corrected P-Value
short	organization of chromosome structure	6.730e−12	1.346e−11
	DNA damage response	5.872e−8	1.174e−7
	vacuolar/lysosomal transport	1.821e−7	3.643e−7
	DNA conformation modification (e.g. chromatin)	3.588e−7	7.177e−7
	transcription elongation	5.137e−5	0.000 10
	transcription repression	6.702e−5	0.000 13
	DNA synthesis and replication	0.000 11	0.000 22
	protein targeting, sorting and translocation	0.000 13	0.000 26
	DNA repair	0.000 16	0.000 31
	cell cycle checkpoints	0.000 18	0.000 37
	general transcription activities	0.000 29	0.000 59
	transcriptional control	0.000 46	0.000 92
	vesicular transport (Golgi network, etc	0.001 98	0.003 95
	RNA degradation	0.002 36	0.004 72
	regulation of phosphate metabolism	0.003 12	0.006 25
	G2/M transition of mitotic cell cycle	0.003 26	0.006 51
	polynucleotide degradation	0.003 96	0.007 92
	phosphate metabolism	0.004 26	0.008 52
	chromosome condensation	0.004 46	0.008 93
	modification by acetylation, deacetylation	0.006 55	0.013 10
	meiotic recombination	0.010 63	0.021 26
	modification by phosphorylation, dephosphorylation, autophosphorylation	0.011 64	0.023 29

Continued on next page.

Continued from previous page.

tlm Phenotype	Functional Category	P-Value	Corrected P-Value
short	posttranslational modification of amino acids (e.g. hydroxylation, methylation)	0.012 20	0.024 41
	actin cytoskeleton	0.012 24	0.024 47
	regulation of C-compound and carbohydrate metabolism	0.012 95	0.025 89
	meiosis I	0.013 50	0.026 99
	regulation of DNA processing	0.014 78	0.029 56
	intra Golgi transport	0.016 38	0.032 77
	endocytosis	0.016 88	0.033 76
	rRNA processing	0.033 84	0.033 84
	translational control	0.038 65	0.038 65
	proteasomal degradation (ubiquitin/proteasomal pathway)	0.019 72	0.039 44
	lysosomal and vacuolar protein degradation	0.020 24	0.040 49
	regulator of transcription factor	0.021 36	0.042 72
	DNA recombination	0.043 83	0.043 83
	vacuole or lysosome	0.022 86	0.045 73
	vacuole or lysosome	0.022 86	0.045 73
long	ribosomal proteins	2.526e−9	5.052e−9
	rRNA processing	0.000 99	0.001 98
	DNA recombination	0.001 42	0.002 84
	metabolism of secondary products derived from primary amino acids	0.001 90	0.003 81
	DNA damage response	0.003 95	0.003 95
	mitotic cell cycle and cell cycle control	0.002 04	0.004 08
	nuclear and chromosomal cycle	0.003 74	0.007 49
	DNA repair	0.008 18	0.008 18
	modification by acetylation, deacetylation	0.013 44	0.013 44
	polyphosphoinositol mediated signal transduction	0.007 11	0.014 22
	DNA synthesis and replication	0.017 74	0.017 74
	organization of chromosome structure	0.017 74	0.017 74
	RNA binding	0.009 64	0.019 28
	general transcription activities	0.030 57	0.030 57
	kinase activator	0.016 34	0.032 68
	translational control	0.030 90	0.038 65
	homeostasis of phosphate	0.020 66	0.041 33

Table C.3.: Overview of the original *tlm* phenotypes as defined in [183–185, 195, 197].

Original Category	Abbreviation	Length Difference	New Category
Very short	VS	$>$ 150 bp	shorter
Short	S	50–150 bp	shorter
Slightly short	SS	$<$ 50 bp	shorter
Very long	VL	$>$ 150 bp	longer
Long	L	50–150 bp	longer
Slightly long	SL	$<$ 50 bp	longer

Table C.4.: Proteins connecting ESCRT-0 and Cdc13 or Rad53 in the PPI-network presented in fig. 3.23. Descriptions were derived from YeastMine [192].

Gene Symbol	Description from YeastMine	In-Between
AIM3	Protein that inhibits barbed-end actin filament elongation	Hse1 and Rad53
LAS17	Actin assembly factor	Hse1 and Rad53
SLA1	Cytoskeletal protein binding protein	Hse1 and Rad53, Stp22 and Rad53
BCK1	MAPKKK acting in the protein kinase C signalling pathway	Vps27 and Cdc13
DBF2	Serine/threonine kinase involved in transcription and stress response	Vps27 and Cdc13
KSP1	Serine/threonine protein kinase	Vps27 and Cdc13
PRK1	Protein serine/threonine kinase	Vps27 and Cdc13, Hse1 and Cdc13
PRR2	Serine/threonine protein kinase	Vps27 and Cdc13
YCK2	Palmitoylated plasma membrane-bound casein kinase I (CK1) isoform	Vps27 and Cdc13
YPL150W	Protein kinase of unknown cellular role	Vps27 and Cdc13, Vps27 and Rad53

Bibliography

[1] Tacutu, R. ; Craig, T. ; Budovsky, A. ; Wuttke, D. ; Lehmann, G. ; Taranukha, D. ; Costa, J. et al.: Human Ageing Genomic Resources: integrated databases and tools for the biology and genetics of ageing. *Nucleic Acids Res.* 2013, January; **41**: pp. D1027–D1033. http://dx.doi.org/10.1093/nar/gks1155. – DOI 10.1093/nar/gks1155

[2] Stenmark, H. and Aasland, R.: FYVE-finger proteins–effectors of an inositol lipid. *J Cell Sci.* 1999, December; **112**(Pt 23): pp. 4175–4183

[3] Gene Ontology Consortium: Gene Ontology Consortium: going forward. *Nucleic Acids Res.* 2015, January; **43**: pp. D1049–D1056. http://dx.doi.org/10.1093/nar/gku1179. – DOI 10.1093/nar/gku1179

[4] Ashburner, M. ; Ball, C. A. ; Blake, J. A. ; Botstein, D. ; Butler, H. ; Cherry, J. M. ; Davis, A. P. et al.: Gene ontology: tool for the unification of biology. The Gene Ontology Consortium. *Nat Genet.* 2000, May; **25**(1): pp. 25–29. http://dx.doi.org/10.1038/75556. – DOI 10.1038/75556

[5] Kanehisa, M. and Goto, S.: KEGG: kyoto encyclopedia of genes and genomes. *Nucleic Acids Res.* 2000, January; **28**(1): pp. 27–30

[6] Kanehisa, M. ; Goto, S. ; Sato, Y. ; Furumichi, M. ; and Tanabe, M.: KEGG for integration and interpretation of large-scale molecular data sets. *Nucleic Acids Res.* 2012, January; **40**(Database issue): pp. D109–D114. http://dx.doi.org/10.1093/nar/gkr988. – DOI 10.1093/nar/gkr988. – ISSN 1362–4962

[7] Kanehisa, M. ; Goto, S. ; Sato, Y. ; Kawashima, M. ; Furumichi, M. ; and Tanabe, M.: Data, information, knowledge and principle: back to metabolism in KEGG. *Nucleic Acids Res.* 2014, January; **42**(Database issue): pp. D199–D205. http://dx.doi.org/10.1093/nar/gkt1076. – DOI 10.1093/nar/gkt1076

[8] Ruepp, A. ; Zollner, A. ; Maier, D. ; Albermann, K. ; Hani, J. ; Mokrejs, M. ; Tetko, I. et al.: The FunCat, a functional annotation scheme for systematic classification of proteins from whole genomes. *Nucleic Acids Res.* 2004; **32**(18): pp. 5539–5545. http://dx.doi.org/10.1093/nar/gkh894. – DOI 10.1093/nar/gkh894

[9] Mewes, H. W. ; Ruepp, A. ; Theis, F. ; Rattei, T. ; Walter, M. ; Frishman, D. ; Suhre, K. et al.: MIPS: curated databases and comprehensive secondary data resources in 2010. *Nucleic Acids Res.* 2011, January; **39**(Database issue): pp. D220–D224. http://dx.doi.org/10.1093/nar/gkq1157. – DOI 10.1093/nar/gkq1157

[10] Cherry, J. M. ; Hong, E. L. ; Amundsen, C. ; Balakrishnan, R. ; Binkley, G. ; Chan, E. T. ; Christie, K. R. et al.: *Saccharomyces* Genome Database: the genomics resource of budding yeast. *Nucleic Acids Res.* 2012, January; **40**(Database issue): pp. D700–D705. http://dx.doi.org/10.1093/nar/gkr1029. – DOI 10.1093/nar/gkr1029

[11] J. Michael Cherry: *Saccharomyces cerevisiae – Genetic Nomenclature Guide.* http://www.yeastgenome.org/sgdpub/Saccharomyces_cerevisiae.pdf. version: 1998

[12] Brown, G. R. ; Hem, V. ; Katz, K. S. ; Ovetsky, M. ; Wallin, C. ; Ermolaeva, O. ; Tolstoy, I. et al.: Gene: a gene-centered information resource at NCBI. *Nucleic Acids Res.* 2015, January; **43**(Database issue): pp. D36–D42. http://dx.doi.org/10.1093/nar/gku1055. – DOI 10.1093/nar/gku1055

[13] Dieckmann, A. ; Babin, V. ; Harari, Y. ; Eils, R. ; König, R. ; Kupiec, M. ; and Luke, B.: *Role of the ESCRT complexes in telomere biology.* – (manuscript in preparation, working title)

[14] Harari, Y. ; Dieckmann, A. ; and Kupiec, M.: *The relationship between telomere length, cellular aging and fitness in Saccharomyces cerevisiae.* – (manuscript in preparation)

[15] Schellhaas, R. ; Dieckmann, A. ; and Luke, B.: *The regulation of telomere looping.* – (manuscript in preparation, working title)

[16] Erika Check Hayden: Human genome at ten: Life is complicated. *Nature.* 2010, April; **464**(7289): pp. 664–667. http://dx.doi.org/10.1038/464664a. – DOI 10.1038/464664a

[17] Sir Paul Nurse: The great ideas of Biology. *Clinical Medicine.* 2003, November/December; **3**(6): pp. 560–568

[18] Denis Noble: *The Music of Life.* Oxford University Press Inc., New York, 2006

[19] Oltvai, Z. N. and Barabási, A.-L.: Systems biology. Life's complexity pyramid. *Science.* 2002, October; **298**(5594): pp. 763–764. http://dx.doi.org/10.1126/science.1078563. – DOI 10.1126/science.1078563

[20] Barabási, A.-L. and Oltvai, Z. N.: Network biology: understanding the cell's functional organization. *Nat Rev Genet.* 2004, February; **5**(2): pp. 101–113. http://dx.doi.org/10.1038/nrg1272. – DOI 10.1038/nrg1272. – ISSN 1471–0056

[21] Marc Vidal: A unifying view of 21st century systems biology. *FEBS Lett.* 2009, December; **583**(24): pp. 3891–3894. http://dx.doi.org/10.1016/j.febslet.2009.11.024. – DOI 10.1016/j.febslet.2009.11.024

[22] Lee, T. I. ; Rinaldi, N. J. ; Robert, F. ; Odom, D. T. ; Bar-Joseph, Z. ; Gerber, G. K. ; Hannett, N. M. et al.: Transcriptional Regulatory Networks in Saccharomyces cerevisiae. *Science.* 2002, October; **298**(5594): pp. 799–804. http://dx.doi.org/10.1126/science.1075090. – DOI 10.1126/science.1075090. – ISSN 1095–9203

[23] Arnold Munnich: Casting an eye on the Krebs cycle. *Nat Genet.* 2008, October; **40**(10): pp. 1148–1149. http://dx.doi.org/10.1038/ng1008-1148. – DOI 10.1038/ng1008–1148. – ISSN 1061–4036

[24] Gerstein, M. B. ; Bruce, C. ; Rozowsky, J. S. ; Zheng, D. ; Du, J. ; Korbel, J. O. ; Emanuelsson, O. et al.: What is a gene, post-ENCODE? History and updated definition. *Genome Res.* 2007, June; **17**(6): pp. 669–681. http://dx.doi.org/10.1101/gr.6339607. – DOI 10.1101/gr.6339607

[25] Hafner, L. and Hoff, P.: *Grüne Reihe. Materialien für die Sekundarstufe II: Genetik.* Schroedel Verlag, 1995

[26] Finkel, T. ; Serrano, M. ; and Blasco, M. A.: The common biology of cancer and ageing. *Nature.* 2007, August; **448**(7155): pp. 767–774. http://dx.doi.org/10.1038/nature05985. – DOI 10.1038/nature05985. – ISSN 1476–4687

[27] Bohgaki, T. ; Bohgaki, M. ; and Hakem, R.: DNA double-strand break signaling and human disorders. *Genome Integr.* 2010; **1**(15). http://dx.doi.org/10.1186/2041-9414-1-15. – DOI 10.1186/2041–9414–1–15

[28] R&D Systems: *Genomic Instability Syndromes.* https://www.rndsystems.com/resources/articles/genomic-instability-syndromes. version: 2004

[29] Negrini, S. ; Gorgoulis, V. G. ; and Halazonetis, T. D.: Genomic instability–an evolving hallmark of cancer. *Nat Rev Mol Cell Biol.* 2010, March; **11**(3): pp. 220–228. http://dx.doi.org/10.1038/nrm2858. – DOI 10.1038/nrm2858

[30] Jackson, S. P. and Bartek, J.: The DNA-damage response in human biology and disease. *Nature.* 2009, October; **461**(7267): pp. 1071–1078. http://dx.doi.org/10.1038/nature08467. – DOI 10.1038/nature08467

[31] Harper, J. W. and Elledge, S. J.: The DNA damage response: ten years after. *Mol Cell.* 2007, December; **28**(5): pp. 739–745. http://dx.doi.org/10.1016/j.molcel.2007.11.015. – DOI 10.1016/j.molcel.2007.11.015

[32] Razqallah Hakem: DNA-damage repair; the good, the bad, and the ugly. *EMBO J.* 2008, February; **27**(4): pp. 589–605. http://dx.doi.org/10.1038/emboj.2008.15. – DOI 10.1038/emboj.2008.15

[33] Anna Dieckmann: *A systems biological study of nuclear receptors and their co-regulation*, Ludwig-Maximilians-Universität & Technische Universität München, Diplomarbeit, July 2011. – Conducted at the Institute of Bioinformatics and Systems Biology, Helmholtz Zentrum München.

[34] Alberts, B. ; Johnson, A. ; Lewis, J. ; Raff, M. ; Roberts, K. ; and Walter, P.: *Molecular Biology of the Cell.* 4th. Garland Science, 2002

[35] Kim Thanos: *Human Anatomy and Physiology – Chapter 4. The CellCell Level of Organization.* https://courses.candelalearning.com/anatomyphysiology/chapter/chapter-3-the-cellular-level-of-organization-2/

[36] Campbell, N. A. ; Reece, J. B. ; Urry, L. A. ; Cain, M. L. ; Wasserman, S. A. ; Minorsky, P. V. ; and Jackson, R. B.: *Biology.* 8th. Pearson Benjamin Cummings, 2008

[37] Lingner, J. ; Cooper, J. P. ; and Cech, T. R.: Telomerase and DNA end replication: no longer a lagging strand problem? *Science.* 1995, September; **269**(5230): pp. 1533–1534

[38] Schluth-Bolard, C. ; Ottaviani, A. ; Bah, A. ; Boussouar, A. ; Gilson, E. ; and Magdinier, F.: Dynamics and plasticity of chromosome ends: consequences in human pathologies. *Atlas of Genetics and Cytogenetics in Oncology and Haematology.* 2011, November; (5). http://dx.doi.org/10.4267/2042/44767. – DOI 10.4267/2042/44767. – ISSN 1768–3262

[39] Soudet, J. ; Jolivet, P. ; and Teixeira, M. T.: Elucidation of the DNA end-replication problem in Saccharomyces cerevisiae. *Mol Cell.* 2014, March; **53**(6): pp. 954–964. http://dx.doi.org/10.1016/j.molcel.2014.02.030. – DOI 10.1016/j.molcel.2014.02.030

[40] James D. Watson: Origin of concatemeric T7 DNA. *Nat New Biol.* 1972, October; **239**(94): pp. 197–201

[41] Olovnikov, A. M.: Principle of marginotomy in template synthesis of polynucleotides. *Dokl Akad Nauk SSSR.* 1971; **201**(6): pp. 1496–1499

[42] Olovnikov, A. M.: A theory of marginotomy. The incomplete copying of template margin in enzymic synthesis of polynucleotides and biological significance of the phenomenon. *J Theor Biol.* 1973, September; **41**(1): pp. 181–190

[43] Dewar, J. M. and Lydall, D.: Similarities and differences between "uncapped" telomeres and DNA double-strand breaks. *Chromosoma.* 2011, December;. http://dx.doi.org/10.1007/s00412-011-0357-2. – DOI 10.1007/s00412–011–0357–2. – ISSN 1432–0886

[44] Mao, Z. ; Bozzella, M. ; Seluanov, A. ; and Gorbunova, V.: DNA repair by nonhomologous end joining and homologous recombination during cell cycle in human cells. *Cell Cycle.* 2008, September; **7**(18): pp. 2902–2906

[45] Papamichos-Chronakis, M. and Peterson, C. L.: Chromatin and the genome integrity network. *Nature Reviews Genetics.* 2012, December; **14**(1): pp. 62–75. http://dx.doi.org/10.1038/nrg3345. – DOI 10.1038/nrg3345. – ISSN 1471–0064

[46] Jim E. Haber: *An Introduction to Break-induced Recombination.* pubished online – Haber Lab Web Site. http://www.bio.brandeis.edu/haberlab/jehsite/resDSBR.html

[47] Mao, Z. ; Bozzella, M. ; Seluanov, A. ; and Gorbunova, V.: Comparison of nonhomologous end joining and homologous recombination in human cells. *DNA Repair.* 2008, October; **7**(10): pp. 1765–1771. http://dx.doi.org/10.1016/j.dnarep.2008.06.018. – DOI 10.1016/j.dnarep.2008.06.018

[48] Nguyen, A. T. and Zhang, Y.: The diverse functions of Dot1 and H3K79 methylation. *Genes & Development.* 2011, July; **25**(13): pp. 1345–1358. http://dx.doi.org/10.1101/gad.2057811. – DOI 10.1101/gad.2057811. – ISSN 0890–9369

[49] O'Sullivan, R. J. and Karlseder, J.: Telomeres: protecting chromosomes against genome instability. *Nat Rev Mol Cell Biol.* 2010, March; **11**(3): pp. 171–181. http://dx.doi.org/10.1038/nrm2848. – DOI 10.1038/nrm2848

[50] David Lydall: Hiding at the ends of yeast chromosomes: telomeres, nucleases and checkpoint pathways. *J Cell Sci.* 2003, October; **116**(Pt 20): pp. 4057–4065. http://dx.doi.org/10.1242/jcs.00765. – DOI 10.1242/jcs.00765

[51] Gilson, E. and Géli, V.: How telomeres are replicated. *Nat Rev Mol Cell Biol.* 2007, October; **8**(10): pp. 825–38. http://dx.doi.org/10.1038/nrm2259. – DOI 10.1038/nrm2259. – ISSN 1471–0080

[52] Willeit, P. ; Willeit, J. ; Mayr, A. ; and al. et: Telomere length and risk of incident cancer and cancer mortality. *JAMA.* 2010, July; **304**(1): pp. 69–75. http://dx.doi.org/10.1001/jama.2010.897. – DOI 10.1001/jama.2010.897

[53] Vega, L. R. ; Mateyak, M. K. ; and Zakian, V. A.: Getting to the end: telomerase access in yeast and humans. *Nat Rev Mol Cell Biol.* 2003, December; **4**(12): pp. 948–959. http://dx.doi.org/10.1038/nrm1256. – DOI 10.1038/nrm1256. – ISSN 1471–0080

[54] Lue, N. F. (ed.) and Autexier, C. (ed.): *Telomerases – Chemistry, Biology, and Clinical Applications.* John Wiley & Sons, Inc., 2012

[55] Giraud-Panis, M.-J. ; Pisano, S. ; Benarroch-Popivker, D. ; Pei, B. ; Le Du, M.-H. ; and Gilson, E.: One Identity or More for Telomeres? *Frontiers in Oncology.* 2013, March; **3**(48). http://dx.doi.org/10.3389/fonc.2013.00048. – DOI 10.3389/fonc.2013.00048. – ISSN 2234–943X

[56] Bianchi, A. and Shore, D.: Telomeres: Maintenance and Replication. *Encyclopedia of Biological Chemistry.* 2004;. http://dx.doi.org/10.1016/b0-12-443710-9/00671-2. – DOI 10.1016/b0–12–443710–9/00671–2

[57] Zhu, X. and Gustafsson, C. M.: Distinct Differences in Chromatin Structure at Subtelomeric X and Y' Elements in Budding Yeast. *PLoS ONE.* 2009, July; **4**(7): p. e6363. http://dx.doi.org/10.1371/journal.pone.0006363. – DOI 10.1371/journal.pone.0006363. – ISSN 1932–6203

[58] Louis, E. J. ; Naumova, E. S. ; Lee, A. ; Naumov, G. ; and Haber, J. E.: The chromosome end in yeast: its mosaic nature and influence on recombinational dynamics. *Genetics.* 1994, March; **136**(3): pp. 789–802

[59] Wellinger, R. J. and Zakian, V. A.: Everything you ever wanted to know about Saccharomyces cerevisiae telomeres: beginning to end. *Genetics.* 2012, August; **191**(4): pp. 1073–1105. http://dx.doi.org/10.1534/genetics.111.137851. – DOI 10.1534/genetics.111.137851

[60] Salvati, E. ; Leonetti, C. ; Rizzo, A. ; Scarsella, M. ; Mottolese, M. ; Galati, R. ; Sperduti, I. et al.: Telomere damage induced by the G-quadruplex ligand RHPS4 has an antitumor effect. *J Clin Invest.* 2007, November; **117**(11): pp. 3236–3247. http://dx.doi.org/10.1172/JCI32461. – DOI 10.1172/JCI32461

[61] Leonetti, C. ; Scarsella, M. ; Riggio, G. ; Rizzo, A. ; Salvati, E. ; D'Incalci, M. ; Staszewsky, L. et al.: G-quadruplex ligand RHPS4 potentiates the antitumor activity of camptothecins in preclinical models of solid tumors. *Clin Cancer Res.* 2008, November; **14**(22): pp. 7284–7291. http://dx.doi.org/10.1158/1078-0432.CCR-08-0941. – DOI 10.1158/1078–0432.CCR–08–0941

[62] Berman, A. J. and Cech, T. R.: SnapShot: Telomeres and Telomerase. *Cell.* 2012, November; **151**(5): pp. 1138–1138.e1. http://dx.doi.org/10.1016/j.cell.2012.11.008. – DOI 10.1016/j.cell.2012.11.008. – ISSN 00928674

[63] Smogorzewska, A. and Lange, T. de: Regulation of telomerase by telomeric proteins. *Annu Rev Biochem.* 2004, January; **73**: pp. 177–208. http://dx.doi.org/10.1146/annurev.biochem.73.071403.160049. – DOI 10.1146/annurev.biochem.73.071403.160049. – ISSN 0066–4154

[64] Rubtsova, M. P. ; Vasilkova, D. P. ; Malyavko, A. N. ; Naraikina, Y. V. ; Zvereva, M. I. ; and Dontsova, O. A.: Telomere lengthening and other functions of telomerase. *Acta Naturae.* 2012, April; **4**(2): pp. 44–61

[65] Conomos, D. ; Pickett, H. A. ; and Reddel, R. R.: Alternative lengthening of telomeres: remodeling the telomere architecture. *Front Oncol.* 2013; **3**(27). http://dx.doi.org/10.3389/fonc.2013.00027. – DOI 10.3389/fonc.2013.00027

[66] Roger R. Reddel: Alternative lengthening of telomeres, telomerase, and cancer. *Cancer Lett.* 2003, May; **194**(2): pp. 155–162

[67] Stewart, J. A. ; Chaiken, M. F. ; Wang, F. ; and Price, C. M.: Maintaining the end: Roles of telomere proteins in end-protection, telomere replication and length regulation. *Mutat Res.* 2012, February; **730**(1-2): pp. 12–19. http://dx.doi.org/10.1016/j.mrfmmm.2011.08.011. – DOI 10.1016/j.mrfmmm.2011.08.011. – ISSN 0027–5107

[68] Nandakumar, J. and Cech, T. R.: Finding the end: recruitment of telomerase to telomeres. *Nat Rev Mol Cell Biol.* 2013, January; **14**(2): pp. 69–82. http://dx.doi.org/10.1038/nrm3505. – DOI 10.1038/nrm3505. – ISSN 1471–0080

[69] Hug, N. and Lingner, J.: Telomere length homeostasis. *Chromosoma.* 2006, December; **115**(6): pp. 413–425. http://dx.doi.org/10.1007/s00412-006-0067-3. – DOI 10.1007/s00412–006–0067–3

[70] Nugent, C. I. ; Hughes, T. R. ; Lue, N. F. ; and Lundblad, V.: Cdc13p: a single-strand telomeric DNA-binding protein with a dual role in yeast telomere maintenance. *Science.* 1996, October; **274**(5285): pp. 249–252

[71] Taggart, A. K. P. ; Teng, S.-C. ; and Zakian, V. A.: Est1p as a cell cycle-regulated activator of telomere-bound telomerase. *Science.* 2002, August; **297**(5583): pp. 1023–1026. http://dx.doi.org/10.1126/science.1074968. – DOI 10.1126/science.1074968

[72] Zhou, J. ; Hidaka, K. ; and Futcher, B.: The Est1 subunit of yeast telomerase binds the Tlc1 telomerase RNA. *Mol Cell Biol.* 2000, March; **20**(6): pp. 1947–1955

[73] Maillet, L. ; Boscheron, C. ; Gotta, M. ; Marcand, S. ; Gilson, E. ; and Gasser, S. M.: Evidence for silencing compartments within the yeast nucleus: a role for telomere proximity and Sir protein concentration in silencer-mediated repression. *Genes Dev.* 1996, July; **10**(14): pp. 1796–1811

[74] Schober, H. ; Ferreira, H. ; Kalck, V. ; Gehlen, L. R. ; and Gasser, S. M.: Yeast telomerase and the SUN domain protein Mps3 anchor telomeres and repress subtelomeric recombination. *Genes Dev.* 2009, April; **23**(8): pp. 928–938. http://dx.doi.org/10.1101/gad.1787509. – DOI 10.1101/gad.1787509

[75] Garvik, B. ; Carson, M. ; and Hartwell, L.: Single-stranded DNA arising at telomeres in cdc13 mutants may constitute a specific signal for the RAD9 checkpoint. *Mol Cell Biol.* 1995, November; **15**(11): pp. 6128–6138

[76] Grandin, N. ; Reed, S. I. ; and Charbonneau, M.: Stn1, a new Saccharomyces cerevisiae protein, is implicated in telomere size regulation in association with Cdc13. *Genes Dev.* 1997, February; **11**(4): pp. 512–527

[77] Teixeira, M. T. ; Arneric, M. ; Sperisen, P. ; and Lingner, J.: Telomere length homeostasis is achieved via a switch between telomerase- extendible and -nonextendible states. *Cell.* 2004, April; **117**(3): pp. 323–335

[78] Loayza, D. and Lange, T. de: Telomerase Regulation at the Telomere. *Cell.* 2004, April; **117**(3): pp. 279–280. http://dx.doi.org/10.1016/s0092-8674(04)00409-x. – DOI 10.1016/s0092–8674(04)00409–x. – ISSN 0092–8674

[79] Maria Pia Longhese: DNA damage response at functional and dysfunctional telomeres. *Genes & Development.* 2008, January; **22**(2): pp. 125–140. http://dx.doi.org/10.1101/gad.1626908. – DOI 10.1101/gad.1626908. – ISSN 0890–9369

[80] Raymund J. Wellinger: When the caps fall off: responses to telomere uncapping in yeast. *FEBS Lett.* 2010, September; **584**(17): pp. 3734–3740. http://dx.doi.org/10.1016/j.febslet.2010.06.031. – DOI 10.1016/j.febslet.2010.06.031

[81] Sabatier, L. ; Ricoul, M. ; Pottier, G. ; and Murnane, J. P.: The loss of a single telomere can result in instability of multiple chromosomes in a human tumor cell line. *Mol Cancer Res.* 2005, March; **3**(3): pp. 139–150. http://dx.doi.org/10.1158/1541-7786.MCR-04-0194. – DOI 10.1158/1541–7786.MCR–04–0194

[82] Blasco, M. A. ; Lee, H. W. ; Hande, M. P. ; Samper, E. ; Lansdorp, P. M. ; DePinho, R. A. ; and Greider, C. W.: Telomere shortening and tumor formation by mouse cells lacking telomerase RNA. *Cell.* 1997, October; **91**(1): pp. 25–34

[83] Bodnar, A. G. ; Ouellette, M. ; Frolkis, M. ; Holt, S. E. ; Chiu, C. P. ; Morin, G. B. ; Harley, C. B. et al.: Extension of life-span by introduction of telomerase into normal human cells. *Science.* 1998, January; **279**(5349): pp. 349–352

[84] Fuster, J. J. and Andrés, V.: Telomere biology and cardiovascular disease. *Circ Res.* 2006, November; **99**(11): pp. 1167–1180. http://dx.doi.org/10.1161/01.RES.0000251281.00845.18. – DOI 10.1161/01.RES.0000251281.00845.18

[85] Heiss, N. S. ; Knight, S. W. ; Vulliamy, T. J. ; Klauck, S. M. ; Wiemann, S. ; Mason, P. J. ; Poustka, A. et al.: X-linked dyskeratosis congenita is caused by mutations in a highly conserved gene with putative nucleolar functions. *Nat Genet.* 1998, May; **19**(1): pp. 32–38. http://dx.doi.org/10.1038/ng0598-32. – DOI 10.1038/ng0598–32

[86] Minamino, T. ; Orimo, M. ; Shimizu, I. ; Kunieda, T. ; Yokoyama, M. ; Ito, T. ; Nojima, A. et al.: A crucial role for adipose tissue p53 in the regulation of insulin resistance. *Nat Med.* 2009, September; **15**(9): pp. 1082–1087. http://dx.doi.org/10.1038/nm.2014. – DOI 10.1038/nm.2014

[87] Mitchell, J. R. ; Wood, E. ; and Collins, K.: A telomerase component is defective in the human disease dyskeratosis congenita. *Nature.* 1999, December; **402**(6761): pp. 551–555. http://dx.doi.org/10.1038/990141. – DOI 10.1038/990141

[88] Lendvay, T. S. ; Morris, D. K. ; Sah, J. ; Balasubramanian, B. ; and Lundblad, V.: Senescence mutants of Saccharomyces cerevisiae with a defect in telomere replication identify three additional EST genes. *Genetics.* 1996, December; **144**(4): pp. 1399–1412

[89] Singer, M. S. and Gottschling, D. E.: TLC1: template RNA component of Saccharomyces cerevisiae telomerase. *Science.* 1994, October; **266**(5184): pp. 404–409

[90] Foster, S. S. ; Zubko, M. K. ; Guillard, S. ; and Lydall, D.: MRX protects telomeric DNA at uncapped telomeres of budding yeast cdc13-1 mutants. *DNA Repair.* 2006, July; **5**(7): pp. 840–851. http://dx.doi.org/10.1016/j.dnarep.2006.04.005. – DOI 10.1016/j.dnarep.2006.04.005

[91] Maringele, L. and Lydall, D.: EXO1-dependent single-stranded DNA at telomeres activates subsets of DNA damage and spindle checkpoint pathways in budding yeast yku70Delta mutants. *Genes Dev.* 2002, August; **16**(15): pp. 1919–1933. http://dx.doi.org/10.1101/gad.225102. – DOI 10.1101/gad.225102

[92] Dewar, J. M. and Lydall, D.: Pif1- and Exo1-dependent nucleases coordinate checkpoint activation following telomere uncapping. *EMBO J.* 2010, December; **29**(23): pp. 4020–4034. http://dx.doi.org/10.1038/emboj.2010.267. – DOI 10.1038/emboj.2010.267

[93] Negrini, S. ; Ribaud, V. ; Bianchi, A. ; and Shore, D.: DNA breaks are masked by multiple Rap1 binding in yeast: implications for telomere capping and telomerase regulation. *Genes Dev.* 2007, February; **21**(3): pp. 292–302. http://dx.doi.org/10.1101/gad.400907. – DOI 10.1101/gad.400907

[94] Duncan M. Baird: Telomeres. *Elsevier Inc.* 2007;

[95] Buseman, C. ; Wright, W. ; and Shay, J.: Is telomerase a viable target in cancer? *Mutation Research/Fundamental and Molecular Mechanisms of Mutagenesis.* 2011, July; **730**(1–2): pp. 90–97. http://dx.doi.org/10.1016/j.mrfmmm.2011.07.006. – DOI 10.1016/j.mrfmmm.2011.07.006. – ISSN 00275107

[96] Hemann, M. T. ; Strong, M. A. ; Hao, L.-Y. ; and Greider, C. W.: The Shortest Telomere, Not Average Telomere Length, Is Critical for Cell Viability and Chromosome Stability. *Cell.* 2001, October; **107**(1): pp. 67–77. http://dx.doi.org/10.1016/s0092-8674(01)00504-9. – DOI 10.1016/s0092–8674(01)00504–9. – ISSN 0092–8674

[97] María A. Blasco: Telomeres and human disease: ageing, cancer and beyond. *Nat Rev Genet.* 2005, August; **6**(8): pp. 611–622. http://dx.doi.org/10.1038/nrg1656. – DOI 10.1038/nrg1656

[98] Nair, S. K. ; Heiser, A. ; Boczkowski, D. ; Majumdar, A. ; Naoe, M. ; Lebkowski, J. S. ; Vieweg, J. et al.: Induction of cytotoxic T cell responses and tumor immunity against unrelated tumors using telomerase reverse transcriptase RNA transfected dendritic cells. *Nat Med.* 2000, September; **6**(9): pp. 1011–1017. http://dx.doi.org/10.1038/79519. – DOI 10.1038/79519

[99] Nava-Parada, P. and Emens, L. A.: GV-1001, an injectable telomerase peptide vaccine for the treatment of solid cancers. *Curr Opin Mol Ther.* 2007, October; **9**(5): pp. 490–497

[100] Kyo, S. ; Takakura, M. ; Fujiwara, T. ; and Inoue, M.: Understanding and exploiting hTERT promoter regulation for diagnosis and treatment of human cancers. *Cancer Sci.* 2008, August; **99**(8): pp. 1528–1538. http://dx.doi.org/10.1111/j.1349-7006.2008.00878.x. – DOI 10.1111/j.1349–7006.2008.00878.x

[101] Komata, T. ; Kondo, Y. ; Kanzawa, T. ; Hirohata, S. ; Koga, S. ; Sumiyoshi, H. ; Srinivasula, S. M. et al.: Treatment of malignant glioma cells with the transfer of constitutively active caspase-6 using the human telomerase catalytic subunit (human telomerase reverse transcriptase) gene promoter. *Cancer Res.* 2001, August; **61**(15): pp. 5796–5802

[102] *Biology.* 1st. OpenStax College, 2013

[103] Field, M. C. and Dacks, J. B.: First and last ancestors: reconstructing evolution of the endomembrane system with ESCRTs, vesicle coat proteins, and nuclear pore complexes. *Curr Opin Cell Biol.* 2009, February; **21**(1): pp. 4–13. http://dx.doi.org/10.1016/j.ceb.2008.12.004. – DOI 10.1016/j.ceb.2008.12.004

[104] Hurley, J. H. and Emr, S. D.: The ESCRT complexes: structure and mechanism of a membrane-trafficking network. *Annu Rev Biophys Biomol Struct.* 2006; **35**: pp. 277–298. http://dx.doi.org/10.1146/annurev.biophys.35.040405.102126. – DOI 10.1146/annurev.biophys.35.040405.102126

[105] Markus Babst: A protein's final ESCRT. *Traffic.* 2005, January; **6**(1): pp. 2–9. http://dx.doi.org/10.1111/j.1600-0854.2004.00246.x. – DOI 10.1111/j.1600–0854.2004.00246.x

[106] Hurley, J. H. and Hanson, P. I.: Membrane budding and scission by the ESCRT machinery: it's all in the neck. *Nat Rev Mol Cell Biol.* 2010, August; **11**(8): pp. 556–566. http://dx.doi.org/10.1038/nrm2937. – DOI 10.1038/nrm2937

[107] Raiborg, C. and Stenmark, H.: The ESCRT machinery in endosomal sorting of ubiquitylated membrane proteins. *Nature.* 2009, March; **458**(7237): pp. 445–452. http://dx.doi.org/10.1038/nature07961. – DOI 10.1038/nature07961

[108] Hartmann, C. ; Chami, M. ; Zachariae, U. ; Groot, B. L. ; Engel, A. ; and Grütter, M. G.: Vacuolar Protein Sorting: Two Different Functional States of the AAA-ATPase Vps4p. *Journal of Molecular Biology.* 2008, March; **377**(2): pp. 352–363. http://dx.doi.org/10.1016/j.jmb.2008.01.010. – DOI 10.1016/j.jmb.2008.01.010. – ISSN 0022–2836

[109] Leung, K. F. ; Dacks, J. B. ; and Field, M. C.: Evolution of the multivesicular body ESCRT machinery; retention across the eukaryotic lineage. *Traffic.* 2008, September; **9**(10): pp. 1698–1716. http://dx.doi.org/10.1111/j.1600-0854.2008.00797.x. – DOI 10.1111/j.1600–0854.2008.00797.x

[110] Mahul-Mellier, A.-L. ; Hemming, F. J. ; Blot, B. ; Fraboulet, S. ; and Sadoul, R.: Alix, making a link between apoptosis-linked gene-2, the endosomal sorting complexes required for transport, and neuronal death in vivo. *J Neurosci.* 2006, January; **26**(2): pp. 542–549. http://dx.doi.org/10.1523/JNEUROSCI.3069-05.2006. – DOI 10.1523/JNEUROSCI.3069–05.2006

[111] Pornillos, O. ; Higginson, D. S. ; Stray, K. M. ; Fisher, R. D. ; Garrus, J. E. ; Payne, M. ; He, G.-P. et al.: HIV Gag mimics the Tsg101-recruiting activity of the human Hrs protein. *J Cell Biol.* 2003, August; **162**(3): pp. 425–434. http://dx.doi.org/10.1083/jcb.200302138. – DOI 10.1083/jcb.200302138

[112] Thompson, B. J. ; Mathieu, J. ; Sung, H.-H. ; Loeser, E. ; Rørth, P. ; and Cohen, S. M.: Tumor suppressor properties of the ESCRT-II complex component Vps25 in Drosophila. *Dev Cell.* 2005, November; **9**(5): pp. 711–720. http://dx.doi.org/10.1016/j.devcel.2005.09.020. – DOI 10.1016/j.devcel.2005.09.020

[113] Bonangelino, C. J. ; Chavez, E. M. ; and Bonifacino, J. S.: Genomic screen for vacuolar protein sorting genes in Saccharomyces cerevisiae. *Mol Biol Cell.* 2002, July; **13**(7): pp. 2486–2501. http://dx.doi.org/10.1091/mbc.02-01-0005. – DOI 10.1091/mbc.02–01–0005

[114] Katzmann, D. J. ; Odorizzi, G. ; and Emr, S. D.: Receptor downregulation and multivesicular-body sorting. *Nat Rev Mol Cell Biol.* 2002, December; **3**(12): pp. 893–905. http://dx.doi.org/10.1038/nrm973. – DOI 10.1038/nrm973

[115] Raymond, C. K. ; Howald-Stevenson, I. ; Vater, C. A. ; and Stevens, T. H.: Morphological classification of the yeast vacuolar protein sorting mutants: evidence for a prevacuolar compartment in class E vps mutants. *Mol Biol Cell.* 1992, December; **3**(12): pp. 1389–1402

[116] Babst, M. ; Katzmann, D. J. ; Snyder, W. B. ; Wendland, B. ; and Emr, S. D.: Endosome-associated complex, ESCRT-II, recruits transport machinery for protein sorting at the multivesicular body. *Dev Cell.* 2002, August; **3**(2): pp. 283–289

[117] Babst, M. ; Katzmann, D. J. ; Estepa-Sabal, E. J. ; Meerloo, T. ; and Emr, S. D.: Escrt-III: an endosome-associated heterooligomeric protein complex required for mvb sorting. *Dev Cell.* 2002, August; **3**(2): pp. 271–282

[118] Katzmann, D. J. ; Babst, M. ; and Emr, S. D.: Ubiquitin-dependent sorting into the multivesicular body pathway requires the function of a conserved endosomal protein sorting complex, ESCRT-I. *Cell.* 2001, July; **106**(2): pp. 145–155

[119] Spitzer, C. ; Schellmann, S. ; Sabovljevic, A. ; Shahriari, M. ; Keshavaiah, C. ; Bechtold, N. ; Herzog, M. et al.: The Arabidopsis elch mutant reveals functions of an ESCRT component in cytokinesis. *Development.* 2006, December; **133**(23): pp. 4679–4689. http://dx.doi.org/10.1242/dev.02654. – DOI 10.1242/dev.02654

[120] Carlton, J. G. and Martin-Serrano, J.: Parallels between cytokinesis and retroviral budding: a role for the ESCRT machinery. *Science.* 2007, June; **316**(5833): pp. 1908–1912. http://dx.doi.org/10.1126/science.1143422. – DOI 10.1126/science.1143422

[121] Morita, E. ; Sandrin, V. ; Chung, H.-Y. ; Morham, S. G. ; Gygi, S. P. ; Rodesch, C. K. ; and Sundquist, W. I.: Human ESCRT and ALIX proteins interact with proteins of the midbody and function in cytokinesis. *EMBO J.* 2007, October; **26**(19): pp. 4215–4227. http://dx.doi.org/10.1038/sj.emboj.7601850. – DOI 10.1038/sj.emboj.7601850

[122] Morita, E. and Sundquist, W. I.: Retrovirus budding. *Annu Rev Cell Dev Biol.* 2004; **20**: pp. 395–425. http://dx.doi.org/10.1146/annurev.cellbio.20.010403.102350. – DOI 10.1146/annurev.cellbio.20.010403.102350

[123] Fujii, K. ; Hurley, J. H. ; and Freed, E. O.: Beyond Tsg101: the role of Alix in 'ESCRTing' HIV-1. *Nat Rev Microbiol.* 2007, December; **5**(12): pp. 912–916. http://dx.doi.org/10.1038/nrmicro1790. – DOI 10.1038/nrmicro1790

[124] Filimonenko, M. ; Stuffers, S. ; Raiborg, C. ; Yamamoto, A. ; Malerød, L. ; Fisher, E. M. C. ; Isaacs, A. et al.: Functional multivesicular bodies are required for autophagic clearance of protein aggregates associated with neurodegenerative disease. *J Cell Biol.* 2007, November; **179**(3): pp. 485–500. http://dx.doi.org/10.1083/jcb.200702115. – DOI 10.1083/jcb.200702115

[125] Lee, I. ; Li, Z. ; and Marcotte, E. M.: An improved, bias-reduced probabilistic functional gene network of baker's yeast, Saccharomyces cerevisiae. *PLoS ONE.* 2007, January; **2**(10): p. e988. http://dx.doi.org/10.1371/journal.pone.0000988. – DOI 10.1371/journal.pone.0000988. – ISSN 1932–6203

[126] Djeddi, A. ; Michelet, X. ; Culetto, E. ; Alberti, A. ; Barois, N. ; and Legouis, R.: Induction of autophagy in ESCRT mutants is an adaptive response for cell survival in C. elegans. *Journal of Cell Science.* 2012, February; **125**(3): pp. 685–694. http://dx.doi.org/10.1242/jcs.091702. – DOI 10.1242/jcs.091702. – ISSN 1477–9137

[127] Vietri, M. ; Schink, K. O. ; Campsteijn, C. ; Wegner, C. S. ; Schultz, S. W. ; Christ, L. ; Thoresen, S. B. et al.: Spastin and ESCRT-III coordinate mitotic spindle disassembly and nuclear envelope sealing. *Nature.* 2015, June; **522**(7555): pp. 231–235. http://dx.doi.org/10.1038/nature14408. – DOI 10.1038/nature14408. – ISSN 1476–4687

[128] Gaur, N. A. ; Hasek, J. ; Brickner, D. G. ; Qiu, H. ; Zhang, F. ; Wong, C.-M. ; Malcova, I. et al.: Vps Factors Are Required for Efficient Transcription Elongation in Budding Yeast. *Genetics.* 2013, January; **193**(3): pp. 829–851. http://dx.doi.org/10.1534/genetics.112.146308. – DOI 10.1534/genetics.112.146308. – ISSN 0016–6731

[129] Stauffer, D. R. ; Howard, T. L. ; Nyun, T. ; and Hollenberg, S. M.: CHMP1 is a novel nuclear matrix protein affecting chromatin structure and cell-cycle progression. *J Cell Sci.* 2001, July; **114**(Pt 13): pp. 2383–2393

[130] Morita, E. ; Colf, L. A. ; Karren, M. A. ; Sandrin, V. ; Rodesch, C. K. ; and Sundquist, W. I.: Human ESCRT-III and VPS4 proteins are required for centrosome and spindle maintenance. *Proceedings of the National Academy of Sciences.* 2010, June; **107**(29): pp. 12889–12894. http://dx.doi.org/10.1073/pnas.1005938107. – DOI 10.1073/pnas.1005938107. – ISSN 1091–6490

[131] Reid, R. J. D. ; González-Barrera, S. ; Sunjevaric, I. ; Alvaro, D. ; Ciccone, S. ; Wagner, M. ; and Rothstein, R.: Selective ploidy ablation, a high-throughput plasmid transfer protocol, identifies new genes affecting topoisomerase I-induced DNA damage. *Genome Res.* 2011, March; **21**(3): pp. 477–486. http://dx.doi.org/10.1101/gr.109033.110. – DOI 10.1101/gr.109033.110

[132] James H Hurley: ESCRT complexes and the biogenesis of multivesicular bodies. *Curr Opin Cell Biol.* 2008, February; **20**(1): pp. 4–11. http://dx.doi.org/10.1016/j.ceb.2007.12.002. – DOI 10.1016/j.ceb.2007.12.002

[133] Williams, R. L. and Urbé, S.: The emerging shape of the ESCRT machinery. *Nat Rev Mol Cell Biol.* 2007, May; **8**(5): pp. 355–368. http://dx.doi.org/10.1038/nrm2162. – DOI 10.1038/nrm2162

[134] Gaullier, J. M. ; Simonsen, A. ; D'Arrigo, A. ; Bremnes, B. ; Stenmark, H. ; and Aasland, R.: FYVE fingers bind PtdIns(3)P. *Nature.* 1998, July; **394**(6692): pp. 432–433. http://dx.doi.org/10.1038/28767. – DOI 10.1038/28767

[135] Raiborg, C. ; Bremnes, B. ; Mehlum, A. ; Gillooly, D. J. ; D'Arrigo, A. ; Stang, E. ; and Stenmark, H.: FYVE and coiled-coil domains determine the specific localisation of Hrs to early endosomes. *J Cell Sci.* 2001, June; **114**(Pt 12): pp. 2255–2263

[136] Hofmann, K. and Falquet, L.: A ubiquitin-interacting motif conserved in components of the proteasomal and lysosomal protein degradation systems. *Trends Biochem Sci.* 2001, June; **26**(6): pp. 347–350

[137] Teis, D. ; Saksena, S. ; and Emr, S. D.: Ordered assembly of the ESCRT-III complex on endosomes is required to sequester cargo during MVB formation. *Dev Cell.* 2008, October; **15**(4): pp. 578–589. http://dx.doi.org/10.1016/j.devcel.2008.08.013. – DOI 10.1016/j.devcel.2008.08.013

[138] Wollert, T. and Hurley, J. H.: Molecular mechanism of multivesicular body biogenesis by ESCRT complexes. *Nature.* 2010, April; **464**(7290): pp. 864–869. http://dx.doi.org/10.1038/nature08849. – DOI 10.1038/nature08849

[139] Wollert, T. ; Wunder, C. ; Lippincott-Schwartz, J. ; and Hurley, J. H.: Membrane scission by the ESCRT-III complex. *Nature.* 2009, March; **458**(7235): pp. 172–177. http://dx.doi.org/10.1038/nature07836. – DOI 10.1038/nature07836

[140] Nickerson, D. P. ; Russell, M. R. G. ; and Odorizzi, G.: A concentric circle model of multivesicular body cargo sorting. *EMBO Rep.* 2007, July; **8**(7): pp. 644–650. http://dx.doi.org/10.1038/sj.embor.7401004. – DOI 10.1038/sj.embor.7401004

[141] Babst, M. ; Sato, T. K. ; Banta, L. M. ; and Emr, S. D.: Endosomal transport function in yeast requires a novel AAA-type ATPase, Vps4p. *EMBO J.* 1997, April; **16**(8): pp. 1820–1831. http://dx.doi.org/10.1093/emboj/16.8.1820. – DOI 10.1093/emboj/16.8.1820

[142] Rusten, T. E. and Stenmark, H.: How do ESCRT proteins control autophagy? *J Cell Sci.* 2009, July; **122**(Pt 13): pp. 2179–2183. http://dx.doi.org/10.1242/jcs.050021. – DOI 10.1242/jcs.050021

[143] Lee, J.-A. ; Beigneux, A. ; Ahmad, S. T. ; Young, S. G. ; and Gao, F.-B.: ESCRT-III dysfunction causes autophagosome accumulation and neurodegeneration. *Curr Biol.* 2007, September; **17**(18): pp. 1561–1567. http://dx.doi.org/10.1016/j.cub.2007.07.029. – DOI 10.1016/j.cub.2007.07.029

[144] Rusten, T. E. ; Vaccari, T. ; Lindmo, K. ; Rodahl, L. M. W. ; Nezis, I. P. ; Sem-Jacobsen, C. ; Wendler, F. et al.: ESCRTs and Fab1 regulate distinct steps of autophagy. *Curr Biol.* 2007, October; **17**(20): pp. 1817–1825. http://dx.doi.org/10.1016/j.cub.2007.09.032. – DOI 10.1016/j.cub.2007.09.032

[145] Slagsvold, T. ; Pattni, K. ; Malerød, L. ; and Stenmark, H.: Endosomal and non-endosomal functions of ESCRT proteins. *Trends Cell Biol.* 2006, June; **16**(6): pp. 317–326. http://dx.doi.org/10.1016/j.tcb.2006.04.004. – DOI 10.1016/j.tcb.2006.04.004

[146] Pilecka, I. ; Banach-Orlowska, M. ; and Miaczynska, M.: Nuclear functions of endocytic proteins. *Eur J Cell Biol.* 2007, September; **86**(9): pp. 533–547. http://dx.doi.org/10.1016/j.ejcb.2007.04.004. – DOI 10.1016/j.ejcb.2007.04.004

[147] Kamura, T. ; Burian, D. ; Khalili, H. ; Schmidt, S. L. ; Sato, S. ; Liu, W. J. ; Conrad, M. N. et al.: Cloning and characterization of ELL-associated proteins EAP45 and EAP20. a role for yeast EAP-like proteins in regulation of gene expression by glucose. *J Biol Chem.* 2001, May; **276**(19): pp. 16528–16533. http://dx.doi.org/10.1074/jbc.M010142200. – DOI 10.1074/jbc.M010142200

[148] Zhong, Q. ; Chen, Y. ; Jones, D. ; and Lee, W. H.: Perturbation of TSG101 protein affects cell cycle progression. *Cancer Res.* 1998, July; **58**(13): pp. 2699–2702

[149] Xie, W. ; Li, L. ; and Cohen, S. N.: Cell cycle-dependent subcellular localization of the TSG101 protein and mitotic and nuclear abnormalities associated with TSG101 deficiency. *Proc Natl Acad Sci U S A.* 1998, February; **95**(4): pp. 1595–1600

[150] Burgdorf, S. ; Leister, P. ; and Scheidtmann, K. H.: TSG101 interacts with apoptosis-antagonizing transcription factor and enhances androgen receptor-mediated transcription by promoting its monoubiquitination. *J Biol Chem.* 2004, April; **279**(17): pp. 17524–17534. http://dx.doi.org/10.1074/jbc.M313703200. – DOI 10.1074/jbc.M313703200

[151] Shim, J.-H. ; Xiao, C. ; Hayden, M. S. ; Lee, K.-Y. ; Trombetta, E. S. ; Pypaert, M. ; Nara, A. et al.: CHMP5 is essential for late endosome function and down-regulation of receptor signaling during mouse embryogenesis. *J Cell Biol.* 2006, March; **172**(7): pp. 1045–1056. http://dx.doi.org/10.1083/jcb.200509041. – DOI 10.1083/jcb.200509041

[152] Wagner, K.-U. ; Krempler, A. ; Qi, Y. ; Park, K. ; Henry, M. D. ; Triplett, A. A. ; Riedlinger, G. et al.: Tsg101 is essential for cell growth, proliferation, and cell survival of embryonic and adult tissues. *Mol Cell Biol.* 2003, January; **23**(1): pp. 150–162

[153] Obita, T. ; Saksena, S. ; Ghazi-Tabatabai, S. ; Gill, D. J. ; Perisic, O. ; Emr, S. D. ; and Williams, R. L.: Structural basis for selective recognition of ESCRT-III by the AAA ATPase Vps4. *Nature.* 2007, October; **449**(7163): pp. 735–739. http://dx.doi.org/10.1038/nature06171. – DOI 10.1038/nature06171

[154] Eggib: *Openclipart: Building Blocks.* https://openclipart.org/detail/214574/building-blocks. version: February 2015. – downloaded: 24/09/2015

[155] Stuffers, S. ; Brech, A. ; and Stenmark, H.: ESCRT proteins in physiology and disease. *Exp Cell Res.* 2009, May; **315**(9): pp. 1619–1626. http://dx.doi.org/10.1016/j.yexcr.2008.10.013. – DOI 10.1016/j.yexcr.2008.10.013

[156] Philips, J. A. ; Porto, M. C. ; Wang, H. ; Rubin, E. J. ; and Perrimon, N.: ESCRT factors restrict mycobacterial growth. *Proc Natl Acad Sci U S A.* 2008, February; **105**(8): pp. 3070–3075. http://dx.doi.org/10.1073/pnas.0707206105. – DOI 10.1073/pnas.0707206105

[157] Nixon, R. A. and Cataldo, A. M.: Lysosomal system pathways: genes to neurodegeneration in Alzheimer's disease. *J Alzheimers Dis.* 2006; **9**(3 Suppl): pp. 277–289

[158] Spencer, B. ; Emadi, S. ; Desplats, P. ; Eleuteri, S. ; Michael, S. ; Kosberg, K. ; Shen, J. et al.: ESCRT-mediated uptake and degradation of brain-targeted α-synuclein single chain antibody attenuates neuronal degeneration in vivo. *Mol Ther.* 2014, October; **22**(10): pp. 1753–1767. http://dx.doi.org/10.1038/mt.2014.129. – DOI 10.1038/mt.2014.129

[159] Tu, C. ; Ahmad, G. ; Mohapatra, B. ; Bhattacharyya, S. ; Ortega-Cava, C. ; Chung, B. M. ; Wagner, K.-U. et al.: ESCRT proteins. *BioArchitecture.* 2011, January; **1**(1): pp. 45–48. http://dx.doi.org/10.4161/bioa.1.1.15173. – DOI 10.4161/bioa.1.1.15173. – ISSN 1949–100X

[160] Westerhoff, H. V. ; Winder, C. ; Messiha, H. ; Simeonidis, E. ; Adamczyk, M. ; Verma, M. ; Bruggeman, F. J. et al.: Systems biology: the elements and principles of life. *FEBS Lett.* 2009, December; **583**(24): pp. 3882–3890. http://dx.doi.org/10.1016/j.febslet.2009.11.018. – DOI 10.1016/j.febslet.2009.11.018

[161] Snyder, M. and Gallagher, J. E. G.: Systems biology from a yeast omics perspective. *FEBS Lett.* 2009, December; **583**(24): pp. 3895–3899. http://dx.doi.org/10.1016/j.febslet.2009.11.011. – DOI 10.1016/j.febslet.2009.11.011

[162] Westerhoff, H. V. and Kell, D. B.: 2 - The methodologies of systems biology. version: 2007. http://dx.doi.org/10.1016/B978-044452085-2/50004-8. in: Boogerd, F. C. (ed.) and Westerhoff, F. J. B.-H. S. H. V. (ed.): *Systems Biology.* Amsterdam : Elsevier, 2007. – DOI 10.1016/B978–044452085–2/50004–8. – ISBN 978–0–444–52085–2, pp. 23–70

[163] Klipp, E. ; Liebermeister, W. ; Wierling, C. ; Kowald, A. ; Lehrach, H. ; and Herwig, R.: *Systems Biology.* Wiley-Blackwell, 2009. – ISBN 3527318747

[164] Bruggeman, F. J. and Westerhoff, H. V.: The nature of systems biology. *Trends Microbiol.* 2007, January; **15**(1): pp. 45–50. http://dx.doi.org/10.1016/j.tim.2006.11.003. – DOI 10.1016/j.tim.2006.11.003

[165] Harari, Y. and Kupiec, M.: Genome-wide studies of telomere biology in budding yeast. *Microbial Cell.* 2014, March; **1**(3): pp. 70–80. http://dx.doi.org/10.15698/mic2014.01.132. – DOI 10.15698/mic2014.01.132. – ISSN 2311–2638

[166] Botstein, D. and Fink, G. R.: Yeast: an experimental organism for 21st Century biology. *Genetics.* 2011, November; **189**(3): pp. 695–704. http://dx.doi.org/10.1534/genetics.111.130765. – DOI 10.1534/genetics.111.130765

[167] Horst Feldmann: *Yeast – Molecular and Cell Biology.* Wiley-Blackwell, 2010

[168] Herschel L. Roman: Development of Yeast as an Experimental Organism. in: *The Molecular Biology of the Yeast Saccharomyces: Life Cycle and Inheritance* vol. 11A. Cold Spring Harbor Laboratory Press, 1981, pp. 1–9

[169] Duina, A. A. ; Miller, M. E. ; and Keeney, J. B.: Budding yeast for budding geneticists: a primer on the Saccharomyces cerevisiae model system. *Genetics.* 2014, May; **197**(1): pp. 33–48. http://dx.doi.org/10.1534/genetics.114.163188. – DOI 10.1534/genetics.114.163188

[170] Masur: *Yeast Life Cycle.* https://commons.wikimedia.org/wiki/File:Yeast_lifecycle.svg. version: February 2007

[171] Heinicke, S. ; Livstone, M. S. ; Lu, C. ; Oughtred, R. ; Kang, F. ; Angiuoli, S. V. ; White, O. et al.: The Princeton Protein Orthology Database (P-POD): a comparative genomics analysis tool for biologists. *PLoS One.* 2007; **2**(8): p. e766. http://dx.doi.org/10.1371/journal.pone.0000766. – DOI 10.1371/journal.pone.0000766

[172] Giaever, G. ; Chu, A. M. ; Ni, L. ; Connelly, C. ; Riles, L. ; Véronneau, S. ; Dow, S. et al.: Functional profiling of the Saccharomyces cerevisiae genome. *Nature.* 2002, July; **418**(6896): pp. 387–391. http://dx.doi.org/10.1038/nature00935. – DOI 10.1038/nature00935

[173] Winzeler, E. A. ; Shoemaker, D. D. ; Astromoff, A. ; Liang, H. ; Anderson, K. ; Andre, B. ; Bangham, R. et al.: Functional characterization of the S. cerevisiae genome by gene deletion and parallel analysis. *Science.* 1999, August; **285**(5429): pp. 901–906

[174] Brachmann, C. B. ; Davies, A. ; Cost, G. J. ; Caputo, E. ; Li, J. ; Hieter, P. ; and Boeke, J. D.: Designer deletion strains derived from Saccharomyces cerevisiae S288C: a useful set of strains and plasmids for PCR-mediated gene disruption and other applications. *Yeast.* 1998, January; **14**(2): pp. 115–132

[175] Breslow, D. K. ; Cameron, D. M. ; Collins, S. R. ; Schuldiner, M. ; Stewart-Ornstein, J. ; Newman, H. W. ; Braun, S. et al.: A comprehensive strategy enabling high-resolution functional analysis of the yeast genome. *Nat Methods.* 2008, August; **5**(8): pp. 711–718. http://dx.doi.org/10.1038/nmeth.1234. – DOI 10.1038/nmeth.1234

[176] Li, Z. ; Vizeacoumar, F. J. ; Bahr, S. ; Li, J. ; Warringer, J. ; Vizeacoumar, F. S. ; Min, R. et al.: Systematic exploration of essential yeast gene function with temperature-sensitive mutants. *Nat Biotechnol.* 2011, April; **29**(4): pp. 361–367. http://dx.doi.org/10.1038/nbt.1832. – DOI 10.1038/nbt.1832

[177] Huh, W.-K. ; Falvo, J. V. ; Gerke, L. C. ; Carroll, A. S. ; Howson, R. W. ; Weissman, J. S. ; and O'Shea, E. K.: Global analysis of protein localization in budding yeast. *Nature.* 2003, October; **425**(6959): pp. 686–691. http://dx.doi.org/10.1038/nature02026. – DOI 10.1038/nature02026

[178] Ghaemmaghami, S. ; Huh, W.-K. ; Bower, K. ; Howson, R. W. ; Belle, A. ; Dephoure, N. ; O'Shea, E. K. et al.: Global analysis of protein expression in yeast. *Nature.* 2003, October; **425**(6959): pp. 737–741. http://dx.doi.org/10.1038/nature02046. – DOI 10.1038/nature02046

[179] Kemmeren, P. ; Sameith, K. ; van de Pasch, L. A. L. ; Benschop, J. J. ; Lenstra, T. L. ; Margaritis, T. ; O'Duibhir, E. et al.: Large-scale genetic perturbations reveal regulatory networks and an abundance of gene-specific repressors. *Cell.* 2014, April; **157**(3): pp. 740–752. http://dx.doi.org/10.1016/j.cell.2014.02.054. – DOI 10.1016/j.cell.2014.02.054

[180] Yoshikawa, K. ; Tanaka, T. ; Furusawa, C. ; Nagahisa, K. ; Hirasawa, T. ; and Shimizu, H.: Comprehensive phenotypic analysis for identification of genes affecting growth under ethanol stress in Saccharomyces cerevisiae. *FEMS Yeast Res.* 2009, February; **9**(1): pp. 32–44. http://dx.doi.org/10.1111/j.1567-1364.2008.00456.x. – DOI 10.1111/j.1567–1364.2008.00456.x. – ISSN 1567–1364

[181] Costanzo, M. ; Baryshnikova, A. ; Bellay, J. ; Kim, Y. ; Spear, E. D. ; Sevier, C. S. ; Ding, H. et al.: The genetic landscape of a cell. *Science.* 2010, January; **327**(5964): pp. 425–431. http://dx.doi.org/10.1126/science.1180823. – DOI 10.1126/science.1180823. – ISSN 1095–9203

[182] Baryshnikova, A. ; Costanzo, M. ; Dixon, S. ; Vizeacoumar, F. J. ; Myers, C. L. ; Andrews, B. ; and Boone, C.: Synthetic genetic array (SGA) analysis in Saccharomyces cerevisiae and Schizosaccharomyces pombe. *Methods Enzymol.* 2010; **470**: pp. 145–179

[183] Askree, S. H. ; Yehuda, T. ; Smolikov, S. ; Gurevich, R. ; Hawk, J. ; Coker, C. ; Krauskopf, A. et al.: A genome-wide screen for *Saccharomyces cerevisiae* deletion mutants that affect telomere length. *Proceedings of the National Academy of Sciences.* 2004, May; **101**(23): pp. 8658–8663. http://dx.doi.org/10.1073/pnas.0401263101. – DOI 10.1073/pnas.0401263101. – ISSN 0027–8424, 1091–6490

[184] Gatbonton, T. ; Imbesi, M. ; Nelson, M. ; Akey, J. M. ; Ruderfer, D. M. ; Kruglyak, L. ; Simon, J. A. et al.: Telomere length as a quantitative trait: genome-wide survey and genetic mapping of telomere length-control genes in yeast. *PLoS Genet.* 2006, March; **2**(3): p. e35. http://dx.doi.org/10.1371/journal.pgen.0020035. – DOI 10.1371/journal.pgen.0020035. – ISSN 1553–7404

[185] Ungar, L. ; Yosef, N. ; Sela, Y. ; Sharan, R. ; Ruppin, E. ; and Kupiec, M.: A genome-wide screen for essential yeast genes that affect telomere length maintenance. *Nucleic Acids Res.* 2009, April; **37**(12): pp. 3840–3849. http://dx.doi.org/10.1093/nar/gkp259. – DOI 10.1093/nar/gkp259. – ISSN 0305–1048, 1362–4962

[186] Krogan, N. J. ; Cagney, G. ; Yu, H. ; Zhong, G. ; Guo, X. ; Ignatchenko, A. ; Li, J. et al.: Global landscape of protein complexes in the yeast Saccharomyces cerevisiae. *Nature.* 2006, March; **440**(7084): p. 637–643. http://dx.doi.org/10.1038/nature04670. – DOI 10.1038/nature04670. – ISSN 1476–4679

[187] Uetz, P. ; Giot, L. ; Cagney, G. ; Mansfield, T. A. ; Judson, R. S. ; Knight, J. R. ; Lockshon, D. et al.: A comprehensive analysis of protein-protein interactions in Saccharomyces cerevisiae. *Nature.* 2000, February; **403**(6770): pp. 623–627. http://dx.doi.org/10.1038/35001009. – DOI 10.1038/35001009

[188] Yu, H. ; Braun, P. ; Yildirim, M. A. ; Lemmens, I. ; Venkatesan, K. ; Sahalie, J. ; Hirozane-Kishikawa, T. et al.: High-Quality Binary Protein Interaction Map of the Yeast Interactome Network. *Science.* 2008, October; **322**(5898): p. 104–110. http://dx.doi.org/10.1126/science.1158684. – DOI 10.1126/science.1158684. – ISSN 1095–9203

[189] GE Healthcare Dharmacon Inc.: *Yeast Mata Knock Out Strain Collection (YSC1053).* http://dharmacon.gelifesciences.com/uploadedFiles/Resources/Mat_a_v5.0.xlsx

[190] GE Healthcare Dharmacon Inc.: *Yeast Matα Knock Out Strain Collection (YSC1054).* http://dharmacon.gelifesciences.com/uploadedFiles/Resources/Mat_alpha_obs_v6.0.xls

[191] GE Healthcare Dharmacon Inc.: *Yeast DAmP Library for essential genes haploid (YSC5090).* http://dharmacon.gelifesciences.com/uploadedFiles/Resources/YSC5090%20-%20Yeast%20DAmP%20HAPLOID.xls

[192] Balakrishnan, R. ; Park, J. ; Karra, K. ; Hitz, B. C. ; Binkley, G. ; Hong, E. L. ; Sullivan, J. et al.: YeastMine–an integrated data warehouse for Saccharomyces cerevisiae data as a multipurpose tool-kit. *Database.* 2012, January; **2012**(bar062). http://dx.doi.org/10.1093/database/bar062. – DOI 10.1093/database/bar062. – ISSN 1758–0463

[193] Koh, J. L. Y. ; Ding, H. ; Costanzo, M. ; Baryshnikova, A. ; Toufighi, K. ; Bader, G. D. ; Myers, C. L. et al.: DRYGIN: a database of quantitative genetic interaction networks in yeast. *Nucleic Acids Res.* 2010, January; **38**(Database issue): pp. D502–D507. http://dx.doi.org/10.1093/nar/gkp820. – DOI 10.1093/nar/gkp820

[194] Fred Sherman: Getting started with yeast. *Methods Enzymol.* 2002; **350**

[195] Shachar, R. ; Ungar, L. ; Kupiec, M. ; Ruppin, E. ; and Sharan, R.: A systems-level approach to mapping the telomere length maintenance gene circuitry. *Mol Syst Biol.* 2008, March; **4**(172). http://dx.doi.org/10.1038/msb.2008.13. – DOI 10.1038/msb.2008.13. – ISSN 1744–4292

[196] Yosef, N. ; Ungar, L. ; Zalckvar, E. ; Kimchi, A. ; Kupiec, M. ; Ruppin, E. ; and Sharan, R.: Toward accurate reconstruction of functional protein networks. *Mol Syst Biol.* 2009, March; **5**(248). http://dx.doi.org/10.1038/msb.2009.3. – DOI 10.1038/msb.2009.3. – ISSN 1744–4292

[197] Ben-Shitrit, T. ; Yosef, N. ; Shemesh, K. ; Sharan, R. ; Ruppin, E. ; and Kupiec, M.: Systematic identification of gene annotation errors in the widely used yeast mutation collections. *Nat Methods.* 2012, February;. http://dx.doi.org/10.1038/nmeth.1890. – DOI 10.1038/nmeth.1890. – ISSN 1548–7105

[198] Rog, O. ; Smolikov, S. ; Krauskopf, A. ; and Kupiec, M.: The yeast VPS genes affect telomere length regulation. *Curr Genet.* 2005, January; **47**(1): pp. 18–28. http://dx.doi.org/10.1007/s00294-004-0548-y. – DOI 10.1007/s00294–004–0548–y. – ISSN 0172–8083

[199] Romano, G. H. ; Harari, Y. ; Yehuda, T. ; Podhorzer, A. ; Rubinstein, L. ; Shamir, R. ; Gottlieb, A. et al.: Environmental Stresses Disrupt Telomere Length Homeostasis. *PLoS Genet.* 2013, September; **9**(9): p. e1003721. http://dx.doi.org/10.1371/journal.pgen.1003721. – DOI 10.1371/journal.pgen.1003721

[200] Addinall, S. G. ; Downey, M. ; Yu, M. ; Zubko, M. K. ; Dewar, J. ; Leake a ; Hallinan, J. et al.: A genomewide suppressor and enhancer analysis of *cdc13-1* reveals varied cellular processes influencing telomere capping in *Saccharomyces cerevisiae*. *Genetics.* 2008, December; **180**(4): pp. 2251–2266. http://dx.doi.org/10.1534/genetics.108.092577. – DOI 10.1534/genetics.108.092577. – ISSN 0016–6731

[201] Addinall, S. G. ; Holstein, E.-M. ; Lawless, C. ; Yu, M. ; Chapman, K. ; Banks, A. P. ; Ngo, H.-P. et al.: Quantitative fitness analysis shows that NMD proteins and many other protein complexes suppress or enhance distinct telomere cap defects. *PLoS Genet.* 2011, April; **7**(4): p. e1001362. http://dx.doi.org/10.1371/journal.pgen.1001362. – DOI 10.1371/journal.pgen.1001362. – ISSN 1553–7404

[202] Poschke, H. ; Dees, M. ; Chang, M. ; Amberkar, S. ; Kaderali, L. ; Rothstein, R. ; and Luke, B.: Rif2 Promotes a Telomere Fold-Back Structure through Rpd3L Recruitment in Budding Yeast. *PLoS Genet.* 2012, September; **8**(9): p. e1002960. http://dx.doi.org/10.1371/journal.pgen.1002960. – DOI 10.1371/journal.pgen.1002960. – ISSN 1553–7404

[203] Chang, H.-Y. ; Lawless, C. ; Addinall, S. G. ; Oexle, S. ; Taschuk, M. ; Wipat, A. ; Wilkinson, D. J. et al.: Genome-wide analysis to identify pathways affecting telomere-initiated senescence in budding yeast. *G3.* 2011, August; **1**(3): pp. 197–208. http://dx.doi.org/10.1534/g3.111.000216. – DOI 10.1534/g3.111.000216. – ISSN 2160–1836

[204] Yibmantasiri, P. ; Leahy, D. C. ; Busby, B. P. ; Angermayr, S. A. ; Sorgo, A. G. ; Boeger, K. ; Heathcott, R. et al.: Molecular basis for fungicidal action of neothyonidioside, a triterpene glycoside from the sea cucumber, *Australostichopus mollis*. *Mol Biosyst.* 2012, March; **8**(3): pp. 902–912. http://dx.doi.org/10.1039/c2mb05426d. – DOI 10.1039/c2mb05426d

[205] Carmen McRae: *Blues Is a Woman.* Speech at Newport Jazz Festival, New York City, July 1980. – (U.S. jazz singer)

[206] R Core Team: *R: A Language and Environment for Statistical Computing.* Vienna, Austria: R Foundation for Statistical Computing, 2015. http://www.R-project.org/. – v3.2.1

[207] Huber, W. ; Carey, V. J. ; Gentleman, R. ; Anders, S. ; Carlson, M. ; Carvalho, B. S. ; Bravo, H. C. et al.: Orchestrating high-throughput genomic analysis with Bioconductor. *Nat Meth.* 2015, January; **12**(2): pp. 115–121. http://dx.doi.org/10.1038/nmeth.3252. – DOI 10.1038/nmeth.3252. – ISSN 1548–7105

[208] Carlson, M.: *Package ‘ Genome wide annotation for Yeast. ’*

[209] Carlson, M.: *Package ‘ KEGG.db: A set of annotation maps for KEGG. ’*

[210] Ruepp, A. ; Zollner, A. ; Maier, D. ; Albermann, K. ; Hani, J. ; Mokrejs, M. ; Tetko, I. et al.: *MIPS Functional Catalogue Database (FunCat) v2.1 [8].* ftp://ftpmips.gsf.de/fungi/catalogue/

[211] Chapple, C. E. ; Robisson, B. ; Spinelli, L. ; Guien, C. ; Becker, E. ; and Brun, C.: Extreme multifunctional proteins identified from a human protein interaction network. *Nat Commun.* 2015; **6**: p. 7412. http://dx.doi.org/10.1038/ncomms8412. – DOI 10.1038/ncomms8412

[212] Csardi, G. and Nepusz, T.: The igraph software package for complex network research. *InterJournal.* 2006; **Complex Systems**. http://igraph.org

[213] Shannon, P. ; Markiel, A. ; Ozier, O. ; Baliga, N. S. ; Wang, J. T. ; Ramage, D. ; Amin, N. et al.: Cytoscape: a software environment for integrated models of biomolecular interaction networks. *Genome Res.* 2003, November; **13**(11): pp. 2498–2504. http://dx.doi.org/10.1101/gr.1239303. – DOI 10.1101/gr.1239303. – v3.2.1

[214] Subramanian, A. ; Tamayo, P. ; Mootha, V. K. ; Mukherjee, S. ; Ebert, B. L. ; Gillette, M. A. ; Paulovich, A. et al.: Gene set enrichment analysis: A knowledge-based approach for interpreting genome-wide expression profiles. *Proceedings of the National Academy of Sciences.* 2005, September; **102**(43): pp. 15545–15550. http://dx.doi.org/10.1073/pnas.0506580102. – DOI 10.1073/pnas.0506580102. – ISSN 1091–6490. – v2.2.1.0

[215] Mootha, V. K. ; Lindgren, C. M. ; Eriksson, K.-F. ; Subramanian, A. ; Sihag, S. ; Lehar, J. ; Puigserver, P. et al.: PGC-1α-responsive genes involved in oxidative phosphorylation are coordinately downregulated in human diabetes. *Nat Genet.* 2003, June; **34**(3): pp. 267–273. http://dx.doi.org/10.1038/ng1180. – DOI 10.1038/ng1180. – ISSN 1061–4036

[216] Taiyun Wei: *corrplot: Visualization of a correlation matrix*, 2013. http://CRAN.R-project.org/package=corrplot. – R package version 0.73

[217] Lee, S. E. ; Moore, J. K. ; Holmes, A. ; Umezu, K. ; Kolodner, R. D. ; and Haber, J. E.: Saccharomyces Ku70, mre11/rad50 and RPA proteins regulate adaptation to G2/M arrest after DNA damage. *Cell.* 1998, August; **94**(3): pp. 399–409

[218] André Maicher: *The impacts of deregulated telomere transcription and increased telomeric RNA: DNA hybrid llevel on telomere length homeostasis and cellular senescence*, Ruperto-Carola University of Heidelberg, Combined Faculties for the Natural Sciences and for Mathematics, Dissertation, September 2013

[219] Bettina Balk: *The influence of induced telomeric transcription and accumulation of RNA-DNA hhybrid on telomere maintenance in the absence of telomerase*, Ruperto-Carola University of Heidelberg, Combined Faculties for the Natural Sciences and for Mathematics, Dissertation, 2014

[220] Julia Klermund: *The influence of rapamycin-induced TORC1 inhibition on adaptation to the cellular DNA damage checkpoint*, Ruperto-Carola University of Heidelberg, Combined Faculties for the Natural Sciences and for Mathematics, Dissertation, July 2015

[221] Amberg, D. C. ; Burke, D. J. ; and Strathern, J. N.: *Methods in Yeast Genetics.* Cold Spring Harbor Laboratory Press, 2005

[222] Sherman, F. and Hicks, J.: Micromanipulation and dissection of asci. *Methods Enzymol.* 1991; **194**: pp. 21–37

[223] Trovesi, C. ; Falcettoni, M. ; Lucchini, G. ; Clerici, M. ; and Longhese, M. P.: Distinct Cdk1 requirements during single-strand annealing, noncrossover, and crossover recombination. *PLoS Genet.* 2011, August; **7**(8): p. e1002263. http://dx.doi.org/10.1371/journal.pgen.1002263. – DOI 10.1371/journal.pgen.1002263

[224] *KEGG Mapper – Search&Color Pathway.* http://www.genome.jp/kegg/tool/map_pathway2.html

[225] Mazón, G. ; Mimitou, E. P. ; and Symington, L. S.: SnapShot: Homologous recombination in DNA double-strand break repair. *Cell.* 2010, August; **142**(4): pp. 646–646.e1. http://dx.doi.org/10.1016/j.cell.2010.08.006. – DOI 10.1016/j.cell.2010.08.006

[226] Chankova, S. G. ; Dimova, E. ; Dimitrova, M. ; and Bryant, P. E.: Induction of DNA double-strand breaks by zeocin in *Chlamydomonas reinhardtii* and the role of increased DNA double-strand breaks rejoining in the formation of an adaptive response. *Radiat Environ Biophys.* 2007, November; **46**(4): pp. 409–416. http://dx.doi.org/10.1007/s00411-007-0123-2. – DOI 10.1007/s00411–007–0123–2

[227] Park, M. S. ; Ludwig, D. L. ; Stigger, E. ; and Lee, S. H.: Physical interaction between human RAD52 and RPA is required for homologous recombination in mammalian cells. *J Biol Chem.* 1996, August; **271**(31): pp. 18996–19000

[228] Mortensen, U. H. ; Bendixen, C. ; Sunjevaric, I. ; and Rothstein, R.: DNA strand annealing is promoted by the yeast Rad52 protein. *Proc Natl Acad Sci U S A.* 1996, October; **93**(20): pp. 10729–10734

[229] Clerici, M. ; Trovesi, C. ; Galbiati, A. ; Lucchini, G. ; and Longhese, M. P.: Mec1/ATR regulates the generation of single-stranded DNA that attenuates Tel1/ATM signaling at DNA ends. *EMBO J.* 2014, February; **33**(3): pp. 198–216. http://dx.doi.org/10.1002/embj.201386041. – DOI 10.1002/embj.201386041

[230] Strathern, J. N. ; Klar, A. J. ; Hicks, J. B. ; Abraham, J. A. ; Ivy, J. M. ; Nasmyth, K. A. ; and McGill, C.: Homothallic switching of yeast mating type cassettes is initiated by a double-stranded cut in the MAT locus. *Cell.* 1982, November; **31**(1): pp. 183–192

[231] Dyer, P. S. and O'Gorman, C. M.: Sexual development and cryptic sexuality in fungi: insights from Aspergillus species. *FEMS Microbiol Rev.* 2012, January; **36**(1): pp. 165–192. http://dx.doi.org/10.1111/j.1574-6976.2011.00308.x. – DOI 10.1111/j.1574–6976.2011.00308.x

[232] Pellicioli, A. ; Lucca, C. ; Liberi, G. ; Marini, F. ; Lopes, M. ; Plevani, P. ; Romano, A. et al.: Activation of Rad53 kinase in response to DNA damage and its effect in modulating phosphorylation of the lagging strand DNA polymerase. *EMBO J.* 1999, November; **18**(22): pp. 6561–6572. http://dx.doi.org/10.1093/emboj/18.22.6561. – DOI 10.1093/emboj/18.22.6561

[233] Ma, J.-L. ; Lee, S.-J. ; Duong, J. K. ; and Stern, D. F.: Activation of the checkpoint kinase Rad53 by the phosphatidyl inositol kinase-like kinase Mec1. *J Biol Chem.* 2006, February; **281**(7): pp. 3954–3963. http://dx.doi.org/10.1074/jbc.M507508200. – DOI 10.1074/jbc.M507508200

[234] Weinert, T. A. ; Kiser, G. L. ; and Hartwell, L. H.: Mitotic checkpoint genes in budding yeast and the dependence of mitosis on DNA replication and repair. *Genes Dev.* 1994, March; **8**(6): pp. 652–665

[235] Sidorova, J. M. and Breeden, L. L.: Rad53-dependent phosphorylation of Swi6 and down-regulation of CLN1 and CLN2 transcription occur in response to DNA damage in Saccharomyces cerevisiae. *Genes & Development.* 1997, November; **11**(22): pp. 3032–3045. http://dx.doi.org/10.1101/gad.11.22.3032. – DOI 10.1101/gad.11.22.3032. – ISSN 0890–9369

[236] Managbanag, J. R. ; Witten, T. M. ; Bonchev, D. ; Fox, L. A. ; Tsuchiya, M. ; Kennedy, B. K. ; and Kaeberlein, M.: Shortest-path network analysis is a useful approach toward identifying genetic determinants of longevity. *PLoS One.* 2008; **3**(11): p. e3802. http://dx.doi.org/10.1371/journal.pone.0003802. – DOI 10.1371/journal.pone.0003802

[237] Witten, T. M. and Bonchev, D.: Predicting aging/longevity-related genes in the nematode Caenorhabditis elegans. *Chem Biodivers.* 2007, November; **4**(11): pp. 2639–2655. http://dx.doi.org/10.1002/cbdv.200790216. – DOI 10.1002/cbdv.200790216

[238] Gasch, A. P. ; Spellman, P. T. ; Kao, C. M. ; Carmel-Harel, O. ; Eisen, M. B. ; Storz, G. ; Botstein, D. et al.: Genomic expression programs in the response of yeast cells to environmental changes. *Mol Biol Cell.* 2000, December; **11**(12): pp. 4241–4257

[239] Prag, G. ; Watson, H. ; Kim, Y. C. ; Beach, B. M. ; Ghirlando, R. ; Hummer, G. ; Bonifacino, J. S. et al.: The Vps27/Hse1 complex is a GAT domain-based scaffold for ubiquitin-dependent sorting. *Dev Cell.* 2007, June; **12**(6): pp. 973–986. http://dx.doi.org/10.1016/j.devcel.2007.04.013. – DOI 10.1016/j.devcel.2007.04.013

[240] Vera Babin: *Regulation of Telomere Length Homeostasis By Telomere Length Maintenance (TLM) Genes in Saccharomyces cerevisiae*, Tel-Aviv University, George S. Wise Faculty of Life Sciences Graduate School, Masterthesis, November 2014

[241] Churikov, D. ; Corda, Y. ; Luciano, P. ; and Géli, V.: Cdc13 at a crossroads of telomerase action. *Frontiers in Oncology.* 2013, February; **3**(39). http://dx.doi.org/10.3389/fonc.2013.00039. – DOI 10.3389/fonc.2013.00039. – ISSN 2234–943X

[242] Evans, S. K. and Lundblad, V.: Est1 and Cdc13 as Comediators of Telomerase Access. *Science.* 1999, October; **286**(5437): pp. 117–120. http://dx.doi.org/10.1126/science.286.5437.117. – DOI 10.1126/science.286.5437.117. – ISSN 1095–9203

[243] Morvan, J. ; Rinaldi, B. ; and Friant, S.: Pkh1/2-dependent phosphorylation of Vps27 regulates ESCRT-I recruitment to endosomes. *Mol Biol Cell.* 2012, October; **23**(20): pp. 4054–4064. http://dx.doi.org/10.1091/mbc.E12-01-0001. – DOI 10.1091/mbc.E12–01–0001

[244] Mattissek, C. and Teis, D.: The role of the endosomal sorting complexes required for transport (ESCRT) in tumorigenesis. *Mol Membr Biol.* 2014, June; **31**(4): p. 111–119. http://dx.doi.org/10.3109/09687688.2014.894210. – DOI 10.3109/09687688.2014.894210. – ISSN 1464–5203

[245] Toyoshima, M. ; Tanaka, N. ; Aoki, J. ; Tanaka, Y. ; Murata, K. ; Kyuuma, M. ; Kobayashi, H. et al.: Inhibition of tumor growth and metastasis by depletion of vesicular sorting protein Hrs: its regulatory role on E-cadherin and beta-catenin. *Cancer Res.* 2007, June; **67**(11): pp. 5162–5171. http://dx.doi.org/10.1158/0008-5472.CAN-06-2756. – DOI 10.1158/0008–5472.CAN–06–2756

[246] Robert, T. ; Vanoli, F. ; Chiolo, I. ; Shubassi, G. ; Bernstein, K. A. ; Rothstein, R. ; Botrugno, O. A. et al.: HDACs link the DNA damage response, processing of double-strand breaks and autophagy. *Nature.* 2011, March; **471**(7336): pp. 74–79. http://dx.doi.org/10.1038/nature09803. – DOI 10.1038/nature09803

[247] Shubassi, G. ; Robert, T. ; Vanoli, F. ; Minucci, S. ; and Foiani, M.: Acetylation: A Novel Link between Double-Strand Break Repair and Autophagy. *Cancer Research.* 2012, March; **72**(6): pp. 1332–1335. http://dx.doi.org/10.1158/0008-5472.can-11-3172. – DOI 10.1158/0008–5472.can–11–3172. – ISSN 1538–7445

[248] Luo, S. and Rubinsztein, D. C.: Atg5 and Bcl-2 provide novel insights into the interplay between apoptosis and autophagy. *Cell Death and Differentiation.* 2007, April; **14**(7): pp. 1247–1250. http://dx.doi.org/10.1038/sj.cdd.4402149. – DOI 10.1038/sj.cdd.4402149. – ISSN 1476–5403

[249] Kametaka, S. ; Matsuura, A. ; Wada, Y. ; and Ohsumi, Y.: Structural and functional analyses of APG5, a gene involved in autophagy in yeast. *Gene.* 1996, October; **178**(1-2): pp. 139–143

[250] Kuma, A. ; Hatano, M. ; Matsui, M. ; Yamamoto, A. ; Nakaya, H. ; Yoshimori, T. ; Ohsumi, Y. et al.: The role of autophagy during the early neonatal starvation period. *Nature.* 2004, December; **432**(7020): pp. 1032–1036. http://dx.doi.org/10.1038/nature03029. – DOI 10.1038/nature03029

[251] Kaeberlein, M. ; Burtner, C. R. ; and Kennedy, B. K.: Recent Developments in Yeast Aging. *PLoS Genet.* 2007; **3**(5): p. e84. http://dx.doi.org/10.1371/journal.pgen.0030084. – DOI 10.1371/journal.pgen.0030084. – ISSN 1553–7404

[252] S. Michal Jazwinski: Longevity, genes, and aging: a view provided by a genetic model system. *Exp Gerontol.* 1999, January; **34**(1): pp. 1–6

[253] Mortimer, R. K. and Jonhnston, J. R.: Life span of individual yeast cells. *Nature.* 1959, June; **183**(4677): pp. 1751–1752

[254] Matt Kaeberlein: Lessons on longevity from budding yeast. *Nature.* 2010, March; **464**(7288): pp. 513–519. http://dx.doi.org/10.1038/nature08981. – DOI 10.1038/nature08981

[255] Longo, V. ; Shadel, G. ; Kaeberlein, M. ; and Kennedy, B.: Replicative and Chronological Aging in Saccharomyces cerevisiae. *Cell Metabolism.* 2012, July; **16**(1): pp. 18–31. http://dx.doi.org/10.1016/j.cmet.2012.06.002. – DOI 10.1016/j.cmet.2012.06.002. – ISSN 1550–4131